RESPONSE ANALYSIS AND DAMAGE MITIGATION OF BURIED CONTINUOUS PIPES SUBJECTED TO FAULTING ACTIONS

by

Dardan Perdibuka

B.S., Civil Engineering, Yildiz Technical University, 2015

M.S., Structural Engineering, Yildiz Technical University, 2017

Submitted to the Kandilli Observatory and Earthquake Research Institute
in partial fulfillment of the requirements for the degree of
Doctor of Philosophy

Graduate Program in Earthquake Engineering

Boğaziçi University

2022

RESPONSE ANALYSIS AND DAMAGE MITIGATION OF BURIED CONTINUOUS PIPES SUBJECTED TO FAULTING ACTIONS

APPROVED BY:

Prof. Ayşe Edinçliler (Thesis Supervisor)	……
Prof. M. Eren Uçkan (Thesis Co-Supervisor)	……
Prof. Ali Pınar	……
Prof. Selçuk Toprak (Gebze Technical University)	……
Assoc. Prof. Gülüm Tanırcan	……
Prof. Yasin Fahjan (Istanbul Technical University)	……

DATE OF APPROVAL: 28/12/2022

ACKNOWLEDGEMENTS

I would like to take and use this opportunity to express my deep sense of gratitude and respect to my thesis supervisor Prof. Ayşe EDİNÇLİLER. Her endless support, patience, interest and guidance has been instrumental while working on this thesis. If not for her meticulous suggestions and whenever necessary astute criticism this thesis would not have been complete. My special thanks and gratitude are also to the co-advisor of the thesis Prof. M. Eren UÇKAN whose attitude of generously sharing his extensive knowledge on the topic and guidance throughout this journey has truly enlightened my path.

The members of the thesis monitoring committee Prof. Ali PINAR and Prof. Selçuk TOPRAK are also to be greatly thanked for their delicate and detailed evaluation of this work throughout the last couple of years. Their valuable suggestions and critics have elevated and enriched the quality of this work and broadened my understanding of the topic.

I also feel in debt to express my sincere thankfulness to the whole department of Earthquake Engineering at Boğaziçi University Kandili Observatory, the faculty members, the staff and friends I have met there during my studies whom never spared their valuable knowledge and help. My sincere thanks are also due to EDGE Consulting Engineers, my dear co-workers there and my employer, their understating of my absence during the busiest times of this thesis has contributed a great deal to its completion today.

Last, but not the least, I cannot imagine of a way of even remotely expressing my feelings of thankfulness to my dear family. My late father who kept supporting and trusted me up to his last moment and my dear mother and sister were pillars of mine who motivated me and kept me moving even during the hardest time. Finally, my warmest thanks are to my dearest darling spouse Hülya Yüksel Perdibuka, her endless support, love, and patience were my driving forces.

ABSTRACT

RESPONSE ANALYSIS AND DAMAGE MITIGATION OF BURIED CONTINUOUS PIPES SUBJECTED TO FAULTING ACTIONS

Buried continuous steel pipelines are critical lifelines failure of which under fault rupture incidents may lead to significant and deteriorating environmental and socio-economic outcomes. Proper understanding and estimation of the mechanical behavior of buried steel pipes under such geohazards and investigation of means of mitigating these deleterious effects is of paramount importance. This thesis aimed at developing rigorous and simplified numerical models of the problem to realistically simulate the behavior of buried continuous pipes under strike-slip fault rupture-induced permeant ground deformations. The response of buried pipe cases under the fault load was investigated with respect to the variation of fault crossing angle (β) and pipe wall thickness (t). The second phase of this dissertation involved the investigation of the effect of four mitigation techniques to protect the buried pipe against fault rupture-induced damages. Lastly, a case study involving the evaluation of the effect of using CFRP wraps on the response of Thames Water Pipe which suffered great damage during the devastating 1999 Izmit is presented.

The outcomes of this thesis indicate that the performance of the pipeline is sensitive to the variation of fault crossing angle and pipe wall thickness, increasing both parameters lead to overall improved pipe performance. Results indicate that all mitigation approaches offer certain degrees of improvement, where most effective mitigation approach is the wrapping of the pipeline surface with CFRP wraps while the use of controlled-low strength material was the least effective approach. Comparison of simplified and rigorous numerical models revealed that a good agreement exist between the approaches. Lastly, evaluation of the response of Thames Water Pipe protected using CFRP indicates that despite the considerable reduction in stresses and strains complete avoidance of failure for this particular case does not seem to be attainable.

ÖZET

FAY ETKİLERİNE MARUZ KALMIŞ GÖMÜLÜ SÜREKLİ BORU HATLARININ DAVRANIŞ ANALİZİ VE HASAR AZALTILMASI

Kritik yaşam hatları olarak gömülü çelik borularda fay kırılmaları esnasında meydana gelebilecek hasarlar yıkıcı çevresel ve sosyo-ekonomik sonuçlara yol açabilmektedir. Bu tür doğal afet durumlarında gömülü çelik boruların mekanik davranışının uygun şekilde anlaşılması ve tahmin edilmesi ve bu zararlı etkilerin azaltılmasına yönelik araçların araştırılması büyük önem taşımaktadır. Bu tez, yanal atımlı fay kırılmasının neden olduğu kalıcı zemin deformasyonları altında gömülü sürekli boruların davranışını gerçekçi bir şekilde simüle etmek için problemin gelişmiş ve basitleştirilmiş sayısal modellerini geliştirmeyi amaçlamıştır. Gömülü borunun artımsal fay yükü altındaki davranışı, fay geçiş açısı (β) ve boru duvar kalınlık (t) değişimine göre incelenmiştir. Tezin ikinci kısmı, gömülü boruyu fay kırılmasının neden olduğu hasarlara karşı korumak amacıyla dört hasar azaltma tekniğinin etkisinin araştırılmasını içermektedir. Tezin son bölümünde, 1999 İzmit depreminde büyük hasar gören Thames Su Borusu hatının davranışı üzerine CFRP sargı kullanımının etkisinin değerlendirilmesini içeren bir vaka çalışması sunulmuştur

Elde edilen neticeler, boru hattının performansının fay geçiş açısı ve boru duvar kalınlığı değişimine duyarlı olduğunu göstermektedir, bu parmetre değerlerinin artılıması boru performansı iyileştirmektedir. Elde edilen sonuçlar tüm iyileşitirme yaklaşımlarının performansı belirli ölçüde iyeliştirdiğini göstermekte, ve en etkili yöntemin CFRP sargıları ile boru hattı yüzeyinin sarılması olduğunu göstermektedir. Diğer taraftan, kontrollü düşük mukavemetli malzemenin kullanımının, en az etkili yaklaşım olduğu belirlenmiştir. Basitleştirilmiş ve gelişmiş sayısal modellerin karşılaştırılması bu yaklaşımlar arasında iyi bir uyumun olduğunu göstermiştir. Son olarak, CFRP kullanılarak iyileştirilen Thames Su Borusunun davranışının değerlendirilmesi, gerilim ve gerinimlerdeki önemli azalmaya rağmen, bu özel durum için göçme durumundan tamamen kaçınmanın mümkün görünmediğini göstermektedir.

TABLE OF CONTENTS

LIST OF FIGURES

LIST OF TABLES

LIST OF SYMBOLS / ABBREVIATIONS

a	API X65 Steel material constant
A_s	Steel pipe cross-sectional area
c	Soil cohesion value
c_{CLSM}	Cohesion of CLSM material
C_R	R-Wave velocity
D	External diameter of buried steel pipe
d_{cr}	Critical fault displacement value leading to the structural failure of the pipe
E	Modulus of elasticity of pipeline steel
E_1	Steel material modulus of elasticity
E_{11}	FRP material longitudinal modulus of elasticity in direction 1-1
E_{12}	FRP material shear modulus in direction 1-2
E_{13}	FRP material shear modulus in direction 1-3
E_2	Steel material modulus of plasticity
E_{22}	FRP material longitudinal modulus of elasticity in direction 2-2
E_{23}	FRP material shear modulus in direction 2-3
E_{33}	FRP material longitudinal modulus of elasticity in direction 3-3
E_{cCL}	Young's Modulus of CLSM material
E_{cE}	Young's Modulus of EPS geofoam material
E_g	Young's Modulus of geogrid material
EI	Flexural stiffness of beam on elastic foundation
E_i	Steel material initial Young's modulus
E_s	Soil modulus of elasticity
f	Ovalization factor
f_{cCL}	Compressive strength of CLSM material
f_{cE}	Compressive strength of EPS geofoam material
F_{max}	Maximum pipeline axial force
H	Pipe burial depth
k	Elastic foundation spring constant
K_o	Soil pressure coefficient at rest condition
L_1	Pipeline anchor length from the far end

L_2	Pipeline anchor length from the far end
$L_{avlb.}$	Available pipeline elongation
L_{cl}	Lateral displacement length
L_{cl}	Pipe bent length
L_{cv}	Vertical displacement length
$L_{req.}$	Required pipeline elongation
$l_{unanch.}$	Unsupported length of the buried pipe
M_p	Steel pipe moment capacity considering the effect of axial force
M_{pc}	Steel pipe moment capacity excluding axial force effect
N_c	Vertical downwards direction bearing capacity factor for clay soil
N_{ch}	Horizontal bearing capacity factor for clay soil
N_{cv}	Vertical upwards direction bearing capacity factor for clay soil
N_q	Vertical downwards direction bearing capacity factor for sandy soil
N_{qh}	Horizontal bearing capacity factor for sandy soil
N_{qv}	Vertical upwards direction bearing capacity factor for sandy soil
N_γ	Vertical downwards soil bearing capacity
P_u	Soil limit force in lateral direction
P_u	Steel pipe ultimate axial force resisting capacity
Q_d	Soil limit force in vertical downwards direction
q_u	Limit stress for transverse soil springs defined per length of the pipe
Q_u	Soil limit force in vertical upwards direction
r	Radius of curvature of deformed pipeline
r	API X65 Steel material constant
R_{cl}	Pipe radius of curvature in the horizontal plane
S_{12}	FRP material shear strength in direction 1-2
S_{13}	FRP material shear strength in direction 1-3
S_{23}	FRP material shear strength in direction 2-3
t	Wall thickness of buried steel pipe
t_c	FRP layer thickness
t_u	Limit soil-pipe friction force defined per length of the pipe
T_u	Soil limit force in axial direction
V_{max}	Maximum seismic wave velocity
V_s	S-Wave velocity

w	Deflection of beam
α	Pipeline local buckling factor
$\alpha_{adh.}$	Adhesion factor used in the calculation of soil spring in axial direction
β	Fault crossing angle
γ_{CLSM}	CLSM material unit weight
γ_{EPS}	EPS geofoam material unit weight
γ_{ms}	Soil unit weight
γ_s	Incidence angle
δ	Pipeline weld toughness
ΔD	Change of the external pipeline diameter
δ_h	Lateral fault displacement
$\Delta L_{avlb.}$	Available pipeline elongation
ΔL_{cl}	Pipe elongation near the fault in the horizontal plane
ΔL_r	Required pipeline elongation
Δx	Fault movement component in x direction
Δy	Fault movement component in y direction
ε_1	Steel material yield strain
ε_2	Steel material failure strain
ε_{cr}	Critical strain value
ε_{cu}	Ultimate compressive strain capacity of pipeline steel material
ε_{el}	Elastic strain value
ε_{etrue}	True strain value
ε_g	Ground strain
$\varepsilon_{inl.}$	Inealastic strain value
ε_{pl}	Plastic strain value
ε_t	Total strain value
ε_{TM}	Ultimate tensile strain capacity of pipeline steel material
ε_x	Axial pipeline strain in x direction
η	Ratio of defect height to pipe wall thickness
θ	Pipeline bending angle
λ	Pipeline yield-tensile strength ratio
μ	Soil-pipe friction parameter

ν	Poisson's ratio
ν_{12}	Poisson's ratio of FRP material in direction 1-2
ν_{13}	Poisson's ratio of FRP material in direction 1-3
ν_{23}	Poisson's ratio of FRP material in direction 2-3
ξ	Ratio of defect length to pipe wall thickness
σ_1	Steel material yield stress
σ_2	Steel material failure stress
σ_a	Pipeline yield stress
σ_h	Pipeline hoop stress
σ_{max}	Maximum pipeline axial stress
σ_{ttrue}	True stress value
σ_x	Axial pipeline stress in x direction
σ_y	Axial pipeline stress in y direction
τ_{CLSM}	Shear strength of CLSM material
Φ	Soil internal friction angle
ψ	Soil dilation angle
BFRP	Basalt fiber reinforced polymer
CFRP	Carbon fiber reinforced polymer
CLSM	Controlled-low strength material
EPS	Expanded polystyrene
FEA	Finite element analysis
FRP	Fiber reinforced polymer
GFRP	Glass fiber reinforced polymer
HDPE	High density polyethylene
PGD	Permanent ground deformation

1. INTRODUCTION

This dissertation concerns with the analysis of the behavioral aspects of welded steel continuous pipes buried underneath a soil deposit and located at the vicinity of active strike-slip faults and investigation of means of reducing and/or eliminating the determinantal effects arising from the rupture of these faults. Often termed as lifelines due to the importance of the content they are used to transport, buried pipes are crucial elements of modern-day world which tend to occupy large areas beneath the surface. As a result, a variety of geohazards have the potential of imposing serious demands on these structures, magnitude of which may become so large that may hinder the operational safety of them. In particular, buried steel pipes may suffer damage either due to permanent ground deformations (PGD) or the seismic waves propagating through the earth's crust during a strong ground shaking (O'Rourke and Liu, 2012). PGD associated damages tend to be localized but severe, whereas those resulting from wave propagation typically affect large areas but are less severe, for instance, the earthquake that hit San Francisco in 1906 caused severe damage on the city's pipeline network with 52% of failures occurring in a single block of the city and the remaining spreading across the city, despite the close percentage the rate of damage at the localized city zone subjected to PGD was nearly 20 times higher than at the much larger zone affected by seismic wave propagation (O'Rourke et al., 1985). Due to their high probability of causing irreparable damage and being the primary design concern for buried pipes, this thesis only deals with the evaluation of pipeline response under PGD induced demands.

Occurring due to earthquake related perils such as fault ruptures, landslides, spreading of earth's surface due to liquefaction and other PGD shattering are the primary causes of failures in buried pipes. Under these deformations acting quasi-statically buried steel pipes typically suffer deformations that lead to the exceeding of the elastic limits of the pipe steel and cause it to undergo breaks in the walls of the pipe which in turn may lead to leakages imposing serious environmental risks. Under these circumstances, the traditional stress-based approach of designing buried pipes would not yield realistic results due to the fact that this approach would only be valid up to a maximum loading limit and whenever this limit is

exceeded at large deformations its applicability is hindered, therefore, need calls for the utilization of a strain-based design and evaluation approach.

Accurate forecasting and determination of the reaction of buried steel pipes sustaining large loads due to faulting actions is vital towards ensuring proper design and safeguarding these structures from the detrimental effects arising from the rupture of active faults. Over the last three decades, a significant body of work and research has been conducted on this matter which gave birth to numerous approaches developed for the estimation of the pipeline response, moreover, this studies also helped establish strain-based deformation limits and performance criteria for pipeline evaluation subjected to a variety of PGD deformations. Despite the existence of many simplified analytical approaches the complexity of the problem resulting from the highly non-linear nature of it and the need of accurately simulating the interaction between contacting mediums (i.e., the buried pipe and the soil deposit backfilling it) necessitates the utilization of sophisticated modelling approaches. The field of sophisticated finite element numerical simulation of buried steel pipe-soil model incorporating the explicit modelling of the interaction between these materials along with the quasi-static simulation of the fault movement is relatively new, with the earliest complete models going back to no longer than 10-15 years (Vazouras et al., 2010). The first part of this thesis is devoted to the building up of such a model, competent enough to capture this complex behavior, where the validation of the developed models was proved via comparing the obtained result with the ones resulting from the widely accepted ones. Influence of pipe design related properties such as the variation of the fault crossing angle and the D/t ratio (i.e. pipeline wall thickness) is studied through the close monitoring of the pre-determined strain limit states and the displacement value (d_{cr}) leading to the violation of these limits.

Prediction of the pipeline damages and evaluation of danger associated with the installation of buried pipes along areas with known histories of natural hazards is important as it would allow proper design and/or changing of the planned installation location. However, circumstances may often make it inevitable to locate the pipe along geohazard areas. Under such conditions, protection of the pipe utilizing available methods becomes important to safeguard it against deformations that may otherwise lead to structural failure. A variety of applications have long been used to improve the pipeline performance against mainly vertical loads, such as improvement of the backfill soil material (Saadeldin et al.,

2015), use of EPS geofoam blocks (Bartlett et al., 2015) and etc. However, research on protection of pipes against faut rupture induced deformations is scarce, with very limited experimental and numerical studies available. One of the primary goals of this dissertation was to develop comprehensive understanding of the effect of utilizing various mitigation strategies to improve buried continuous (welded) steel pipe seismic performance via developing rigorous numerical models capable of realistically simulating the contact properties of the materials as well as the beyond elastic behavior of these materials itself. Changes in the critical fault displacement (d_{cr}) value leading to failure due to exceedance of one of the strain limit, variation of stresses and the changes in the overall damage distribution along the pipeline were the criteria used to evaluate the influence of the investigated mitigation technique on the pipeline performance.

1.1. Objectives and Scope of the Study

This dissertation concerns itself with the estimation of the behavioral aspects of buried continuous (welded) steel pipes subjected to fault actions resulting from the rupture of a strike-slip fault. Scrupulous numerical models of the problem incorporating the modelling of material and geometric non-linearities as well as explicit simulation of the interaction and occurring between the buried pipe and the backfill soil interfaces have been developed and utilized to estimate the mechanical behavior of the pipe under the fault action applied as a quasi-static displacement load. Influence of design considerations such as angle of intersection with the fault trace and pipe D/t ratio on the performance of the buried pipe have been investigated within the scope of this thesis. A strain-based approach was utilized for performance evaluation purpose where strain limits defining the failure of the pipe due to the occurrence of phenomena such as local buckling, exceedance of tensile strains and cross-sectional distortion have been calculated for each investigated case. Apart from developing numerical models to simulate the buried pipe behavior under fault movement, this thesis also investigated the effect of four mitigation techniques to improve the seismic capacity and response of the steel pipe. In particular, utilization of FRP composite wraps (three types, CFRP, GFRP and BFRP with layer thicknesses varying from 1mm to 10mm), EPS geofoam blocks (low and high strength), controlled-low strength material (low and high strength) and Tensar Nr. 3 geogrid meshes (single and double mesh configurations) has been investigated to assess the level of improvement that might offered following the same strain-based

evaluation scheme. In addition to the developed complex numerical models this thesis also aimed at proposing a simplified-easier to construct and use-numerical model to accurately predict the peak longitudinal pipe strains and to be adopted for preliminary design and evaluation purposes. A case study involving the investigation of the efficacy of utilizing CFRP wraps for seismic damage mitigation was conducted within the scope of this thesis where the Thames Water Pipe which suffered severe damage during the notorious 1999 Izmit earthquake and was shut down as a consequence of this event was modeled and evaluated.

The body of work in this dissertation is divided into seven chapters in total. Initially Chapter 2 of the thesis covers a bibliographic review of the research and studies regarding the response evaluation of buried pipes subjected to faulting actions with a special emphasis on the strike-slip fault cases along with main findings emerging from these studies. In this context, main analytical, experimental, and numerical approaches contributed to the evolvement of this field have been reviewed. A short description of strain-based design approach is also provided within this section. Further on the chapter, a short discussion on the philosophy of damage mitigation of buried pipes subjected to seismic actions is provided, where the main applications and the existing research on their effectiveness are thoroughly reviewed. The chapter closes with the review of available commercial software widely utilized to simulate the behavior of buried pipes subject to fault movements.

Chapter 3 of the thesis contains information on the numerical modelling approach. Detailed description of the model dimensions, boundary conditions, fault load application, performance parameters, material properties, and modeling of the contact between pipe-soil and mitigation material interfaces are provided within this chapter. Further parts of the chapter provide descriptions on the material models utilized to define the behavior of pipe steel, native soil, FRP wraps, EPS geofoam, CLSM and geogrid. Computation of strain limits for definition of local buckling, 3 and 5% tensile strain, cross sectional distortion (ovalization), rupture of FRP and EPS, cracking of CLSM and breaking of geogrid are provided under this chapter.

Analysis results obtained using the numerical models described in previous chapter are provided under Chapter 4. Initial parts of the chapter present the results of models used for validation purpose, the plots and figures showing the variation of the distribution of

strains in axial direction spread along the length of the pipe are graphically compared with results available in literature. Second part of the chapter is devoted to the evaluation of pipeline performance apropos of the variation of fault crossing angle-β-(10^o, 15^o, and 30^o) and D/t ratio (58, 96, and 144). Changes in axial strains, and d_{cr} value are compared through the relevant plots and graphics. The chapter also includes the results obtained from analysis cases incorporating the considered mitigation approaches. Each mitigation strategy is initially evaluated separately considering their effect on buried pipe strains and stress levels and distribution. The last part of the chapter covers the comparison of the utilized mitigation approaches in terms of their influence on pipeline performance through the review of their effect on the d_{cr} values and damage distribution, lastly a cost comparison of the methods is presented along with a discussion on the cost-effectiveness of the utilized methods.

Chapter 5 of the thesis provides details on the simplified numerical models developed for the estimation of maximum pipeline strains. Description on the modelling approach and strain computation scheme is provided under the chapter. Later parts present the analysis results obtained using these models. The chapter concludes with the comparison of the strain results obtained using the simplified and the rigorous models.

In Chapter 6, a case study incorporating the use of CFRP wraps as seismic damage mitigation approach is presented. In this context, the Thames Water Pipe which underwent irreversible damage during the 1999 Izmit earthquake was modeled considering the soil and fault crossing angle conditions. Validity of the models is proven through comparison with literature work. Later the results of conventional (no mitigation) case are compared with those obtained from the model improved using CFRP wraps with a layer thickness of 5mm.

The last chapter of the thesis (Chapter 7) present the concluding remarks and main findings of this study along with discussions on future work.

2. LITERATURE SURVEY: RESPONSE ANALYSIS AND DAMAGE MITIGATION OF BURIED CONTINUOUS STEEL PIPE SUBJECTED TO FAULTING ACTIONS

2.1. Introduction

This chapter examines the existing literature and research conducted on the understating and description of the response and mechanical behavior of buried continuous steel pipes exposed to deformations induced by fault rupture. Being the primary cause of pipeline failure, this research area has attained significant interest over the last decades, resulting in the development of a considerable number of approaches and evaluation tools. Furthermore, the chapter also reviews the existing approaches and studies regarding the mitigation of seismic damages, by paying special emphasis on the techniques utilized in this study.

Buried continuous steel pipes subjected to faulting actions exhibit a rather complex behavior due to the exceedance of elastic limits of the steel material (i.e., highly nonlinear response) and the interaction of the pipe with the surrounding backfill soil material. As a result, accurate simulation of this behavior requires the utilization of rigorous numerical models of the problem. However, due to lack of adequate computer tools and software, the earliest attempts on developing response evaluation methods were limited to analytical and theoretical models. Section 2.2 of this chapters briefly presents the chronology of the analytical models developed for buried pipes subjected to faulting actions. With the progressions in the field of computers and availability of finite element software capable of accurately capturing this complex response, the interest in this field of research gravitated towards numerical models. Section 2.3 reviews the outstanding studies in this matter starting from simplified ones going the way up to latest and most comprehensive approaches. Experimental work on the response of buried pipes subjected to fault loads is very limited compared to theoretical work, the available literature is presented under Section 2.4. Mitigation strategies used to improve the seismic capacity and response of these pipes are presented under Section 2.5, where initially the main philosophy behind the concept of damage mitigation for these infrastructure is discussed with latter parts focusing on the past studies related to the utilization of techniques investigated in this thesis. Section 2.6

describes the concept of strain-based design-the approach utilized in this dissertation for performance evaluation of buried pipes-emphasizing the main differing points with stress-based design. The last section (Section 2.7) of this chapter reviews the available analysis software, highlighting their main advantages and shortcomings.

2.2. Analytical Methods of Response Analysis

The behavior of buried pipes under fault rupture induced seismic loads, in particular to permanent ground deformation hazards induced by the rupture of the fault they intersect is evaluated either via simple analytical approaches enabling a practical computation of demands and strain on the pipeline, however, tend to ignore certain considerations, or analysis is performed via utilizing numerical methods which could be either simplified models or more sophisticated three-dimensional finite element models. The main analytical models developed for this purpose are presented under this section.

2.2.1. Newmark and Hall Approach

The work conducted by Newmark and Hall was among the pioneering endeavors developed to understand the mechanical behavior of a buried pipeline subjected a fault rupture induced displacement load using a simplified analytical modeling approach (Newmark and Hall, 1975). This model assumes the pipe to behave as a cable sufficiently long which is subjected to displacement loads of low magnitude. The approach relates the slip of the pipe occurring due to friction with the native backfill soil directly to the pressure enforced by the gravity effect on this soil deposit. The method considered lateral and axial deformation of pipe as the deformation of soil, while ignoring the relative displacement between the two interacting parts. The outcomes of the study pointed out that the resistance ability and extent of a steel pipe to the applied fault displacement load depends on the properties of the backfill soil, steel pipe, and features of the fault it crosses. Outcomes of this approach suggests that the seismic resistance of the pipe enhances with the reduction of soil resistance in lateral and longitudinal directions. The study also concludes that if the steel pipe is located within a trench with almost no or very shallow slopes it would in turn perform much better in terms of resisting the transverse and longitudinal components of the fault movement.

The approach proposed by Newmark and Hall is structures upon three basic assumptions. The first among these premises, typically encountered in almost all deterministic approaches of this kind, considers the effects related to the ground motion itself. The constituents of this earths motion (i.e., earthquake induced ground acceleration, displacement, and velocity) appearing at two disjointed points over the path followed by propagating waves are presupposed to stand apart each other by a very short time gap. Meaning, the proposed approach assumes the earthquake excitation to fundamentally possess the features of a traveling wave. The next consideration of the approach regards the inertial effects sustained by the pipe suggesting them to be very small, thus negligible (Hansen, 1961). Experimental data (Trautmann, 1983) as well as later analytical studies (Kennedy et al., 1977) support this to an acceptable expectation. The last basic supposition of the model suggests that there would not be any relative motion occurring at the contacting surfaces of pipe and native soil resulting in net strains of the pipe be equal to that of ground. Figure 2.1 shows a pipeline undergoing S-wave propagation along a vertical plane with a certain incidence angle γ_s beside this vertical plane. The strain sustained by the ground itself (ε_g) acting in the direction coherent with that of pipe in this case is calculated using the wave velocities (V_{max} and V_s) as follows:

$$\varepsilon_g = \frac{V_{max}}{V_s} \sin\gamma_s \cos\gamma_s \tag{2.1}$$

For a R-wave traveling in the same direction with that of pipe axis, the strain sustained by the ground itself is similarly calculated as follows:

$$\varepsilon_g = \frac{V_{max}}{C_R} \sin\gamma_s \cos\gamma_s \tag{2.2}$$

The equations provided above typically result in overestimated pipe strain values, especially at large fault displacements. Moreover, due to negligence of flexural rigidity, the required equilibrium condition would be satisfied for fault movements causing compression built-up on the pipeline, hence, the methodology cannot be utilized for such instances. Despite its drawbacks, the Newmark and Hall method is considered to be the pioneering work offering a strong and reliable approach to the problem.

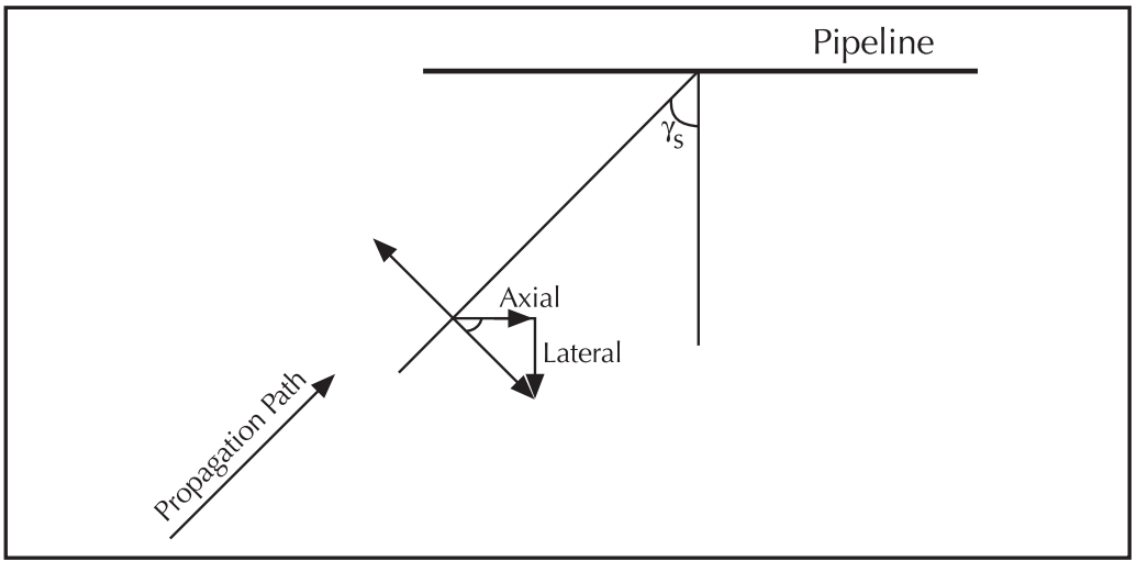

Figure 2.1. Buried pipeline subjected to S-Wave propagation (Newmark and Hall, 1975)

2.2.2. Kennedy et al. Methodology

Another widely used and accepted methodology is the that of Kennedy et al. (1977, 1983). The approach proposed in this research improved the basic formulation of Newmark and Hall (1975). In general, this approach as well treats the buried pipes as a relatively long cable, where the flexural or bending stiffness of the pipe is ignored for simplicity of calculations. Due to this limitation, the proposed methodology is only valid for fault crossing angles resulting in net tension on the pipe. The general outline of this methodology is shown in Figure 2.2, indicating a buried pipe intersection with a strike-slip fault (right lateral motion) with an angle of orientation β defined based on the features of fault movement. The buried pipe is suggested to be propped up at length denoted as L_1, and L_2 from fault trace on two far ends. The steps followed in the solution scheme of this analytical methodology are as described below:

(i) Initially the maximum pipeline axial stress (σ_{max}) and axial force (F_{max}) at pipe-fault intersection are estimated.

(ii) The radius of curvature at lateral and vertical direction is approximated.

(iii) The length (L_{cl} and L_{cv}) where displacement components in vertical and lateral directions occur are calculated.

(iv) The available pipeline elongation ($L_{avlb.}$) is calculated summing the extensions of the pipe occurring in the locations of high curvatures and outside.

(v) If equilibrium among the required ($L_{req.}$) and available ($L_{avlb.}$) elongation is not achieved step above are repeated for updated σ_{max} and F_{max} values. This continuous until convergence is achieved.

(vi) Once convergence is ensured, the axial pipe strain (ε_x) is computed using the following equation:

$$\varepsilon_x = \frac{\sigma_x}{E}\left[1 + \left(\frac{a}{r+1}\right)\left(\frac{|\sigma_x|}{\sigma_y}\right)^r\right] \tag{2.3}$$

Investigating the scenarios involving the development of extensive deformations (elongations) on the pipe leading to solely tensile effects happening due to the faulting actions, the proposed approach evaluated the correlation among the fault movement induced tensile forces in axial direction, resulting moments, and the lastly the emerging strains causing flexural and axial deformations. The followings are the main outcome of this study:

- The pipe tensile force in axial direction is independent of the curvature of it, providing that strains causing bending are not more than 80% of these leading to the development of strains in axial direction of the pipe.
- Assuming the net tension is acting on the pipe the flexural effects might be disregarded, such that the buried pipe possesses the behavioral patterns of a cable.

Due its limiting assumptions this methodology only becomes applicable under situations when the buried pipe experience's large fault loads and is capable of undergoing elongation without suffering any ruptures. However, in practice this is hardly ever achievable and would require the use of special construction measures. Hence, the analytical strain predictions of this approach typically would overestimate the pipeline strains resulting in strain values manifolding the real strains.

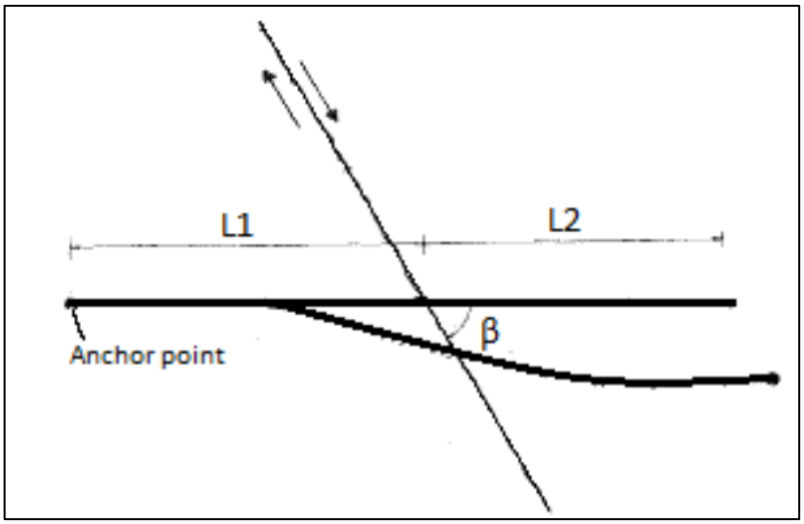

Figure 2.2. Deformation diagram of a buried pipe subjected to horizontal fault displacement load (Kennedy et al., 1977)

2.2.3. Wang and Yeh Methodology

Wang and Yeh (1985) have proposed an approach with more complete attributes than the predecessors that might be utilized for circumstances incorporating the effects of strike-slip and also reverse slip faulting conditions. Their approaches basically modified the main aspects and assumptions of the existing ones. The main attribute and refinement offered in this method is the dividing of the buried pipe segment into four parts, as depicted in Figure 2.3. The method assumes that at Point A the buried pipe crosscuts the fault, Points B and C on the other hand are used to define the borders of areas associated with high curvature occurrence during the act of the fault, lastly zones between BB' and CC' represent the points of anchorage where axial stress developing on the pipe is nearly absent. Segment AB and AC located on both ends of the fault and stretching along the zone of high curvature are assumed to be circular arcs. The remainder of segments (i.e., BB' and CC') located in the zone of minute displacement are considered to behave as beams-on-elastic foundation. Using this partitioning, the flexural effects (i.e., moments) occurring at the union locations of each arc segment with the straight segment are calculated via the use elastic beam theories can and eventually compared to the fundamental (ultimate) flexural capacity of the buried, which allows the derivation of safety factor countering failure might be estimated using the following expression:

$$\frac{M_{pc}}{M_P} = \cos\frac{\pi}{2}\left(\frac{P}{P_U}\right) \tag{2.4}$$

where, M_{pc} and M_P denote the resisting moment capacities of pipeline steel including and excluding axial load P, respectively, while P_u is the ultimate axial force capacity of the steel pipe without considering any bending effects.

Furthermore, the approach enables the calculation of a second factor of safety using the relationship between the ultimate strain capacity of the pipe and the calculated axial strain coinciding to the point where the pipe intersects the fault.

Although clearly a refinement to the existing methodologies, compared to that of Kennedy et al. (1977) this methodology also possesses certain shortcomings:

- The reduction in pipes ultimate bending capacity due to axial deformations is merely accounted for, moreover, its adverse impact to the stiffness of the pipe against flexural effect it totally neglected.
- Despite the adopted suggestion, the worst, unfavorable concentration of deformations does not definitely and always appear at borders of areas associated with high curvature, instead it occurs in the vicinity of fault.
- Evaluation of the safety of buried pipe-based om bending moments solely may be misleading and incomplete, in particular for displacement-controlled cases, where performance criteria based on deformation instead of stress appear to be more relevant.

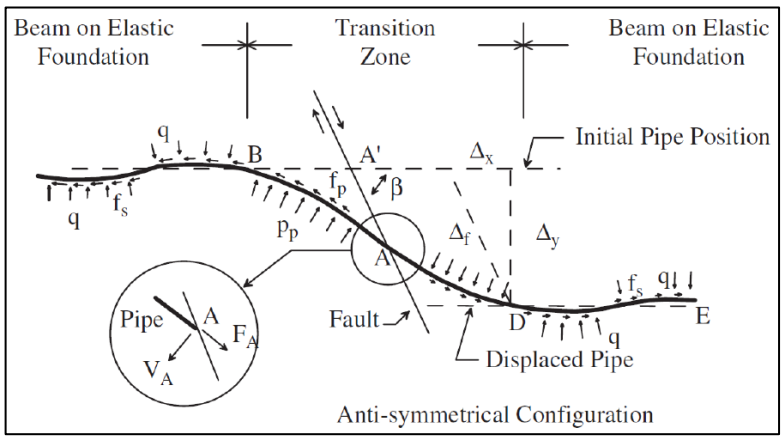

Figure 2.3. Pipeline analysis model proposed by Wang and Yeh (1985)

2.2.4. Karamitros et al. Methodology

A more recent methodology proposed by Karamitros et al. (2007) was developed and proposed by further improving the existing and renowned concepts of the earlier attempts describe in sections above. This study combines within its approach the earlier studies, where the expression developed by Kennedy et al., (2007) to underline and determine the influence of pipe axial tensile effects, and the Wang and Yeah (1985) division of the pipe into four distinct zones of deformation have been unified by also suggesting important modifications and additions.

Reviewing its details, the approach proposed in this particular research attempt essentially aimed at obtaining of axial and flexural deformations of a buried pipe underdoing large deformations due to faulting action. Similar to earlier research, beam on elastic foundation formulations as well the elastic beam theory solutions aided the computation procedure, however, in contrast to earlier works, this method took into account the stiffness of the buried pipe against bending, and the interaction or contact between the steel material of the pipe and native soil considered in transverse and axial directions. The anticipated non-linear response of the pipe steel material under the applied fault load was reckoned with the adoption of a bilinear force deformation pattern. The method follows an iterative solution scheme based on the update of secant elastic modulus of steel material up until convergence is ensured between the stresses and strains calculated at each particular step. The pipe and the fault were assumed to intersect each other at a single point possessing zero thickness. Figure 2.4 schematically illustrates the main assumptions of this method. The strike-slip fault load is assumed to be applied in x and y directions, hence has two components of motion defined per a Cartesian system of coordinates, these two are related to each other through the angle of orientation of the pipe with respect to fault plane. The current proposed form of this approach holds to be valid for crossing angles of $\beta \leq 90^{o}$, resulting in pipeline elongation.

Similar to the approach of Yang and Yeh (1985) this methodology assumes a four-segment partitioning of the buried pipe (see Figure 2.5). Here, under the imposed fault displacement segments AA’ and CC’ are solved with a theoretical approach (i.e., beam resting on an elastic ground) with the purpose of establishing relations between the flexural

deformation (moment), shear force and angle of rotations occurring at point A and C, the generic form of this differential expression for a bean element is as follows:

$$EI\frac{d^4w}{dx^4} + \text{kw} = 0 \tag{2.5}$$

where EI defines the flexural stiffness of the beam, w the deflection of it and k being the spring constant for the elastic foundation.

Maximum flexural effects acting on the buried pipe due to faut load is determined through the solution of pipe portion along AB and AC as elastic beams. This approach involves the computation of forces in axial direction of pipe corresponding to its junction point with the fault trace using the need of equilibrium among the required (load induced) and available (geometric) pipe elongations. Following steps of the solution procedure involve the computation of maximum pipeline strains by also regarding for the higher order effects, where the equality between the acting forces and the resulting pipeline stresses is used. These steps follow an iterative solution approach based on the updating of secant Young's modulus after each cycle until convergence is achieved. Strain results obtained using this methodology were compared to results emerging from sophisticated numerical models, where a satisfactory agreement was noted with a margin of error being below 10%.

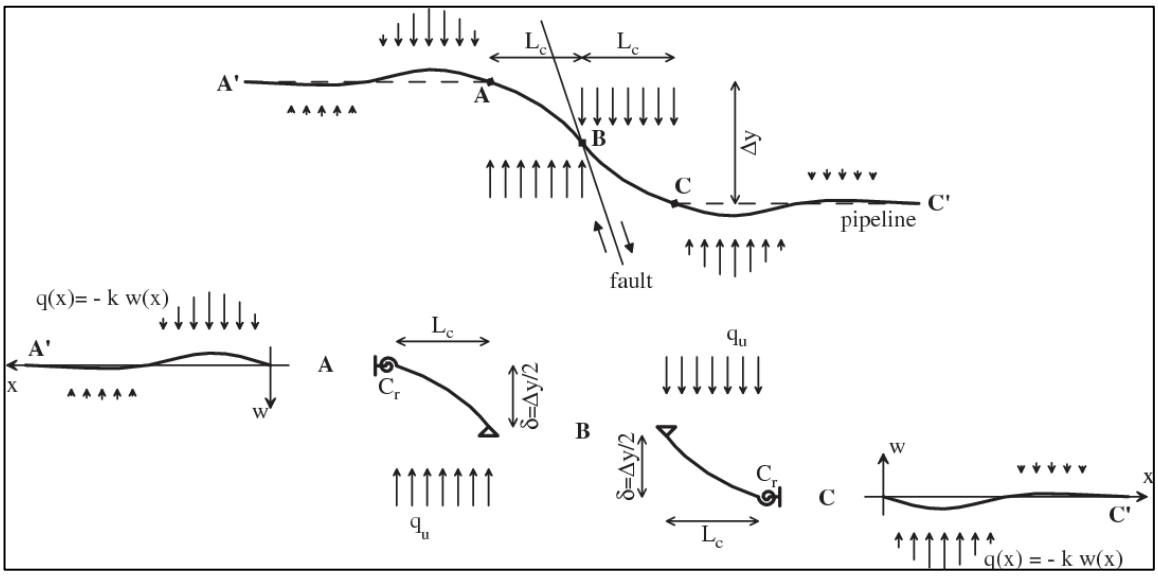

Figure 2.4. Pipeline partitioning and model proposed by Karamitros et al. (2007)

Other notable efforts in the field of developing analytical approaches for response evaluation of buried pipes undergoing deformations dur to seismic effects include the publications of McCaffrey and O'Rourke (1983) and Desmond et al. (1995) which studied the accumulation of strains in buried gas and water pipe that suffered damage at the destructive 1971 earthquake of San Fernando. Wang and Wang (1995) have also proposed an analytical model and solution approach assuming the buried pipe to act as a beam resting on elastic basis.

2.3. Numerical Methods of Response Analysis

Apart from analytical and theoretical approaches and following the developments in the field of computational structural analysis ana availability of efficient software, numerical modeling of the response of buried pipes suffering from a variety of loading condition became a prominent method for performance evaluation of these structures. The complex nature of the problem involving the analysis of a buried pipe under a fault rupture induced loading acting quasi-statically requires adequate material modeling so as to capture the highly non-linear behavior. Moreover, being a buried structure accurate definition of the contact properties among the pipe steel material and backfill soil deposit at the interface is crucial. This section briefly discusses the main numerical models developed for buried pipes subjected to fault movements.

2.3.1. Karamitros, Bouckovalas and Kouretzis Model

In addition to their analytical method Karamitros et al. (2007) have also proposed a 3D FE numerical model so as to evaluate and prove the accuracy of the predictions of analytical methodology. As seen in Figure 2.5 the developed numerical model consists of 1000m long pipe model of which 900m are modelled using beam elements, whereas, the remaining portions were modelled as shell elements. The soil surrounding the pipe and the interaction among the pipe and soil were represented by nonlinear springs. A pipeline with a diameter of 914.4mm and wall thickness of 12mm assumed to be placed within a sandy backfill soil. Analysis of the developed model was performed for three fault angle values (30^o, 45^o, and 60^o). The peak value of fault displacement applied onto the model was assumed to be equal to two pipe diameters. Results obtained in terms of maximum axial,

bending and longitudinal strains were then compared with the values obtained through the use of analytical methodology. A good overall agreement was observed among the two approaches with only minor deviations in values.

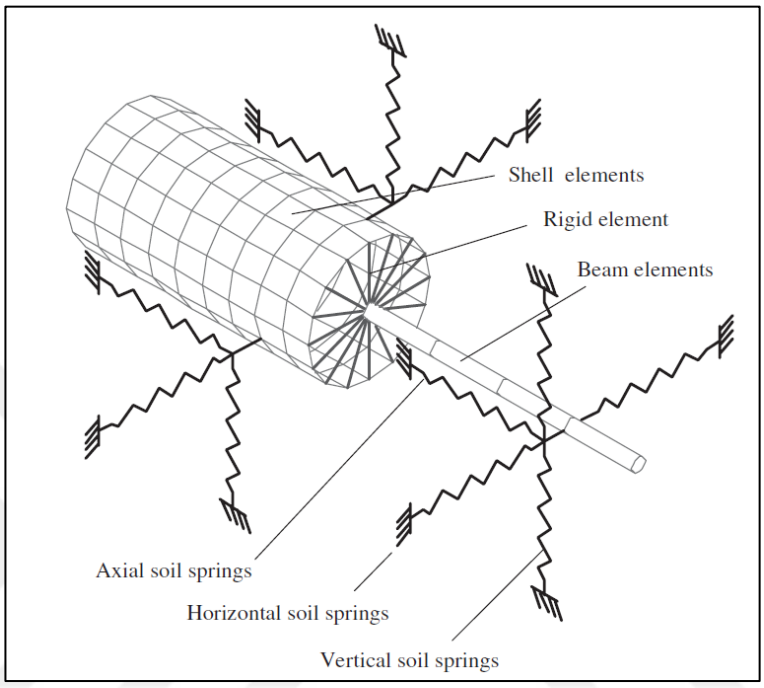

Figure 2.5. 3D numerical FE model proposed by Karamitros et al. (2007)

2.3.2. Liu, Wang and Yu Model

The numerical model proposed by Liu et al. (2008) resembles to the one proposed by Karamitros et al. (2007). A shell FE model with a total length of 4100 meters was developed to predict the variation of pipeline performance with respect to internal pressure, fault angle and variation of Lüder's extension (a state defined as the point where for small ranges of strains the pipe material yields and leads to a plateau in the stress-strain curve of steel material). The reason behind choosing such a large value for pipe length is for the purpose of reducing the relative difference among the movements of pipe and soil at far ends of model. The findings obtained through this study indicate that as the fault intersection angle gets lower the net tension force along pipe's axial direction becomes larger and eventually leads to a predominant tension failure mode. However, the finding of this approach suggests that as the value of fault intersection angle value increases the buried pipe suffers from bending instead of tension and majority of strains accumulate at locations far from the fault

trace. Consequently, the outcomes of the study suggest that the fault intersection value can be arranged such that the axial tensile strains and stresses on the pipeline during the fault movement would be minimum and therefor mitigate the seismic demands.

2.3.3. Liu et al. Model

Liu et al. (2016) have presented a numerical modeling approach for buried steel pipes subjected to reverse faulting actions where the occurrence of local buckling appears as the dominant mode of failure. The proposed FE model made use of shell elements to simulate the behavior of buried pipe, while the interaction among the pipe and the soil deposit was represented through the use of spring type elements. The study focused on the investigation of the pipe steel material properties on its seismic performance. Influence of steel material characteristics such as the yield strength and strain hardening have been studied assuming three different steel grades. Findings of this study showed that the Von Mises stresses generated on the pipe during the act of reverse fault loading were in magnitude equal to about 1.1 times the strength of the steel material. Increasing the yield strength of the pipe steel appeared to increase the critical value of fault displacement and the resulting axial stresses, whereas a decrement in these parameters was observed for increasing values of strain hardening. Both parameters (i.e., yield strength and strain hardening) were determined to have a very limited effect on the variation of axial strains.

2.3.4. Shitamoto et al. Model

The study conducted by Shitamoto et al. (2010) aimed at establishing a compressive strain limit for a pipeline possessing a steel grade of API X80 via constructing a numerical FE model of the pipe. As seen in Figure 2.6, the proposed FE model considers only half of the pipe and utilizes eight-node three dimensional solid elements to represent it. The pipe maximum demands in terms of strains was computed for a fault displacement value of 3m. Interaction characteristic between the steel pipe and the native soil were modeled via the use of non-linear springs at bottom and top faces of pipe shell element. The strain demand for peak bending effects was computed and compared to the fundamental capacity of the pipe.

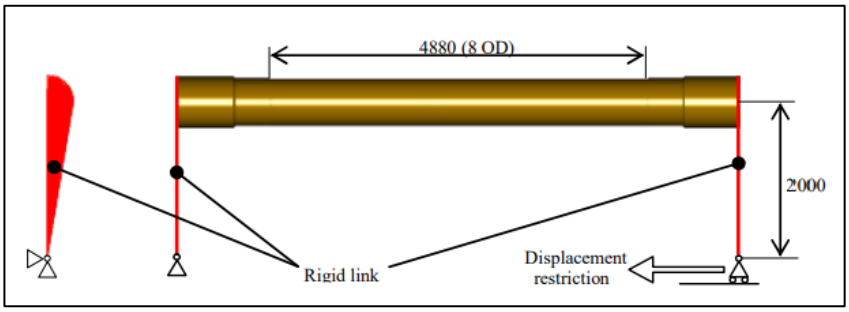

Figure 2.6. Configuration of numerical model proposed by Shitamoto et al. (2010)

2.3.5. Odina et al. Model

In a study published in 2009 Odina and Tan (2009) proposed a FE model of buried pipes constituting of beam form elements to assess the performance of these pipelines under detrimental faulting actions. A year later the proposed approach was further improved in a study published by Odina and Conder (2010) where the impact of the plateau of Lüder on the overall behavior of the steel pipe was also investigated. The study investigated the response of a 1400m long pipe with a wall thickness value of 17.1mm, the grade of steel material was assumed to be API X65. The developed 3D FE model utilized 3D beam elements (2-node elastic-plastic bean element with 6 degrees of freedom considered at each node of the pipe circular section).

Equivalent soil springs in lateral and vertical axial directions were employed for the modeling of the backfill soil material. The fault intersection angle was assumed to be equal to 22^{o}. The configuration of the utilized model is shown in Figure 2.7. The study investigated the pipeline performance considering the effect of using three different steel material models. The first case defined the post elastic response of the steel material of pipe using the Ramberg-Osgood stress-strain relationship. The second one defined the stress-strain curve based on Lüder's plateau, whereas the last case used a modified version of Ramberg-Osgood model assuming a 10% reduction in bending capacity at the locations of localized strains. The findings of the study indicate that the material model significantly influences the magnitude of axial strains.

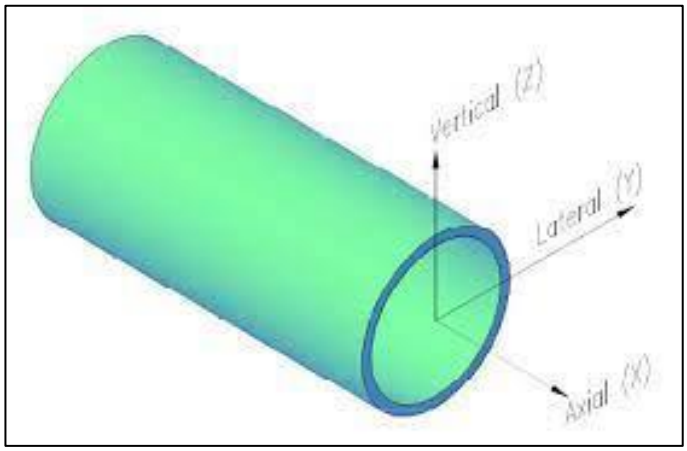

Figure 2.7. FE Model and soil springs proposed by Odina et al. (2009)

2.3.6. Fredj and Dinovitzer Model

A significant attempt to develop a numerical model for buried pipeline response against the effect of slope movements was proposed by Fredj and Dinovitzer (2012). The method followed for pipeline response analysis made use of 3D continuum modeling technique using LS-DYNA 971 (2007) software. The utilized FE model illustration is shown in Figure 2.8. The Smoothed-Particle Hydrodynamics (SPH) method-typically adopted for simulating fluid flows-was used during the response analysis procedure. Shell elements were utilized for pipe modelling, whereas a double-hardening plasticity model was used for soil modelling. Verification of the accuracy of the proposed method was achieved via comparing the obtained results with the experimental results of Karimian et al. (2009). An acceptable agreement among the two was observed. Analysis results indicate that the axial strain demands get larger as the pipeline D/t ratio increases (i.e. the wall thickness of pipe reduces). Obtained results were also compared to experimental findings of Scarpelli et al. (2003) performed on pipes wrapped with polyethylene, where again a good overall agreement between the two was observed.

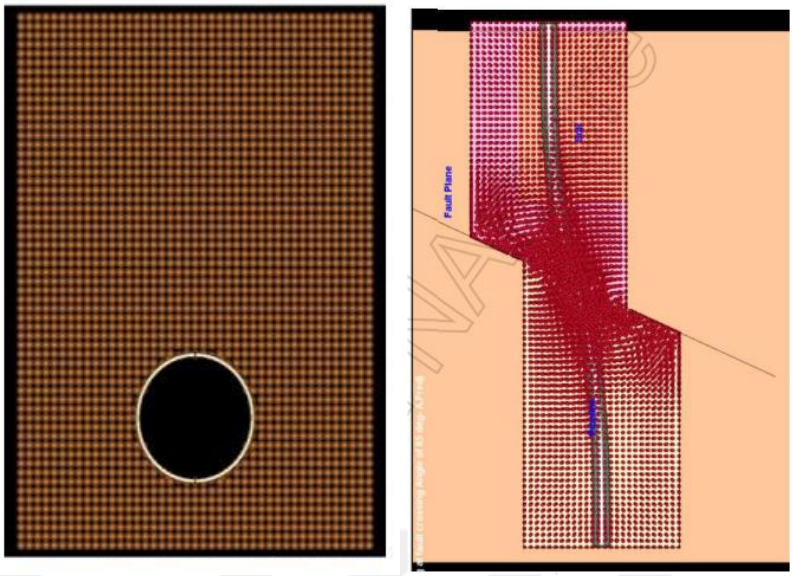

Figure 2.8. Configuration of FE model proposed by Fredj and Dinovitzer (2012)

2.3.7. Bartolini et al. Model

A study performed by Bartolini et al. (2013) proposed a strain-based evaluation approach for buried pipes located at active fault zones. Two evaluation approaches were utilized to observe the occurrence of damage patterns such as tensile and compressive failure, rupture of pipeline walls, weld failure under the imposed seismic load. The first scenario involved the consideration of an earthquake with a recurrence period of two hundred years to assess the operational safety of the pipe under such seismic demand. The second approach utilized an event with 1000 years return period in order to investigate the occurrence of detrimental damages and prevailing modes of failure. The study also rated the impact of design variables including the wall thickness of the pipe, steel material strength class, and trench conditions.

2.3.8. Gantes and Boukovalas Model

The study performed by Gantes and Boukovalas (2013) evaluated the performance of natural gas (high pressure) pipes subjected to fault movements in Greece. The configuration of the proposed analysis method made use of beam and shell elements to mathematically represent the buried where while modeling the soil around it using spring type elements. The NASTRAN FE analysis software was used to describe and understand the characteristic of

a buried pipe which was assumed to have an external diameter of 0.9144m and wall thicknesses varying between 12mm and 17.5mm. The pipeline steel material was API X65 grade steel and the pressure within the pipe was equal to 7.5MPa, represented in the analysis model using the Ramberg-Osgood curve. Analyzed under an oblique fault displacement of 0.8m, the total model length for the pipe was assumed to be equal to 1700m. Performance evaluation of the buried pipe suggested that the tensile strain limit defined as per Eurocode 8 was satisfied and therefor mitigation was deemed necessary to improve the performance of the pipeline under seismic loads.

2.3.9. Vazouras et al. Model

A vast majority of studies presented above typically involve rather simple numerical models where the pipeline is model either via the use of beam and/or shell type elements, whereas, the soil cover surrounding the pipeline is modeled using linear or non-linear soil springs. However, more recent studies have made use of more sophisticated finite element analysis software to model not only the pipeline but also the surrounding soil. Among these works the numerical models developed by Vazouras et al. (2010) exhibit a rather significant effort to establish the concepts of numerical modeling of pipe-soil system. ABAQUS CAE (2020) general purpose finite element software was utilized in their study. The typical configuration of the developed model is presented in Figure 2.9. Elements used for pipeline and soil modelling were chosen from the element library of the software. Shell elements with reduced integration and four nodes (S4R) were utilized for pipeline modelling, whereas, brick or solid elements of possessing eight nodes (C3D8R) were employed for soil simulation. The advantage of S4R elements is in their capacity to capture the large strains on membranes and large rotational occurrences and hence are appropriate for the analysis of cases where large strains do take place. The C3D8R brick solid element are also capable of providing accurate results for large stress and/or displacement analysis. As depicted in Figure 2.9 below, the study assumes a finer mesh pattern in the vicinity of fault trace for both soil and pipe so as to reduce the required computational effort and time. The strike-slip fault plane is modelled as a discontinuity plane that divides the soil into two equal blocks. The analysis consists of two steps: initially, gravity loading along with internal pipeline pressure are applied, in this step both soil blocks are restrained to move in horizontal directions; in step two as shown in Figure 2.10 one of the soil bocks is set free to move

horizontally and a fault displacement load is enforced to the outer nodes of shell and solid elements used to model the pipe and backfill soil respectively, a displacement load involving the gradually increment of fault displacement value is utilized to observe the evolution of stresses and strains. The outcomes of this study offer some significant insight regarding the seismic behavior characteristic of buried pipes subjected to faulting actions arising from the rupture incident of a strike-slip type faults and present a significant tool for design improvement of pipes located at areas of large geohazard potential. The model proposed by Vazouras et al. (2010) also served the basis for the development of numerical models presented in this dissertation. Main concepts offered in this study have been adopted and further refined in the present work. Moreover, validation of the developed numerical models and the overall approach was made via comparing the obtained results with the ones derived from the work of this study.

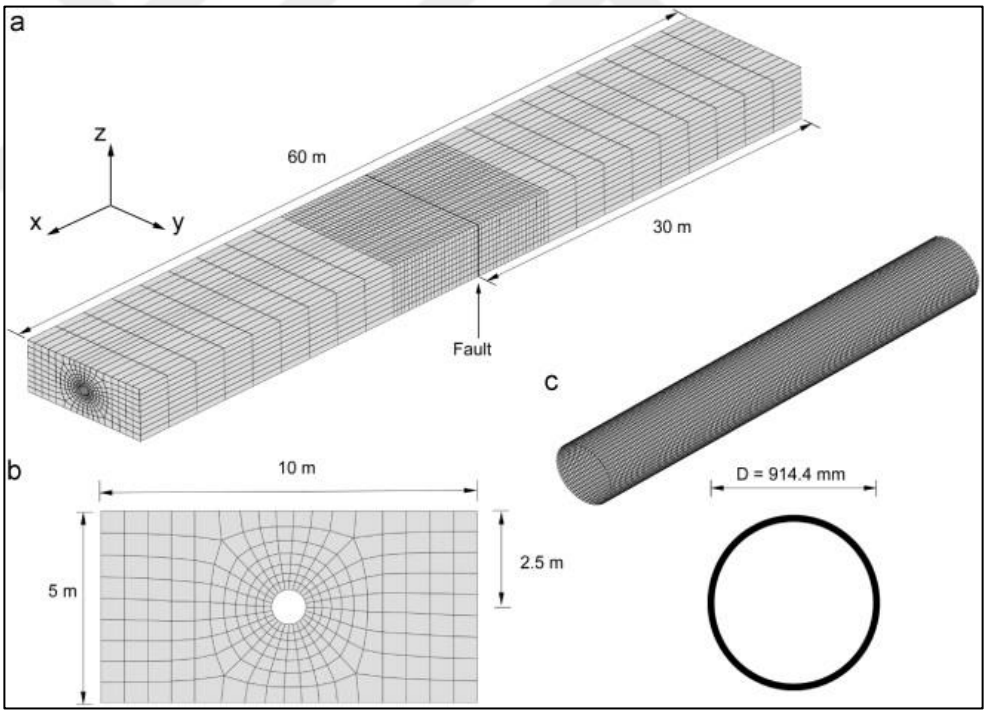

Figure 2.9. Detailed numerical model proposed by Vazouras et al. (2010)

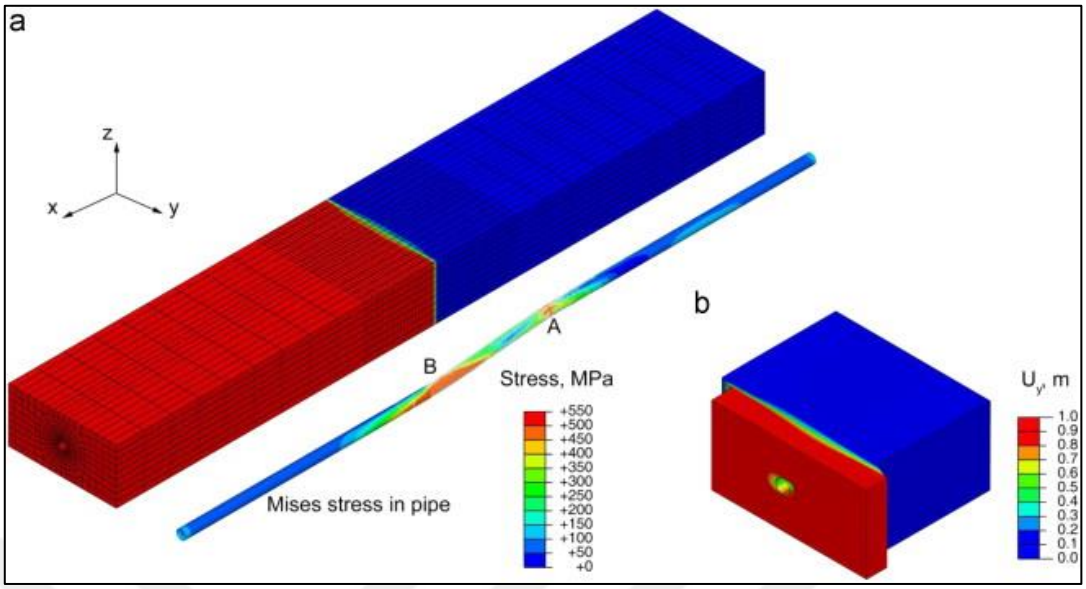

Figure 2.10. Fault load application and development of Von Mises stresses in Vazouras et al. (2010) model

2.4. Experimental Methods of Response Analysis

In addition to analytical and numerical approaches the response of buried pipelines under seismic demands imposed by fault movements is also studies through experimental research efforts. This section summarizes the most notable examples in this field.

The experimental studies performed by Yoshizaki et al. (2001) studied the aftermath of ground deformations on buried pipes with elbow type elements. The testing configuration (see Figure 2.11) consisted of a steel pipe with an outer diameter of 100mm and wall thickness of 4.1mm. The performance of buried pipe was testes assuming four different soil and/or water content scenarios. Data obtained in this experimental program was used to calibrate the numerical model developed for these cases. The proposed model consisted of a beam and shell elements with a pipe placed in a total depth of 0.9m within the soil deposit. The interaction at soil-pipe interface was modeled using spring elements with force deformation curves defined based on experimental data. Outcomes of the experimental program pointed into an acceptable coherence among the data obtained through experiments and numerical results. Furthermore, obtained data reveled that soil conditions, in particular the water content of the backfill soil material significantly influences the performance of buried steel pipe.

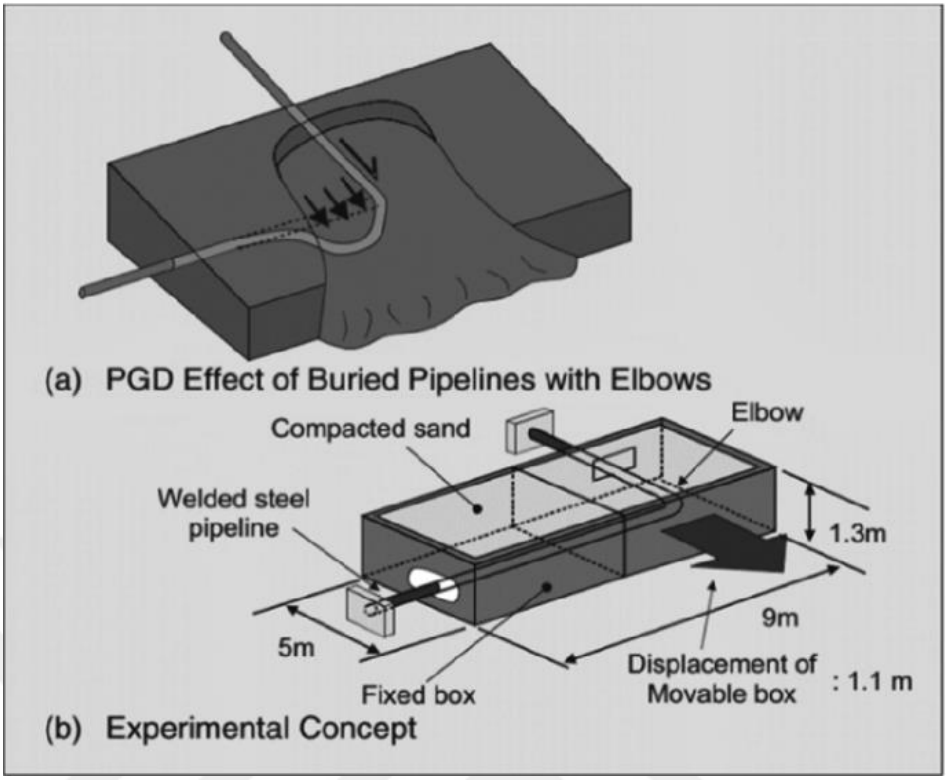

Figure 2.11. Experimental configuration proposed by Yoshizaki et al. (2001)

A series of experiments performed by Ha et al. (2008) and subsequent published papers present a valuable contribution on the understanding of the response of buried high-density polyethylene (HDPE) pipes exposed to faulting actions induced by the rupture of normal and strik-slip faults. Two experimental setups were constructed within the scope of their research resulting in two separate papers. As shown in Figure 2.12 the first experimental program investigated the reaction of a pipe at the crossing of a strike-slip fault (with an intersection angle of 5^{o}) and a normal fault, whereas as seen in Figure 2.13 the second tests evaluated the cases involving strike-slip faults crossed by the pipe at various intersection angle values. Accurate pressure sensors and strain gages were used as instruments to measure the changes in accumulated stresses and strain as the deformation due to fault rupture increased. The soil surrounding the pipe was divided into two blocks with the division line representing the fault trace. Fault movements was simulated via gradual movement of one these blocks while the second block remained stationary. Results obtained in terms of pressures in transverse direction and bending strains were utilized to establish curves defining the relationship among the soil and pipe. Resulting curves were than compared to the ones proposed by ASCE pipeline guidelines (1984).

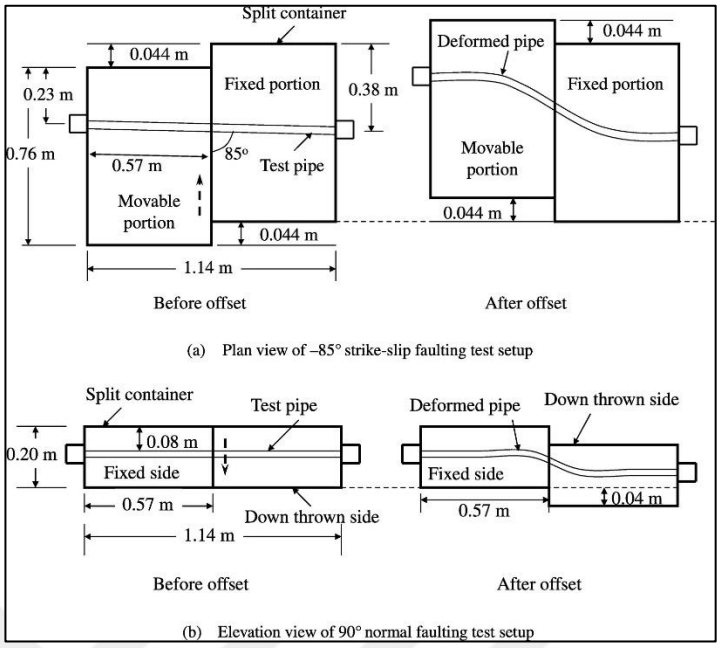

Figure 2.12. HDPE pipeline experimental setup developed by Ha et al. (2008) for, a) case of a strike-slip fault with β=5º and b) normal fault case

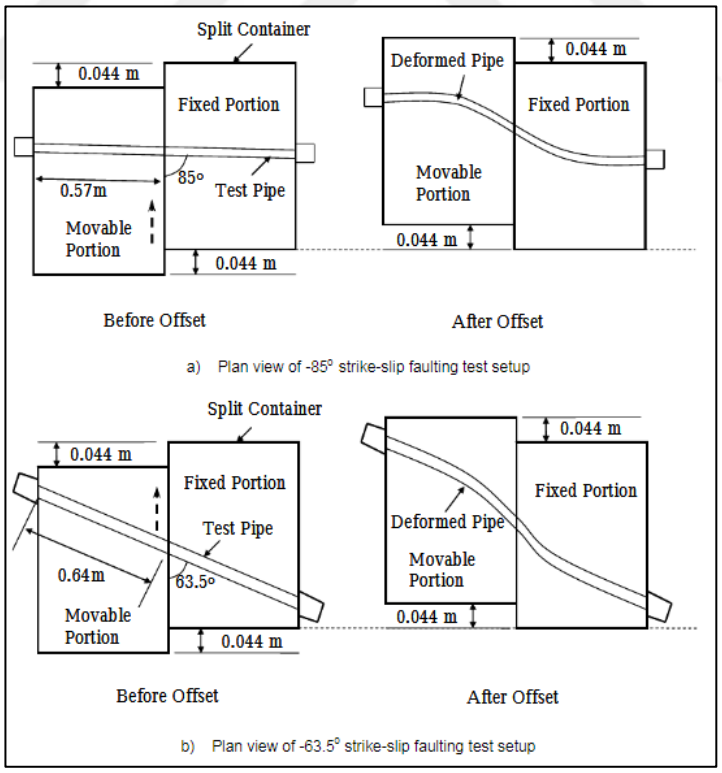

Figure 2.13. HDPE pipeline experimental setup developed by Ha et al. (2008) for, a) case of a strike-slip fault with β=5º and b) strike-slip fault case with β=26.5º

Full scale experimental studies performed at Cornell University by O'Rourke et al. (2008) present another significant effort and contribution to the understanding of the behavior of buried HDPE pipes. Split boxes with sizes of 10.7m in length and 3.3m in width as shown in Figure 2.14 were utilized to perform the experiments. HDPE pipes with diameters of 250 and 400mm and thickness of 24mm and steel pipes with a diameter of 150m and wall thickness of 3mm were tested within the scope of the study. The fault crossing angle was kept constant at 65^{o} for all tests performed. A fault displacement load reaching up to 1.2m was applied gradually to on the blocks, inducing net tension of the pipes. Parameters used for performance evaluation were the strain and stress values measured using adequate instrumentation. Results emerging from these experiments were compared with centrifuge tests, where an acceptable agreement was determined to exist between them.

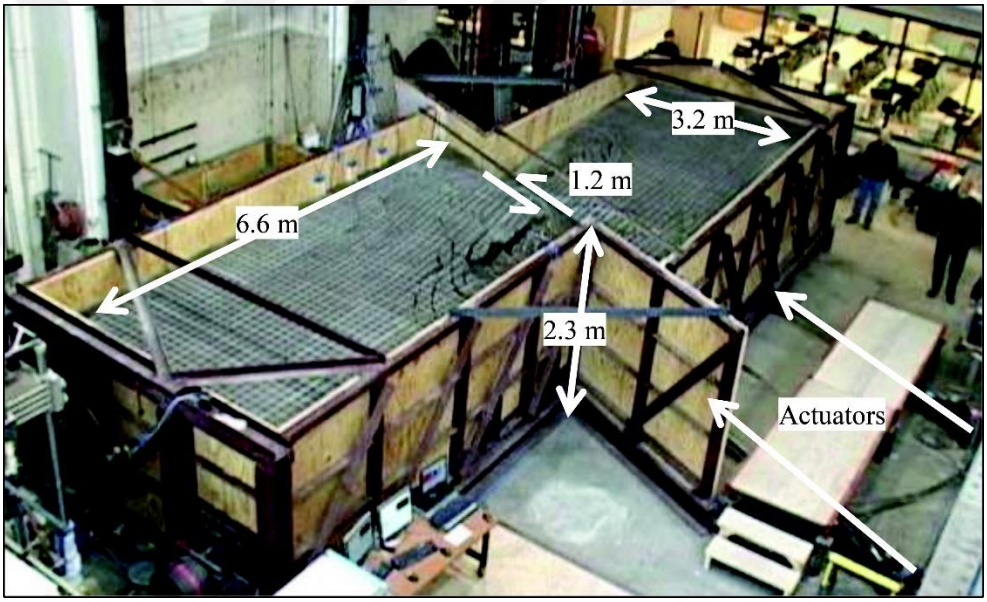

Figure 2.14. Split-box test setup developed by O'Rourke et al. (2009)

Oskouei et al., (2019) have performed a series of experimental studies to estimate the influence of burial depth as a design parameter on the seismic performance of buried steel pipes undergoing damage due to strike-slip fault actions. The surfaces representing the two constituting parts of the strike-slip fault (i.e., the footwall and the hanging wall parts) were simulated using two steel boxes with lengths equal to 1.5m and width and height fixed to 1.5m and 1.4m respectively. The total length of the pipe was 3.5m, with 25cm remaining outside of boxes at both ends. Figure 2.15 shows the assumed testing setup where a total of 10 different configurations have been tested. The box representing the footwall portion was

fixed by being attached to the floor, while the second box moved on rails. An actuator placed on the movable box ensured the application of a total displacement of 0.6m. LVDT devices were mounted to the pipe and box to measure the displacements, while the load cell and a total of 11 strain gauge devices were used to determine the generated stresses and strains respectively. Data obtained through these physical investigations showed that the majority of strains on the buried pipe induced by the fault action is localized over a distance equal to the half length of pipe portion on each side of the fault (i.e. 1.75/2= 0.875m). Experimental data indicated that the burial depth definitively influences the pipe performance, a non-linear increment of strains was determined for increasing burial depth values. Evaluation of the obtained experimental data eventually led to the conclusion that burying the steel as shallow and near to the surface as possible improved its performance under strike-slip fault actions. Two of the buried pipe configurations studied in these experiments (SM01 and SM02 cases) was also modeled within the scope of this thesis to validate the accuracy of the numerical modeling approach. Comparison between experimental and numerical results can be found under Chapter 4.

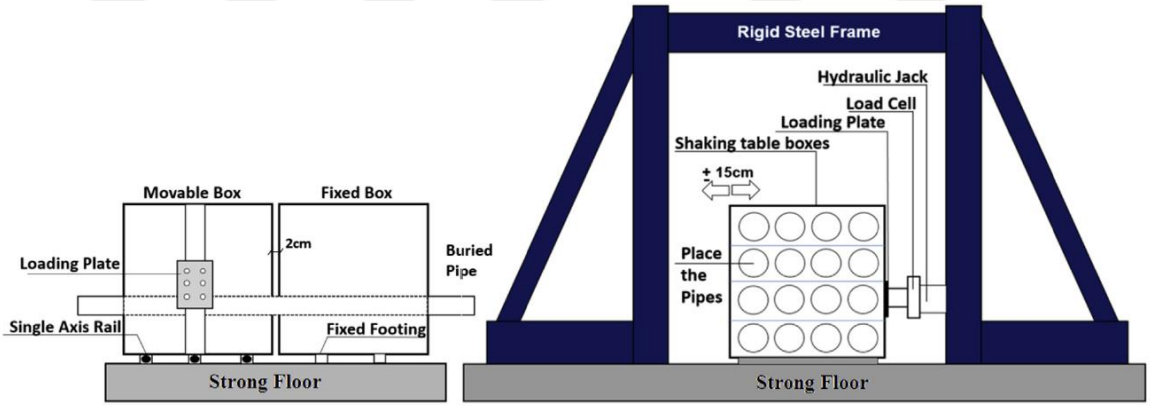

Figure 2.15. Experimental test setup developed by Oskouei et al. (2019)

An experimental and numerical modeling effort performed by Demirci et al. (2021) studied the response of buried HDPE and steel pipes under strike-slip fault actions. Experimental work performed on 4 different cases of HDPE pipes investigated the influence of design parameters including the burial depth, fault crossing angle, curved length, and the flexibility of the pipe defined in terms of relative soil pipe stiffness value. The experimental program initially incorporated the development of scaling laws based on past studies for various parameters (including soil size, pipe dimensions, burial depth, anchor length,

magnitude of fault movement, and the rate of fault offset) known to influence the response of the pipe. The developed physical testing setup consisted of two aluminum boxes with identical length equal to 1m and width and height equal to 1m and 0.75m respectively. Similar to previously mentioned experimental setups, one of the boxes was fixed to the ground with movement constrained in any direction while the other box could move laterally on constructed rails and bearings. An electric actuator connected to the moving box enabled the imposition of a controlled displacement up to a peak value of 0.3m. Figure 2.16 shows the sketch and the actual setup used in physical tests. The developed setup allowed the pipe to be placed at fault crossing angle values equal to 90^o and $\pm 75^o$. Various instruments capable of capturing and recording different types of data were utilized and attached to the components. Load cells were used to record the applied load, while strain gauges placed along the length of the HDPE pipe to capture the longitudinal strain data resulting from the application of the fault load. Resulting emerging from these extensive experimental and numerical studies revealed that the pipe should be placed as close as possible to the surface and minimizing the burial depth improves its seismic performance. Moreover, results indicate that the closer the fault intersection angle value gets to 90^o the better is its seismic performance, also pipes with thicker walls were determined to attain improved seismic performance under strike-slip fault loads. The T-1 test setup was also modeled within the scope of this study to validate the adopted numerical modeling approach. Comparisons and details are presented under Chapter 4.

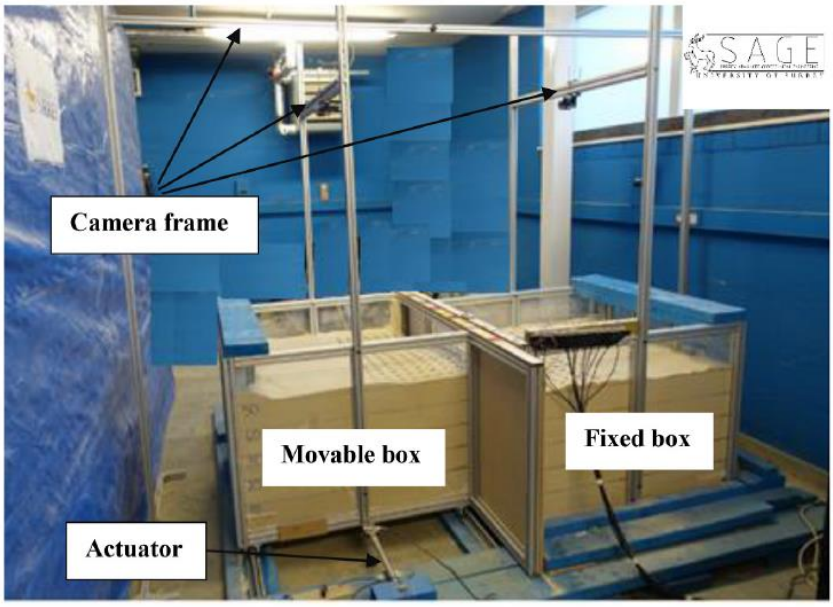

Figure 2.16. Experimental test setup developed by Demirci et al. (2021)

2.5. Mitigation of Seismic Damage for Buried Steel Pipes

This section covers literature survey on mitigation approaches commonly utilized for buried stee pipes subjected to a variety of loading conditions, placing particular emphasis on method used for the mitigation of seismic demands. Being crucial lifelines used for the transport of valuable and hazardous material contents such as fuel, oil, gas, water and etc. Buried steel pipes are important elements of a society with critical economic significance, however, these lifelines are extremely vulnerable to failures induced by seismic actions, in particular by those induced due to permanent ground deformations. Typically running over large areas inevitably leads to crossings of buried pipes with active faults. The demands forced to the pipe due to the rupture of these faults causes significant deformations that could endanger the safety and structural integrity of it. As a result, mitigation of these potentially dreadful effects occurring during faulting actions is of paramount interest and is among top design priorities for buried steel pipes.

According to Gantes and Melissianos (2016) the current practices typically used to mitigate seismic hazard on buried pipelines can be gathered and reviewed under three main groups. The first approach toward damage mitigation is to decrease the frictional effects among the pipe and backfill soil, which might be achieved through the use of various geosynthetic wraps or using low density such as EPS geofoam for backfilling instead of traditional soil or alternatively placing the pipe inside of a concrete culvert. Applying geosynthetics for pipeline damage mitigation (see Figure 2.17) aims at reducing the friction among the soil and pipe and increasing pipeline anchor length (Gantes and Bouckovalas, 2013). Placement of buried pipe within a pre-fabricated box concrete culvert (see Figure 2.18) is another option used to shield the pipe from the backfill soil and eliminate the friction in between. The second category of mitigation measures utilized for buried steel pipes is the strengthening of the pipe by selection a higher strength class for the pipe steel material, increasing its wall thickness or wrapping it with composites as will be discussed detailly in the following sections. Lastly, the buried pipes subjected to seismic actions might be protected via the use of flexible joints at locations close to the fault plane (Melissianos et al., 2016). Schematically illustrated in Figure 2.19 the main damage mitigation philosophy behind this approach is the absorption of ground deformation as rotational movements at these joints and ensure the pipe to remain unaffected. Another study published by Hasegawa

et al. (2014) proposed the introduction of a deformation (buckling) pattern prior to the application of fault load so as to supposedly gain some level of control over the location, shape and magnitude of damage.

The study performed within the scope of this thesis on the mitigation of seismic damages induced on buried steel pipes due to the rupture of strike-slip faults investigated the possibility of using, Fiber Reinforced Polymer (FRP) wraps, EPS geofoam blocks, controlled-low strength (CLSM) materials and Tensar Nr. 3 geogrid meshes. Existing research regarding the use of these material is scarce, with very few comprehensive studies. The following section presents literature review on each of these mitigation measures.

Figure 2.17. Wrapping of the pipeline with geosynthetic material to reduce soil-pipe friction (Gantes and Bouckovalas, 2013)

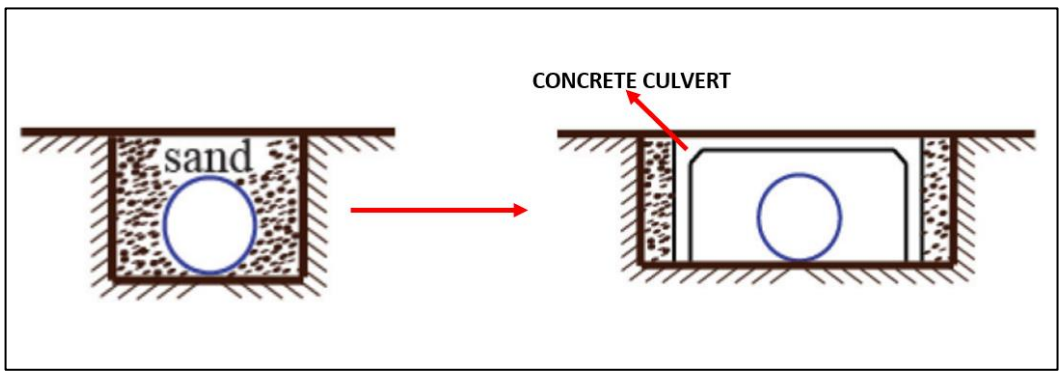

Figure 2.18. Pipeline protection using pre-fabricated concrete box culvert (Gantes and Melissianos, 2016)

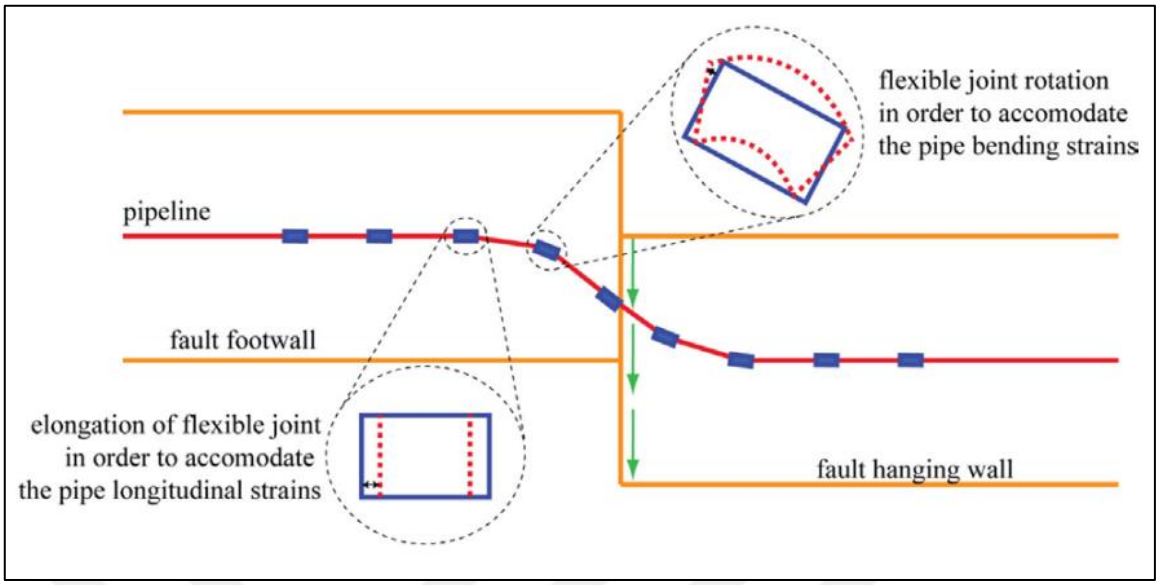

Figure 2.19. Illustration of pipeline mitigation approach incorporating the use of flexible joints (Gantes and Melissianos, 2016)

2.5.1. Use of FRP Composite Wraps for Seismic Damage Mitigation of Buried Pipes

Fiber reinforced polymer (FRP) is composite material consisting of a polymer matrix along with fiber reinforcement component of varying characteristics such carbon, glass, basalt or aramid (Holloway, 2010) with a diversified field of applications such as utilization in construction industry, to rehabilitate existing structures or used as a construction material on their own. FRP materials differ from traditionally utilized materials in construction industry including concrete, steel, wood, aluminum and etc. with respect to their material properties (Humphreys, 2003). FRP composites are anisotropic (non-uniform material properties that tend to be dominant along the direction of the applied load) while, steel and aluminum are isotropic materials (with same properties over all directions independent of the direction of the load). These composite materials consist of a polymer matrix-resins such as polyester, vinyl-ester and epoxy and etc. combined with fibers used to reinforce it (for instance carbon, glass and basalt fibers). The inclusion of these fibers improves the material and mechanical characteristics and results in increased stiffness and strength. The structural role these fibers serve to is resisting bearing the load and provide upgraded durability and stiffness along the direction they are oriented. Fibers utilized as components in FRP composites are made of amorphous and crystalline materials possessing varying material features, but those used for structural purposes typically include glass fiber, carbon fiber,

basalt fiber and aramid fiber are the materials of choice (Humphreys, 2003). Carbon, glass and basalt fiber-reinforced polymers (CFRP, GFRP and BFRP) have demonstrated themselves to be extremely efficient in regaining and promoting the better performance for a variety of civil engineering structures.

Evaluation of the possibility of using these beneficial properties of FRP composites for rehabilitation and/or damage mitigation of buried steel pipes subjected to permanent ground deformations is a relatively new field with few studies performed. Among the earliest attempts investigating the use of FRP wraps to strengthen and repair pipes is the study performed by Alexander and Ochoa (2010), the study presents research on the possibility of extending the procedures adopted for the repair of damaged onshore pipe to offshore pipes using carbon fiber FRP wraps adopting both numerical and experimental investigation techniques.

In their study Shouman and Taheri (2011) investigate the effect of using GFRP (Glass Fiber Reinforced Polymer) for pipe rehabilitation. The study does not directly consider the improvement of buried pipes subjected to faulting actions, but rather investigates the improvement rates of pipes subjected to loading effects such as internal pipeline pressure, axial force and bending. The study is conducted in two stages: the first stage involves the development of numerical analysis models using ABAQUS CAE, whereas, stage two involves laboratory study of pipeline sections. The details of the developed FE numerical model are shown in Figure 2.20, in these simulations the buried pipe is modelled using C3D8R solid elements, the loads acting on the pipe along with the boundary conditions are defined through a reference node assumed to exist on the center line of the pipe. A total eight layers of GFRP with fiber orientation accepted to be around the circumference of the pipeline was utilized in the. numerical analysis. Numerical analysis result indicate that the use of these remedies offers an extremely effective solution for the rehabilitation of pipelines damaged under the act of various loads.

A more recent study performed by Mokhtari and Nia (2015) investigates the effect of utilizing CFRP composite wraps to mitigate the seismic effects induced to buried steel pipes due strike-slip fault actions. Rigorous numerical models (see Figure 2.21) were developed using ABAQUS CAE software, where a model consisting of buried pipe and CFRP wrap

modeled as shell element and soil modeled as solid element was subjected to fault displacement load. Performance evaluation of the buried pipe was achieved via monitoring of the change in pre-defined performance criteria, define based on tensile and compressive strain limits, cross-sectional distortion of the pipe and rupture of FRP wrap. Analysis results obtained using these models clearly indicate that the use of CFRP wraps significantly improved the performance of the buried pipe subjected to strike-slip fault movement. An increment of as much as 560% in d_{cr} (critical fault displacement value) value was shown to be achievable with CFRP wrapping of the pipe.

Another study performed by Mokhtari and Nia (2016) investigated the utilization of same strategy to mitigate the deleterious effects induced on buried pipes by subsurface explosions. Findings of this study showed that utilization of a CFRP wrap with a suitable thickness has the ability to significantly enhance the performance of buried steel pipes subjected blast loads occurring atop of the pipe. Results indicate that, a decreased ranging between 30-64% is achievable with the implementation of CFRP wraps having a layer thickness of 4mm.

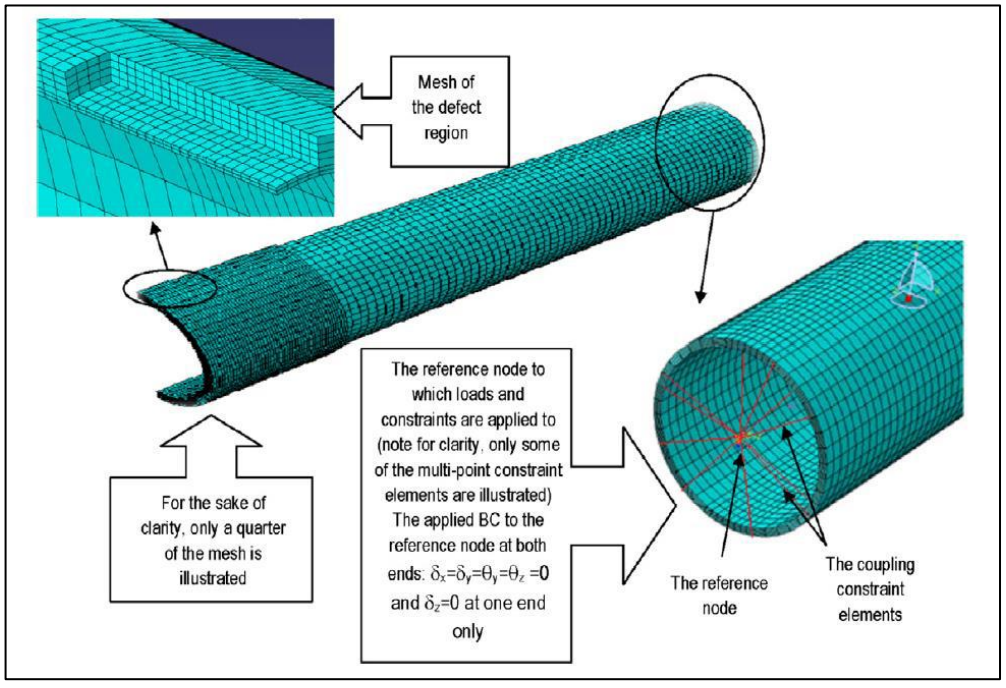

Figure 2.20. Numerical model proposed by Shouman and Taheri (2011)

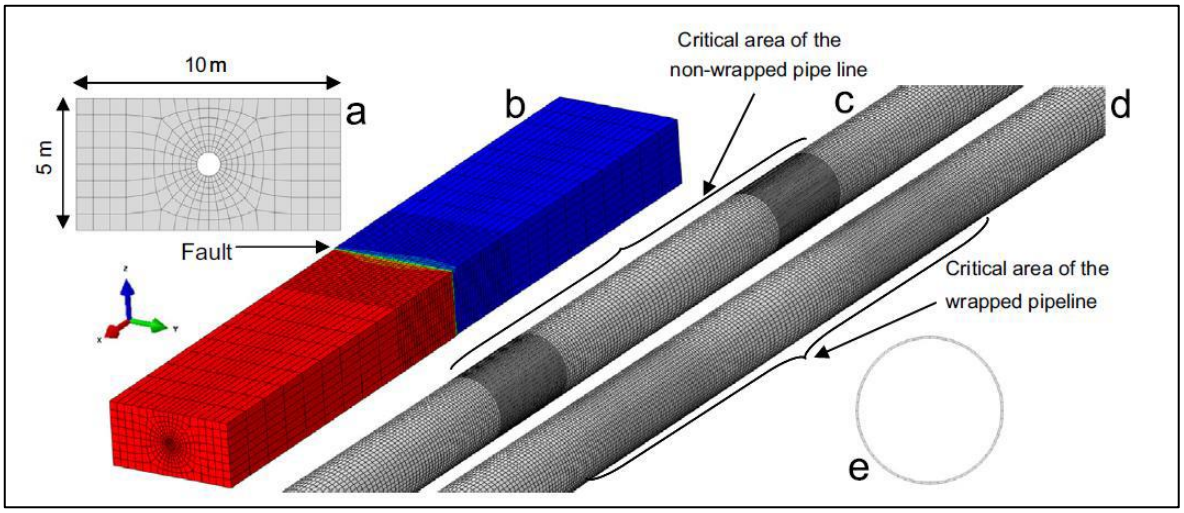

Figure 2.21. Numerical model configuration of Mokhtari and Nia (2015) incorporating CFRP wraps

2.5.2. Use of EPS Geofoam Blocks for Seismic Damage Mitigation of Buried Pipes

Shortly abbreviated as EPS, expanded polystyrene geofoam is cellular geosynthetic material with an ultra-light weight. Currently, this material has a wide range of applications both above and beneath the ground. Being a very lightweight material compared to granular soil traditionally used for backfilling and having the ability to remain undeformed and maintain its initial properties and dimensions when subjected to a great variety of loading conditions make this material to be a very suitable option for the protection of underground structures in particular (AbdelSalam et al., 2019). Owing to their extremely light weight and ability to sustain large deformation, EPS geofoam blocks can be employed for the construction of embankment and backfill systems. Under such case, the EPS inclusion provides reduced weight and hence decreased stresses and strains exerted onto the structures (Taechakumthorn and Rowe, 2013). Following the application of external loads an geofoam blocks will undergo compression and this behavior would in result reduce the static and dynamic load effects.

The use of EPS geofoam with the intention of reducing the demands exerted onto the buried steel pipelines has been investigated by researches either by means of laboratory testing methods or via the development of numerical FEA models using various software. Among the earliest attempts to investigate the effect of use of EPS geofoam blocks for buried

pipes is the study performed by Yoshikazi and Sakanoue (2003). In this study a series of experiments were performed on buried pipes backfilled with EPS geofoam and subjected to horizontal displacements induced by traffic loads. A reduction of as much as 60 percent in lateral pipeline forces was observed as and end result of their study.

Choo et al. (2007) have investigated the possibility of utilizing geofoam as a lightweight shielding system for buried pipes undergoing vertical offset due to faulting actions. Scaled models of buried pipes have been subjected to a series of experiments to evaluate the effectiveness of using EPS geofoam for demand mitigation caused by vertical offsetting caused by fault motions. The strategies utilized in this study successfully reduced the maximum transverse forces at the interface between soil and pipe up to 90 percent. This decrement in the lateral forces resulted in up to 60 percent reduction in bending strain acting on the pipe compared to conventional configuration without EPS blocks. Furthermore, the study showed that EPS also resulted in the decrement of axial strains in the pipe by as much as 30 percent.

Tafreshi et al. (2020) have performed full scale experiments of buried pipes embedded within EPS geofoam and geocell under heavy traffic loads. Obtained results indicate reduction in stresses and strain on top of the buried pipe. In another study, Meguid et al. (2017) have developed numerical models to simulate the response of buried culverts protected using EPS geofoam blocks and have showed that an improved performance is attainable through this mitigation technique. A study performed by Bartlett et al. (2011) investigated the potential of reducing the rupture and stresses due to vertical fault movement by means of developing a trench cover system using geofoam blocks. A series of laboratory, full scale tests as well as development of numerical FAE analysis models were developed for this purpose. The end results of the study indicate considerable reductions in load induced actions by use of EPS geofoam trench.

Research work available in the literature typically involve the damage mitigation of buried pipes subjected to traffic loads, while very few of them investigate the possibility of reducing the hazards associated with fault rupture and even fever to those related to strike-slip fault actions. The most notable work towards the assessment of the efficiency of using EPS geofoam blocks to mitigate strike-slip fault damages include the study of Rasouli and

Fatahi (2020) where advanced 3D numerical models as shown in Figure 2.22 are used to simulate the response of the pipe protected using EPS geofoam blocks atop and on both sides of the pipe under strike-slip induced permanent ground deformation. The study evaluated the effectiveness of using EPS geofoam in terms of performance limits including the axial tensile and compressive strains and cross-sectional deformation of the pipe, where a significant improvement in performance was noted.

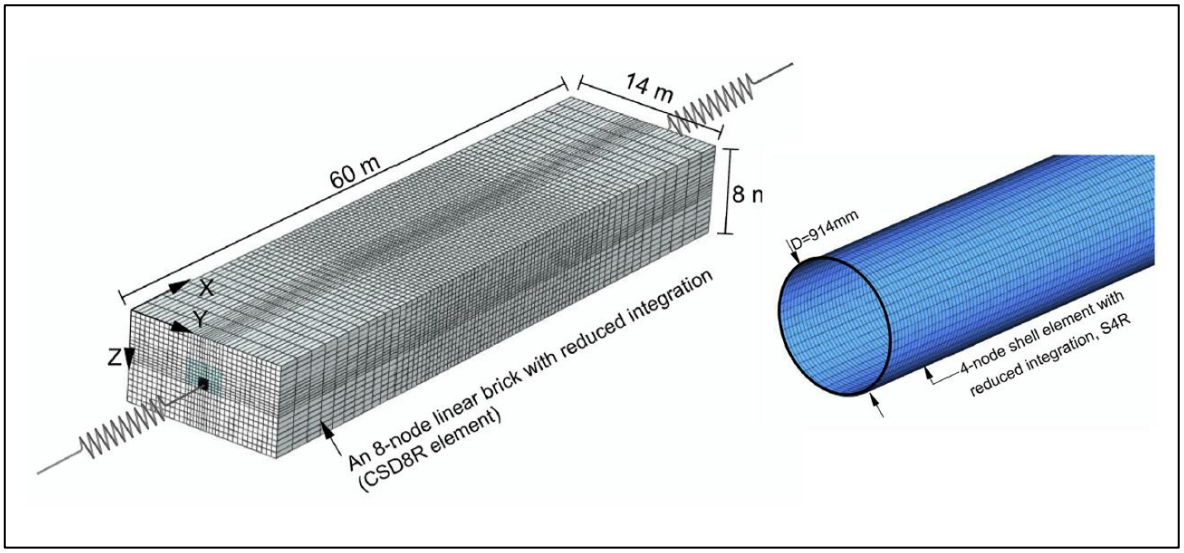

Figure 2.22. Numerical model configuration of Rasouli and Fatahi (2020) incorporating EPS geofoam

2.5.3. Use of CLSM for Seismic Damage Mitigation of Buried Pipes

Commonly described as a self-compacting flowable and cementitious material, a controlled-low strength material (CLSM) is a mixture usually incorporating water, cement, aggregates of various sizes, and commonly fly ash as its main ingredients (Do and Kim, 2016). Proportions of these ingredients in a particular CLSM mixture change greatly with respect to the intended purpose of use (Cheung et al, 2008). With the primary area of use as a backfill material CLSM is characterized with high levels of flowability associated with properties such as self-compaction and self-leveling. These materials have usually been considered as an alternative to traditional compacted soil applications, including the use for backfilling, utility cover up, rapid filling of voids and etc. These materials are used as a backfill for retaining structures, and trench applications. Conduits such as pipes, electrical and water utilities, telecommunication lines and so are rapidly covered up following their

installations using these mixtures (Ling et al., 2018). Excavated voids such as shafts of tunnels, basements, underground facilities are also filled swiftly utilizing these materials. There is a significant number of advantages of using flowable fill to substitute the traditional granular soil. One of the primary benefits of using this material is the reduction in cost required for implementation (due to the ability of this material to level and compact without the need for any external interventions), other benefits include ability to perform rapid construction, and the placement of material in confined spaces (Cheung et al., 2008). Moreover, possessing low compressive strength allows this material to be easily excavated when such need arises.

Literature review reveals numerous attempts and approaches developed to model the material behavior of CLSM in primarily in finite element analysis software. However, the number of studies involving the performance evaluation of buried steel pipes under the effect of faulting actions incorporating CLSM as a backfill material are scarce and possibly far from being complete and well understood. A study presented by Zhan and Rajani (1997) employed a 2D plane strain based numerical model to assess the behavior of buried pipes subjected to traffic live loads. The main goal of the study was to compare the obtained analysis results with data collected from field studies and asses the influence of various backfill type. The study assumed the steel pipe to behave as an elastic material, while a Drucker-Prager material model was assumed for CLSM and other backfill type. A jointed model was employed for soil-pipeline interaction. Obtained results indicated that when used as pipe bedding material CLSM resulted in reduced stresses.

In another study conducted by Masada and Sargand (2002) the effect of using CLSM as backfill for High Density Polyethylene pipe subjected to surcharge loads was investigated through a series of experiments and subsequent development of FEA models. Obtained results indicated that the use of CLSM as a substitute for granular soil reduced pipeline deflections and stresses and improves the overall performance. However, one major drawback of the proposed model is the assumption that the pipe and CLSM are fully bonded and do not undergo separation under the applied load, an assumption that would not be realistic for pipes subjected to lateral displacements induced by faulting actions.

Dezfooli et al. (2015) have performed a laboratory and FEA study to determine the performance of buried steel pipes embedded within three different backfill type. The existing soil around the pipeline was introduced within the FEA model via the adoption of Mohr-Coulomb material model, whereas the CLSM was assumed to behave as concrete, hence was modeled by means of using the damaged plasticity approach available within software package typically utilized for concrete option. Equivalent thermal loading option was chosen as the load pattern for the investigated cases. End results indicated that the developed model results are in good agreement with laboratory data, therefore, the proposed modeling approached might be utilized for such cases.

A more recent study presented by Abdel-Rahman et al. (2020) investigated the behavior of buried steel pipes filled with CLSM exposed to the effects of traffic loads. In the developed 2D FEA model both the native soil and the CLSM are modeled via the use of Mohr-Coulomb constitutive material model. A penalty friction contact was assumed to exist among the pipe and the CLSM. In particular, the response of concrete and flexible plastic (PVC) pipes was investigated in terms of developed vertical, horizontal stresses and bending moments. Results indicate that the use of CLSM as a substitute for granular soils improves the overall performance of pipes under traffic loads.

A study published by Somboonyanon and Halmen (2021) studied the performance of steel pipes backfilled with CLSM under the demands exerted by the rupture of a reverse-fault. The FEA model was developed through ABAQUS CAE, where, similar to the approach assumed in this thesis, soil and CLSM was modelled as solid element, whereas, the buried steel pipe was represented via shell elements. The developed FEA model in presented in Figure 2.23. The soil and CLSM around the pipe are modeled via the Mohr-Coulomb model, whereas a bilinear stress-strain relationship with isotropic hardening was assumed for the steel pipe. A penalty friction was assumed as the contact algorithm among the pipe and CLSM. The study investigated the influence of parameters and factors such as trench continuity, variation of friction coefficient, backfill material properties and D/t ratio. Obtained results indicated that it is possible to attain improved pipeline performance under seismic load effects by utilizing CLSM as pipe backfill material.

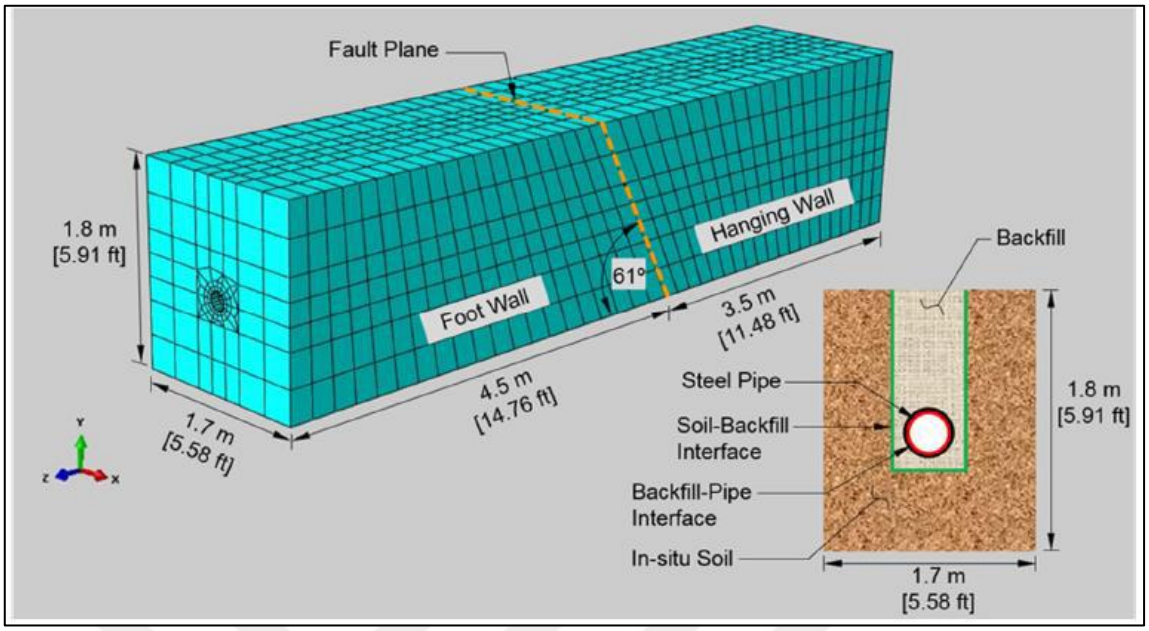

Figure 2.23. Numerical model configuration of Somboonyanon and Halmen (2021) incorporating CLSM

2.5.4. Use of Geogrid Layers for Seismic Damage Mitigation of Buried Pipes

Defined as a geosynthetic materials, geogrids are classified as polymeric materials primarily used as reinforcement for soils, retaining walls, and other highway applications, providing a reduced pavement thickness need. The incorporation of geogrid layers in the soil results in a new composite material possessing improved properties and performance under the applied loads, compared with traditional un-reinforced soil (Adams et al., 2015). Produced in form of grids, the shape of this materials varies anywhere between knitted and/or woven grids, non-woven and also composite fabrics. Materials typically utilized for geogrid production include polyester and polyethylene (Puppala et al., 2020). The main load resisting ability of geogrid reinforcements relays on a tension mechanism which develops as the soil layer incorporating geogrid is subjected to tension which eventually leads to a bonding and interlock with the aggregates of native soil (Marto et al., 2013). The properties of a geogrid strongly depend on the characteristic of constituting materials such as geometric configuration and physical properties. The mechanical behavior of the geogrid reinforcement is tightly related to the geometry of the grid, including the aperture size, open are percentage, and layer thickness (Barqawi et al., 2021). The aperture size for the geogrid should be sufficiently large to ensure the bonding and interlock of geogrid with the aggregates of native

soil. The existence of this interlock among the geogrid and the native soil ensures the composite behavior necessary to achieve the desired soil stability. These materials have been used for decades to improve the properties of soils.

Several studies (Xu et al., 2019; Bathurst and Ezzein, 2017; Tran et al., 2015; Zhou et al., 2012; Ferellec and McDowell, 2012; Pinho et al., 2015) have investigated the relation between the geogrid layers and native soil under applied static loads and showed the use of geogrid reinforcement greatly enhanced the load-bearing capacity of the soil. Experimental research (Elshesheny et al., 2019; El Naggar et al., 2015; Ahmed et al., 2015) on the performance of buried flexible pipes incorporating the use of geogrid reinforcement to mitigate the effects of cyclic loads have revealed that geogrid reinforcement improved the performance of these lifelines via distributing the stresses and providing additional lateral support. In terms of mitigating the effect of permanent ground deformations induced by faulting actions, proposed physical model tests and developed conceptual elasto-plastic models by various study groups (Shewbridge and Sitar, 1996; Seed et al., 2003; Mahrjardi and Tafreshi, 2008; Ballard and Jewell, 2013) indicate that soils reinforced with geogrids are effective in "spreading out" the imposed fault displacement, hence, leading to the formation of a wider shear zone which in turn reduces the horizontal strains associated with fault actions. This mechanism of action presents the idea behind this study which aims at utilizing geogrid layers to mitigate the seismic demands of buried pipes subjected to strike-slip actions.

Early attempts (Yogarajah and Yeo, 1994; Shuwang et al., 1998;, Perkins and Edens, 2003; Sugimoto and Alagiyawanna, 2003) to develop approaches for the design of geogrid reinforced soil rely solely on the equilibrium-based limit states. Despite providing insight enough for preliminary design purposes, yet these methods lack accuracy on the failure mechanisms dominating the behavior of such systems as well are incapable of providing information on displacements and strains, modes that tend to control the performance of the system specifically at large displacement problems. Recent studies, however have made use of powerful software to realistically model the mechanical behavior of the geogrid material, considering its material and geometric properties, in addition, the use of these software have made it possible to model the interaction among the geogrid and soil surfaces. One of the most important and complete contributions in this field is the study of Hussein and Meguid

(2016). This study proposed a 3D FE numerical model for the response analysis of geogrid layers subjected to a variety of loading conditions. The study consists of two phases, where phase one focused on the development of geogrid numerical models fully considering the geometry of the layers, including the modeling of apertures and shifts in geometry at junction points. The developed models were analyzed under tensile pullout loading conditions and compared to existing numerical and experimental data. Obtained results indicate a good overall agreement. The second phase of the study a prismatic subgrade soil model (see Figure 2.24) incorporating geogrid layers was developed and analyzed under surcharge loading. The outcomes of this study indicate that this approach of geogrid modeling is the most suitable one in order to ensure realistic behavior of geogrid material, noting that the use of planer elements usually require a significant reduction in the actual thickness of geogrid layer to achieve acceptable results

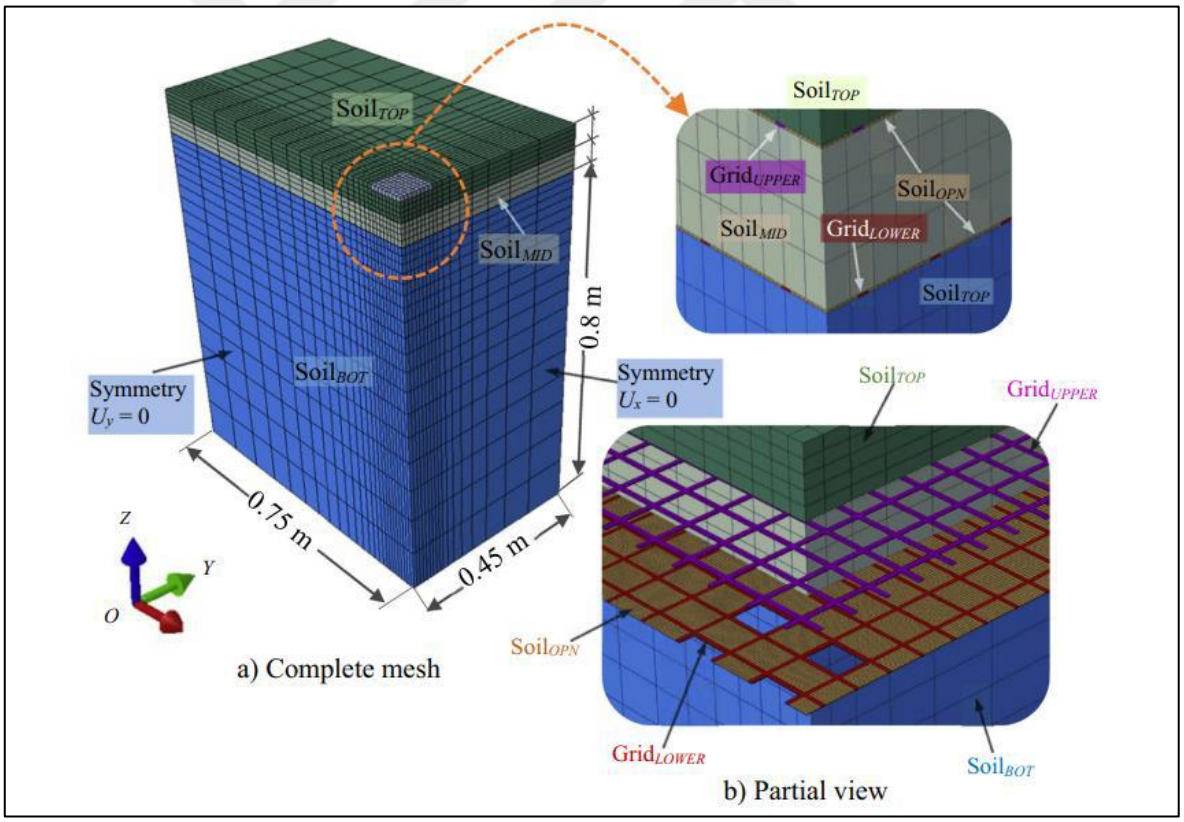

Figure 2.24. Numerical model configuration of Hussein and Meguid (2016) incorporating geogrid layers in a subgrade soil prism

2.6. Strain Based Design of Buried Steel Pipes

Traditionally the engineering evaluation and design of steel pipes buried underneath the earth subjected to faulting actions has been performed using a stress-based approach which involves the consideration of various stress limit states. Despite being widely accepted and used this method of design possess significant drawbacks. Designing a buried pipe only by taking into account the applied forces and the subsequent stresses allows an accurate pipeline behavior description only up to state of maximum loading, however, for cases where deformations (displacement) are of prominence and dominate the response-such as the case of permanent ground deformations caused by faulting actions-these methods tend to result in inaccurate and often non-economic design solutions. Limiting the stress criteria while designing a pipeline may be considered appropriate only for a steel material possessing a clear point of yield and strength. But the stresses on a pipe can exceed the pre-determined stress limit under some extreme loading conditions (such as earthquakes, landslides and etc.) and hence the stress-based design criteria are no longer useful (Crapps et al., 2018). Being so, the introduction and use of pipeline strain-based design has gained a well-deserved use and popularity specifically for the afro-mentioned deformation-controlled cases.

In the simplest terms the strain-based design of pipes incorporates the evaluation of strain demand on the pipe and comparison of it with the strain capacity of the same pipe. The strain-based design allows the extension and improvement of stress-based design methods by making use of the testatum property of steel material to deform beyond elastic limits but at the same time remain stable (Panico et al., 2017). An illustration of difference among stress and strain-based design approaches is presented in Figure 2.25. In essence the strain-based design of pipelines relies of the principles of limit state design which basically refers to circumstances where the pipeline can no longer meet the pre-described design and service requirements. The main philosophy of limit state design approach incorporated within stress-based design includes the following principles (Wang et al., 2010):

- Determination of all related limit states applicable for pipeline design.
- Designation of these limit states into ultimate and service limit states, which is done by defining the results of the violation of each limit state considered.
- Establishment of limit state criteria.

- Development of a design and performance measures provide a safe, effective and economic solution.

The performance criteria of limit typically utilized in pipeline design are:

- Maximum tensile strain limit state.
- Onset of local buckling limit state.
- Pipeline cross-sectional distortion limit state.
- Burst of pipe cause by extreme internal pipeline pressure limit state.

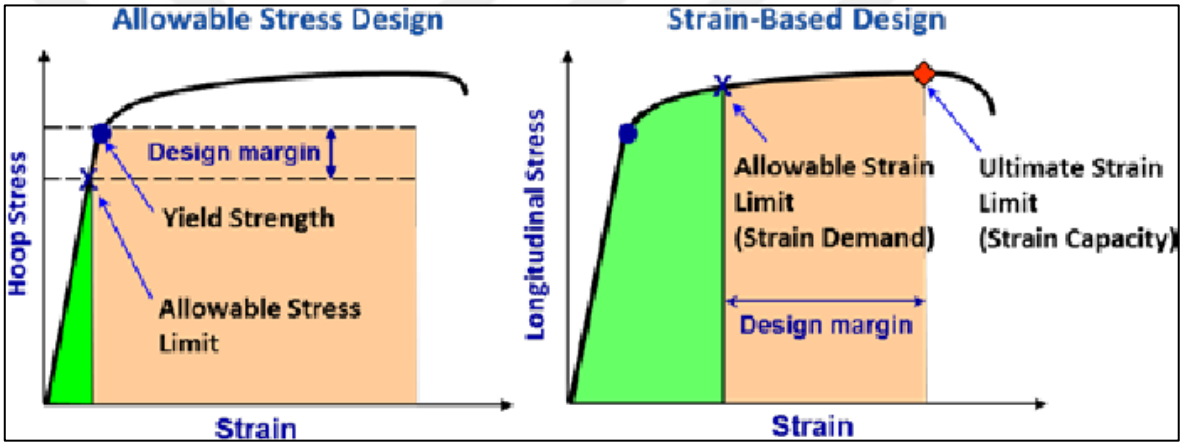

Figure 2.25. Illustration of difference between stress and strain-based design approaches (Panico et al., 2017)

2.7. Computer Software Used for Numerical Analysis of Buried Steel Pipes

Several computer software capable of performing finite element analysis have been adopted for the development of numerical models of buried steel pipes exposed to faulting actions. Some of this software have limited sophistication and therefore cannot realistically capture the pipeline behavior, whereas some other allow the development of rigorous and complex models and yield accurate results. Following sections describe some of the most commonly utilized computation tools for pipeline analysis.

2.7.1. PLE Software

This software is a tool primarily developed to aid the pipeline engineer during the design process to meet certain requirements typically enforced by pipeline codes and regulations. The PLE software is useful for the analysis of both on and offshore pipe systems. PLE makes use of finite element modelling approach to model and analyze pipes subjected to various loading conditions. The pipeline is modelled using beam elements, whereas, the soil surrounding it and the interaction between them are modeled using equivalent soil springs. A typical model developed using this software is given in Figure 2.26. Individual beam elements are analyzed using FE approach and outputs are obtained in terms of stresses, strains, deformations, displacements and etc. In addition to stress-based design the software is also capable of strain-based design. Despite being specifically developed for pipeline analysis, the PLE software has significant drawbacks such as it is not capable of modelling the pipeline behavior beyond the onset of buckling limit state and does not support dynamic analysis.

Figure 2.26. Pipeline beam model supported with linear springs modeled using PLE software (PLE4Win, 2003)

2.7.2. FLAC3D Software

The FLAC3D software is a tool developed for advance numerical modelling and geotechnical analysis of structures embedded within soil and other complex geotechnical models. The software utilizes an exact finite difference formulation and solution to approach the problem and provides a continuum solution and analysis medium. The program is capable of modelling complex scenarios such as cases of large deformations, non-linear behavior, multi-stage loading and analysis cases and etc. Despite being a very powerful tool the FLAC3D software in not a very user-friendly tool when it comes to the modelling of pipeline problems.

2.7.3. PLAXIS 3D Software

PLAXIS 3D is finite element software specifically developed for the analysis of complex geotechnical problems. The program allows the modelling of the soil and structure systems and is capable of modelling the interaction among them by making use of the Mohr-Coulomb soil model. However, the software is not capable of providing realistic outcomes when the system is subjected to large displacements and cannot model the system behavior beyond the elastic limit states.

2.7.4. ABAQUS CAE Software

Defined as a general-purpose finite element analysis software ABAQUS CAE is a tool which allows the modelling and analysis of a very wide range of problems from civil to mechanical, biomedical and other fields of engineering. Equipped with a very rich library of elements and material models the software allows the modelling of virtually any type of geometry regardless of its level of complexity. The software's in-built material models allow the simulation of various engineering materials such as soil materials, composites, metals, rubber, concrete, polymers and etc. Simulation of complex engineering phenomena such as heat transfer, soil mechanics, mass diffusion are possible via the use of ABAQUS CAE. Both linear and non-linear problems are solved with high efficiency and accuracy via the adoption of various iterative solution techniques. The automatic adjustment of load increment values and continuous regulation of convergence tolerances by the software leads to a rather realistic simulation and solution. Possibility of using static and dynamic, implicit and explicit methods also provides the user with a wide spectrum of choices to approach the problem in hand. A typical model of soil-pipeline system modelled using ABAQUS CAE is shown in Figure 2.27. ABAQUS CAE was the software of choice for the study performed within the scope of this dissertation for its obvious superiorities over other software.

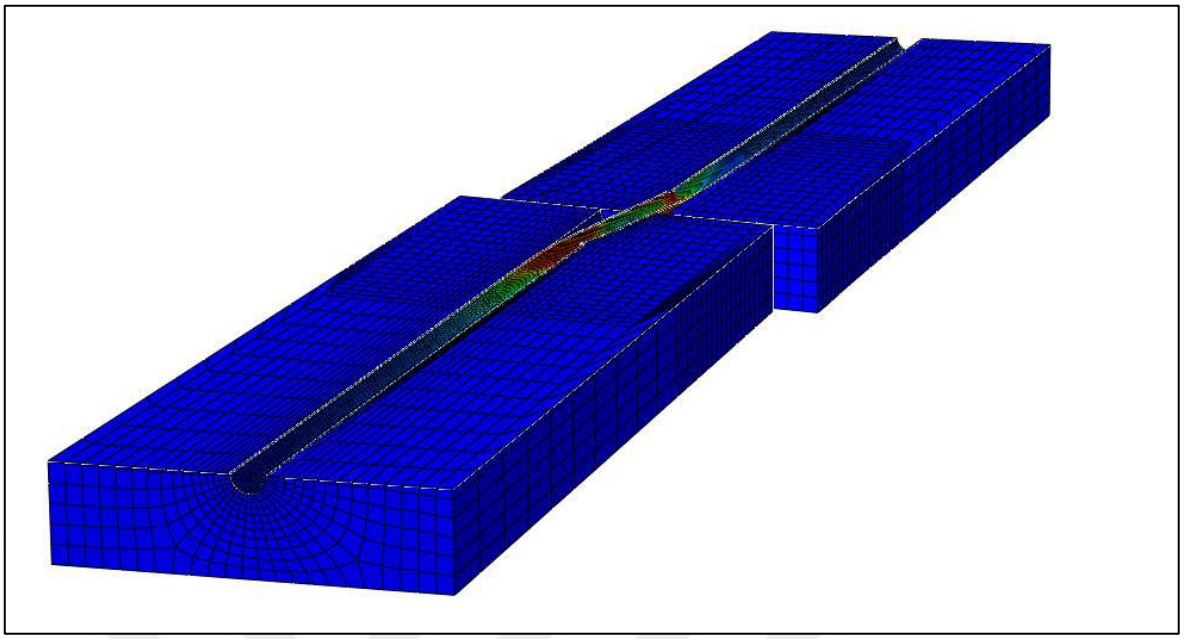

Figure 2.27. FE Model of buried pipeline developed using ABAQUS CAE

3. NUMERICAL MODELING

3.1. Introduction

This chapter presents information regarding the steps followed and assumptions made during the development of numerical models employed to simulate the behavior of buried steel pipes subjected to strike-slip fault actions. The general-purpose finite element software ABAQUS CAE was utilized for modelling the soil-pipe configuration with an exact representation of soil-pipe interaction. Figures 3.1 and 3.2 depict the plan and 3D views of one of the developed numerical models, showing the direction of the pipeline axis and the vector of the tectonic fault plane form an intersection angle denoted as β. The values that this angle may take depend on the motion of the soil blocks relative to each other and it can be either a positive or a negative value. In case when β attains positive values, tensile strains are imposed onto the pipe, whereas, when the β values are negative than compressive strains become dominant. Within the scope of this study the influence of the variation of this angle value was investigated for $\beta = 10^{o}, 15^{o}$ and 30^{o} and so as to evaluate the effects of the variation of this design parameter.

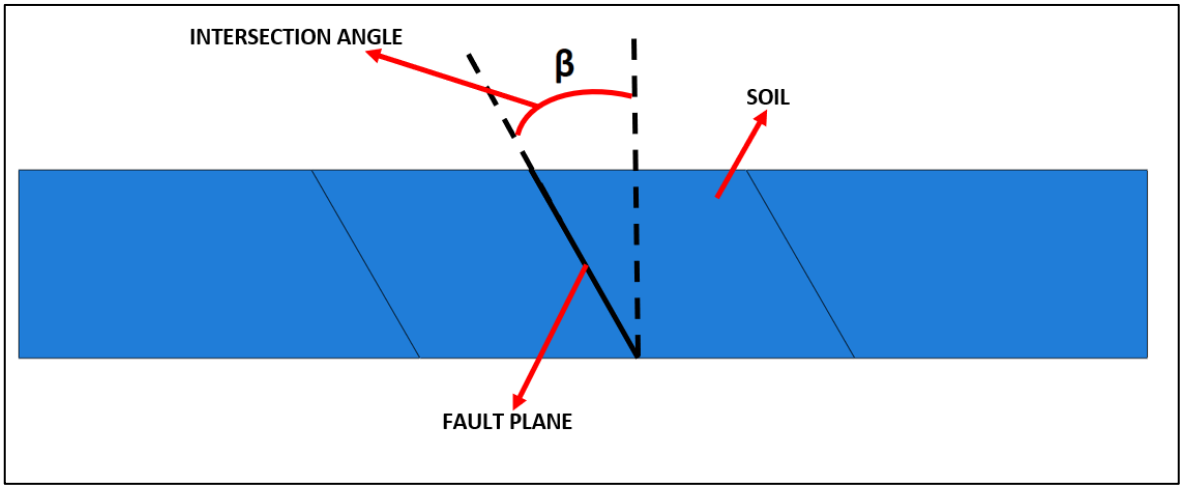

Figure 3.1. Schematic plan view of the developed numerical FE model

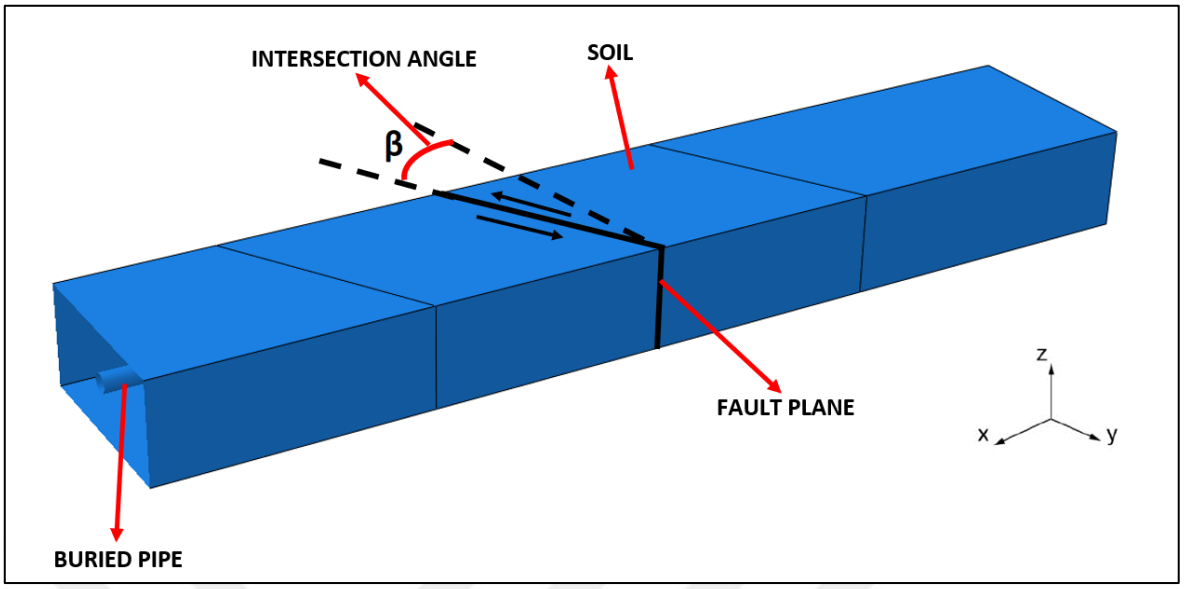

Figure 3.2. Schematic render view of the developed FE model

The path followed to construct the numerical models relies on the well-established concepts proposed by earlier research (Vazouras et al., 2010, 2015 and Sarvanis et al., 2017). These studies involved parametric investigations regarding the optimum model dimension, material properties (friction values), interaction properties and etc., hence, this dissertation did not attempt to repeat the same parametric studies but instead adopted the determined optimum values and accepted them to be viable.

Detailed descriptions of the developed finite element model are provided in Section 3.2, but in summary, the numerical model employed for analysis consisted of two soil blocks divided by a discontinuity plane representing the fault trace modelled using solid elements and the buried pipe modelled using shell elements. The ABAQUS CAE element library was utilized for the selection of these element types. The interaction between soil and the pipe was simulated via a surface-to-surface contact algorithm which took into account the friction and slip among the two elements. Meshing properties utilized in these models assumed a finer mesh size at the vicinity of fault plane for both the pipe and soil blocks and a coarser size at location far from the fault. The reason behind this is the fact that the majority of pipe deformations will occur near the fault trace, hence, adopting such a meshing pattern will significantly reduce the required computational power and effort. The analysis was carried out in two steps: initially, the actions imposed by the soil cover were analyzed under gravity load case, then, in the second step the fault actions was imposed as an external incremental

displacement load onto the nodes of one of the soil blocks. In addition to the investigation of the effect of varying fault angle values and pipeline wall thickness, mitigation of seismic demands was investigated via the use of four mitigation strategies. Namely, cases involving the use of three FRP wrap types, EPS geofoam blocks, controlled-low strength material casing and Tensar Nr. 3 Geogrid meshes were studied within the scope of this work. Similar models but this time incorporating the materials used for mitigation were developed and analyzed. Details of these models are presented under Section 3.3 of this chapter. For all cases studied in this thesis results have been obtained in terms of strains developing on the pipe and performance criteria (limit states) defined in Section 3.4 have been employed to assess the performance of the investigated case.

3.2. Numerical Finite Element Modeling Approach

3.2.1. General Information

In this thesis the behavior of buried steel pipes under the action of strike-slip fault movement was analyzed by developing numerical models of the problem using ABAQUS CAE software. As illustrated in Figures 3.3 and 3.4 the numerical models consist of a pipe buried inside of a soil prism. The fault trace crossed by the pipe was modeled as a discontinuity plane of 30mm width and was assumed to divide the soil prism into to equal soil blocks. Analysis was carried out for different values of fault intersection angle, for instance, Figure 3.3 illustrates the case of pipe axis being perpendicular to the fault plane vector (i.e., $\beta = 0^o$), whereas Figure 3.5 depicts the typical configuration of the numerical models for values of $\beta \neq 0^o$. The element types used for the modelling of soil and the embedded pipe were taken from the library of existing elements of ABAQUS CAE. The so called S4R (four-node reduced integration shell elements with hour-glass control) were utilized to model the cylindrical steel pipe, whereas C3D8R (eight-node reduced integration brick elements with hour-glass control) were used to model the soil blocks. Illustrated in Figure in 3.6, the S4R elements are finite-strain shell elements able to capture the finite membrane strain formations and large nodal rotations, hence, are generically used for the modelling of problems involving large strain analysis. On the other hand, the C3D8R elements also shown in Figure 3.6 are solid (brick) elements specifically designed for the

modelling and simulation of cases involving large stress/strain conditions and are known to yield accurate and realistic solutions. The naming convention utilized in ABAQUS CAE is shown in Figure 3.7.

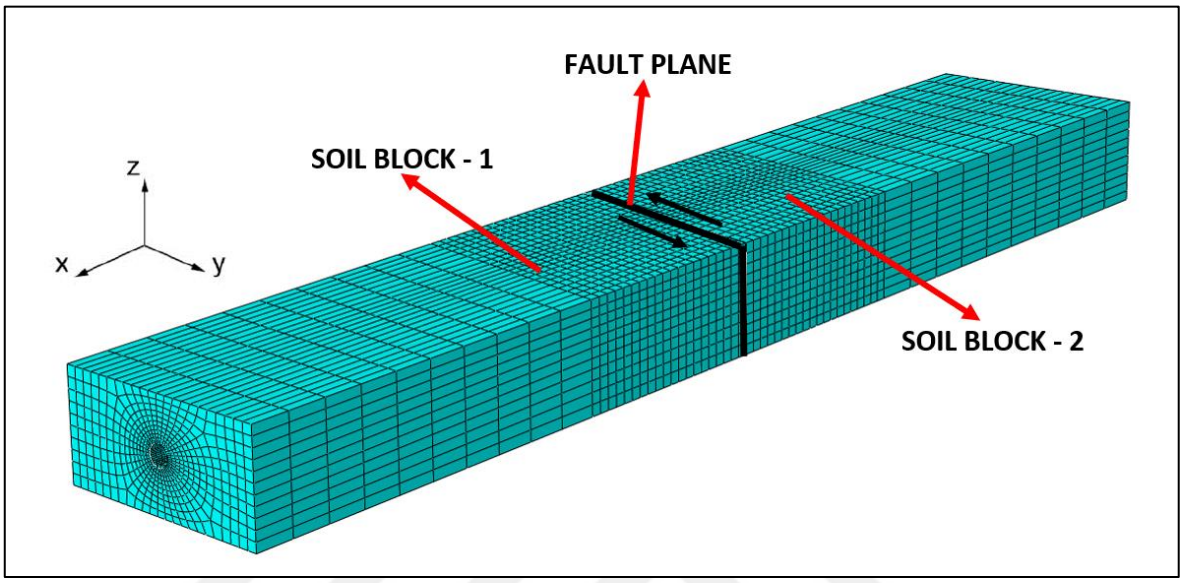

Figure 3.3. Model configuration for analysis cases where β = 0º

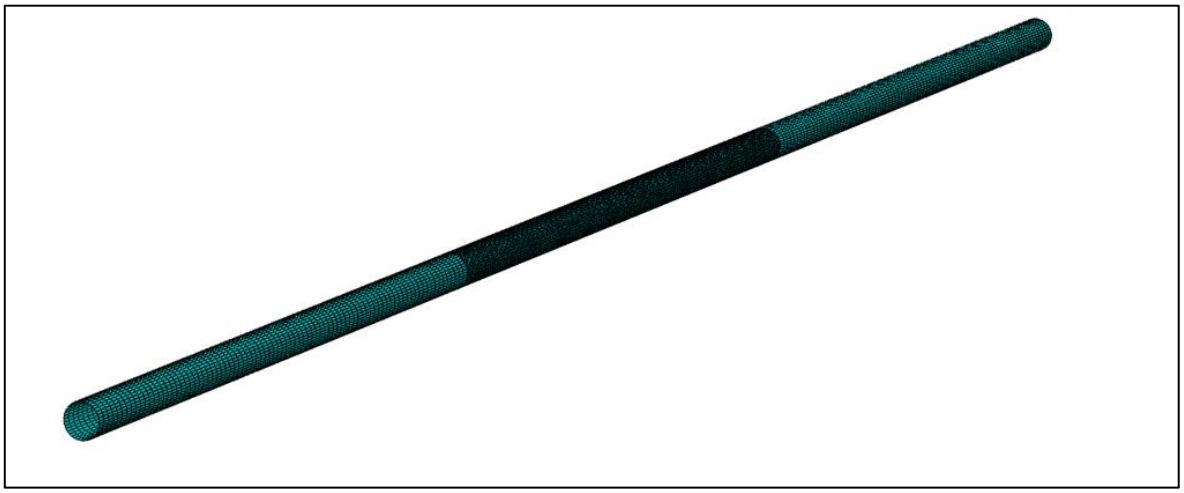

Figure 3.4. Numerical model of the buried pipe (β = 0º)

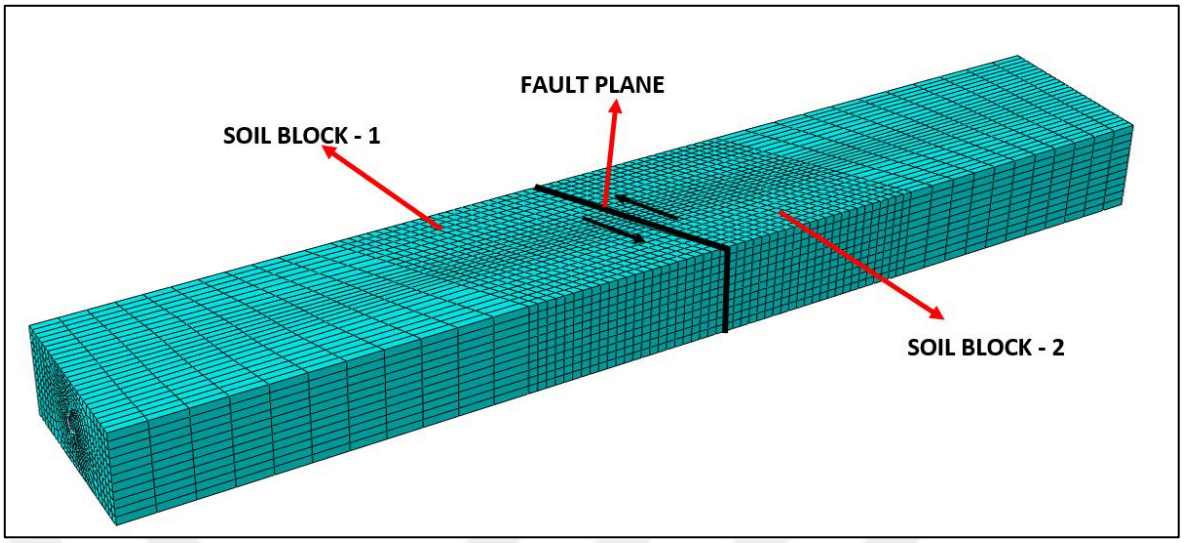

Figure 3.5. Model configuration for analysis cases where $\beta \neq 0^o$

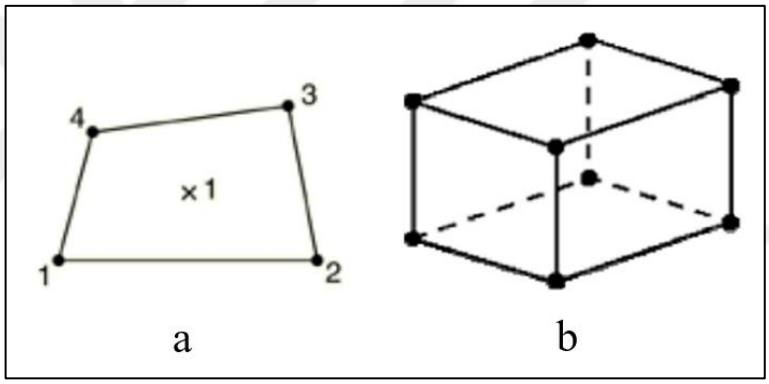

Figure 3.6. ABAQUS CAE illustration of finite elements used in analysis: a) S4R shell element, b) C3D8R solid element (Abaqus CAE, 2020)

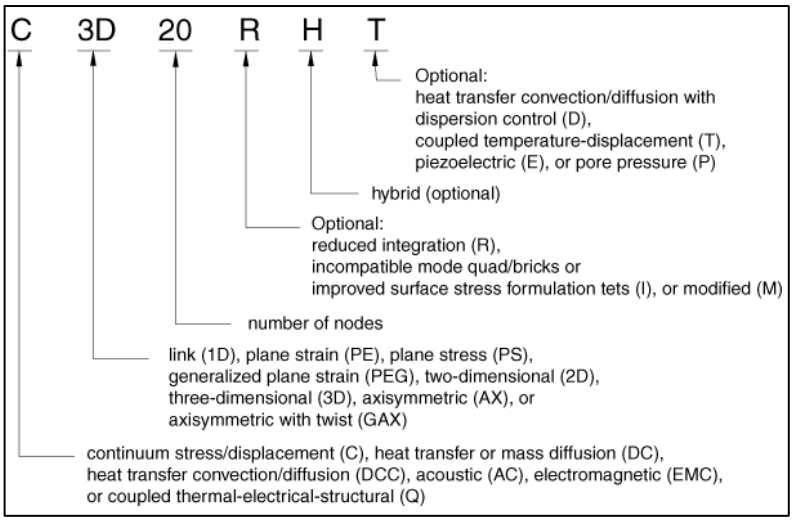

Figure 3.7. Element naming convention of ABAQUS CAE (2020)

3.2.2. Boundary and Loading Conditions

The developed numerical models consist of three parts in total assembled together to form the entire simulation system. The first part of the system is the cylindrical pipe modeled as a continuous shell element. The soil cover is modeled as prism constituting of two equal parts divided by the strike-slip fault plane represented in the model as a discontinuity plane of thickness equal to 30mm. Boundary conditions shown in Figure 3.8 were enforced onto the models so as to achieve a realistic behavior and capture the evolution of strains under the applied fault load. In this context, the bottom surfaces of soil blocks were restrained to move horizontally as well as vertically, the side surfaces were restrained against horizontal movement along with the end nodes of the pipe. The top surface of the soil was set free to move in all directions with no boundary conditions applied on this surface.

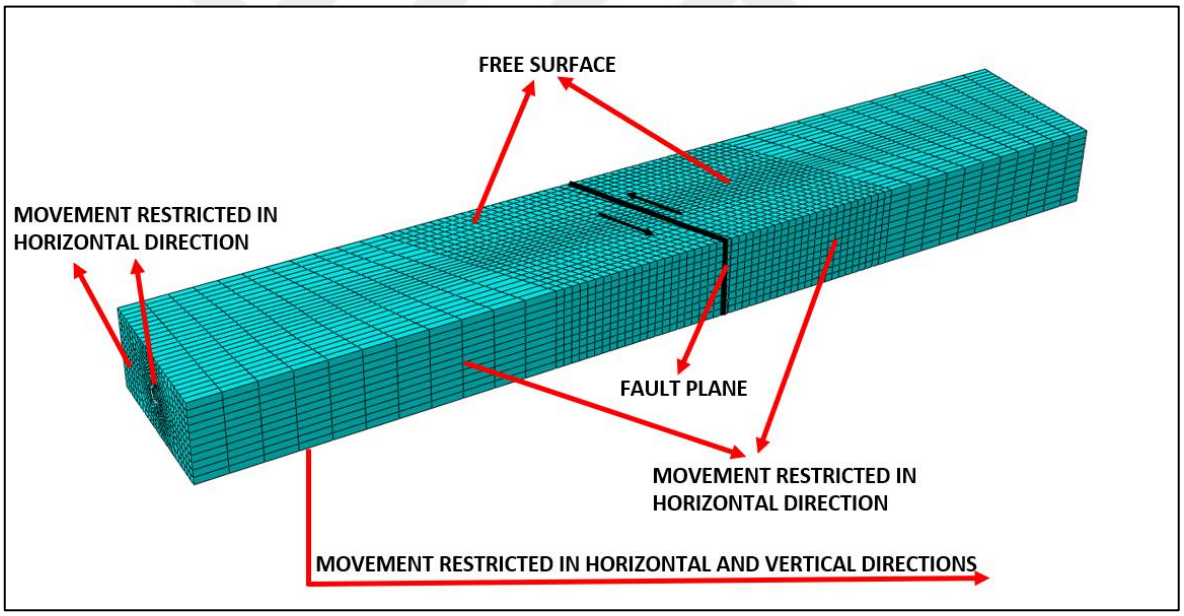

Figure 3.8. Boundary condition assumed in the analysis model

The analysis of the created model involved two steps conducted subsequently. The first stage of analysis involved the gravity load case where the effect of soil load acting on the pipe was analyzed, in this case both soil blocks assumed the boundary condition depicted in Figure 3.8. The “static general” analysis pattern was utilized for this step. The cases investigated in this thesis do not include the effect of internal pipe pressure (i.e. non-pressurized case), therefore, no such loading step exists. Once the analysis for the first step is completed and the effects are calculated, step two which involves the application of the

fault movement initiates. As seen in Figures 3.9 and 3.10 the fault load is applied as a displacement load on the outer nodes of the second soil block by following a displacement-controlled scheme. The fault displacement range considered in this study is 0-4m with intermediate increments of 10mm/s. The imposed fault loading was not rate-dependent and ignored the fault slip-rate, experimental work conducted by Turner (2004) and Jung et al. (2013) showed that the impact of the rate of fault offset is negligible for buried steel pipes, where only minor differences were determined for slip rates changing between 0.03mm/s and 25mm/s (Turner, 2004). Hence, a relatively slow loading scheme was adopted to accurately capture the evolution of damage on the buried pipes. In order to allow movement due to the applied load, the boundary condition defined in step 1 are suppressed for the second soil block at the beginning of this analysis step. The "Dynamic Implicit" method of analysis was employed for this step. This method is useful in the sense of making automatic adjustments in loading increments and iteration steps so as to achieve the required convergence value. Due to the highly non-linear nature of the problem implementing this type of analysis over the "static general" approach which could have also been used for this step allowed a faster solution algorithm with no need for manual adjustments and other intermediate steps. For all buried steel pipe cases investigated within the scope of this thesis the internal pipeline pressure was assumed to be zero, hence, no analysis step was incorporated to account for this load type.

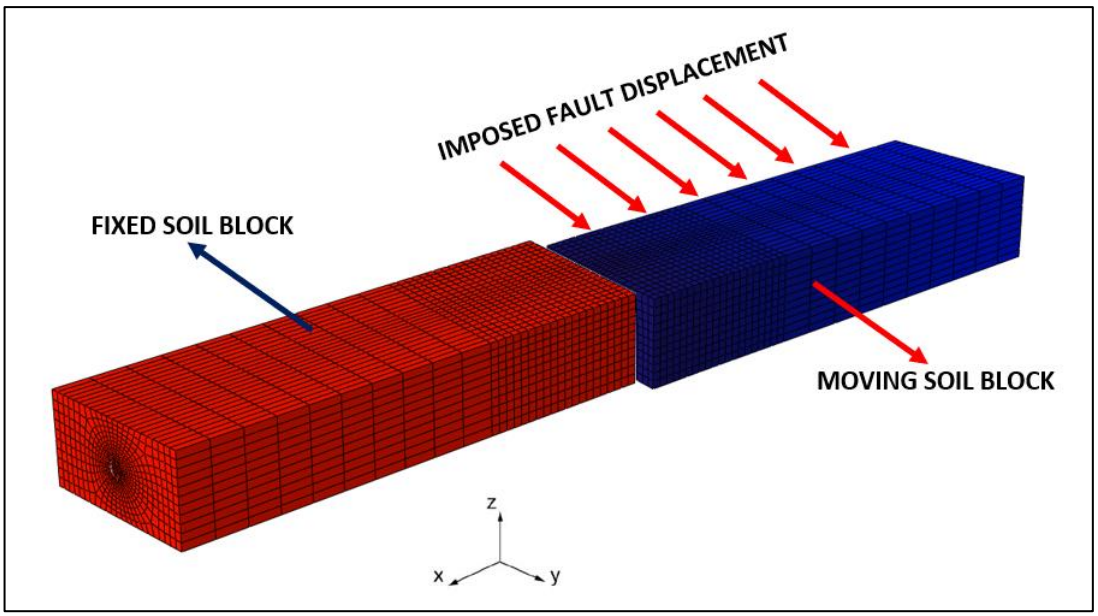

Figure 3.9. Implementation of strike-slip fault movement as displacement load on the nodes of moving soil block

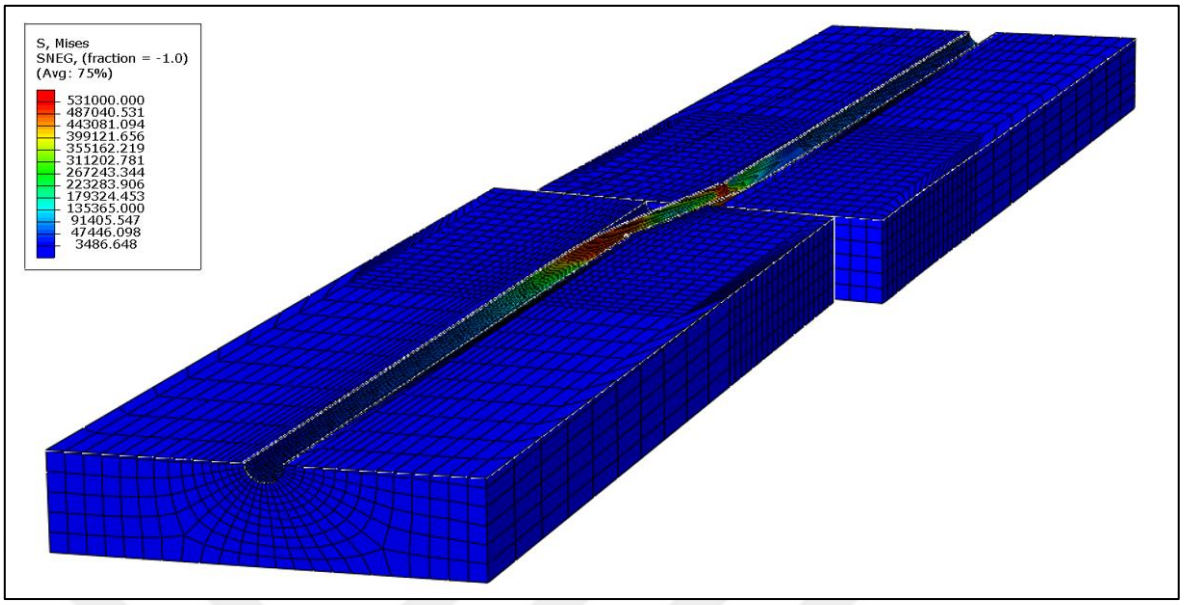

Figure 3.10. Cross-sectional view of a buried pipe subjected to 2m of fault displacement and development of Von Mises stresses

3.2.3. Model Dimensions and Meshing

As mentioned in previous sections past studies performed on numerical modeling of buried pipes subjected to faulting actions involved parametric investigations regarding the optimum model, mesh dimensions as well interaction properties. Among these studies the work performed by Vazouras et al. (2010, 2015) detailly describes the effect of varying values of geometric parameters such as model total length, width, burial depth and width of fault plane. According to their study a model length of at least 65 pipe diameters and width and height of minimum of 11 and 5 pipe diameters respectively are sufficient for a realistic model with a negligible margin of error. These dimensions were also assumed in this dissertation, in addition, as will be discussed in Chapter 4 a model similar to the one developed by Vazouras etl al. (2010) was analyzed so as to validate the models used in this study. Figures 3.11 and 3.12 schematically depict the model dimensions assumed in the present study.

In a finite element analysis approach appropriate meshing of the model is of paramount importance in order to obtain accurate results. However, over meshing of the model or model parts typically significantly increases the required computational power and time to achieve a solution. Therefore, need calls for a trade-off and strategy to apply such a meshing pattern

that neither hinders the accuracy of the model nor overly increases the needed computational time. For the numerical models investigated in this thesis, such an effect was achieved by increasing the fines of the mesh at the location in the vicinity of fault trace, whereas a much coarse meshing pattern was chosen for the regions located away from the fault. The reason behind such a meshing pattern relies on the well-known fact that the majority of deformations (strains) on the pipeline will take place at regions close to the fault plane, a fact proven to be valid by many past studies (Anastasopoulos et al., 2007, 2008; and Gazetas et al., 2007). As a result, 20m (10m in each opposite direction) of the total model length of 60m has more refined mesh (with mesh sizes equal to 0.5m), while the remaining 40m is much coarser (mesh size equal to 2m). In order to prove the validity of the assumed approach a control model with very fine meshing was also analyzed. Comparison of the obtained result indicated that the margin of difference among the two models was acceptable and rather minor, therefore, the meshing pattern presented in Figures 3.11 and 3.12 was considered to be appropriate for the purposes of this thesis.

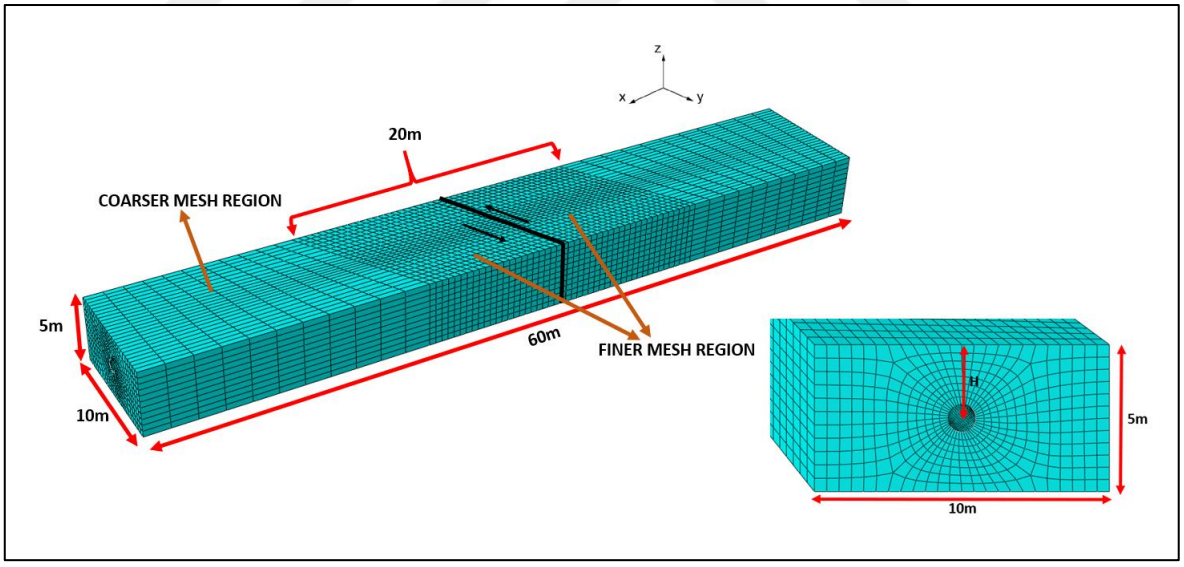

Figure 3.11. Model dimensions and meshing pattern used for soil blocks

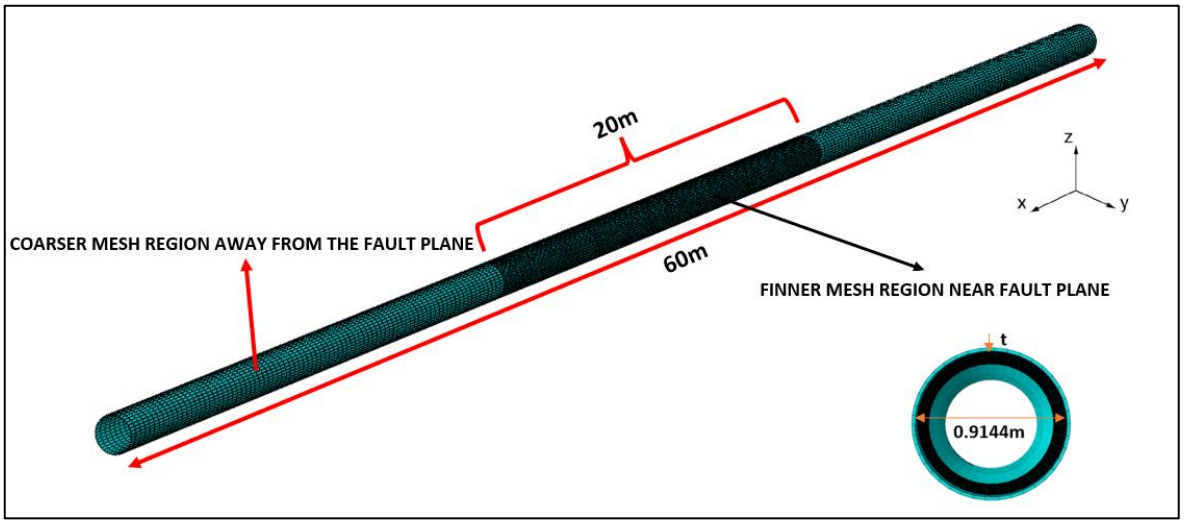

Figure 3.12. Model dimensions and meshing pattern used for buried steel pipe

3.2.4. Material and Pipe-Soil Interaction Properties

Analysis of the numerical models was performed assuming the soil surrounding the pipe is a medium sand, material characteristics of which are summarized in Table 3.1. The properties and behavior of the soil material was described via adopting the elastic-perfectly plastic Mohr Coulomb soil model which is based on the Mohr-Coulomb strength of failure criterion which assumes that maximum shear stress defined based on normal stress rules the failure. This assumption is illustrated through the use of Mohr's circle incorporating the plot of maximum and minimal principal stresses. Then, the line which best fits the circles defines the failure line (Labuz and Zang, 2012). Graphical illustration of these failure criterion is given in Figure 3.13. Characteristic values needed to define this failure criterion such as cohesion (c), internal friction angle (ϕ), Unit Weight (γ_s), Poisson's ratio (ν), Elastic modulus (E_s) and dilation angle (ψ) are summarized in Table 3.1.

Table 3.1. Backfill soil properties (Karamitros et al., 2007)

Soil Type	**c (kPa)**	**ϕ (^{o})**	**γ_{sm} (kN/m^3)**	**E_s (MPa)**	**ν**	**ψ (^{o})**
Medium Sand	0	35	18	25	0.30	0

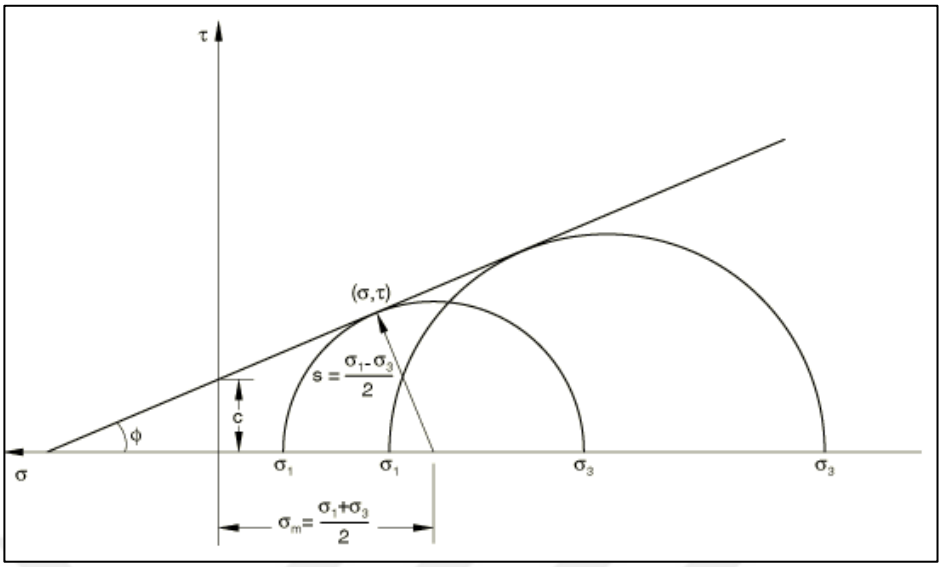

Figure 3.13. Mohr-Coulomb failure criterion (Abaqus CAE, 2020)

A Von Mises plasticity model accounting for large strains and with isotropic hardening was assumed for describing the mechanical behavior of the steel material. A grade API X65 steel was utilized in the analysis. Material properties of this steel including plastic and elastic Young's modulus (E_1 and E_2), yield and failure stress and strain limits (σ_1, σ_2, ε_1 and ε_2) are summarized in Table 3.2. The Ramberg-Osgood stress-strain relation defined as per the equation 3.1 (Talebi and Kiyono, 2021) below was used to model the plastic behavior of steel material in the analysis software. The obtained stress-strain curve for API X65 steel in shown in Figure 3.14.

$$\varepsilon = \frac{\sigma}{E_i}\left[1 + \left(\frac{a}{r+1}\right)\left(\frac{|\sigma|}{\sigma_y}\right)\right] \tag{3.1}$$

Here, ε is the pipeline strain value, σ and σ_y is the applied and yield stress, E_i is the initial elasticity modulus of steel material, a and r are the constants for this steel grade. The equation 3.1 was used to calculate the stress strain curve utilized in this study. The elastic-plastic material model available in the analysis software was used to input these properties.

Table 3.2. Material properties of the API Grade X65 steel (Vazouras et al., 2012)

Material Property	Value	Unit
Yield Stress (σ_1)	490	MPa
Failure Stress (σ_2)	530	MPa
Yield Strain (ε_1)	0.233	%
Failure Strain (ε_2)	4	%
Elastic Young's Modulus (E_1)	210	GPa
Plastic Young's Modulus (E_2)	1.088	GPa
Material Constant 1 (a)	38.31	-
Material Constant 2 (r)	31.51	-

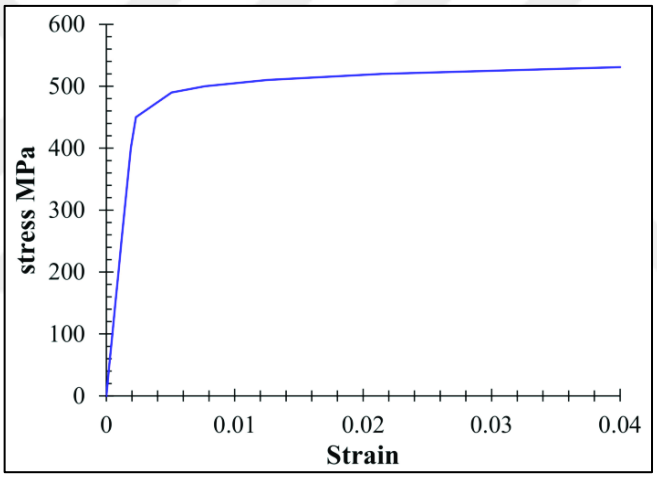

Figure 3.14. Stress-strain curve for API X65 grade steel obtained using Ramberg-Osgood equation

The interaction between the soil and pipe surface was simulated by means of a "surface to surface contact algorithm" available within the material interaction library of ABAQUS CAE. As seen in the Figure 3.15 the utilized interaction property defines the separation behavior among the pipe and soil during the act of fault displacement via a so called "normal behavior" property, whereas a "tangential behavior" property involving the definition of a friction parameter μ is used to simulate the friction behavior and interaction occurring at soil-pipe interface. The Coulomb friction model assuming the μ coefficient to be the same (isotropic) along all direction was utilized. The coefficient of friction μ is calculated as $\tan(\phi_\mu)$, where ϕ_μ is the skin friction angle between the soil and the buried pipe. Extensive experimental studies performed by Potyondy (1961) to determine the values of this angle

between different type of soil and a variety of civil engineering materials revealed that between a sandy soil and steel material this angle attains values between 17^o and 25^o. Similar laboratory experiments performed by Tsubakihira et al. (1993) report that the friction coefficient between steel and sandy soil attains values ranging between 0.23 to 0.56. Experimental studies reported in Canadian Foundation Engineering Manuel (2006) indicate that the skin friction angle values between sand and steel material attain values between 20^o and 30^o. Extensive numerical studies performed by Yimsiri et al. (2004) on the characteristic of the steel-sand interaction in lateral and upward direction indicate that ϕ_μ varies between the soil internal friction angle (ϕ) and $\phi/2$. Moreover, sensitivity investigation regarding the value of μ was reported by various research efforts (Vazouras et al., 2012; Mosadegh and Nikraz, 2015; Somboonyanon and Halmen, 2021; Mokhtari and Nia, 2015) obtained results indicate that there is minimal variation of results for a μ value between 0.15 and 1.00. Therefore, based on reported experimental and numerical data for all cases investigated herein in this dissertation the value of μ was taken to be equal to 0.30

As shown in Figure 3.15 a master-slave surface contact property was also required to be defined along with the above-mentioned interaction properties. The philosophy behind this algorithm is such that it is assumed that nodes of slave surface (soil in this case) are not allowed to penetrate the surfaces (segments) that make the master surface (pipe in this case). Figure 3.16 illustrates the assumption of this contact algorithm. In contrast to slave surface, nodes located on the master surface are able to penetrate the slave surface.

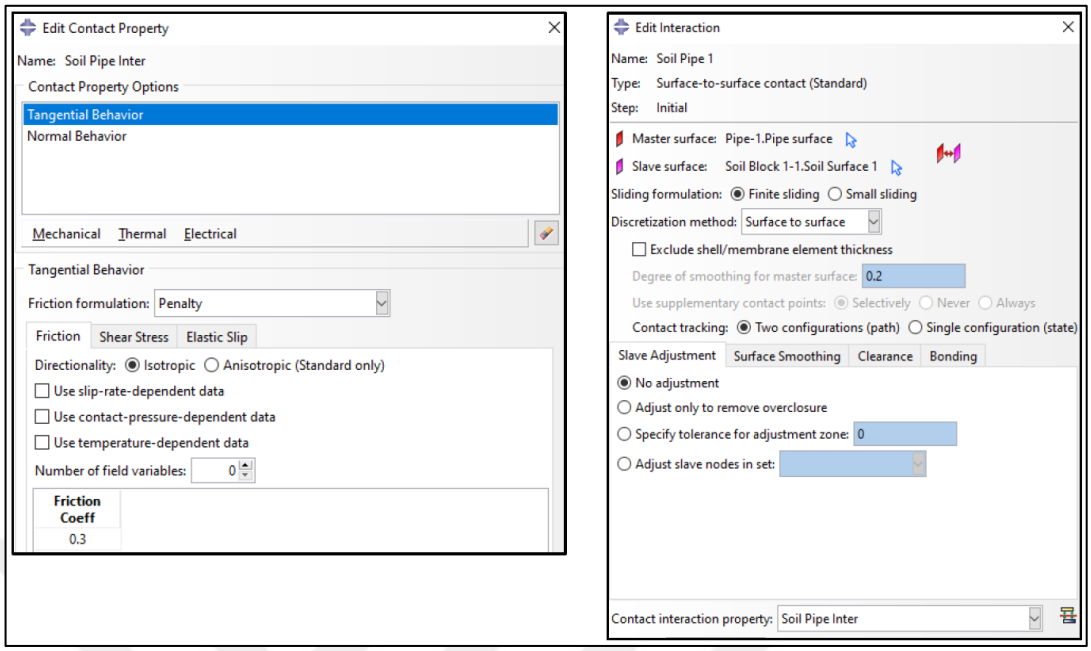

Figure 3.15. Properties of contact algorithm defined at the interface of soil and pipe, tangential and normal behaviour properties (left), and master-slave surface definition (right)

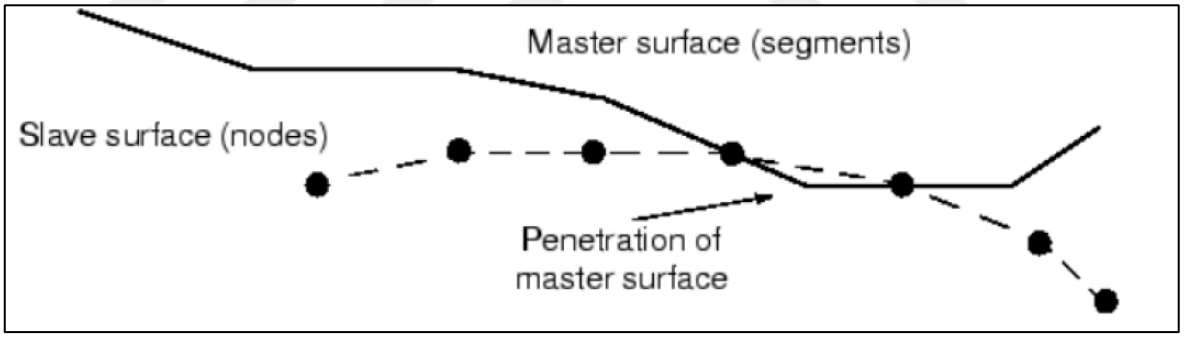

Figure 3.16. Graphical illustration of master-slave surface contact algorithm (Abaqus CAE, 2020)

3.3. Numerical Models Incorporating Mitigation Approaches

This section presents information on numerical FE models of buried soil - pipe system incorporating mitigation strategies investigated within the scope of this thesis. In essence, the approach utilized for these cases is similar to the one used for models described in Section 3.2, with additional material and interaction models adopted for each particular mitigation technique. The scope of this thesis aimed at investigating the effect of using four mitigation

methods. In particular, the variation of seismic performance of buried steel pipes subjected to strike-slip faulting actions was studies for cases incorporating the use of three FRP wrap types (CFRP, GFRP and BFRP), two EPS Geofoam Block encasement types (High and Low Strength), two CLSM types (Low and High strength both modeled using two different material models), and two Tensar Nr. 3 geogrid mesh configurations (single and double layer). Following sections, present information of modeling approaches utilized for each of these methods.

3.3.1. Properties of Numerical Models Incorporating FRP Wraps

Possibility of the mitigation of seismic demands exerted on the pipeline by the strike-slip fault action was investigated via incorporating FRP composite wraps within the analysis models described detailly in Sections 3.1 and 3.2. In particular, the scope of this thesis investigated the impact of utilizing Carbon Fiber (CFRP), Glass Fiber (GFRP) and Basalt Fiber (BFRP) wraps. Fiber reinforced polymer (FRP) composite materials are in essence a combination of multiple components at micro and/or macro level possessing different physical properties, chemical compositions and are not soluble to each other, which are typically bonded using a strong adhesive. These types of materials have gained significant importance for repair, strengthening and rehabilitation of a great variety of structures, owing to their superior abilities such as a high resistance to tensile stresses, light weight, corrosion durability and ease of application. Research indicates that use of FRP composites strengthens the structural element via ensuring a safe cross-section (Günaslan et al., 2014). The ability of these composites to offer improved resistance to tensile stresses by strengthening the cross-section of the buried pipes was main idea behind utilizing them as a mitigation approach. The proposed configuration depicted in Figure 3.17 suggests that the buried pipes would have an improved seismic performance under the applied fault load via having a strengthened cross-section with a much higher resistance.

As shown in Figure 3.18 the FRP wrap was modeled using the same element type (S4R shell element) used for pipeline modelling. Again, a surface-to-surface contact algorithm was utilized to simulate the interaction among the buried pipe and the FRP composite wrap. Details of the properties of these interaction algorithms are presented in Subsection 3.3.2. Besides the investigation of the influence of FRP type, the impact of FRP layer thickness

was as well investigated within study. The layer thicknesses considered for each FRP type are as follows:

- Single Layer of t = 1mm CFRP, GFRP and BFRP Wrap
- Single Layer of t = 3mm CFRP, GFRP and BFRP Wrap
- Single Layer of t = 5mm CFRP, GFRP and BFRP Wrap
- Single Layer of t = 10mm CFRP, GFRP and BFRP Wrap

A total of 12 cases were analyzed and compared with each other and also to the cases with no FRP Wrap as well as to cases utilizing the other mitigation methods so as to study and understand the influence of each wrap type. A performance criterion (limit state) was necessary to be defined so as to account for the rupture of the FRP wrap, owing to the fact that a hard contact with no possibility of slippage among the pipe and FRP was enforced into the analysis model, assuming that once the rupture takes place on the FRP the same amount of tensile strains will also be sustained by the pipeline. Hence, as described detailly in section 3.4 a tensile strain capacity calculated using elastic material properties of the FRP (due to fact that the behavior of FRP is almost linear up to the point of rupture) was utilized as the limit state for FRP wrap rupture. For each case, the application length of the wrap was assumed to be equal to 20m and located at the area of fine mesh pattern due to the obvious fact that the better part of damage occurs at the vicinity of fault trace. The meshing pattern used for the FRP wrap was taken to be the same as the one used for the pipeline. A full bond with a hard contact property was assumed to exist among the pipe and FRP surfaces, while, aa friction value of 0.30m was assumed for FRP and soil surface per experimental data reported by Aksoy et al. (2017).

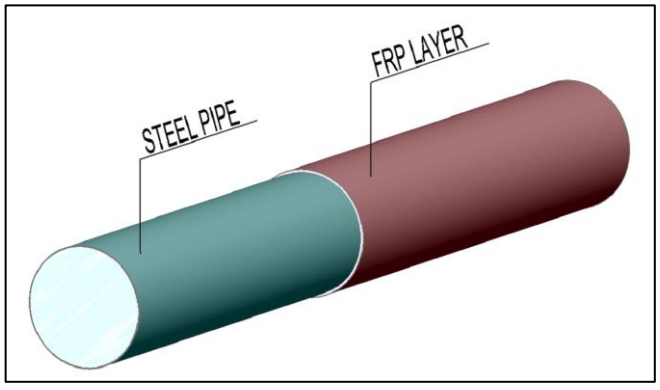

Figure 3.17. Proposed buried pipe configuration incorporating FRP wraps

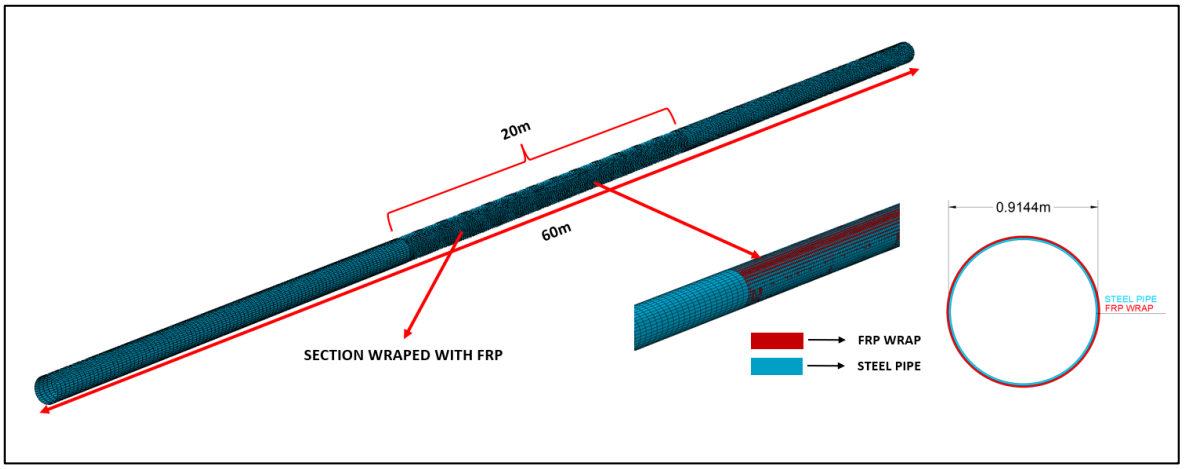

Figure 3.18. Configuration used for the numerical models including FRP Wraps

3.3.2. Material of Numerical Models Incorporating FRP Wraps

Mitigation of seismic damage due to strike-slip fault action was aimed via the use of three FRP composite wraps (CFRP, GFRP and BFRP). As described earlier FRP wraps were modeled using the same element type (S4R shell) used to model the pipeline and the layer thickness for each FRP type ranged from 1mm to 10mm. In addition to accurate modelling of the FRP wrap another crucial input are the material properties utilized for these composite types. The properties summarized is Tables 3.3, 3.4 and 3.5 for CFRP, GFRP and BFRP wraps respectively present the material properties that were input within ABAQUS CAE using the engineering properties option of the software. Being anisotropic materials, FRP composites required the definition of a material model capable of capturing the anisotropic material damage acquired during the application of seismic load. For this purpose, the so-called “Hashin Damage Material Model” already existing within software was utilized. The Hashin damage model (Hashin and Rotem, 1973) is utilized to describe the elastic-brittle material damage characteristics which are anisotropic in nature. Typically, this material model is used for software input of composite materials containing fibers as reinforcements agents. The model is capable of defining the failure modes associated with: tension in fiber elements, compression in fiber elements, and tension and compression occurring in matrix (Hashin, 1980). These properties are also presented in the table below.

Table 3.3. Properties used to define CFRP material (Mokhtari and Nia, 2015)

CFRP Material Properties	**Value**	
Material Property		
E_{11} Young's Modulus in Longitudinal Direction (GPa)	137	**ELASTIC PROPERTIES**
E_{22}= E_{33} Modulus in Longitudinal Direction (GPa)	9.11	
E_{12}= E_{13} Modulus of Shear (GPa)	6.12	
E_{23} Modulus of Shear (GPa)	3.04	
Poisson's Ratio ν_{12} = ν_{13}	0.30	
Poisson's Ratio ν_{23}	0.40	
Tensile Strength in Longitudinal Direction (MPa)	2004	**HASHIN DAMAGE MODEL PROPERTIES**
Compressive Strength in Longitudinal Direction (MPa)	1186	
Tensile Strength in Transverse Direction (MPa)	56	
Compressive Strength in Transverse Direction (MPa)	208	
S_{12} = S_{13} Strength in Shear (MPa)	141	
S_{23} Strength in Shear (MPa)	45	

Table 3.4. Properties used to define GFRP material (Holloway, 2010)

GFRP Material Properties	**Value**	
Material Property		
E_{11} Young's Modulus in Longitudinal Direction (GPa)	55	**ELASTIC PROPERTIES**
E_{22}= E_{33} Modulus in Longitudinal Direction (GPa)	15.20	
E_{12}= E_{13} Modulus of Shear (GPa)	4.70	
E_{23} Modulus of Shear (GPa)	3.28	
Poisson's Ratio ν_{12} = ν_{13}	0.254	
Poisson's Ratio ν_{23}	0.428	
Tensile Strength in Longitudinal Direction (MPa)	1200	**HASHIN DAMAGE MODEL PROPERTIES**
Compressive Strength in Longitudinal Direction (MPa)	800	
Tensile Strength in Transverse Direction (MPa)	39	
Compressive Strength in Transverse Direction (MPa)	128	
S_{12} = S_{13} Strength in Shear (MPa)	250	
S_{23} Strength in Shear (MPa)	25	

Table 3.5. Properties used to define BFRP material (Jayasuriya et al., 2020)

BFRP Material Properties	**Value**	
Material Property		
E_{11} Young's Modulus in Longitudinal Direction (GPa)	25	**ELASTIC PROPERTIES**
E_{22}= E_{33} Modulus in Longitudinal Direction (GPa)	10	
E_{12}= E_{13} Modulus of Shear (GPa)	4.80	
E_{23} Modulus of Shear (GPa)	4.80	
Poisson's Ratio v_{12} = v_{13}	0.30	
Poisson's Ratio v_{23}	0.42	
Tensile Strength in Longitudinal Direction (MPa)	500	**HASHIN DAMAGE MODEL PROPERTIES**
Compressive Strength in Longitudinal Direction (MPa)	260	
Tensile Strength in Transverse Direction (MPa)	45	
Compressive Strength in Transverse Direction (MPa)	60	
S_{12} = S_{13} Strength in Shear (MPa)	35	
S_{23} Strength in Shear (MPa)	20	

3.3.3. Properties of Numerical Models Incorporating EPS Geofoam Blocks

The second mitigation approach investigated within the scope of this thesis involved the use of EPS geofoam blocks to shield the buried pipes against the seismic demands induced due to the rupture of the strike-slip fault. The main idea behind adopting this mitigation technique relied on the well-known ability of the geofoam blocks to undergo deformation without losing much their initial shape and size (Rasouli and Fatahi, 2020; Jiang et al., 2008), hence the approach utilized in this thesis proposed a configuration of buried pipe embedded within blocks of geofoam and suggests that this would isolate the pipeline from the surrounding soil, and the ability of geofoam blocks to compress under fault actions would create a medium that would have a buffering action for the induced stresses and strains and as a result would improve the seismic performance of the pipeline. Figure 3.19 schematically illustrates this buffering effect offered using EPS geofoam blocks by comparing the deformation characteristics of the conventional buried pipe and pipeline mitigated with geofoam blocks. Under strike-slip fault rupture conventional pipeline backfilled only with native soil tends to undergo deformation along a relatively short length

of the pipe, therefore, induced stresses and strain are localized within this length at an amount that typically leads to the structural failure of the pipe. On the other hand, pipes protected using EPS geofoam blocks would undergo the same amount of deformation distributed over a considerably longer length - that due to the geofoam blocks serving as mediator for absorbing and distributing the fault rupture and thus isolating the buried pipe-which in turn would avoid the localized concentration of the stresses and strain that would otherwise lead to failure.

Figure 3.20 shows the EPS geofoam block configuration adopted in this study. The proposed configuration assumed the pipeline to be completely isolated from the surrounding soil and embedded within geofoam blocks at top, bottom where the blocks were assumed to have a width of 4m and thickness of 1.50m and also on both sides at a width of 1.543m and thickness equal to the external pipeline diameter. Similar to cases incorporating FRP wraps, investigation of examples including EPS geofoam considered cases of a steel pipeline with an out-to-out diameter (D) of 914.4mm (36inches)-a commonly utilized 342 steel pipe size in gas and oil transportation industries-and wall thicknesses (t) of 6.35mm (1/4inches), 9.53mm (3/8inches) and 15.88mm (5/8inches) with corresponding D/t ratios of 144, 96 and 58 respectively. The study assumed the pipeline to be placed within a soil block having a width of 10m and depth of 5m, while burial depth for all cases was taken to be equal to 1.8m. Eight –node reduced integration bricks elements (C3D8R) with hour-glass control were used to model the soil deposit surrounding the steel pipe. Same type elements were also utilized for the EPS geofoam blocks. Figure 3.21 shows the adopted model dimensions and configuration. The meshing configuration differs from that of other models such that the EPS geofoam block has a much finer mesh configuration compared to the native soil, a pattern developed based on trial end error, where the configuration that yielded the most stable solution was chosen. The utilized mesh pattern in shown in Figure 3.22. A Coulomb friction model with coefficients of frictions equal to 0.20, 0.30, and 0.60 for pipe-EPS, EPS-EPS, and EPS-soil surfaces were utilized per the numerical and experimental data reported by Meguid and Hussein (2017) for the definition of contact properties.

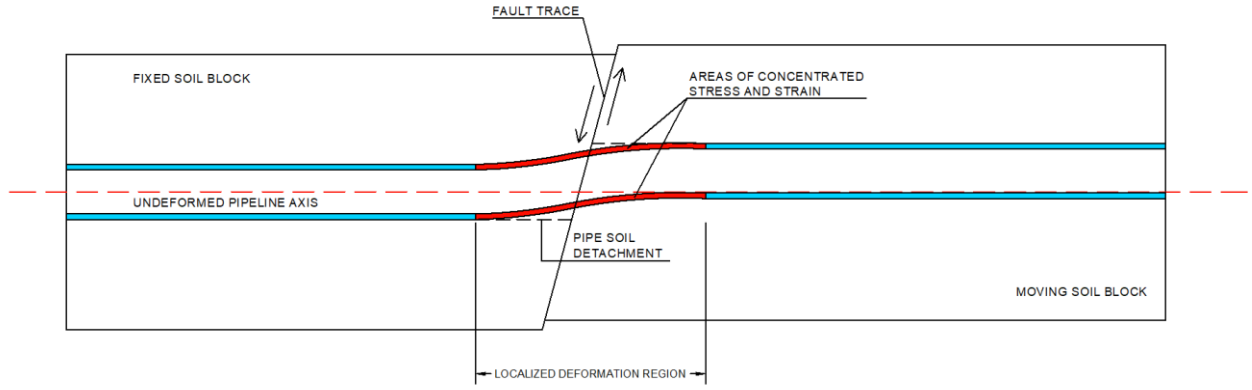

a)

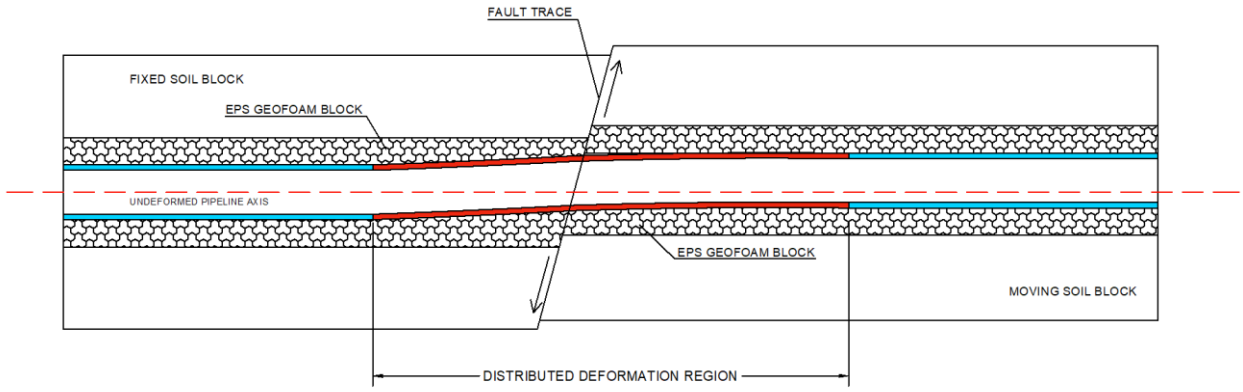

b)

Figure 3.19. Schematic illustration of the response of a) a pipeline placed in native soil and b) pipeline embedded within EPS geofoam blocks

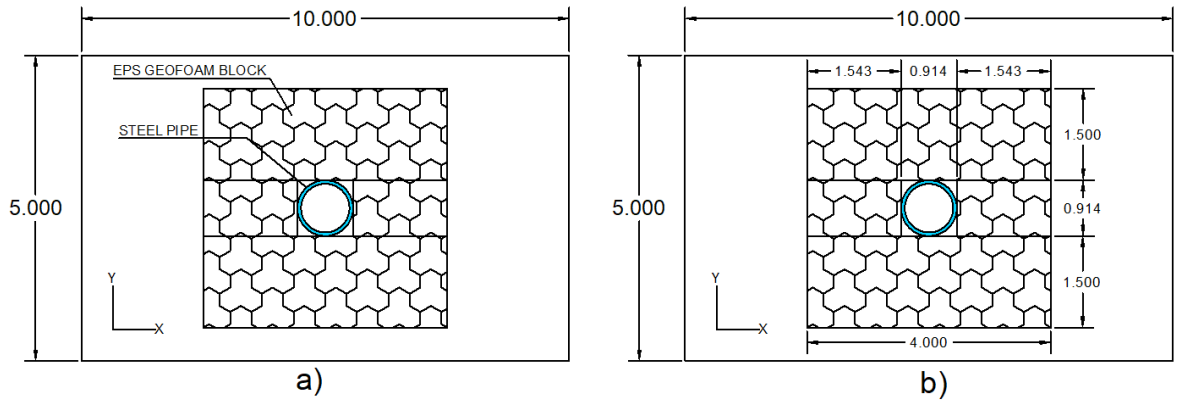

Figure 3.20. EPS geofoam block model configuration a) cross-sectional view, b) model dimensions, c) plan view

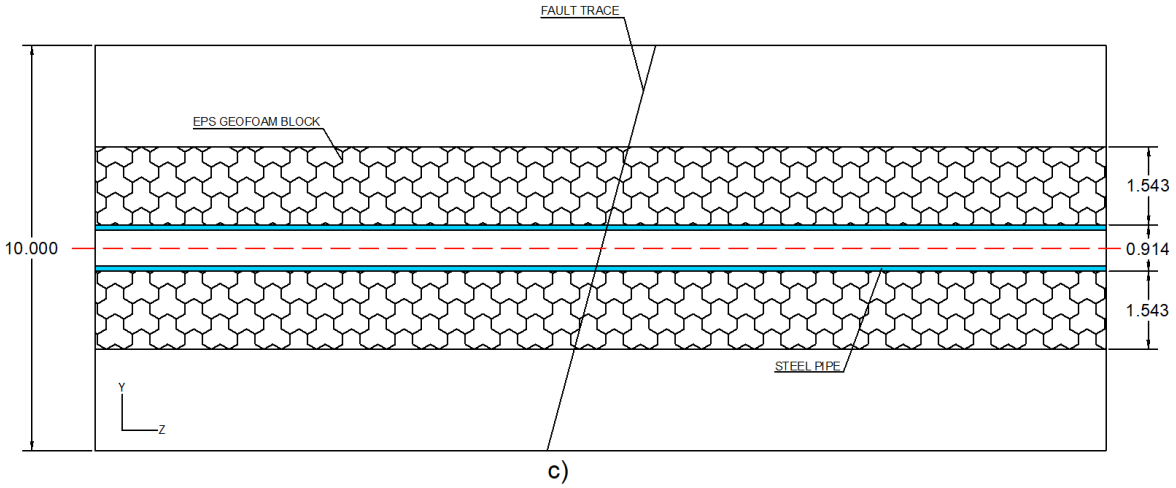

Figure 3.20. EPS geofoam block model configuration a) cross-sectional view, b) model dimensions, c) plan view

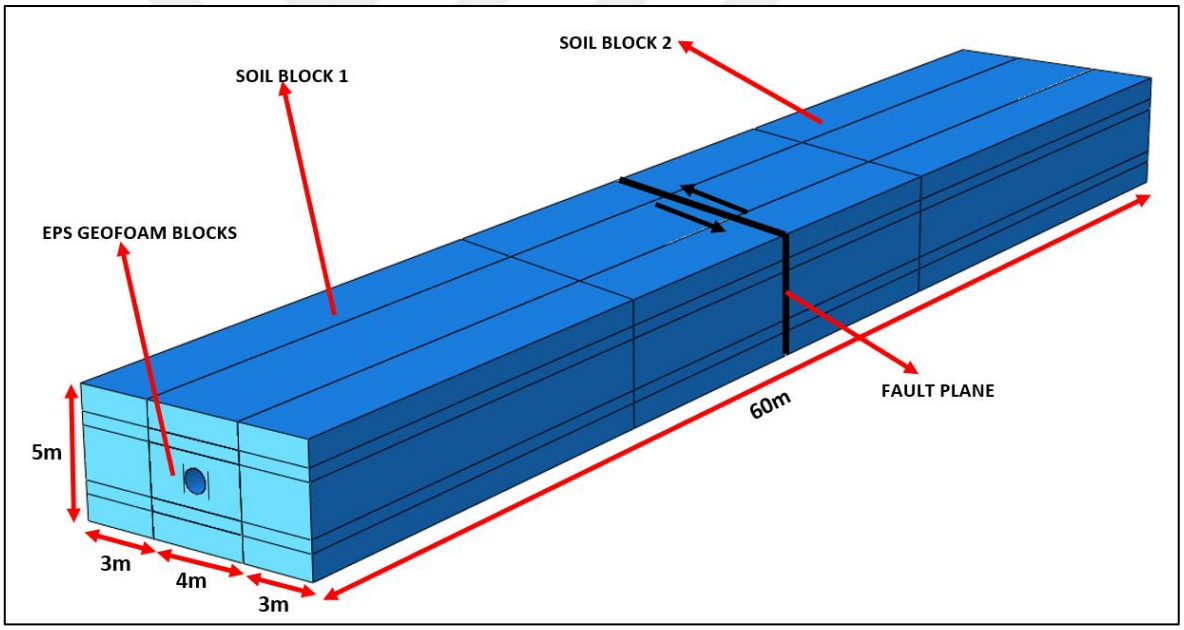

Figure 3.21. Model configuration used for analysis cases incorporating EPS Geofoam

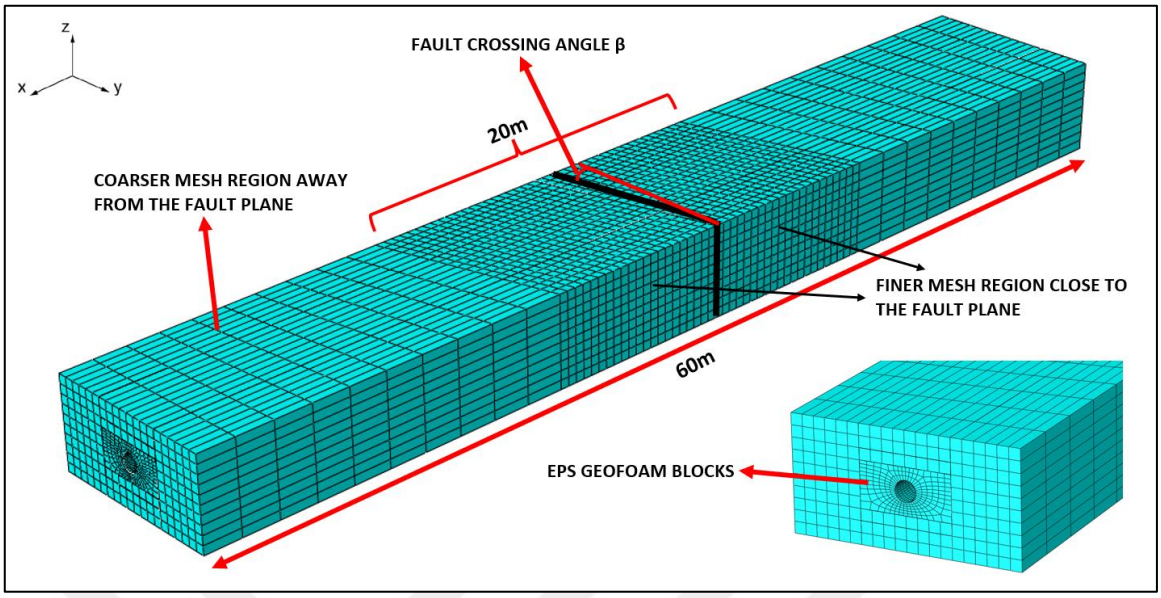

Figure 3.22. Mesh pattern used for analysis cases incorporating EPS Geofoam

The scope of this dissertation investigated the influence of using EPS geofoam block to protect buried steel pipes against faulting actions assuming two strength classes for the geofoam material. Namely, a low-strength and a high-strength EPS geofoam material was utilized in the response analysis of buried pipe subjected to a fault displacement ranging between 0-4m, applied quasi-statically. Table 3.6 present information on the assumed properties of EPS geofoam materials. The anticipated behavior of EPS geofoam blocks was simulated assuming an elastic perfectly plastic material model based on Mises yield formulation with isotropic hardening defined through a flow rule. Material properties were input into the analysis model through the use of true stress-strain data of the EPS material obtained from engineering stress-strain data following the formulation and approach proposed by Meguid and Hussein (2017). In brief, the procedure initially requires the calculation of true stresses and strains from nominal data provided by the EPS geofoam manufacturers (Lingwall and Bartlet, 2014), later the true strains are decomposed into their elastic and plastic components and the steps are finished by entering the determined true stress versus plastic strain values into the analysis model. Figure 3.23 shows the schematic illustration of the theory adopted for this purpose along with the actual computed curve, whereas, Table 3.7 shows the calculated stress-strain values.

Table 3.6. Material properties of EPS geofoam blocks (Meguid and Hussein, 2017)

EPS TYPE	$^{*}f_{cE}$ (kPa)	E_{cE} (MPa)	ν	γ_{EPS} (kg/m^3)
LOW STRENGTH	35	4.50	0.10	40
HIGH STRENGTH	90	18.50	0.15	14.50

*Compressive strength at 10% strain

Table 3.7. Stress-strain data for Low Strength EPS material model

σ_t (kPa)	ε (%)	ν	σ_{ttrue} (kPa)	E_{cE} (kPa)	ε_{el} (%)	ε_{etrue} (%)	ε_{pl} (%)
0.00	0.00	0.15	0.00	17800	0.0000	0.0000	0.0000
177.40	0.01	0.15	177.93	17800	0.0100	0.0100	0.0000
309.20	0.02	0.15	311.06	17800	0.0175	0.0198	0.0023
333.70	0.03	0.15	336.72	17800	0.0189	0.0296	0.0106
343.20	0.04	0.15	347.36	17800	0.0195	0.0392	0.0197
350.00	0.05	0.15	355.31	17800	0.0200	0.0488	0.0288
357.20	0.06	0.15	363.72	17800	0.0204	0.0583	0.0378
363.50	0.07	0.15	371.26	17800	0.0209	0.0677	0.0468
369.50	0.08	0.15	378.53	17800	0.0213	0.0770	0.0557
374.80	0.09	0.15	385.13	17800	0.0216	0.0862	0.0645
380.00	0.10	0.15	391.66	17800	0.0220	0.0953	0.0733
385.40	0.11	0.15	398.44	17800	0.0224	0.1044	0.0820
390.40	0.12	0.15	404.84	17800	0.0227	0.1133	0.0906
395.00	0.13	0.15	410.87	17800	0.0231	0.1222	0.0991
399.60	0.14	0.15	416.93	17800	0.0234	0.1310	0.1076
401.80	0.15	0.15	420.51	17800	0.0236	0.1398	0.1161

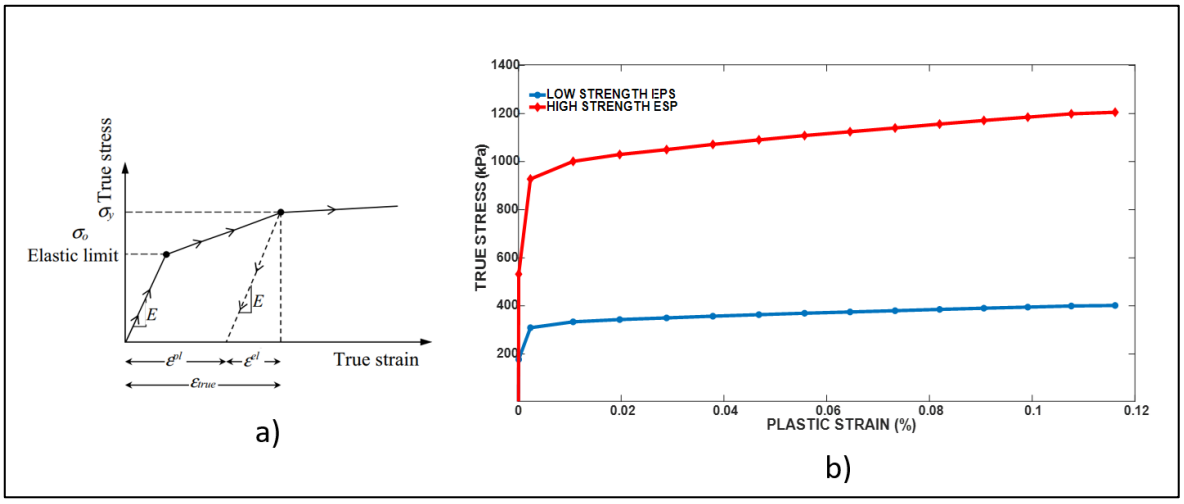

Figure 3.23. Stress strain curve utilized for material definition of EPS geofoam blocks a) stress-strain computation approach, b) computed plastic strain vs true stress value

3.3.4. Properties of Numerical Models Incorporating Controlled-Low Strength Material

Improvement of the seismic performance characteristics of steel pipes subjected the strong ground deformations induced by the rupture of strike-slip faults was also investigated via encasing the buried pipe within a 'box' of controlled-low strength material. These cementitious mixtures are highly flowable material at their fresh state, thus enabling a very rapid and easy field implementation compared to traditional soil backfill which typically requires compaction following the placement procedure. Furthermore, these mixtures are designed to gain their final strength at an extremely short duration, providing immediate resume of daily activity. Another feature of this material is the low compressive strength value, which allows easy future excavation and access to the buried pipe in case of an emergency. Despite having a low strength, this material yet provides a more durable, uniform, and dense embedment to the buried pipe. Similar to the cases incorporating EPS geofoam blocks, the main reason behind utilizing this material as a mitigation approach relies on the idea that the existence of this material around the pipe would provide a deformation medium that would sustain the fault rupture induced demands, absorb the deformations via undergoing cracking and thus reduce the seismic demands that would otherwise be directly applied ono the pipe. Figure 3.24 schematically shows the anticipated mitigation effect of using CLSM, the magnitude of seismic demands (with the red color depicting a more severe action, while yellow, green and blue showing less severe

concentration zones) is thought to reduce with the replacement of native soil with CLSM material, hence resulting in improved seismic performance.

The study performed in this thesis for the cases involving the replacement of native soil surrounding the buried steel pipe with CLSM assumed a configuration where this cementitious material replaced a rectangular soil section having dimensions of 2m x 5m x 60m in width, height, and length respectively. The schematic of this configuration is shown in Figure 3.25. Model dimension were the same with the ones adopted for non-mitigated and EPS geofoam block including models, where the total length of model was 60m, whereas width and length were 10m and 5m respectively. In longitudinal directions blocks were divided into three parts, two of which represented the native soil while the middle block represented the CLSM block. Developed numerical model in presented in Figure 3.26. Similar to previous cases, to reduce the required computational effort but also maintain accuracy a meshing configuration assuming a finer mesh region at zones close to the fault plane (where the majority of deformation will occur) and a coarser pattern away from the fault was employed during the analysis. As a result, 20m (10m in each opposite direction) of the total model length of 60m has more refined mesh, while the remaining 40m is much coarser. Figure 3.27 depicts the meshing configuration assumed for soil, CLSM and buried steel pipe. The element types used for the modelling of the pipeline embedded within soil and CLSM were taken from the library of existing elements of ABAQUS CAE. The so called S4R (four-node reduced integration shell elements with hour-glass control) were utilized to model the cylindrical steel pipe, whereas C3D8R (eight-node reduced integration brick elements with hour-glass control) were used for modelling the soil and CLSM. The developed numerical models consist of four parts in total assembled to form the entire simulation system. The first part of the system is the cylindrical pipe modeled as a continuous shell element. The soil cover and CLMS block is modeled as a prism divided into two equal parts by the strike-slip fault plane represented in the model as a discontinuity plane of thickness equal to 30mm. Boundary conditions shown in Figure 3.8 were enforced onto the models to achieve a realistic behavior and evolution of strains under the applied fault load. Similar to the previous models, analysis was carried out in two steps, where in step one gravity loading of soil and CLSM was applied onto the pipeline, the static general solution approach of ABAQUS CAE was utilized for this purpose. Step two consists of the analysis of soil-CLSM-pipe system subjected to a total fault displacement value of 4m, applied in a

displacement-controlled manner. A friction coefficient (μ) equal to 0.30 was assumed between CLSM-pipe, and CLSM-soil surfaces for the definition of interaction properties per the experimental and numerical data reported by Somboonyanon and Halmen (2021) .

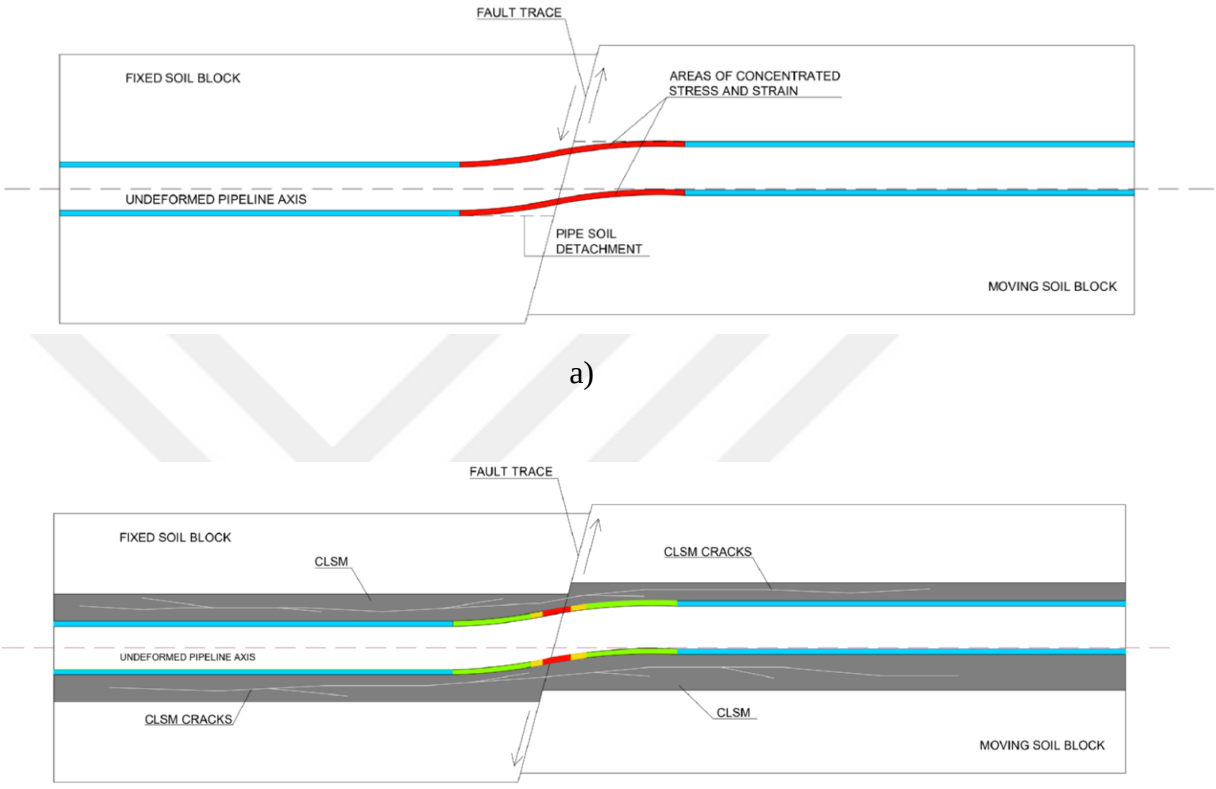

Figure 3.24. Schematic illustration of the response of a) a pipeline placed in native soil and b) pipeline embedded within CLSM encasement

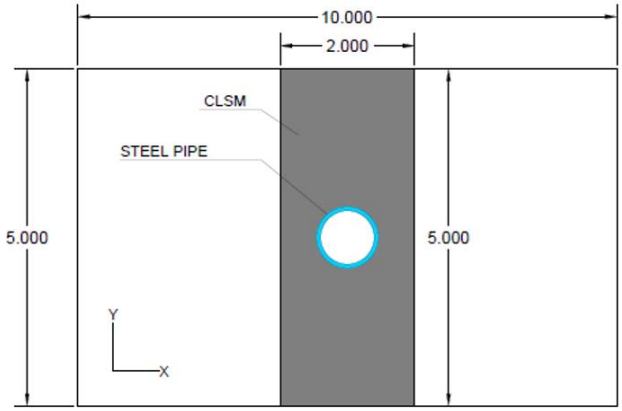

Figure 3.25. CLSM model configuration a) cross-sectional view, b) plan view

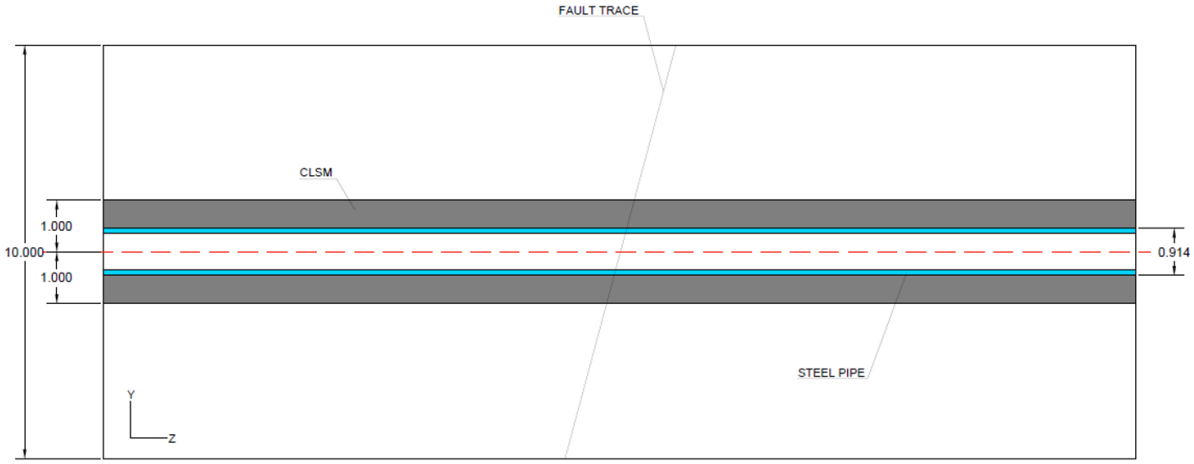

b)

Figure 3.25. CLSM model configuration a) cross-sectional view, b) plan view

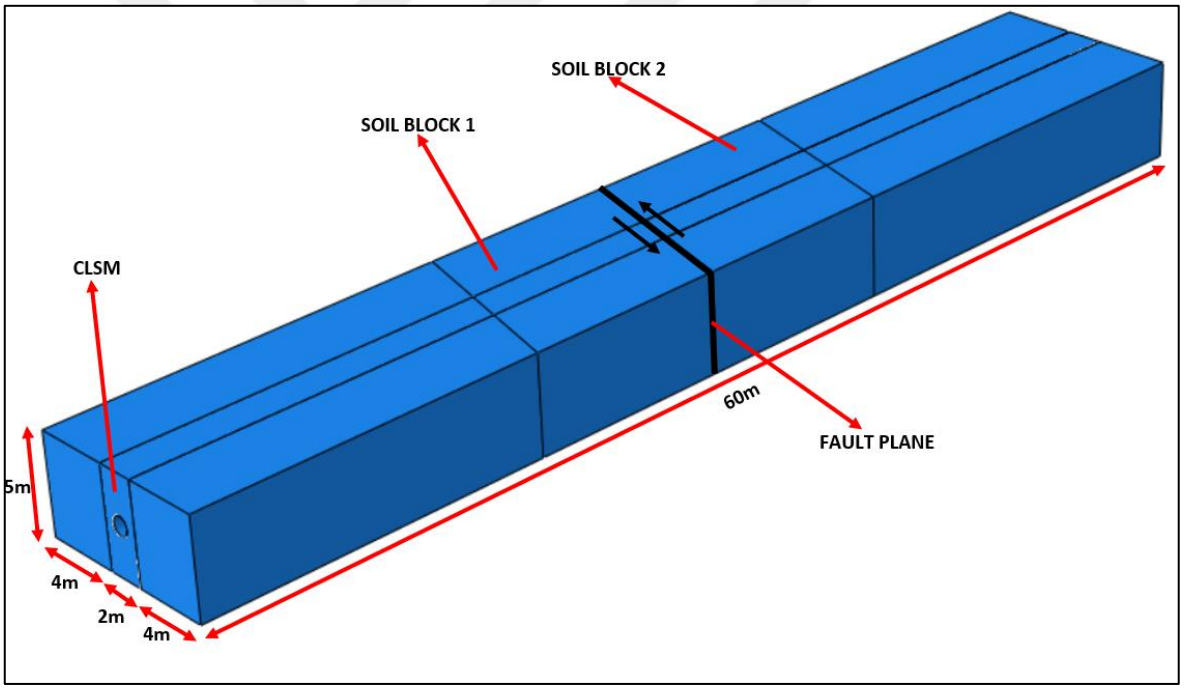

Figure 3.26. Model configuration used for analysis cases incorporating CLSM

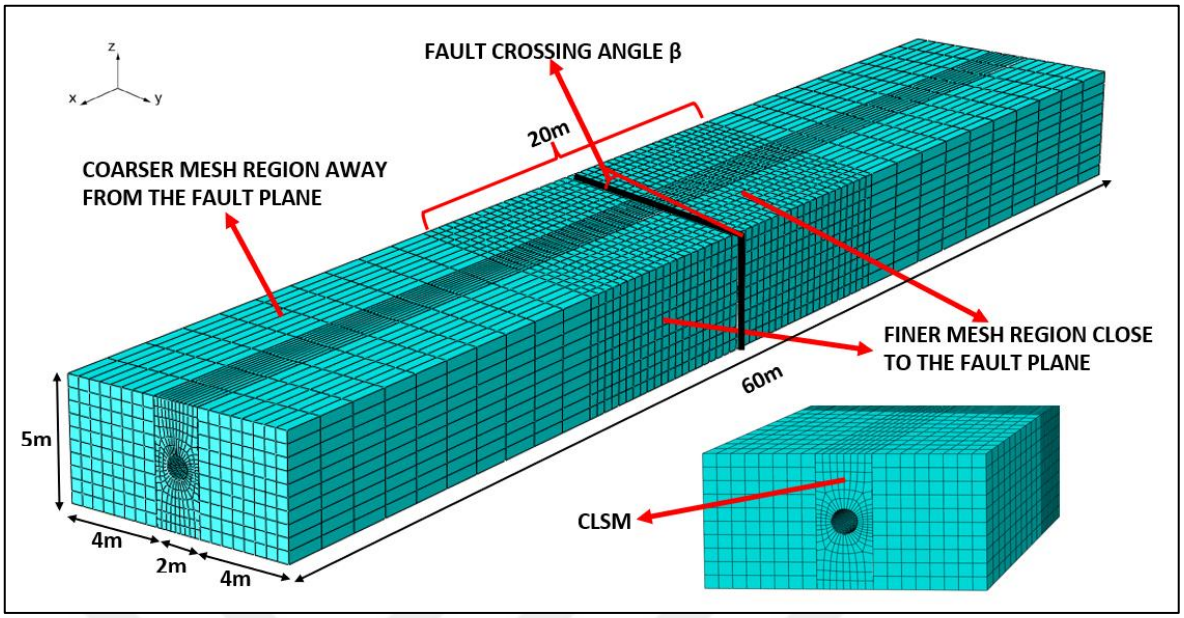

Figure 3.27. Mesh pattern used for analysis cases incorporating CLSM

Evaluation of the performance of buried steel pipes under the effect of applied fault displacement was performed assuming two strength classes for the CLSM material. A low strength CLSM with a compressive strength of 1.50MPa and a high strength mixture with a characteristic compressive strength of 7.60MPa were utilized in this study. Mechanical properties of these CLSM mixtures are presented in Table 3.8. Simulation of the behavior of this material in the numerical models was performed assuming two different modeling approaches. Initially, both mixtures were modeled using the Mohr-Coulomb constitutive material model (the same model used to characterize soil) following the procedure described in Subsection 3.2.4, the second approach utilized the Concrete Damaged Plasticity model. This model is primarily used to define the behavior of concrete material subjected to cyclic and/or dynamic loading conditions which induce plastic deformation. This material model requires the definition of compression and tension behavior of the concrete in order to realistically capture the properties of the investigated material. Literature survey reveals the existence of many models (Carol et al., 2001; Yu et al., 2010; Larsson et al., 2012; Shang et al., 2012) that are used to define this behavior states. The method followed in this dissertation is the simplified damaged plasticity model proposed by Hafezolghorani et al. (2017). In general, when defining the compressive behavior, the compressive stress features of the material are represented via expressing their relationship with the deformation (inelastic) strains, and, if desired and necessary, parameters such as rate of strain, change in temperature, and other related field parameters. The stress-strain curve used to define

compression behavior could also defined for stresses beyond the ultimate value, thus capturing the strain-softening regime as well. The simplified form of the stress-strain curve needed to define the compressive behavior is developed by Hafezolghorani et al. (2017) shown in Figure 3.28. The inelastic compressive strains for the low-strength CLSM mixture computed using this approach and damage parameter of material under the applied compressive stresses is summarized in Table 3.9. The plot of this values is given in Figure 3.28. Same procedure was also utilized for the high-strength mixture, however, the derived data is not shown here to avoid repetition of data and plots. The tension behavior of the material on the other hand is defined via using the tension stiffening properties of it. Tension stiffening on the other hand is employed to define the behavior after failure has occurred allowing the modeling of concrete that has sustained cracking under tension. This approach also allows for the effects of the reinforcement interaction with concrete to be simulated in a simple manner. Figure 3.29 shows the simplified tension behavior model proposed by Hafezolghorani et al. (2017) along with the values computed for the low-strength CLSM material. Computed stress-straina and damage parameter data are presented in Table 3.10. Similarly, same data was also calculated for high-strength mixture but is not shown here. The need to utilize to different material models for CLSM mixtures arises from the fact that this material has properties that by definition fits somewhere between a backfill soil and concrete, hence, this study aimed at pointing out the impact of modeling choice on the obtained results and magnitude of variance between the results and eventually reach to a conclusion regarding the optimal approach to be utilized for modeling this type of material.

Table 3.8. Material properties of CLSM mixtures (Somboonyanon and Halmen, 2021)

CLSM TYPE	**f_{cCL} (kPa)**	**E_{cCL} (MPa)**	**ν**	**γ_{CLSM} (kg/m^3)**	**τ (MPa)**	**c (MPa)**
LOW STRENGTH	1.50	21	0.30	1640	0.05	0.043
HIGH STRENGTH	7.60	100	0.15	1780	0.15	0.098

Table 3.9. Stress Strain Data for Concrete Damaged Plasticity Model (Compression Behavior) for Low Strength CLSM Mixture

Yield Stress (MPa)	ε_t (‰)	$\varepsilon_{inl.}$ (‰)	$\varepsilon_{pl.}$ (‰)	**Damage Parameter**
0	0.000000	0.000000	0.000000	0.0000
0.750	0.000412	0.000000	0.000000	0.0000
0.800	0.000446	0.000006	0.000006	0.0000
0.850	0.000481	0.000014	0.000014	0.0000
0.900	0.000517	0.000023	0.000023	0.0000
0.950	0.000555	0.000033	0.000033	0.0000
1.000	0.000595	0.000045	0.000045	0.0000
1.050	0.000636	0.000059	0.000059	0.0000
1.100	0.000680	0.000076	0.000076	0.0000
1.150	0.000727	0.000095	0.000095	0.0000
1.200	0.000778	0.000118	0.000118	0.0000
1.250	0.000832	0.000146	0.000146	0.0000
1.300	0.000893	0.000179	0.000179	0.0000
1.350	0.000962	0.000220	0.000220	0.0000
1.400	0.001043	0.000274	0.000274	0.0000
1.450	0.001150	0.000353	0.000353	0.0000
1.500	0.001410	0.000583	0.000583	0.0533
1.420	0.001732	0.000951	0.000908	0.1540
1.269	0.001959	0.001262	0.001135	0.2600
1.110	0.002124	0.001514	0.001300	0.4533
0.820	0.002354	0.001903	0.001530	0.5333
0.700	0.002434	0.002049	0.001610	0.6000
0.600	0.002496	0.002167	0.001672	0.0000

Table 3.10. Stress Strain Data for Concrete Damaged Plasticity Model (Tension Behavior) for Low Strength CLSM Mixture

Yield Stress (MPa)	**ε_{cr} (‰)**	**$\varepsilon_{inl.}$ (‰)**	**Damage Parameter**
0.000	0.000000	0.000000	0.0000
0.857	0.000471	0.000000	0.3333
0.572	0.001413	0.001099	0.6250
0.321	0.002767	0.002590	0.8333
0.143	0.004945	0.004867	0.0000

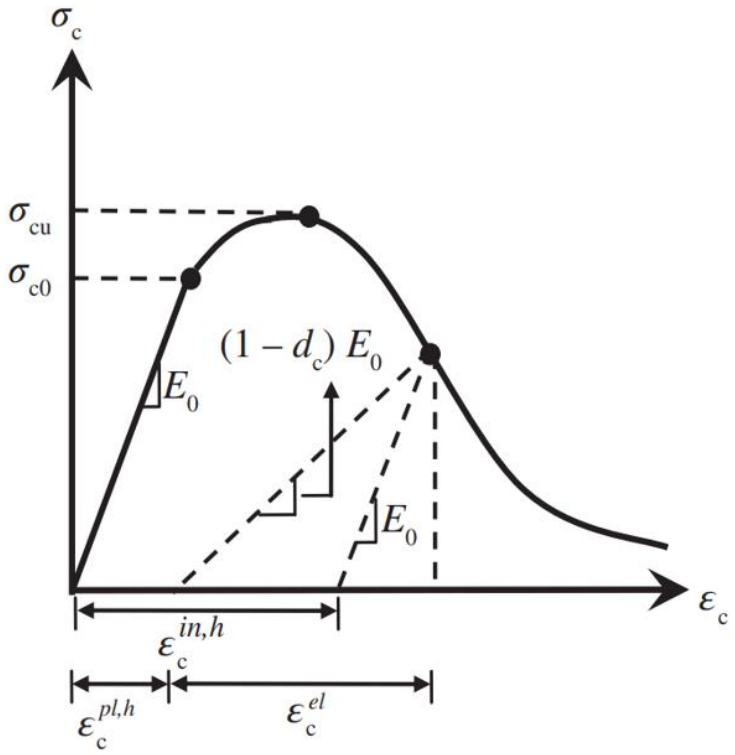

a)

Figure 3.28. CDP compression behavior model, a) simplified model of Hafezolghorani et al. (2017), b) computed data for low-strength CLSM mixture

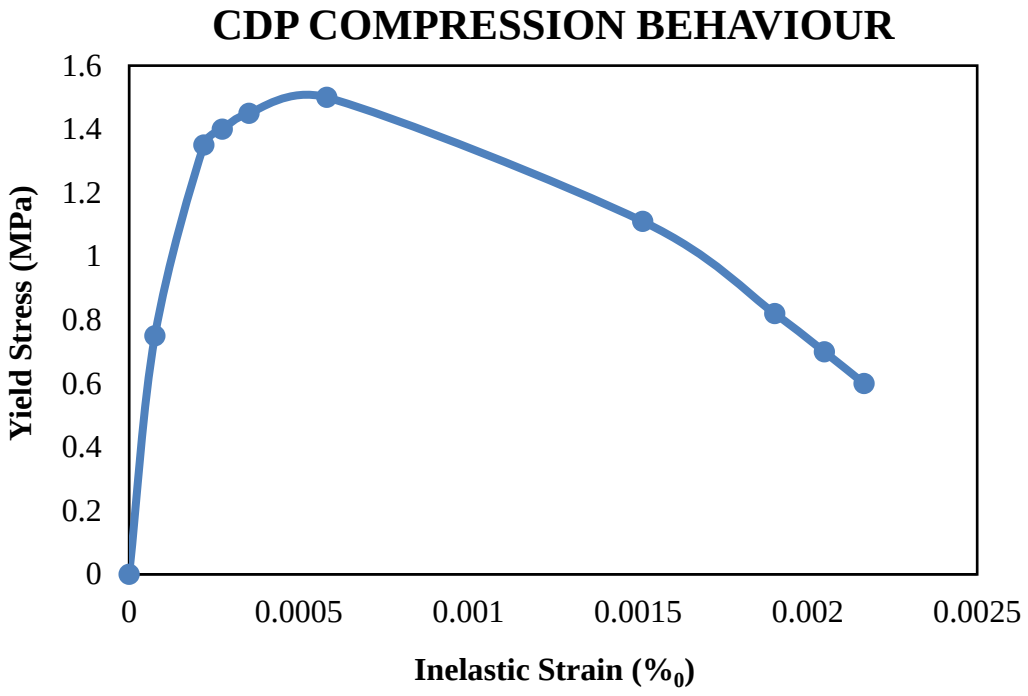

b)

Figure 3.28. CDP compression behavior model, a) simplified model of Hafezolghorani et al. (2017), b) computed data for low-strength CLSM mixture

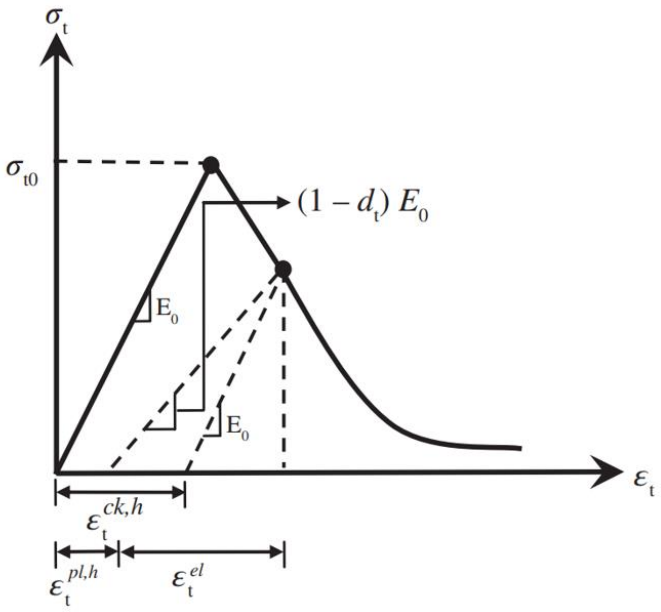

a)

Figure 3.29. CDP tension behavior model, a) simplified model of Hafezolghorani et al. (2017), b) computed data for low-strength CLSM mixture

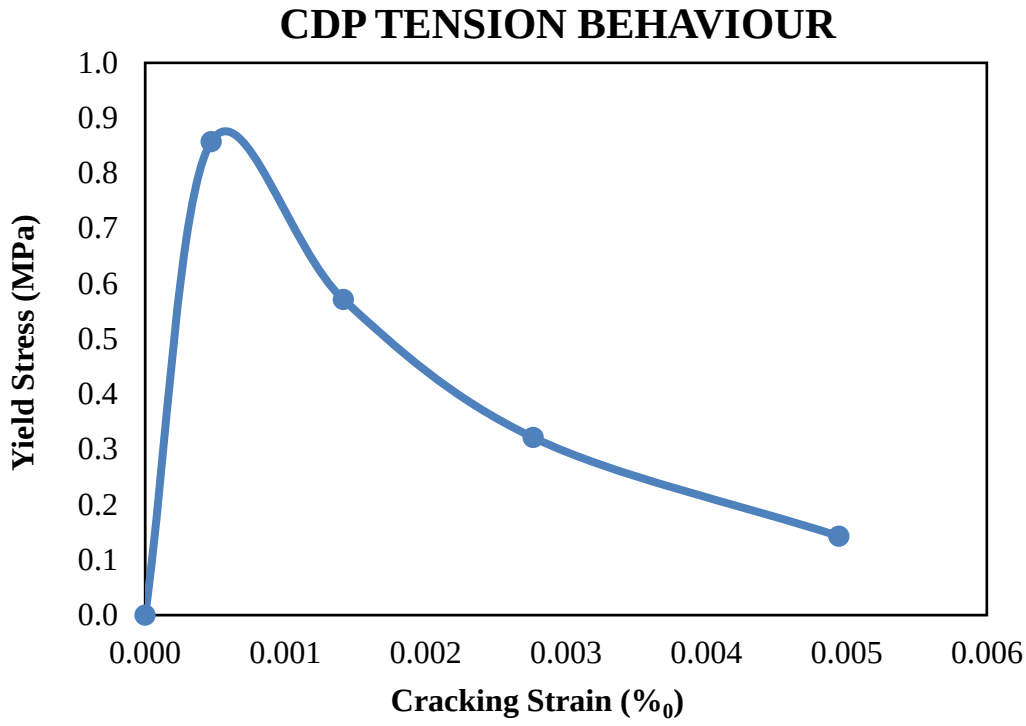

b)

Figure 3.29. CDP tension behavior model, a) simplified model of Hafezolghorani et al. (2017), b) computed data for low-strength CLSM mixture

3.3.5. Properties of Numerical Models Incorporating Geogrid Layers

The last approach utilized within the scope of this thesis as a mitigation strategy for buried steel pipes subjected to strike-slip fault actions was the use of Tensar Nr. 3 geogrid layers. These reinforcement layers improve the soil properties around the buried pipe by spreading out the concentrated seismic effects and widening the shear zone of the fault trace, which in turn leads to the reduction of seismic demands imposed on the buried pipe. Buried pipe model configurations incorporating geogrid layers are shown in Figure 3.30a to 3.30c. To assess the influence of layer number models consisting of single and double geogrid layer configurations have been developed and analyzed. The burial depth of the geogrid layers was assumed to be 1.5m for cases incorporating single layer of geogrid and 1m (first layer) and 1.5m (second layer) for cases with double layers of geogrid. For all cases the geogrid layers were assumed to have a width and length equal to that of soil prism (see Figure 3.30c).

Numerical modeling approach utilized for cases incorporating geogrid layers was in essence similar to that utilized to model cases protected with EPS geofoam blocks. Two solid prisms separated by a gap (i.e. fault trace) with a total length of 60m (approximately equal to 65D) width of 10m and depth of 5m were used to model the soil around the buried pipe, while the pipe was modeled using S4R type shell elements. Cuts of 4mm were made through the soil prisms to enable the inclusion of geogrid layers. Figure 3.31 shows the developed 3D numerical model and considered dimensions. As noted under Chapter 1, review of existing studies suggests that modeling of geogrid layers using planar elements without the consideration for the geometric properties, in particular without the modeling of apertures hinders the accuracy of the obtained results and typically requires modifications to the actual thickness of the layers. As a result, in this study the geogrid layers were modeled using brick type hexahedral elements, the modeling approach initially begin with the construction of a solid layer with thickness of 4mm, later, this solid layer was divided into opening with sizes of 30x30mm along the full width and length of the geogrid layer so as to model the assumed aperture structure. Localized thickness changes in the junction points were ignored due to their minimal effects on the accuracy of the obtained results (Hussein and Meguid, 2016). The same cuts were also made in the soil section in contact with geogrid layers to ensure proper interaction definition among these materials. Figures 3.32a through 3.32c shows the model configuration assumed for geogrid layers, soil section in contact with these layers and deformation sustained by these layers when subjected to fault loading. Utilizing such an approach to model the cases incorporating geogrid increased the element number for these numerical models which in turn significantly affected the solution duration. Yet, such an approach was deemed necessary to ensure accuracy.

The solution algorithm involved the application of gravity loading followed by the fault load applied as displacement on the outer nodes of the moving soil block. The dynamic implicit method with a full Newtonian solution algorithm was also utilized for the geogrid reinforced models. A friction-based surface to surface contact was again assumed to exist among the geogrid and soil, as well as among the native soil and the buried steel pipe. In addition to the definition of the tangential behavior, the normal behavior of the system was also defined as hard contact. The mesh pattern chosen for these models has no difference from that of non-mitigated models except the inclusion of geogrid layers mesh pattern of which is shown in Figure 3.33. In this context a finer mesh region of 20m was adopted for

zones close to the fault trace (both for the pipe and the soil blocks), whereas the geogrid layer consists of constant mesh pattern along the length with members divided into mesh parts with sizes no larger than 10mm.

Definition of the mechanical properties of geogrid material required the employment of a constitutive material model able of accurately describing the beyond linear and inelastic behavior of the material under the applied fault loads. In this study this is achieved through the use of an elastic perfectly plastic material model based on Mises yield formulation with isotropic hardening defined through a flow rule, defined within ABAQUS as a data incorporating yield stresses and corresponding plastic strains all input as numerical data. The stress-strain data provided by manufacturers typically present the nominal or engineering properties of the material which cannot be directly input into the software without a pre-processing phase. This study followed the path proposed by Hussein and Meguid (2016) to obtain the required data. Briefly, this procedure initially uses the nominal stress-strain data to obtain the true stresses and strain. Later, these data is decomposed into its elastic and plastic components, where the true strain values are further processed to obtain the required plastic strains. Finally, the computed true stresses and plastic strain are input into the analysis model. Figure 3.34 schematically illustrates the adopted the computed stress-strain curve. Whereas Tables 3.11 and 3.12 summarize the assumed material properties of geogrid material and computed strain values respectively.

Table 3.11. Material properties of geogrid layers (Hussein and Meguid, 2016)

MATERIAL	**Apeture Size (mm)**	**Ult. Strength (kN/m)**	**Mass/Unit Area (g/m2)**	**Stiffness at 2% strain (kN/m)**	**Modulus of Elasticity (MPa)**
GEOGRID	30x30	20	215	292	605

Table 3.12. Stress-strain data for geogrid material model

σ_t (kPa)	**ε (%)**	**ν**	**σ_{ttrue} (kPa)**	**E_g (kPa)**	**ε_{el} (%)**	**ε_{etrue} (%)**	**ε_{pl} (%)**
0.00	0.00	0.30	0.00	60500	0.0000	0.0000	0.0000
4615.39	0.01	0.30	4643.21	60500	0.0077	0.0100	0.0000
7500.01	0.02	0.30	7590.83	60500	0.0125	0.0198	0.0073

Table 3.12. Stress-strain data for geogrid material model (cont'd)

σ_t (kPa)	ε (%)	ν	σ_{ttrue} (kPa)	E_g (kPa)	ε_{el} (%)	ε_{etrue} (%)	ε_{pl} (%)
10000.02	0.03	0.30	10182.48	60500	0.0168	0.0296	0.0127
11923.10	0.04	0.30	12214.48	60500	0.0202	0.0392	0.0190
13846.18	0.05	0.30	14271.10	60500	0.0236	0.0488	0.0252
15384.64	0.06	0.30	15953.81	60500	0.0264	0.0583	0.0319
16538.49	0.07	0.30	17255.61	60500	0.0285	0.0677	0.0391
17500.03	0.08	0.30	18371.27	60500	0.0304	0.0770	0.0466
18461.57	0.09	0.30	19500.37	60500	0.0322	0.0862	0.0539
19038.49	0.10	0.30	20234.34	60500	0.0334	0.0953	0.0619
19615.42	0.11	0.30	20977.06	60500	0.0347	0.1044	0.0697
20000.03	0.12	0.30	21521.70	60500	0.0356	0.1133	0.0778
20384.65	0.13	0.30	22072.75	60500	0.0365	0.1222	0.0857
20576.96	0.14	0.30	22420.75	60500	0.0371	0.1310	0.0940
20692.34	0.15	0.30	22688.35	60500	0.0375	0.1398	0.1023
20769.26	0.16	0.30	22916.44	60500	0.0379	0.1484	0.1105
20846.19	0.17	0.30	23146.97	60500	0.0383	0.1570	0.1187
20846.19	0.18	0.30	23294.02	60500	0.0385	0.1655	0.1270
20846.19	0.19	0.30	23442.46	60500	0.0387	0.1740	0.1352
20846.19	0.20	0.30	23592.33	60500	0.0390	0.1823	0.1433
20846.19	0.21	0.30	23743.65	60500	0.0392	0.1906	0.1514

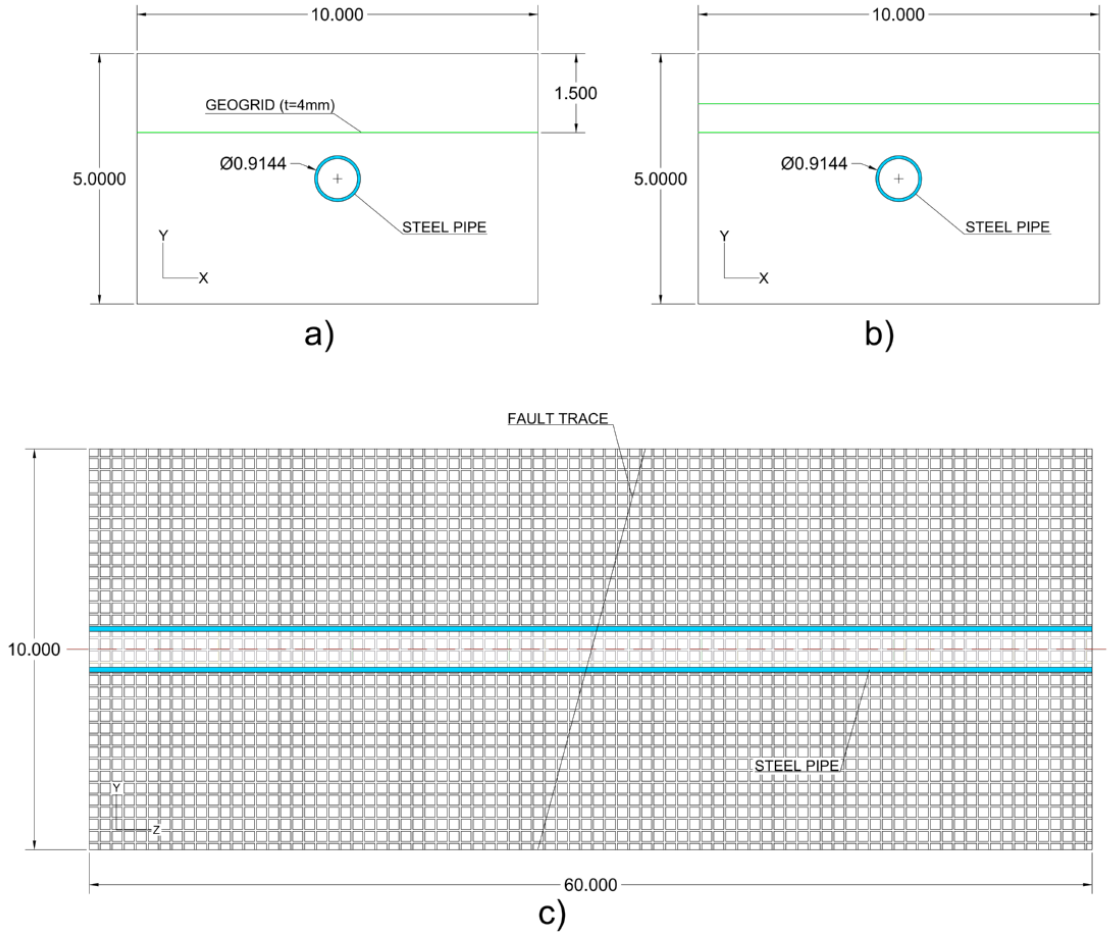

Figure 3.30. Numerical model configurations assumed for cases incorporating geogrid layers, a) single layer, b) double layer configuration, c) plan view

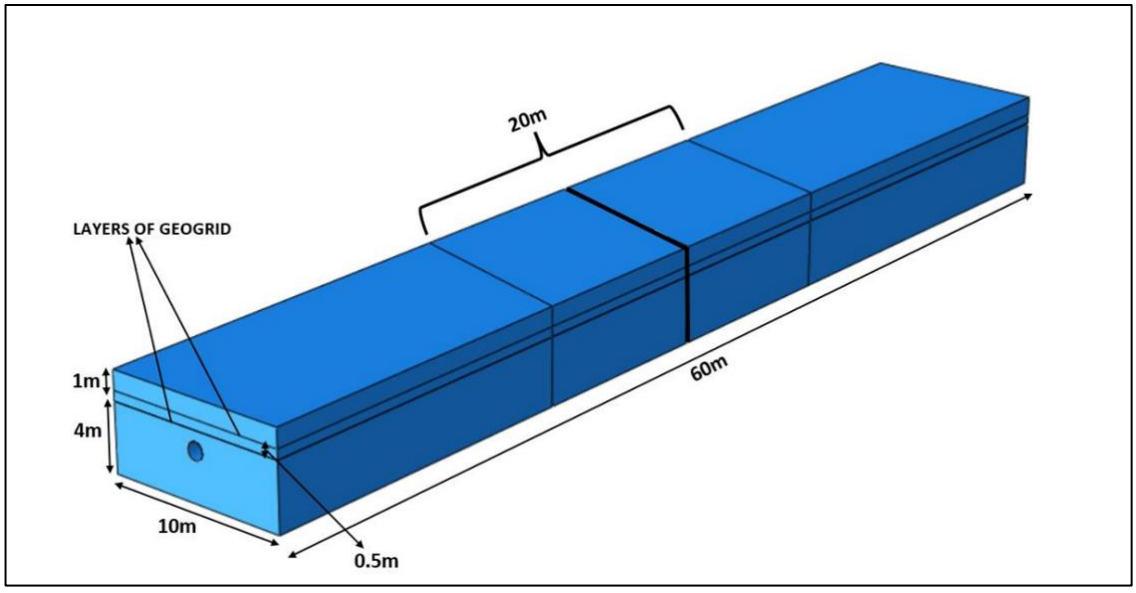

Figure 3.31. Model configuration used for analysis cases incorporating geogrid layers

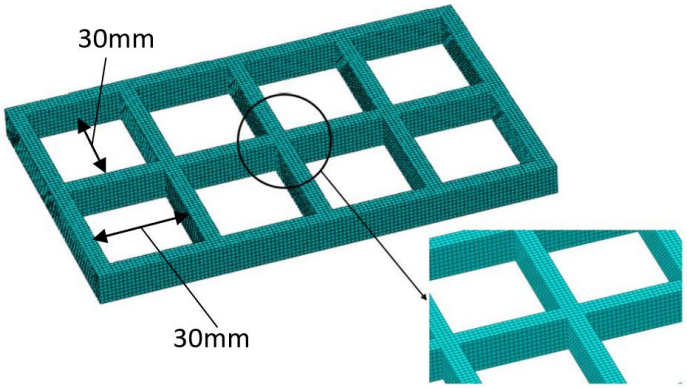

a)

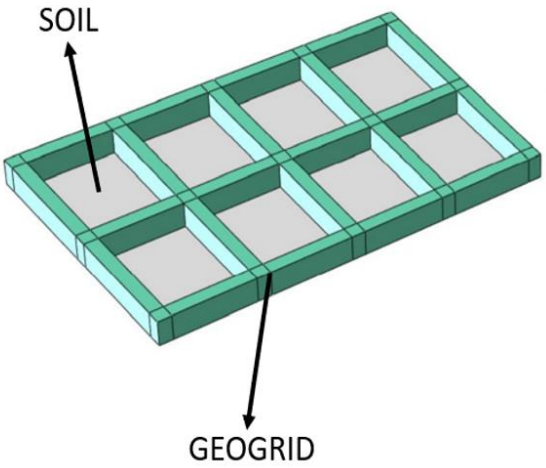

b)

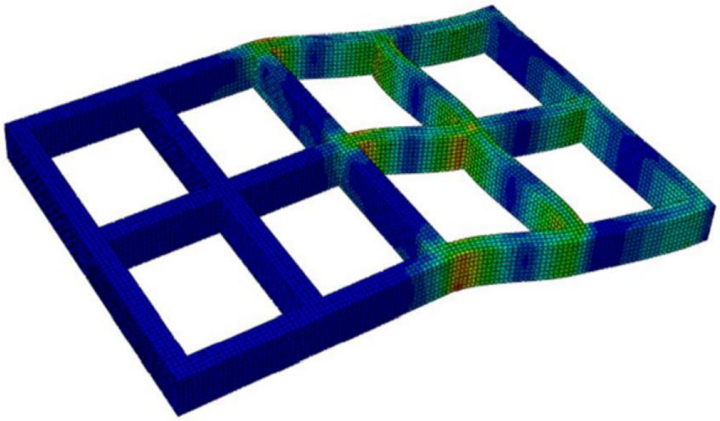

c)

Figure 3.32. Modelling details of geogrid layers; a) mesh pattern, b) participation of soil prism, c) deformation of geogrid layer under the applied fault load

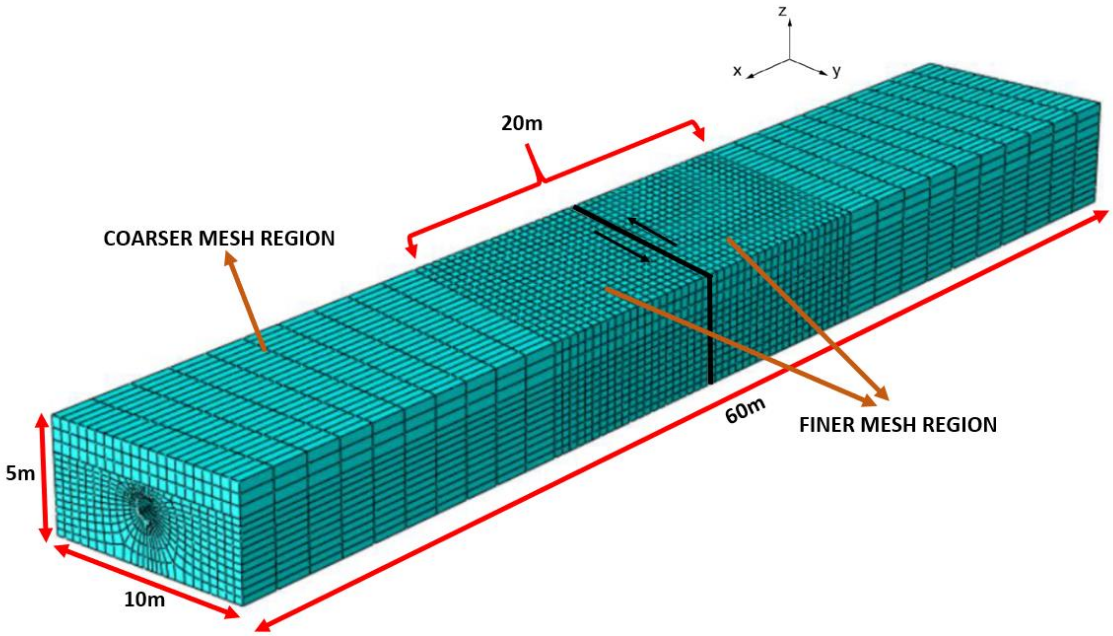

Figure 3.33. Numerical model configuration for cases incorporating the use of geogrid, model dimensions and partitioning

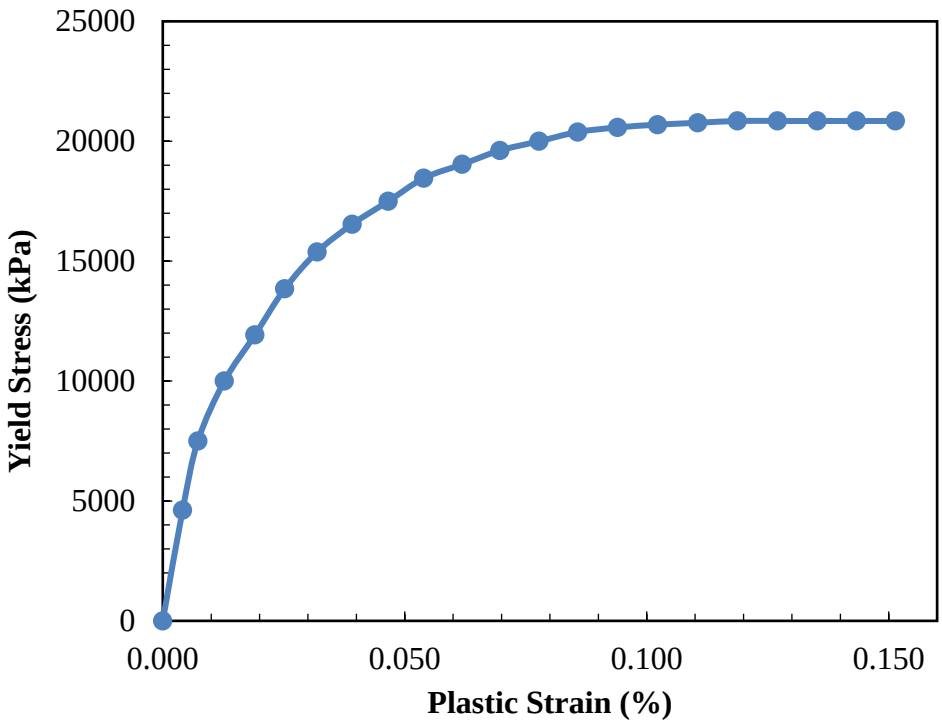

Figure 3.34. Stress strain curve utilized for material definition of geogrid layers

3.4. Performance Criteria Utilized for Buried Steel Pipes

Buried pipelines crossing active fault zones are subjected to large ground deformations leading to the accumulation of large forces and deformations typically exceeding well above the elastic limits of the steel material. Even though the steel material has a high-level ductility and ability to endure large amount of plastic deformations, yet at certain locations along pipeline subjected to fault displacements large tensile strains may develop and cause the pipe wall to rupture and eventually cause the formation of wrinkles (local buckling) at this sections of concentrated compressive strains. Moreover, a phenomenon known as cross-sectional distortion (ovalization) may occur under the effect of soil pressure sustained by the pipeline during the act of fault displacement.

In order to define the damage exerted onto a pipe at large ground displacementss, performance criteria (or limit states) based on pipeline steel and also mitigation material strain or deformation limits need to be defined. Following sections include the definition of limit states utilized in this study, namely: Maximum Tensile Strain limit state leading to the rupture of pipeline wall; Onset of Buckling Limit State; Distortion of the Cross Section of Pipeline, and Onset of Damage (Rupture, Cracking and etc.) in FRP, EPS geofoam, CLSM and geogrid materials at Tension Side of the Deformed Pipe Limit States are detailly described below.

3.4.1. Maximum Tensile Strain Limit State

Significant amount of tensile strain developing on pipeline wall during the seismic ground actions may lead to the rupture of the pipeline wall and eventually operational failure of it. Therefore, accurate estimation of the pipe strain capacity in tension is of paramount importance towards an efficient strain-based design approach. Typically for a steel pipeline possessing no existing fabrication related errors the tensile strain capacity is depended on the properties of girth weld, in particular to its strength (Kibey et al., 2010). There are two possible ways of determining the tensile strain capacity of a steel pipe: laboratory tension tests on steel specimens (ASCE, 2009) or using simplified formulations found in various

codes defining the specifications for pipeline design such as the one given in CSA Z662 standard for oil and gas pipelines (2007):

$$\varepsilon_{TM} = \delta^{(2.36-1.583\lambda-0.101\xi\eta)}(1 + 16.1\lambda^{-4.45})(-0.57 + 0.239\xi^{-0.241}\eta^{-0.315}) \quad (3.2)$$

where ε_{TM} is the pipe steel material ultimate strain capacity in tension, δ is the weld toughness, λ is the yield-tensile strength ratio, ξ is defined as the ratio of length over which defect has occurred on pipeline wall, and η is used to define the relation between the depth of the defect and the pipe wall thickness.

The study performed in this dissertation assumed tensile strain capacities of 3% and 5% to evaluate the performance of buried steel pipe under the applied fault displacement load. These values are found on several standards such as Eurocode 8 (2006) ASCE 2010 Standard (2010).

3.4.2. Onset of Local Buckling Limit State

In addition to the development of areas of large tensile strain concentration the act of large fault deformations may also induce large bending deformations under which the pipeline tends to sustain large compressive strains. Whenever these compressive strains attain values larger than the threshold value (limit state) a pipeline structural deformation manifested in the form of pipeline wall wrinkling (i.e. local buckling) may take place. Despite being structurally instable due to these wrinkles, yet if the ductility of the pipeline steel material is high enough the pipeline may still remain functional. However, due to the concentration of significant amounts of compressive strains, if the pipeline is subjected to cyclic patterns of loading that fatigue cracks may develop and hinder the structural safety and integrity of the pipeline or these buckles may restrict the passage of pipeline content (Dama et al., 2007; Das et al., 2008). In literature there exist a significant number of formulations derived for the estimation of strain value causing local buckling. Some of these are summarized in the below.

Dash and Jain Formulation (2007):

$$\varepsilon_{cu} = 0.6\frac{2t}{D} \quad (3.3)$$

where ε_{cu} is the pipe steel material ultimate strain capacity in compression, t is the wall thickness of the pipe and D is its external diameter.

Gresnigt (1986) formulation based on internal pipeline hoop stresses σ_h:

$$\varepsilon_{cu} = 0.5\frac{t}{D} - 0.0025 + 3000\left(\frac{\sigma_h}{E}\right) \tag{3.4}$$

In the present study the formulation defined by Gresnigt (1986) was adopted for the definition of local buckling limit state.

3.4.3. Pipeline Cross-Sectional Distortion Limit State

Among the structural problems occurring at pipelines subjected to large fault displacement is the restriction of the flow of pipeline content as a result of excessive pipeline cross-section deformation that typically occurs as a sectional ovalization. This type of cross-sectional distortion is simply quantified by means of a dimensionless parameter known as the flattening parameter f, calculated as follows (Gresnigt, 1986) :

$$f = \frac{\Delta D}{D} \tag{3.5}$$

where ΔD is the change of the outer diameter of pipe and D is the initial pipeline diameter.

The limit value of this performance parameter utilized in this thesis is equal to 0.15 based on the research published by Dutch standard NEN 3650 (2006).

3.4.4. Damage Limit States for FRP, EPS Geofoam, CLSM and Geogrid Materials

For cases incorporating the evaluation of the effect of using FRP wraps for seismic damage mitigation purposes the limit state which involves the rupture of the wrap at the tension side of the buckled pipe is important. The reason behind this is based on the assumptions made during the development of the numerical models. In the developed models it was primarily assumed that there exists a “hard” contact among the pipe and the FRP wrap meaning that these two were considered to be inseparable during the act of fault loading.

This assumption leads to the conclusion that both the pipe and FRP composite will undergo the same amount of damage and strains under the applied load. So basically, the tensile strain acting on the pipe will also be sustained by the FRP wrap. The approach utilized in this thesis assumes that the direction of the fibers of each FRP type stretches along the pipe length, hence, whenever the maximum strain limit corresponding to tension exceeded wraps limit of strain corresponding to ultimate tension along the fiber direction the pipeline external surface also begins to experience the same amount of tensile strain. The value of ultimate tensile strain for each FRP type was determined simply by using the Elastic Young Modulus values since the behavior of this composites is essentially linear up to its rupture. The calculated value for each FRP type studied are as follows:

CFRP: $\varepsilon_{TU} = \frac{2400}{1000*138} = 0.01452$

GFRP: $\varepsilon_{TU} = \frac{1200}{1000*55} = 0.02182$

BFRP: $\varepsilon_{TU} = \frac{500}{1000*25} = 0.02000$

The damage limit state utilized for the second mitigation approach incorporating the use of EPS geofoam blocks was derived based on the true stress-strain curve of the material (see Figure 3.23.) computed using the approach described in Subsection 3.3.3. The peak true strain value ($\varepsilon_{true} = 0.1398$) obtained using this method was adopted for both low and high strength EPS geofoam material as it was assumed that the material would fail once reaching this strain values. A similar approach was also assumed to determine the limit states for CLSM geogrid material. The peak inelastic strain (see Tables 3.9 and 3.10) calculated using the related approach were utilized for CLSM mixtures, while the computed peak true strain value (see Table 3.12) was utilized for geogrid meshes.

4. ANALYSIS RESUTLS OF NUMERICAL MODELS

4.1. Introduction

This chapter presents the analysis results of the numerical models developed following the outlines described in Chapter 3. Prior to the evaluation of the response of buried pipe configurations aimed to be investigated within the scope of this thesis, a validation procedure involving the recreation and analysis of a buried pipe model (Vazouras et al., 2012) published and widely accepted to be among the pioneering works in this field was adopted to verify the acceptance of the path and method employed for the models of this study.

Following sections of the chapter present the performance and response assessment of buried pipes possessing varying D/t ratios and angles of intersection β with the idealized fault plane. The developed numerical models were capable of providing stress and strain outputs along the length of the buried for each increment of the applied fault displacement load. Hence, graphical, and numerical distribution of strains along the buried pipe were initially obtained for certain fault displacement values and compared to assess the effect of this design parameters on the performance of buried steel pipes subjected to strike-slip faulting actions. A strain-based evaluation approach applied through the close monitoring of limit states for maximum tensile strains of 3% and 5%, onset of local buckling, and cross-sectional distortion defined per the flattening or ovalization factor served the basis for the assessment of the seismic performance of these investigated cases. Identification of the critical fault displacement value d_{cr} leading to the exceedance of these criterial expressed in terms of limit states served as a crucial way towards a clear understanding of the response of buried pipes possessing differing properties.

Later parts of the chapter cover the evaluation of the response of buried pipes incorporating the use of various strategies to mitigate the seismic demands imposed by strike-slip fault actions. In particular, cases involving the use of three fiber reinforced composites (CFRP, GFRP, and BFRP) with layer thicknesses varying between 3mm and 10mm, EPS geofoam blocks with varying strength classes, controlled-low strength material encasements of again varying strength classes, and geogrid reinforcement of single- and double-layer configurations were numerically modeled as described in Chapter 3 and

analyzed under the applied fault displacement load range. Similar to the evaluation of cases with varying D/t and angle β values initially strain distributions corresponding to various loading states were obtained and graphically compared. Later d_{cr} values leading to the structural failure of the buried pipe were determined and compared. In addition, plots showing the development of both tensile and compressive strains with respect to the applied fault load along with the respective limit values were utilized to better comprehend and visualize the efficiency of these mitigation approaches. Moreover, distribution of Von-Mises stresses at certain fault displacements were recorded and graphically presented for comparison purposes. The chapter closes with the comparison of the utilized mitigation approaches in terms of strain distribution and degree of change in critical fault displacement values, a cost comparison between the selected approaches is also provided at the end of the chapter to enable the assessment of the cost-efficiency of these mitigation strategies.

4.2. Validation of the Numerical Modeling Approach

Prior to the analysis of the intended cases of buried steel pipes and investigation of the influence of design parameters such as the D/t ratio and pipe-fault intersection angle β the path followed for the development of analysis models need to be somehow verified. For this purpose, the numerical modeling pattern developed by Vazouras et al. (2012) which as shown in Figure 4.1 involved the analysis of a buried pipe subjected to the action of a strike-slip fault with a fault intersection angle of β equal to zero degrees was redeveloped. The interacting soil-pipe system was accepted to be embedded within a stiff clay soil properties of which are summarized in Table 4.1. The model configuration developed in the present study is shown in Figure 4.2.

As illustrated in Figures 4.3a and 4.4a the study of Vazouras et al. (2012) investigated the performance of buried pipes via the extraction of maximum axial strain data both in compression and tension side of the buckled pipe under a variety of fault displacement load values. Moreover, the study also depicts the distribution of longitudinal pipeline strains under various fault load values as can be seen in Figure 4.5a. To validate the accuracy of the methodology undertaken to create the same pipe model (which also is the same approach used for the rest of the cases investigated in this study) the model was analyzed under a fault displacement range of 0-4m with intermediate increments of 10mm. The axial strain values

corresponding to the fault displacements shown in Figure 4.3a and 4.4a were taken from the developed model and the same plot was constructed and used for comparison. The obtained data are shown aside the plots derived by control study in Figures 4.3b and 4.4b for the compression and tension sides respectively. The path along which these strains values are derived is depicted in Figures 4.3c and 4.4c. In addition to axial strains the distribution of longitudinal strains along the pipe was also graphically taken from the analysis model for fault displacement value equal to 1m. Figures 4.5a and 4.5b show and compare the longitudinal strains obtained from the two models.

Graphical comparison of the obtained results indicates a clear coherence in between the models. The plots appear to be in accordance with each other both in terms of magnitude and shape. Furthermore, comparison of the distribution of longitudinal strains shows that the resulting maximum longitudinal strain under a fault displacement load of 1m is almost equal for the two models (0.105 and 0.100 respectively). The overall good agreement among the obtained results was accepted and served as a solid validation source for the models developed within the scope of this study.

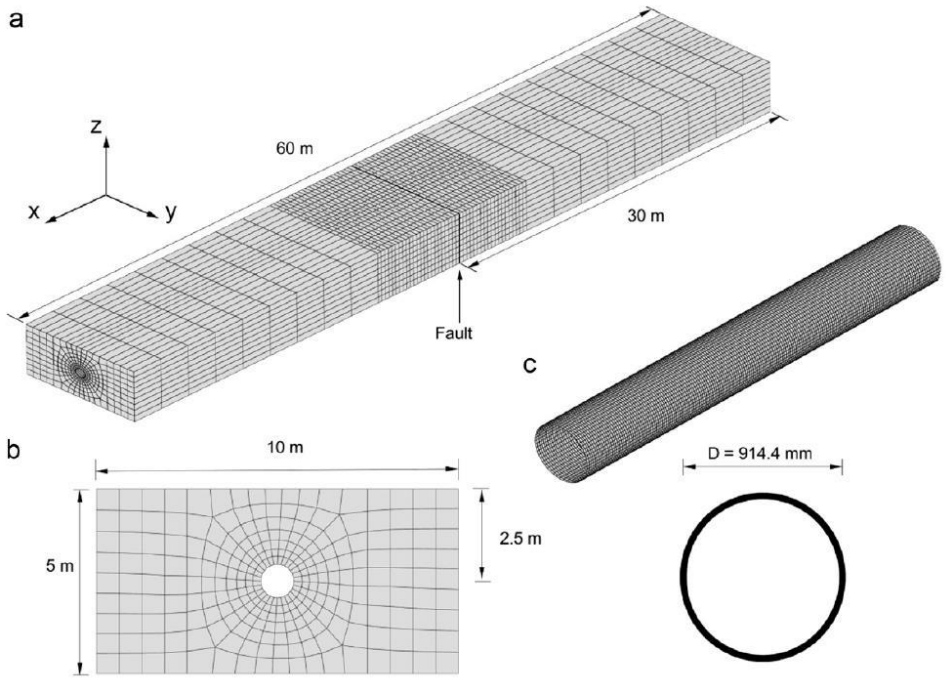

Figure 4.1. Configuration, dimensions, and meshing pattern of the numerical model developed by Vazouras et al. (2012)

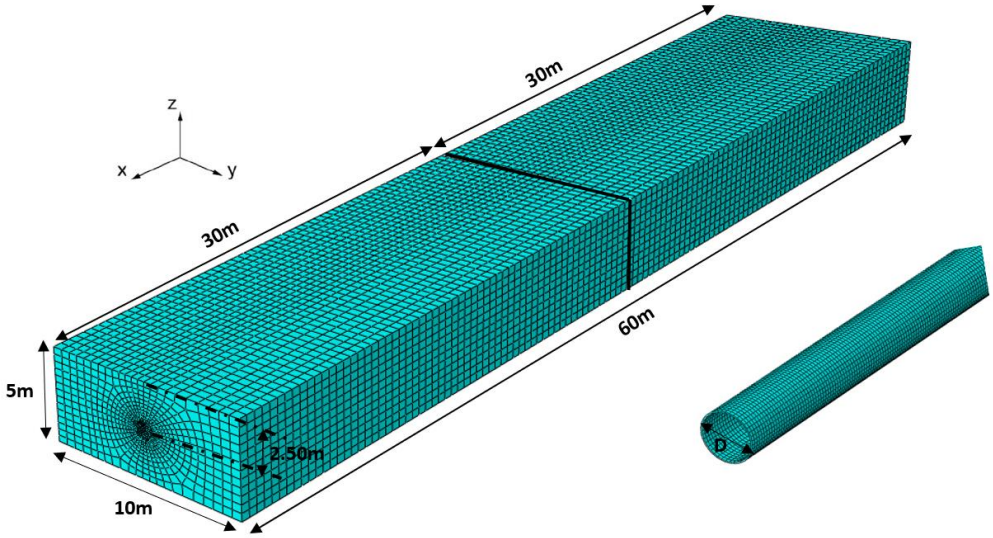

Figure 4.2. Configuration, dimensions, and meshing pattern of the numerical model developed for validation purpose

Table 4.1. Backfill soil properties used for the validation model (Vazouras et al., 2012)

Soil Type	**c (kPa)**	**ϕ (º)**	**γ_{sm} (kN/m^3)**	**E_s (MPa)**	**δ (º)**	**ν**	**ψ (º)**
Stiff Clay	200	0	21	100	25	0.50	0

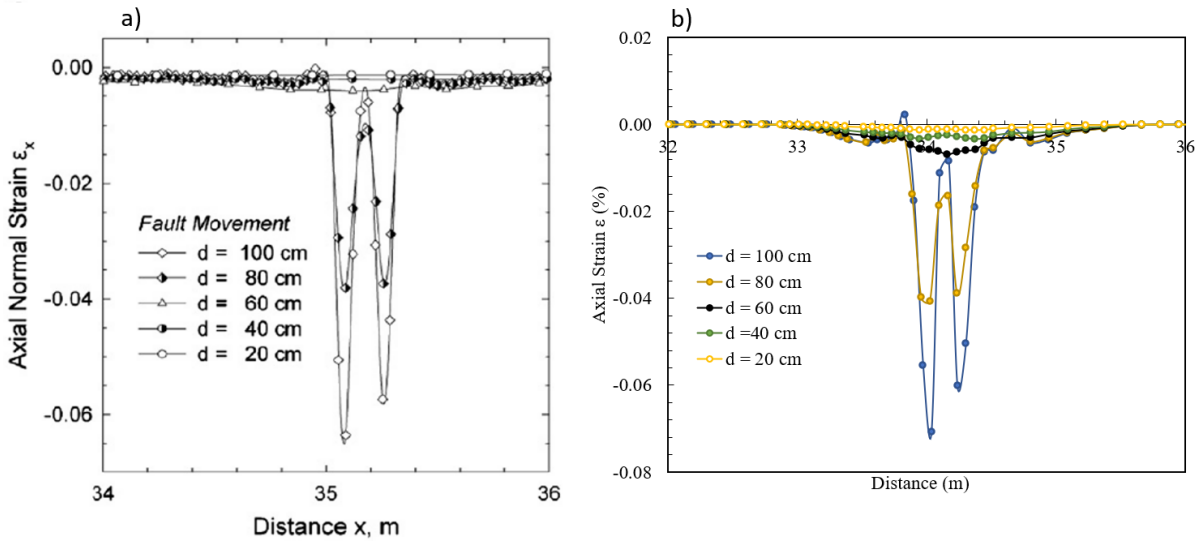

Figure 4.3. Comparison of results in terms of axial strains recorded at the deformed pipe side subjected to compression; a) Vazouras et al. (2012); b) developed model

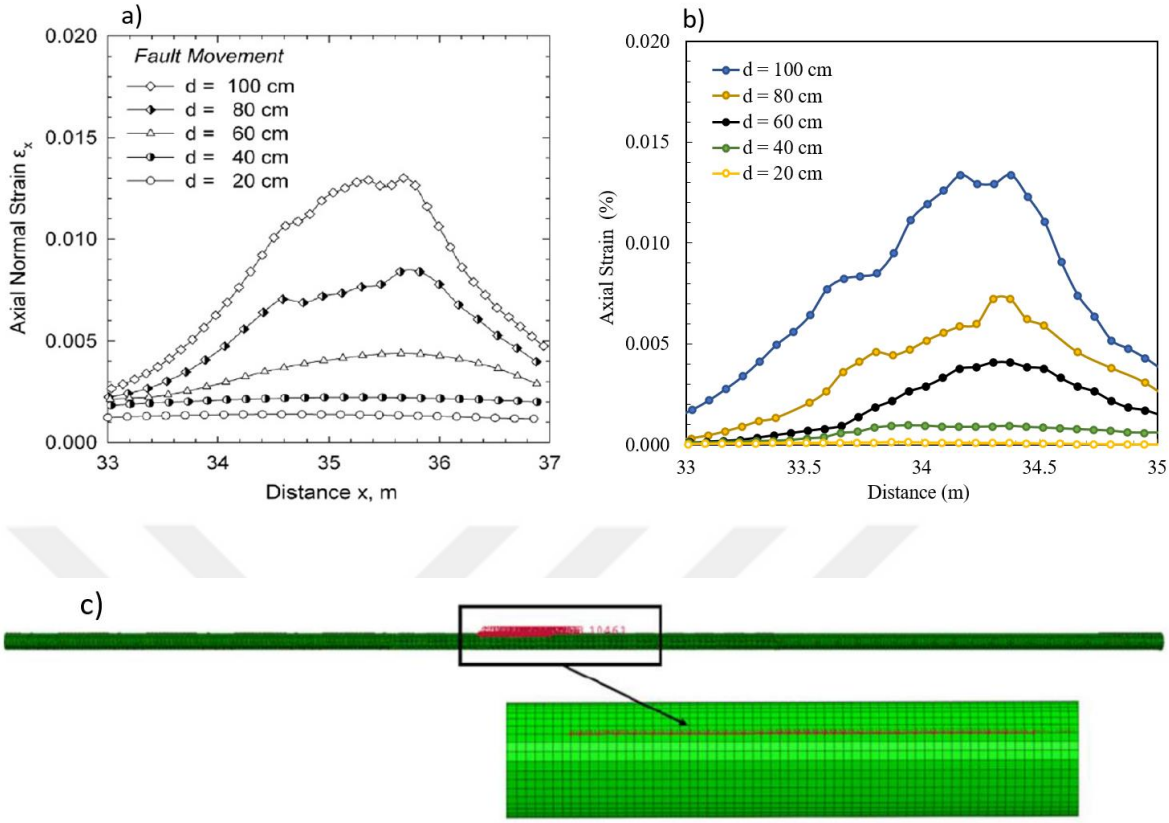

Figure 4.4. Comparison of results in terms of axial strains recorded at the deformed pipe side subjected to tension; a) Vazouras et al. (2012); b) developed model; c) path used to derive the strains

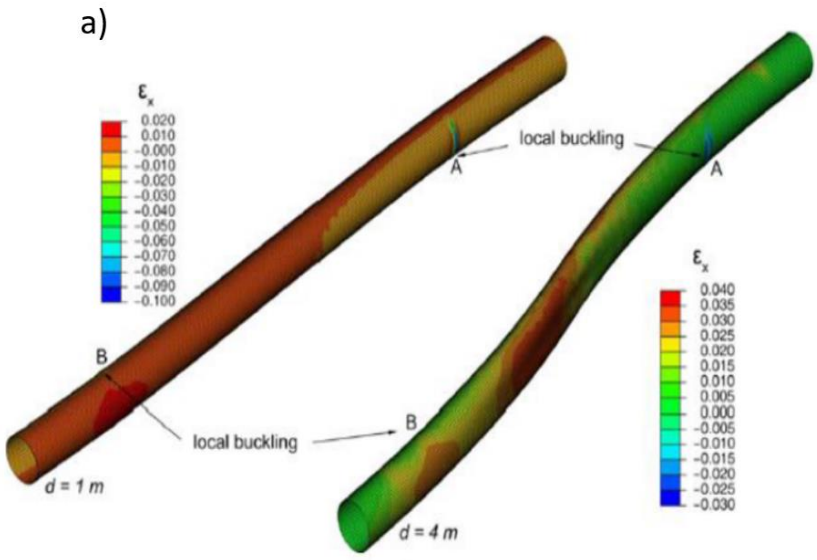

Figure 4.5. Comparison of results in terms of distribution of longitudinal pipeline strains; Vazouras et al. (2012); b) developed model

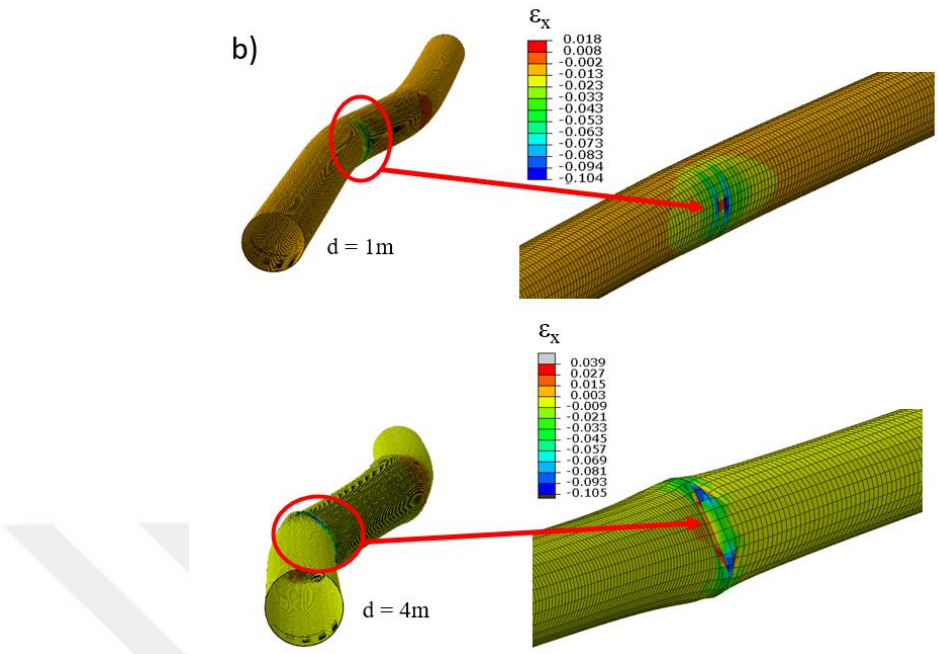

Figure 4.6. Comparison of results in terms of distribution of longitudinal pipeline strains; Vazouras et al. (2012); b) developed model

Apart from the comparison with the numerical models of Vazouras et al. (2012), two of the physical test models developed by Oskouei et al. (2019) to estimate the response of buried steel pipes under strike-slip fault actions were numerically modeled using the methodology adopted in this thesis. As detailly described in under Section 2.4, this experimental program aimed at the investigation of the effect of burial depth on the performance of buried steel pipes subjected to strike-slip fault actions. For this purpose, a test setup consisting of two steel boxes with length, width, and height equal to 3m, 1.5m, and 1.4m respectively was constructed. A total displacement load of 0.6m was applied incrementally on the box moving on rails through an actuator. Proper instrumentation was attached along the length of the buried pipe to measure applied load, as well as the generated stresses and strains.

The SM01 and SM02 test setup incorporating the testing of buried steel pipes with an outer diameter (D) of 0.0634m, wall thickness (t) of 3.2mm and 5.2mm respectively, and burial depth (H) equal to 0.36m and 0.887m respectively were numerically modeled using ABAQUS CAE (2020) software and following the approaches detailly described under Chapter 3. Figures 4.7 shows the numerical model developed for these physical test cases.

The material properties for pipe steel and the soil deposit were determined per laboratory tests performed prior to the actual pipe physical tests. The grade of the pipe steel material was API 5L with a yield stress (σ_y) of 391MPa, a yield strain (ε_y) equal to 0.00175, while the ultimate stress (σ_u) and strain (ε_u) were equal to 453MPa and 0.0137 respectively. The soil around the tested buried pipes was a sea sand with a measured unit weight (γ_s) of 13.5 kN/m^3, and internal friction angle (δ) equal to 38^o. The Mohr-Coulomb constitutive material model was again utilized to model the soil behavior. The friction coefficient required to define the interaction at soil pipe interfaces was taken to be 0.4 following a short parametric study. As shown in Figure 4.8 a fault load increasing from 0m to 0.6m was applied incrementally on the moving soil block to simulate the displacement load applied in the experimental study. The fault crossing angle in these models was equal to 90^o.

Strain gauges attached on the buried pipe were capable of continuously measuring the longitudinal strains developing on the pipe under the applied displacements. The strains were later used to obtain the bending, axial, and shear strains on the pipe. Eventually the distribution of strains was reported as plots of strains recorded at gauge locations vs. the distance from fault trace. The developed numerical models were used to obtain the same data occurring at locations corresponding to the location of strain gauges. Figure 4.9 through 4.11 show the comparison of bending, axial, and shear strains obtained through physical tests (solid blue) and the developed model (dashed orange). Moreover, Figure 4.12 present the comparison of peak strains obtained from experiments (SM02 case) and solution of the numerical models. As evident, a good agreement with small discrepancies exists between experimental and numerical results, indicating the assumed modeling approach to be capable of yielding acceptably accurate results.

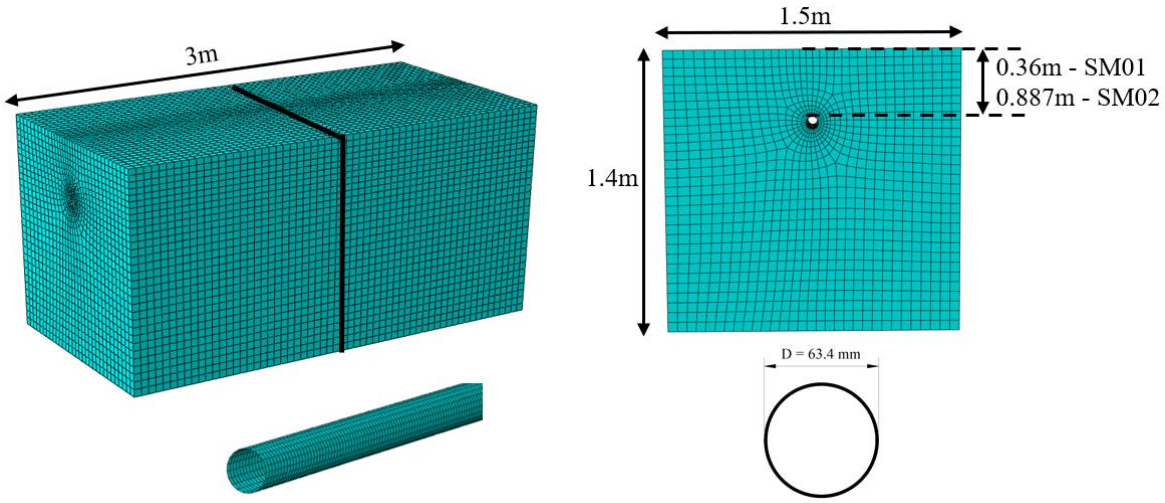

Figure 4.7. Configuration, dimensions, and mesh pattern of the numerical model developed for comparison with experimental studies of Oskouei et al. (2019)

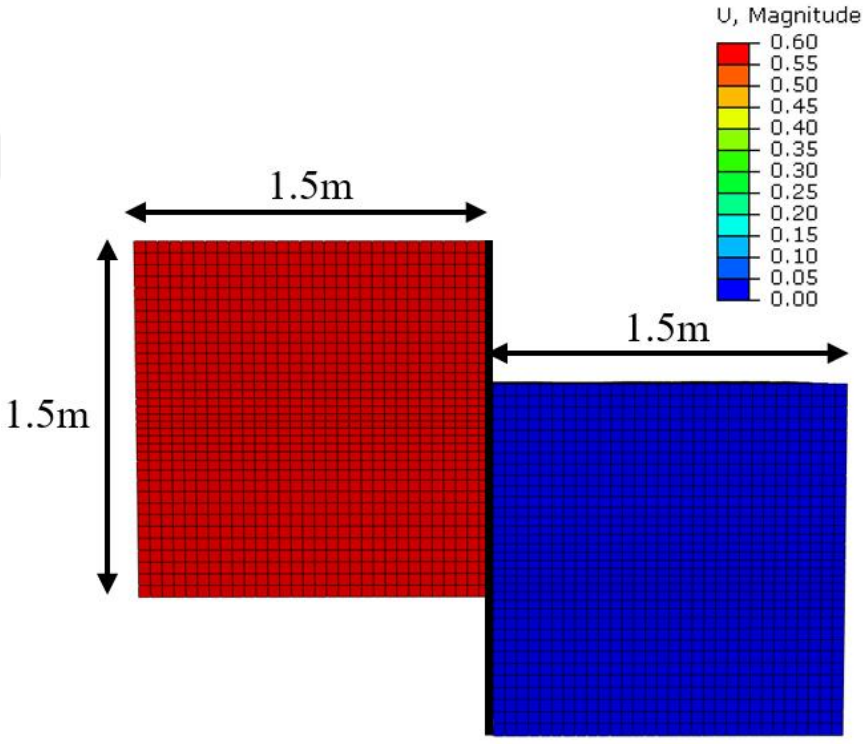

Figure 4.8. Plan view of the moving soil block (red) displaced under the fault load applied as displacement with a peak magnitude of 0.6m

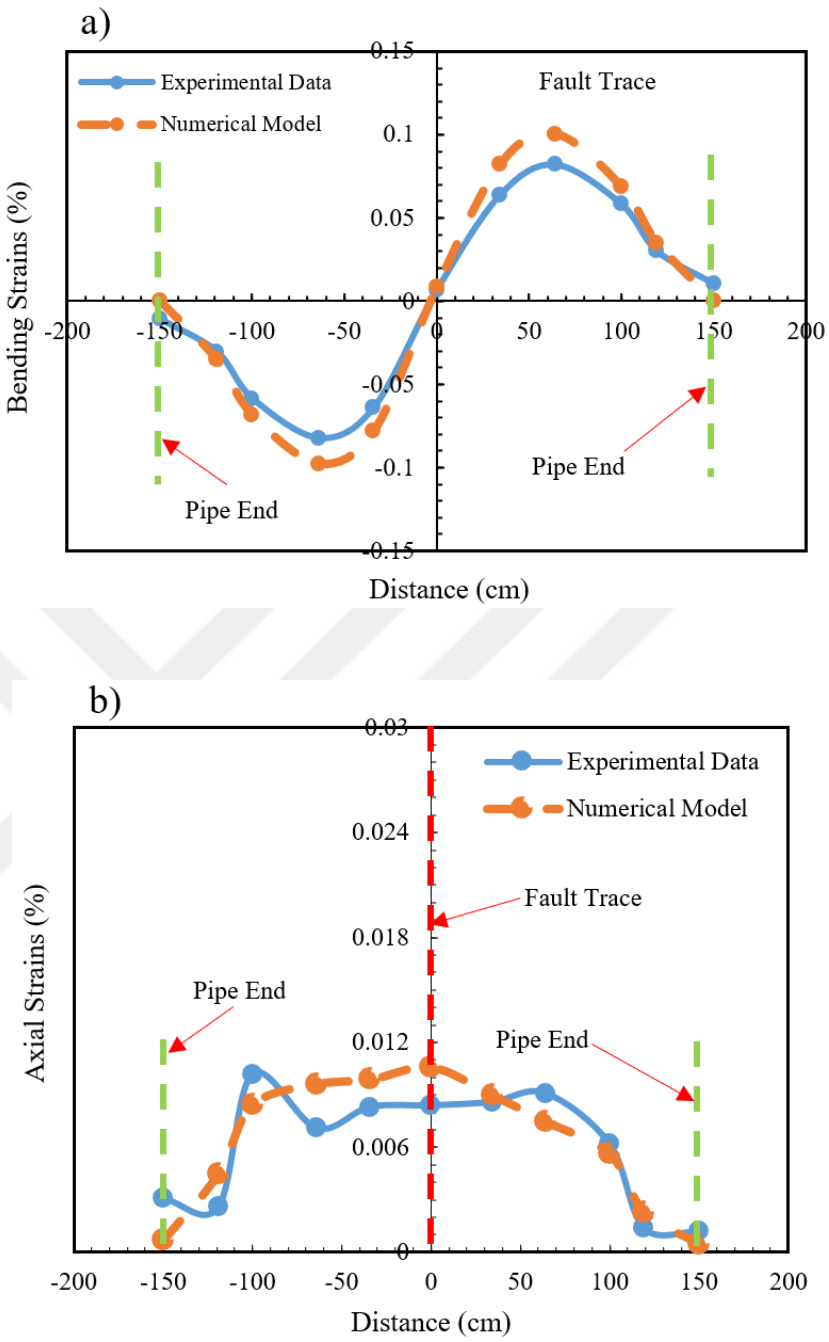

Figure 4.9. Comparison of results obtained through physical test models and numerical predictions, a) bending strains, b) axial strains, and c) shear strains under fault displacement of 0.6m

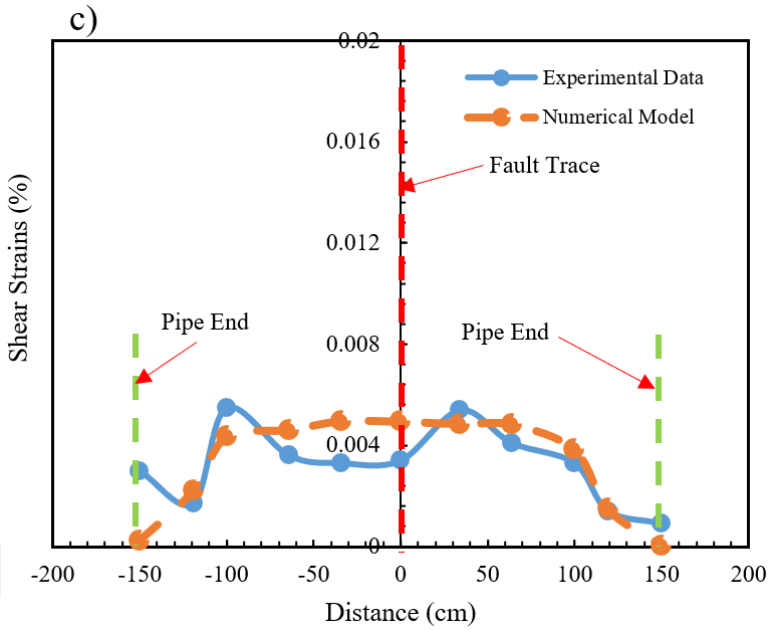

Figure 4.9. Comparison of results obtained through physical test models and numerical predictions, a) bending strains, b) axial strains, and c) shear strains under fault displacement of 0.6m

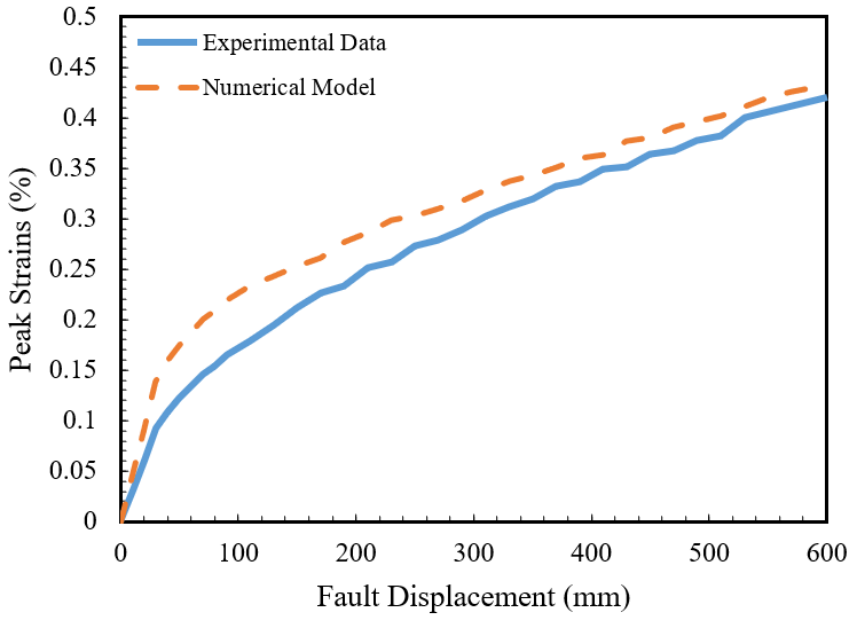

Figure 4.10. Comparison of peak strains under incremental fault displacements obtained through physical test models and numerical predictions

Lastly, the experimental test models developed by Demirci et al. (2021) for HDPE pipes were numerically simulated to verify the acceptance of the modeling approach utilized in this thesis. As described under Section 2.4 the experimental setup developed by Demirci et al. (2021) consisted of two aluminum frame boxes, filled with sandy soil. The combined length of boxes was 2m whereas the width and height were 1m and 0.75m respectively. The actual length of the pipe inside the box was 1.7m, whereas the depth of soil deposit was 0.5m. An electric actuator connected to the moving box imposed a total displacement of 0.3m to simulate the strike-slip fault action, while the second boxed remained stationary. A total of 10 strain gauges attached to cylindrical pipe spring lines and located at 5 locations along the length of the pipe were employed to record the longitudinal strains on the pipe. Four buried pipe configurations were subjected to this experimental evaluation scheme to assess the influence of various design parameters such as burial depth, wall thickness, orientation angle, and soil-pipe relative stiffness.

Among the physical tests performed within the scope of the mentioned experimental study, the model test coded as T1 was numerically modeled to compare the result and assess the validity of the numerical modeling approach used for the development of the models in this thesis. This case incorporated the testing of a HDPE pipe with an external diameter of 50mm and wall thickness of 3mm. The elastic Young's Modulus (E_H) of the HDPE material was 750MPa while the yield strength (σ_{yh}) was 14MPa. The soil deposit around the buried pipe was a silica sand with a unit weight of (γ_s) 13kN/m^3, Poisson's ratio (ν) of 0.40, internal friction angle (δ) of 34^o, dilation angle (ψ) of 6^o, and cohesion (c) equal to 0kPa. The developed numerical model configuration is presented in Figure 4.11. Displaced shape of model under the peak displacement value of 0.3m is shown in Figure 4.12.

The data obtained through these experiments enabled the investigation of the variation of axial and bending strains under different values of the applied displacement load. Moreover, peak bending strains obtained under incremental displacement load was also recorded. To allow comparison with experimental data, the axial and bending strains at the locations corresponding to the locations of strain gauges were obtained from the developed numerical model. Comparison of results obtained under the maximum displacement load of 0.3m presented in Figure 4.13a and 4.13b indicates that a good agreement exists between the results, with numerical model slightly overpredicting both the axial and bending strains.

In addition, Figure 4.14 presents the comparison of peak bending strains, results indicate that again the numerical model results in slightly increased strain values, where a larger deviation is noticed at smaller displacement values, an occurrence that might be related to the inability of the utilized Mohr-Coulomb constitutive material model to account for the strain softening phenomena for sandy soils under low levels of stress. Regardless of this, comparison of results indicate that the discrepancies are at negligible levels, hence, validating the utilized numerical modeling approach.

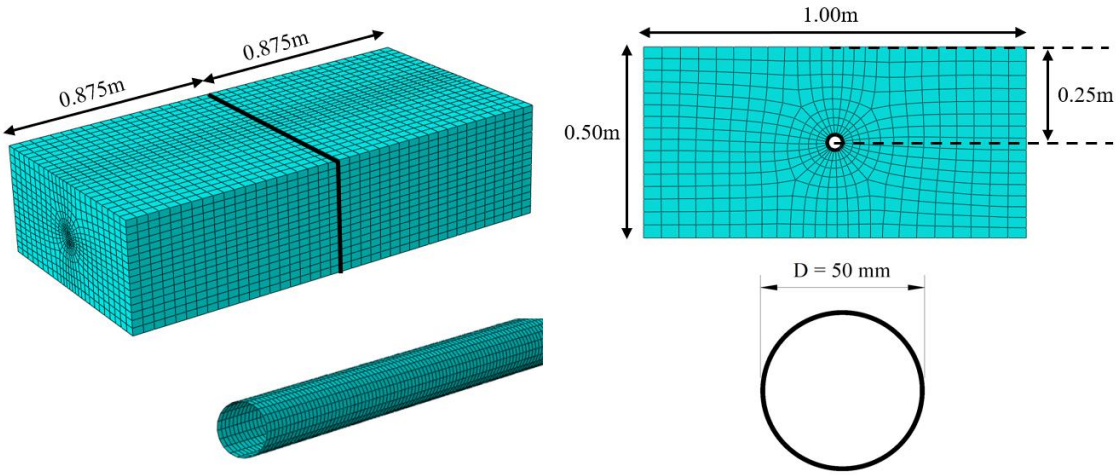

Figure 4.11. Configuration, dimensions, and mesh pattern of the numerical model developed for comparison with experimental studies of Demirci et al. (2021)

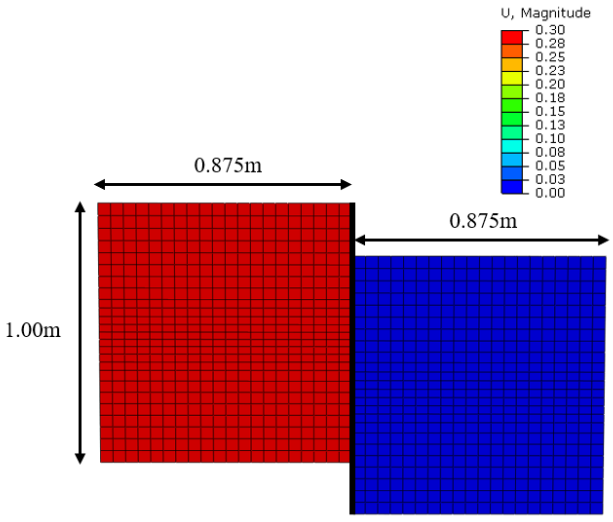

Figure 4.12. Plan view of the moving soil block (red) displaced under the fault load applied as displacement with a peak magnitude of 0.3m

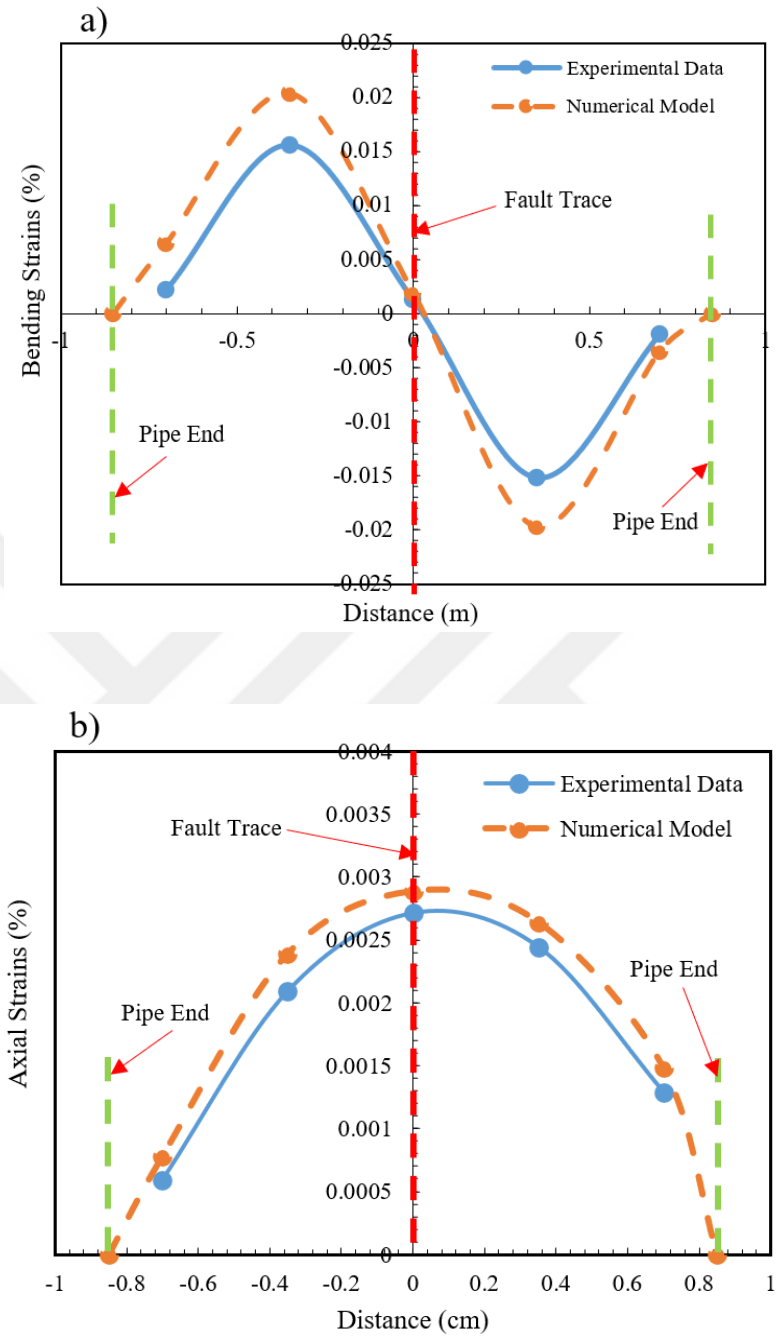

Figure 4.13. Comparison of results obtained through physical test models and numerical predictions, a) bending strains, and b) axial strains under fault displacement of 0.6m

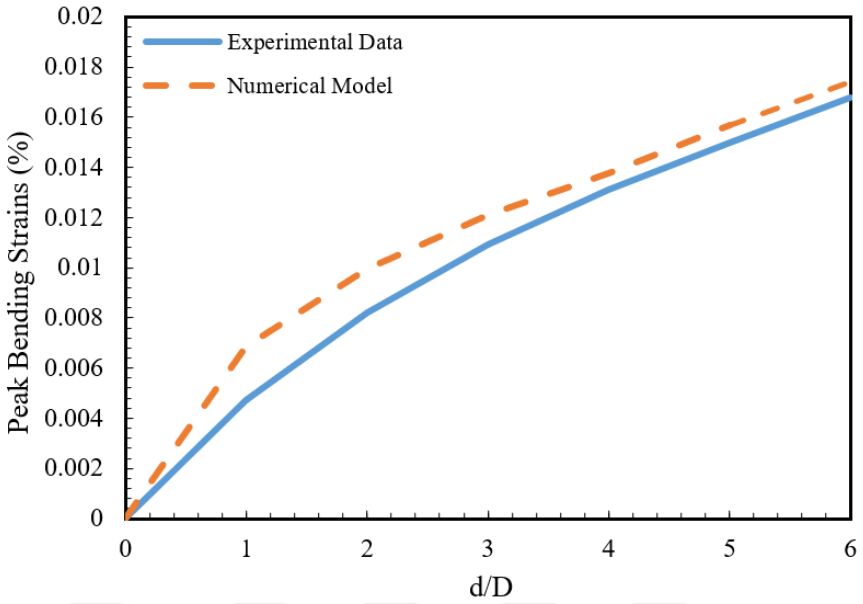

Figure 4.14. Comparison of peak bending strains under incremental fault displacements obtained through physical test models and numerical predictions

4.3. Influence of Fault Intersection Angle β On Buried Pipe Seismic Performance

Among the most critical factors influencing the seismic behavior of steel pipes exposed to ground-induced motion is the fault orientation angle β. Previous research on topic (Vazouras et al., 2010,2012, Karamitros et al., 2016) revealed that for negative β values the non-pressurized pipe dominantly suffers structural failure due to onset of local buckling appearing in form of a wrinkles on the walls of the pipe. Whereas, as the value of β gets larger the failure occurs either due cross-sectional distortion (related to the flattening parameter d) or reaching of maximum tensile strain limits of 3% and 5%.

In the present study the influence of the variation of fault intersection angle was investigated via developing numerical models for cases where the value of this angle was:

- $\beta = 10^{o}$
- $\beta = 15^{o}$
- $\beta = 30^{o}$

The fault load applied as a horizontal displacement load pattern on the external nodes of the moving soil block causes a gradual (step-by-step) evolution of stresses and strains on

the pipe. Figure 4.15 shows the initial (i.e., d = 0m) and final condition (d = 4m) of Von Mises stresses on a pipe subjected to strike-slip fault action.

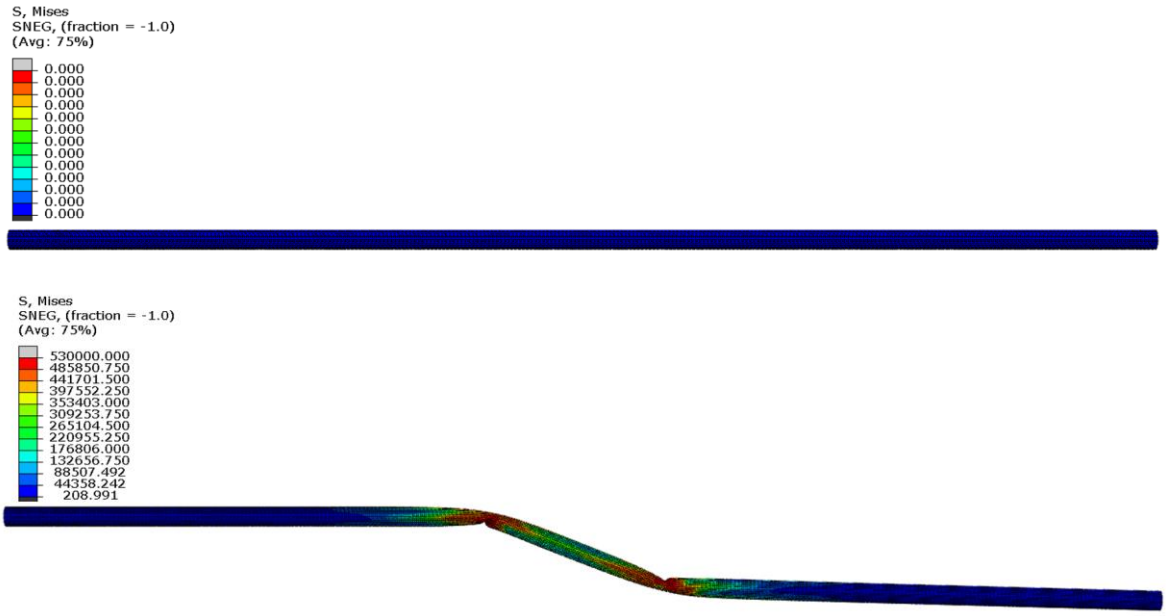

Figure 4.15. Von Mises stresses developed on buried pipe subjected to d = 1m (top) and b) d = 4m (bottom) fault displacement load

Review of analysis results presented in form of graphical and numerical distribution of longitudinal pipeline strains given in Figures 4.16a through 4.17c for fault displacement of 1m and 2m respectively indicates that strains reduce with the increment of fault intersection angle β, where a decrement of as much as 40% was observed for d = 1m. However, results suggest that under larger values of fault load this positive effect tends to reduce, where a reduction of only 36% is noted under d = 2m. Investigation of the change in axial strains developing on the tension and compression side of the buried pipe under fault displacement values of 0.5m, 1m, 1.50m, and 2m respectively given in Figure 4.18a through 4.19c points to a reduction in strain values with the increment of angle β value. However, similar to longitudinal strains this reductive effect loses its magnitude for increased values of fault displacement. Since a similar pattern was attained for D/t cases the data presented only show the cases for D/t = 144.

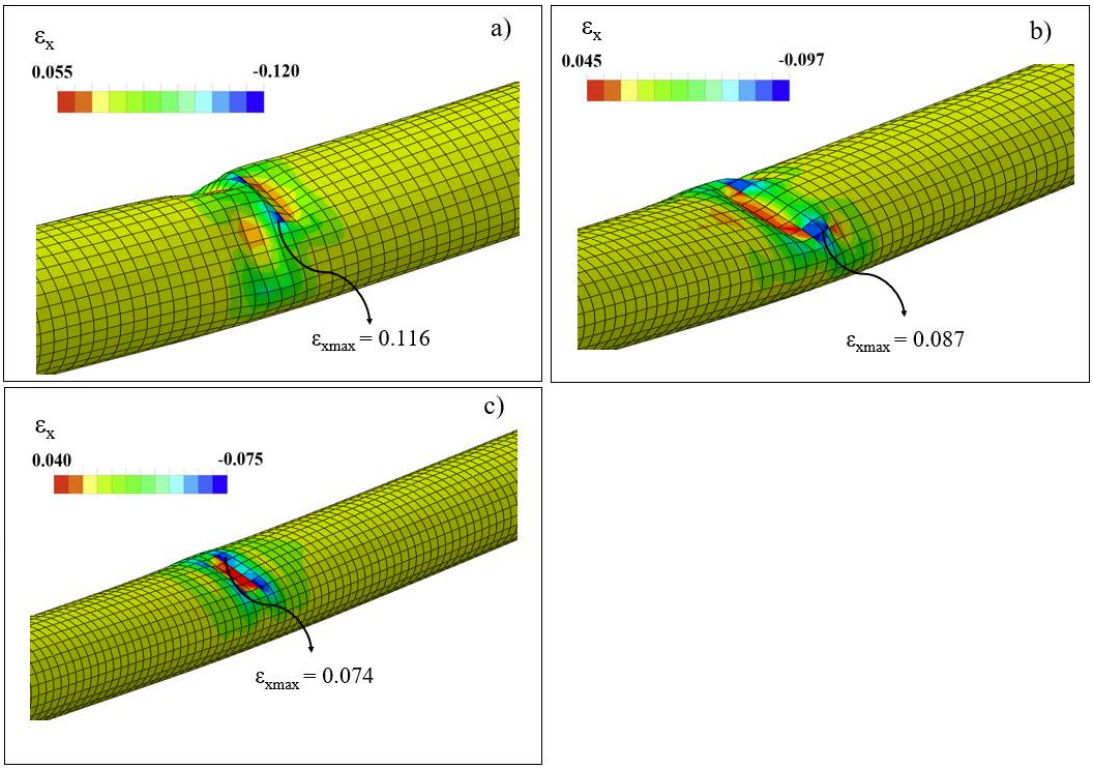

Figure 4.16. Comparison of the distribution of pipeline longitudinal strains for, a) $\beta = 10^o$, b) $\beta = 15^o$, and c) $\beta = 30^o$, where D/t = 144, and d = 1m

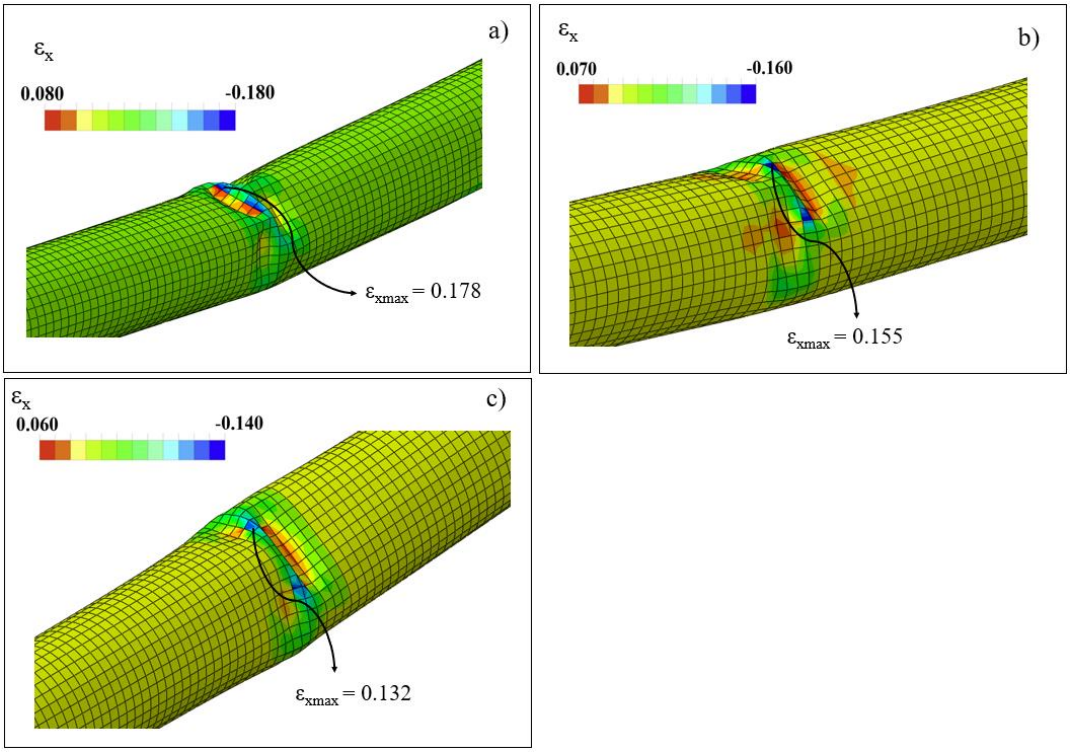

Figure 4.17. Comparison of the distribution of pipeline longitudinal strains for, a) $\beta = 10^o$, b) $\beta = 15^o$, and c) $\beta = 30^o$, where D/t = 144, and d = 2m

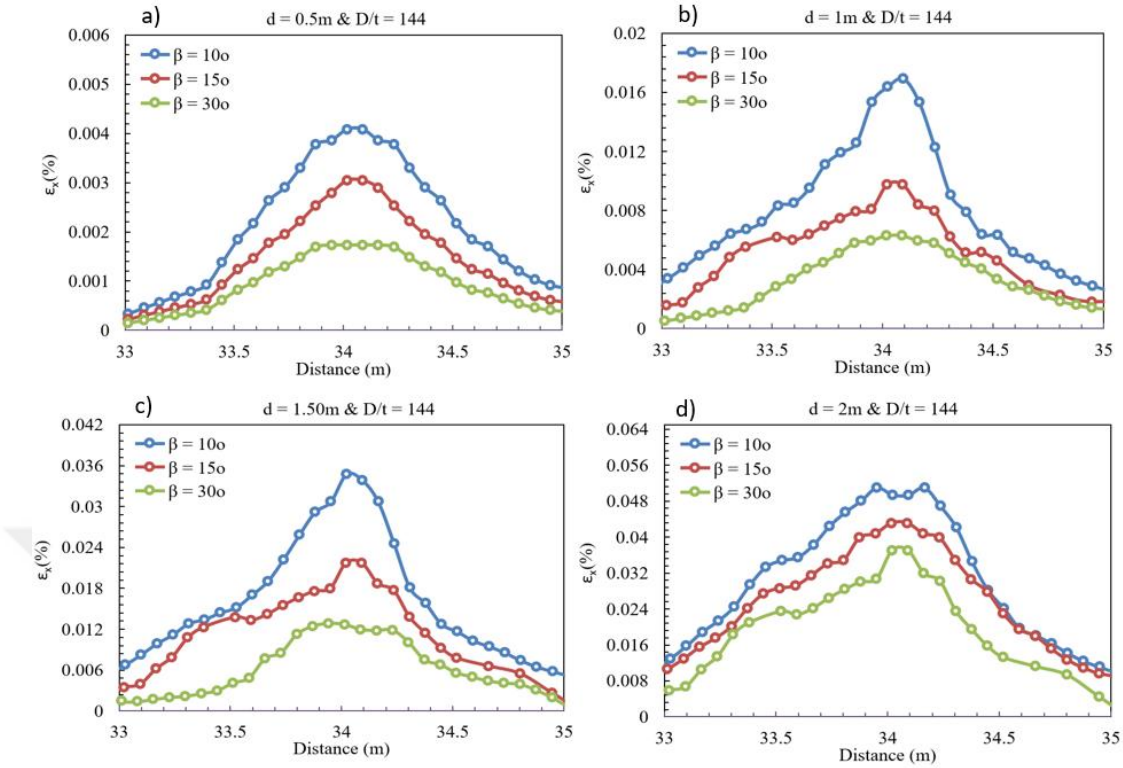

Figure 4.18. Variation of the distribution of axial strains recorded at the deformed pipe side subjected to tension for, β = 10º, β = 15º, β = 30º, D/t = 144, and a) d = 0.5m, b) d = 1.00m, c) d = 1.50m, and d) d = 2.00

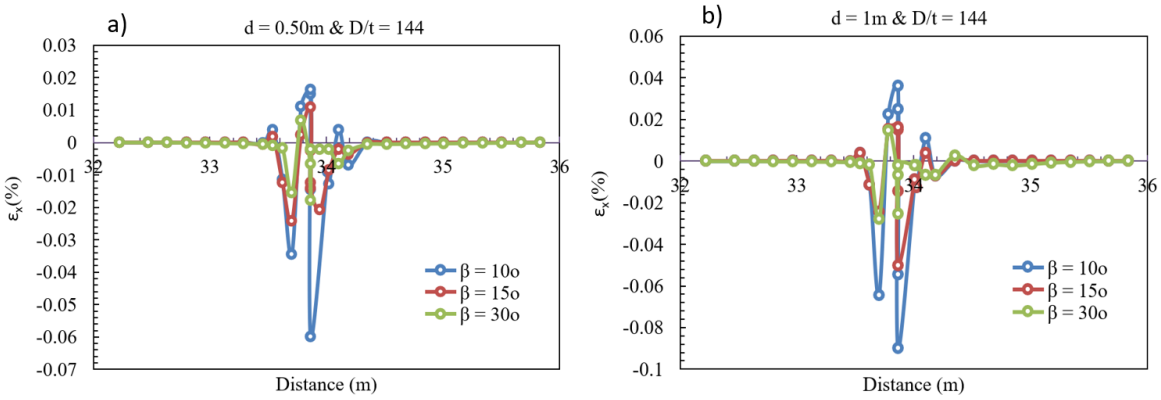

Figure 4.19. Variation of the distribution of axial strains at recorded at the deformed pipe side subjected to compression for, β = 10º, β = 15º, β = 30º, D/t = 144, and a) d = 0.5m, b) d = 1.00m, c) d = 1.50m, and d) d = 2.00

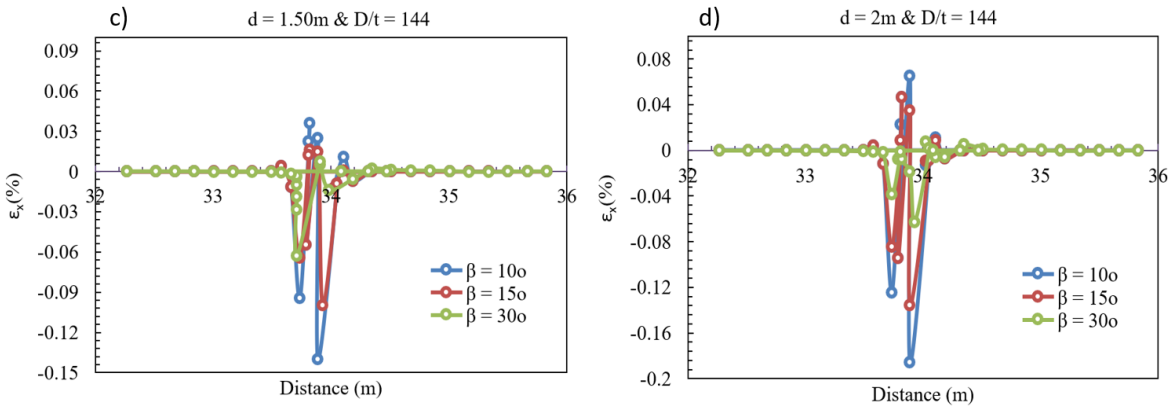

Figure 4.19. Variation of the distribution of axial strains recorded at the deformed pipe side subjected to compression, β = 10º, β = 15º, β = 30º, D/t = 144, and a) d = 0.5m, b) d = 1.00m, c) d = 1.50m, and d) d = 2.00

Evaluation of the response of studied buried steel pipe cases was also performed via deriving the critical values of fault displacement load leading to the occurrence of the pre-defined performance criteria (limit states). In particular, fault displacements resulting to the initiation of local buckling occurance defined based on Dash and Jain (2007), reaching the maximum tensile strain limits of 3% and 5% (per Eurocode 8, 2006) and cross-sectional distortion of the buried pipe defined based on the flattening parameter f taken to be equal to 0.15 according to Gresnigt (1986) were determined for each corresponding D/t ratio and β value. Tables 4.2 to 4.4 summarize the d_{cr} values determined for each limit state and for D/t = 144 and β = 10°, 15°,30° respectively. Figures 4.20 to 4.22 present the plots of normalized critical fault displacement (d_{cr}/D) versus fault intersection angle β for each limit state considered within the scope of this study. As depicted in this tables and figures mentioned above reducing the value of β adversely effects the performance of the pipeline since the d_{cr} value decreases for each limit state.

Table 4.2. Limit States and d_{cr} values for D/t = 144 and β = 10º

Limit State	**Limit State Value**	**d_{cr} (m)**
Maximum Tensile Strain (3%)	3%	0.41
Maximum Tensile Strain (5%)	5%	0.63
Onset of Local Buckling	$-9.73*10^{3}$	0.22
Cross-Sectional Distortion	f = 0.15	0.38

Table 4.3. Limit States and d_{cr} values for D/t = 144 and β = 15°

Limit State	Limit State Value	d_{cr} (m)
Maximum Tensile Strain (3%)	3%	0.46
Maximum Tensile Strain (5%)	5%	0.67
Onset of Local Buckling	$-9.73*10^{3}$	0.31
Cross-Sectional Distortion	f = 0.15	0.42

Table 4.4. Limit States and d_{cr} values for D/t = 144 and β = 30°

Limit State	Limit State Value	d_{cr} (m)
Maximum Tensile Strain (3%)	3%	0.51
Maximum Tensile Strain (5%)	5%	0.76
Onset of Local Buckling	$-9.73*10^{3}$	0.37
Cross-Sectional Distortion	f = 0.15	0.61

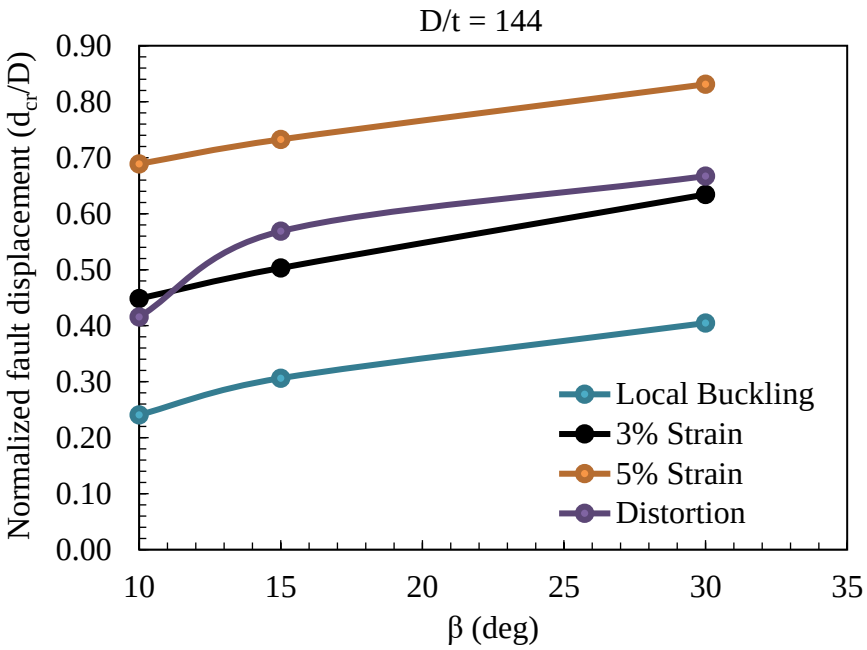

Figure 4.20. Variation of d_{cr} values corresponding to each limit state in regard to the variation of angle β and for D/t = 144

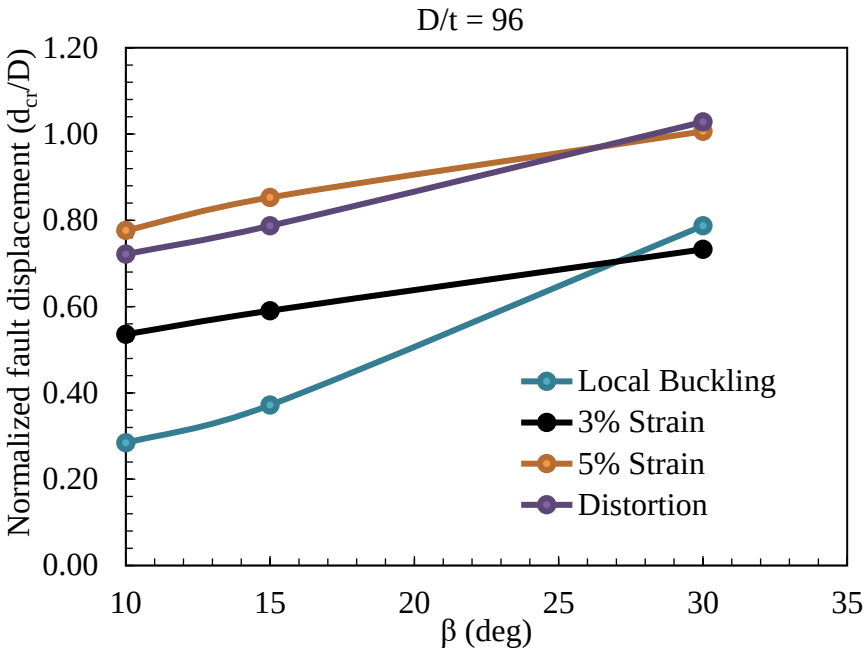

Figure 4.21. Variation of d_{cr} values corresponding to each limit state in regard to the variation of angle β and for D/t = 96

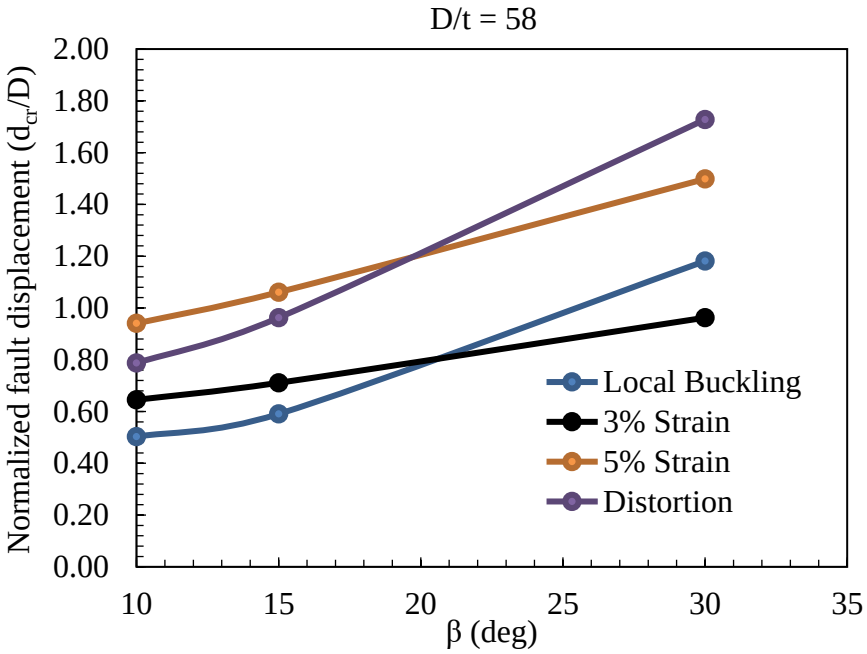

Figure 4.22. Variation of d_{cr} values corresponding to each limit state in regard to the variation of angle β and for D/t = 58

Illustration of the cross-sectional distortion limit state defined based on the flattening parameter f (taken here as 0.15) is given in Figure 4.23 to 4.25 for D/t = 144 and β = 10º, 15º and 30º respectively.

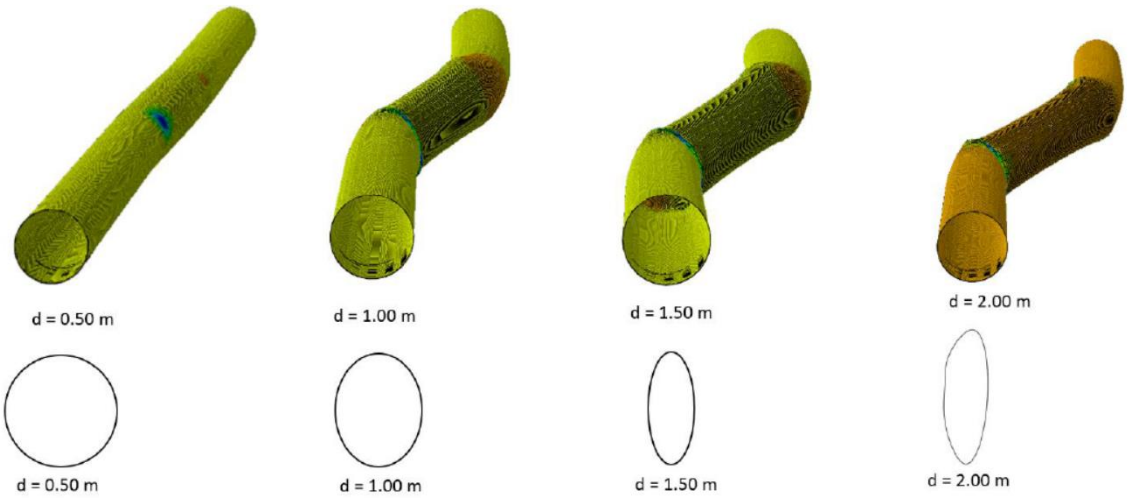

Figure 4.23. Variation of pipeline cross-sectional distortion appearing in form of flattening under various fault displacement loads and for D/t = 144, and β = 10º

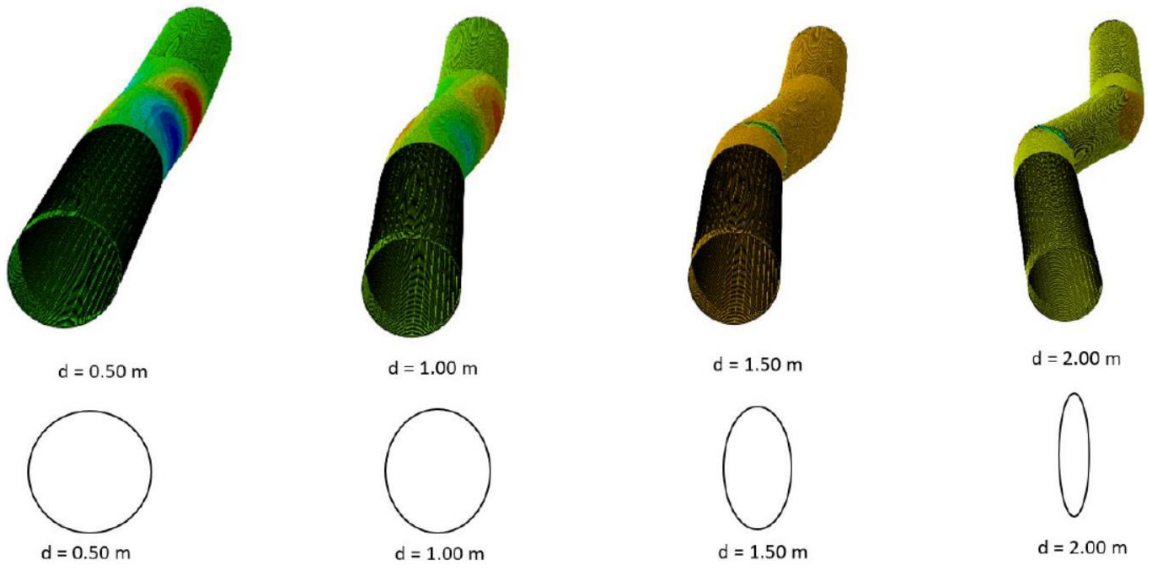

Figure 4.24. Variation of pipeline cross-sectional distortion appearing in form of flattening under various fault displacement loads and for D/t = 144, and β = 15º

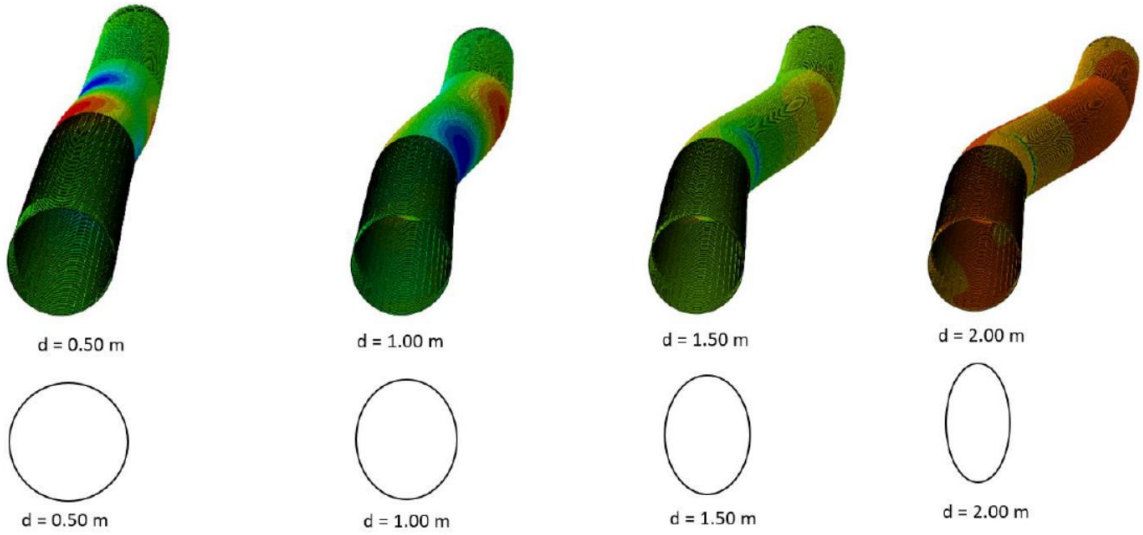

Figure 4.25. Variation of pipeline cross-sectional distortion appearing in form of flattening under various fault displacement loads and for D/t = 144, and β = 30º

4.4. Influence of D/t Ratio on Buried Pipe Seismic Performance

Variation of the pipeline wall thickness or D/t ratio was another parameter influence of which was investigated within the scope of the current study. Previous investigations (Vazouras et al., 2010, 2012) indicate that decreasing the wall thickness of the pipe (i.e., increasing its D/t ratio) makes the pipeline vulnerable to local buckling at increasingly lower fault displacement values. The pipeline cases which differ in terms of the assumed wall thickness value are summarized in Table 4.5. As seen from this data the external pipeline diameter was kept constant at 0.9144m (36inches) whereas the wall thickness varied from 0.00635m to 0.01588m and subsequently the D/t ratio changed between 58 and 144.

Table 4.5. Investigated buried pipe cases with varying D/t ratio

Property	**Case-1**	**Case-2**	**Case-3**
External Diameter (m)	0.9144	0.9144	0.9144
Wall Thickness (m)	0.00635	0.00953	0.01588
D/t Ratio	144	96	58

Numerical models for each pipeline case and fault angle value have been solved separately. However, since the results depicting the impact of fault angle are given in the previous section, and for clarity purposes, this section only included the results for β = 10º

since it represents the worst-case scenario for the cases investigated in the current study. Similar to the investigation of the influence of intersection angle β, results have been initially graphically compared, where Figure 4.17 illustrates the variation of the distribution of longitudinal pipeline strains for all D/t ratios, and β = 10° and under the applied fault displacement load of d = 1m. In addition, the plots presented in Figure 4.26a through 4.27d show the variation of axial normal strains at tension and compression sides of the deformed pipe for d =0.5m, 1m, 1.5m and 2m and pipes with D/t = 144, 96 and 58 respectively, and again only for β = 10°. Reviewed, in terms of strain reductions results indicate that as expected pipes with a higher wall thickness perform better under the applied load. Compared to the effect of angle β, increasing the wall thickness appears to be a more effective intervention, where a reduction of as much as 66% in longitudinal strains was observed, opposed to 40% reduction rate for cases involving the variation of angle β only.

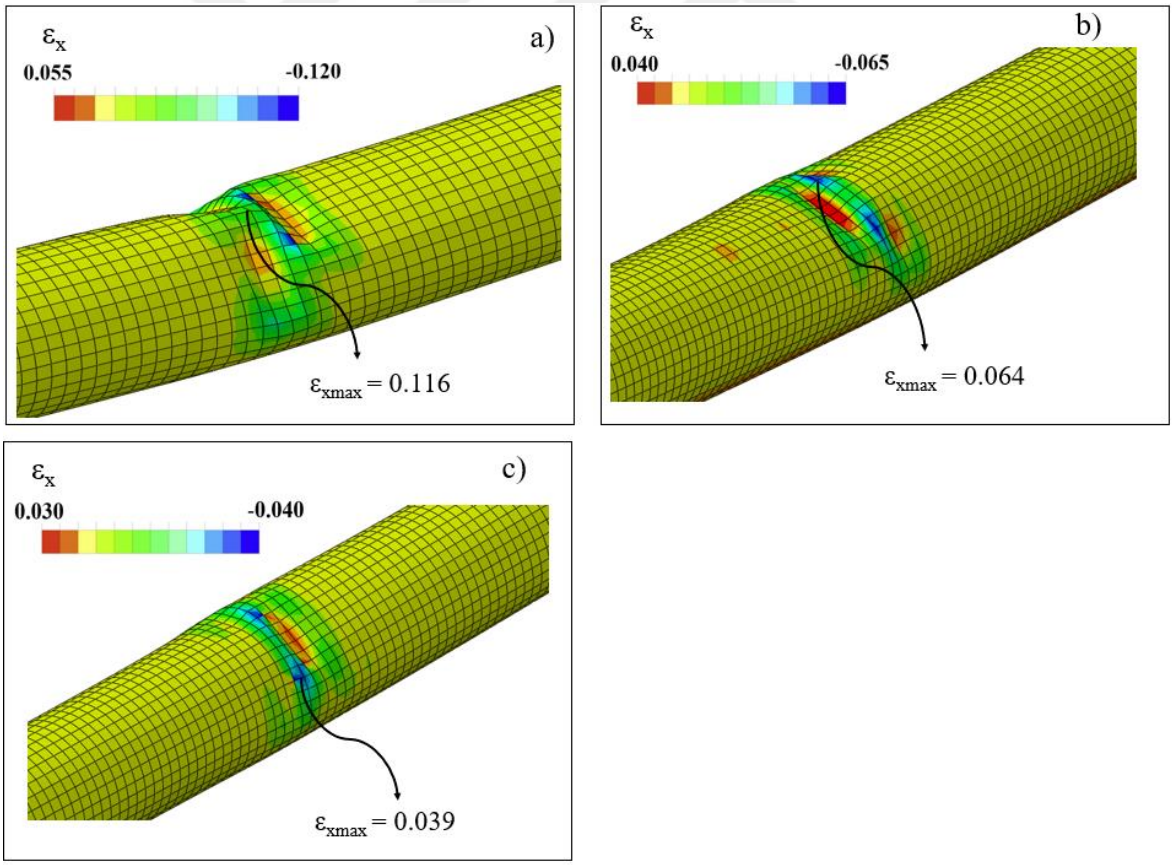

Figure 4.26. Comparison of the distribution of pipeline longitudinal strains for, a) D/t = 144, b) D/t = 96, and c) D/t = 58, where β = 10°, and d = 1m

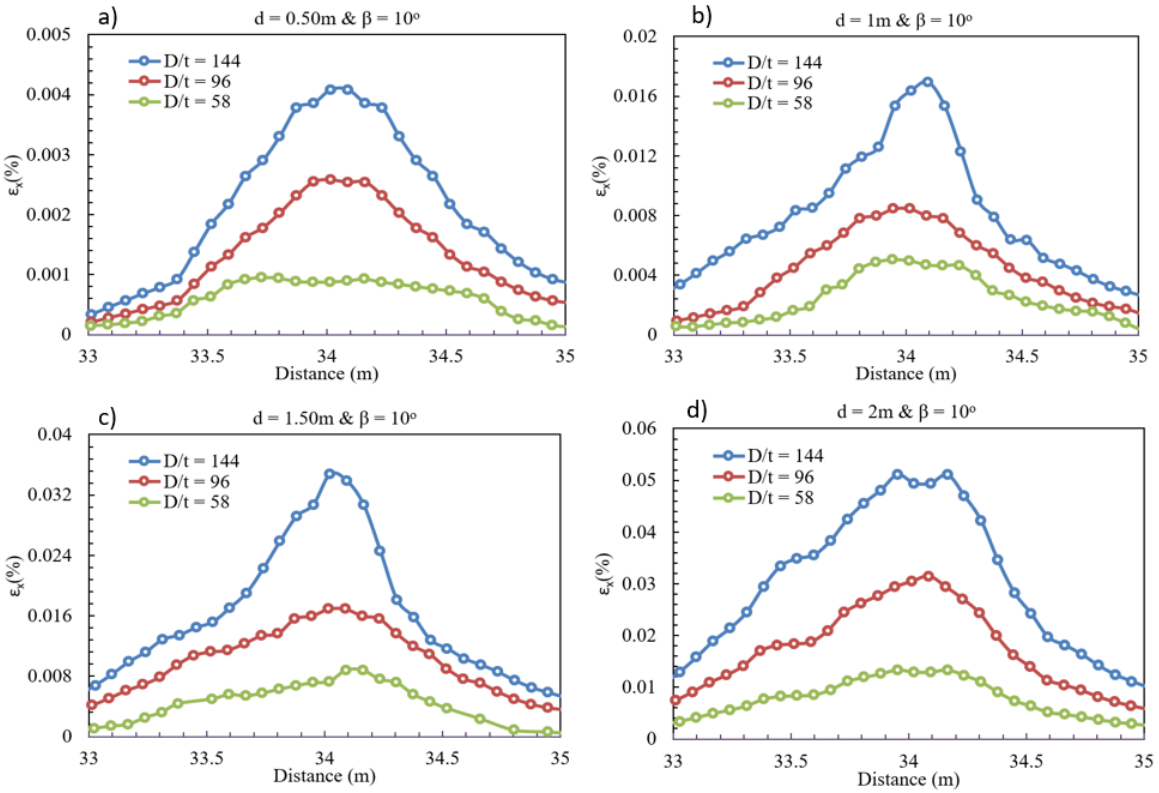

Figure 4.27. Variation of the distribution of axial strains recorded at the deformed pipe side subjected to tension for, D/t =144, D/t =96, D/t =58, β = 10°, and a) d = 0.5m, b) d = 1.00m, c) d = 1.50m, and d) d = 2.00m

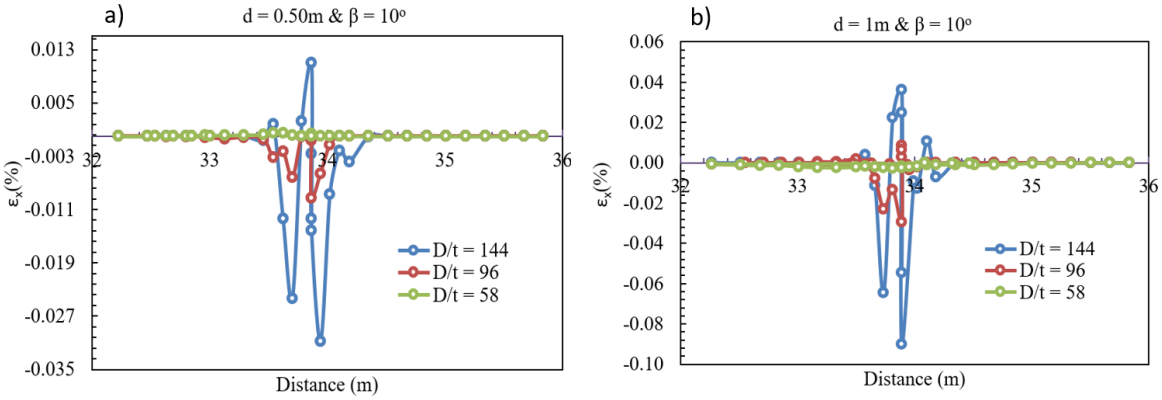

Figure 4.28. Variation of the distribution of axial strains recorded at the deformed pipe side subjected to compression for, D/t =144, D/t =96, D/t =58, β = 10°, and a) d = 0.5m, b) d = 1.00m, c) d = 1.50m, and d) d = 2.00m

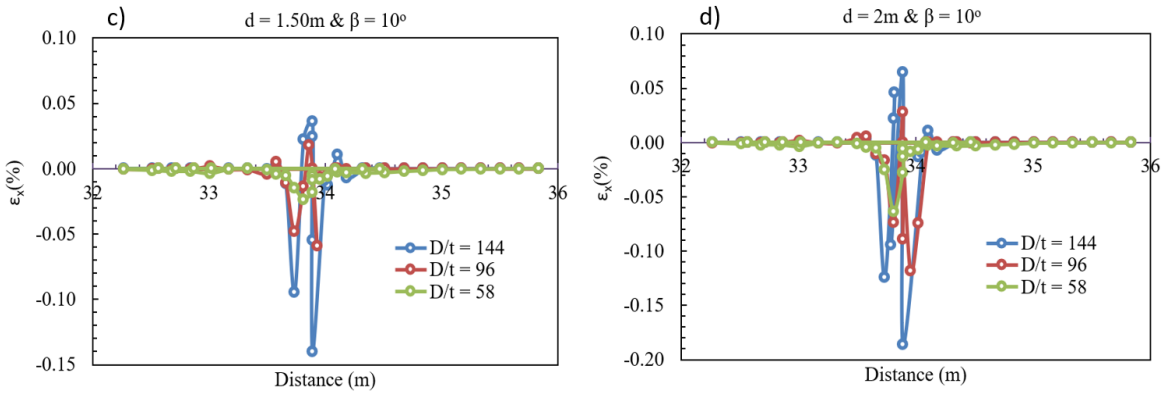

Figure 4.28. Variation of the distribution of axial strains recorded at the deformed pipe side subjected to compression for, D/t =144, D/t =96, D/t =58, β = 10°, and a) d = 0.5m, b) d = 1.00m, c) d = 1.50m, and d) d = 2.00m

Similar to Section 4.3 evaluation of the performance of studied buried steel pipe cases was also performed via deriving the critical values of applied fault displacement load leading to the exceedance of to the pre-defined criteria of performance (limit states). Tables 4.6 to 4.8 summarize the d_{cr} values for each limit state and for D/t = 144, 96 and 58 respectively and β = 10°. Figures 4.29 to 4.31 present the plots of fault displacement values normalized per the outer diameter of the steel pipe (d_{cr}/D) versus D/t ratio for each limit state considered within the scope of this study. As depicted in this table and figures reducing the pipeline wall thickness adversely effects the performance of the pipeline since the d_{cr} value decreases for each limit state. An increment of as much as nearly 90% for d_{cr} leading to failure due to exceedance of ovalization factor of 0.15 was determined to be achievable through the increment of pipe wall thickness to 15.88mm. Furthermore, results indicate that local buckling of the pipeline wall becomes the prevailing mechanism of failure as D/t increases.

Table 4.6. Limit States and d_{cr} values for D/t = 144 and β = 10°

Limit State	**Limit State Value**	**d_{cr} (m)**
Maximum Tensile Strain (3%)	3%	0.41
Maximum Tensile Strain (5%)	5%	0.63
Onset of Local Buckling	$-9.73*10^{3}$	0.22
Cross-Sectional Distortion	f = 0.15	0.38

Table 4.7. Limit States and d_{cr} values for D/t = 96 and β = 10º

Limit State	Limit State Value	d_{cr} (m)
Maximum Tensile Strain (3%)	3%	0.49
Maximum Tensile Strain (5%)	5%	0.71
Onset of Local Buckling	$-9.73*10^{3}$	0.31
Cross-Sectional Distortion	f = 0.15	0.68

Table 4.8. Limit States and d_{cr} values for D/t = 58 and β = 10º

Limit State	Limit State Value	d_{cr} (m)
Maximum Tensile Strain (3%)	3%	0.59
Maximum Tensile Strain (5%)	5%	0.86
Onset of Local Buckling	$-9.73*10^{3}$	0.46
Cross-Sectional Distortion	f = 0.15	0.72

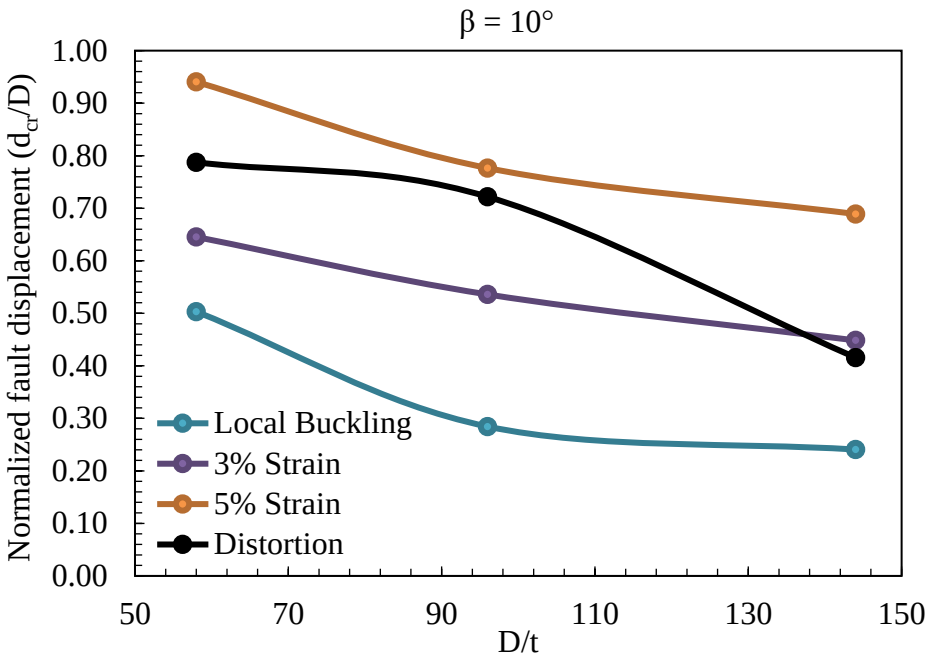

Figure 4.29. Variation of d_{cr} values corresponding to each limit state with regard to the variation of D/t ratio and for β = 10º

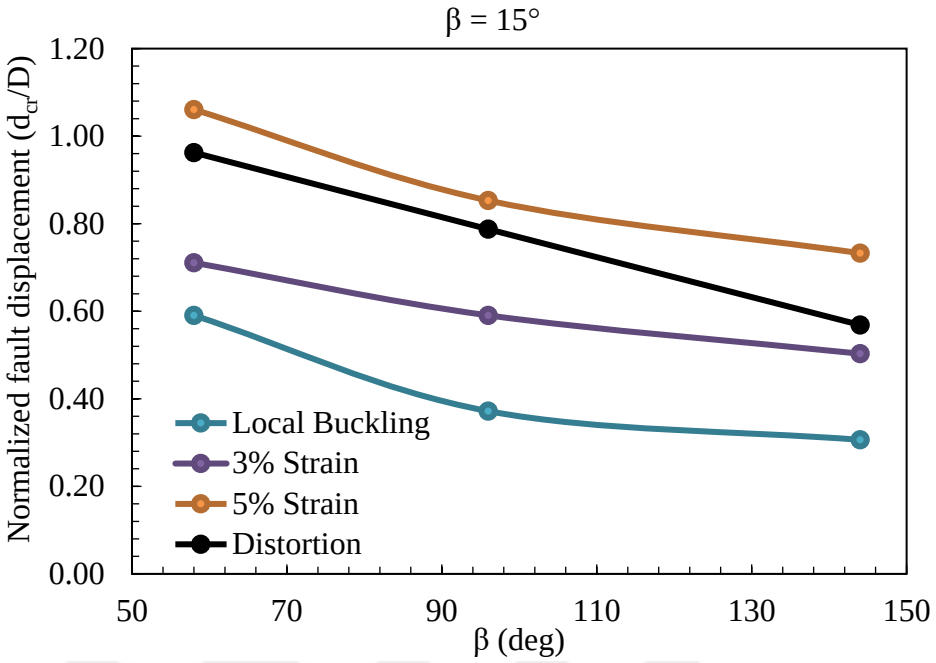

Figure 4.30. Variation of d_{cr} values corresponding to each limit state with regard to the variation of D/t ratio and for β = 15º

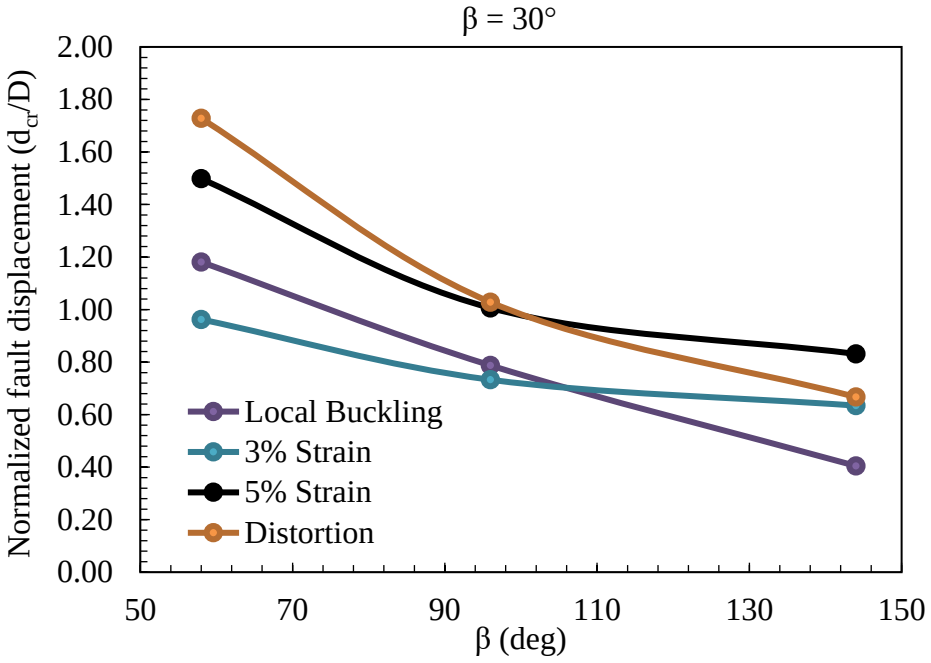

Figure 4.31. Variation of d_{cr} values corresponding to each limit state with regard to the variation of D/t ratio and for β = 30º

Illustration of the cross-sectional distortion limit state defined based on the flattening parameter f (taken here as 0.15) is given in Figure 4.32 to 4.34 for D/t = 144, 96 and 58 respectively, and $\beta = 10^o$.

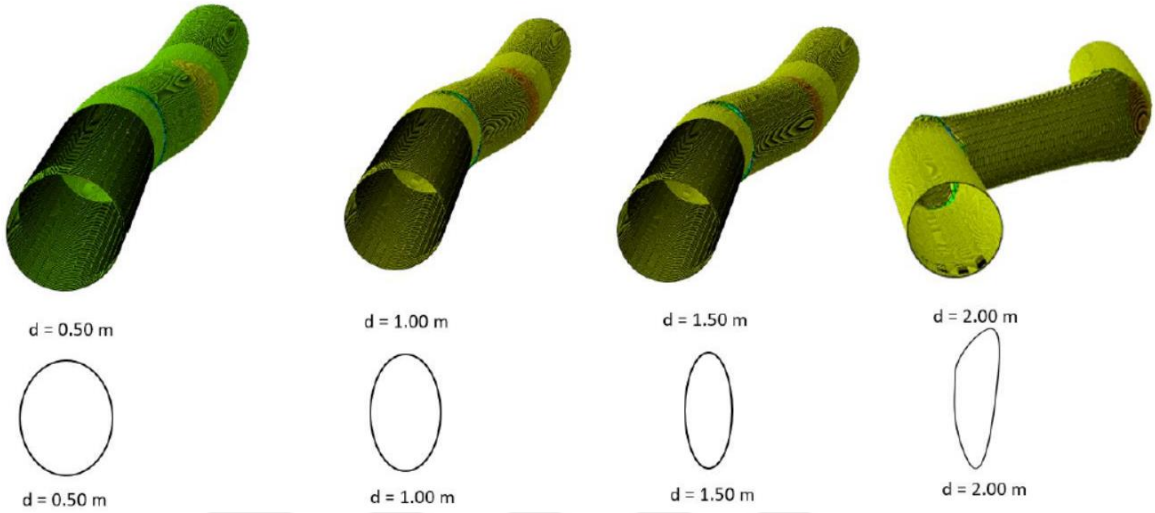

Figure 4.32. Variation of pipeline cross-sectional distortion appearing in form of flattening under various fault displacement loads and for D/t = 144, and $\beta = 10^o$

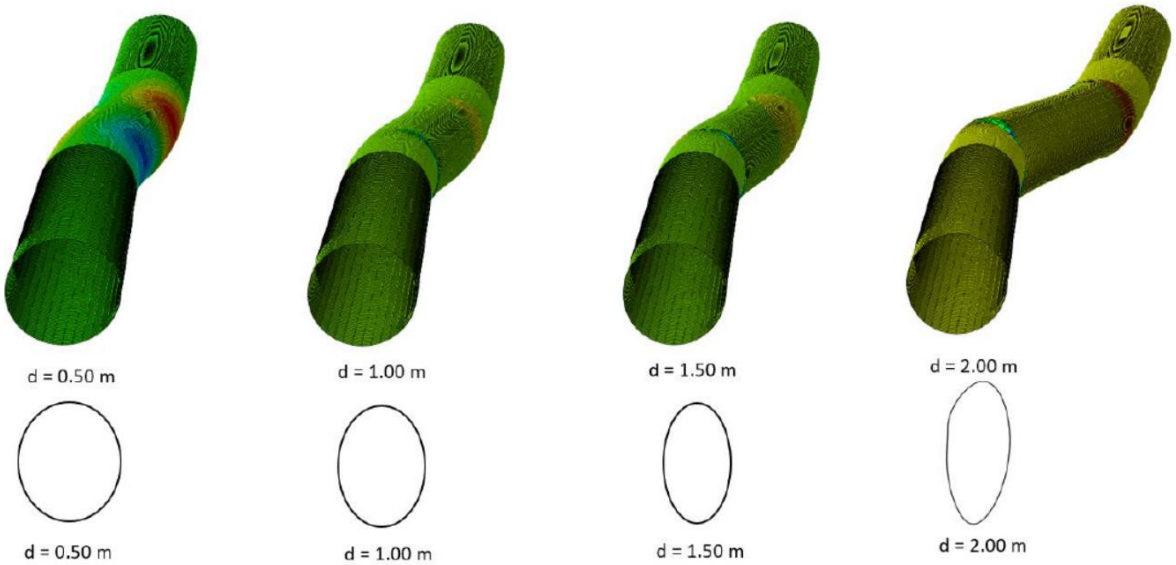

Figure 4.33. Variation of pipeline cross-sectional distortion appearing in form of flattening under various fault displacement loads and for D/t = 96, and $\beta = 10^o$

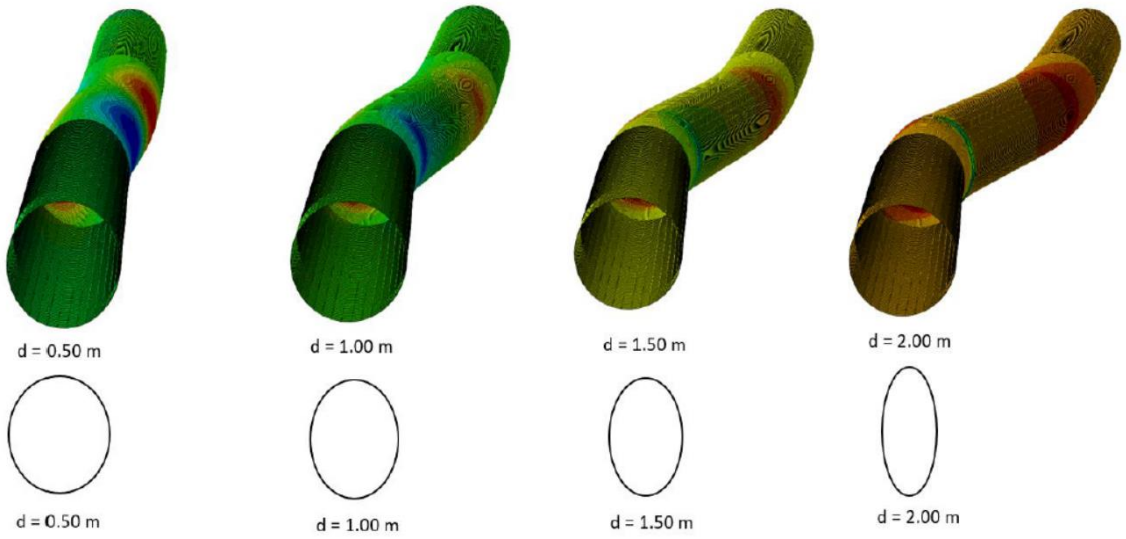

Figure 4.34. Variation of pipeline cross-sectional distortion appearing in form of flattening under various fault displacement loads and for D/t = 58, and $\beta = 10^{o}$

4.5. Damage Mitigation of Buried Steel Pipes Using FRP Wraps

Mitigation of seismic damage and demands on buried steel pipes exposed to strike-slip fault action was investigated via developing numerical models of soil-pipe system where the pipe was wrapped with FRP composites of different types and layer thicknesses. In particular, this dissertation investigated the use of CFRP, GFRP and BFRP wrap types with thicknesses varying between 1mm and 10mm. Following sections present the investigation of the efficiency of each wrap type and the variation of the layer thickness of this wraps on the overall pipeline seismic performance. Initially a validation procedure following the modeling of a sample published work (Mokhtari and Nia, 2015) assumed as a control model and comparing the obtained results is presented. Later sections review the efficacy of wrap types separately in terms of comparing the strain distributions, changes in d_{cr} value, and performance criteria, lastly the effect of wrap types is compared with each other.

4.5.1. Model Validation

Prior to the analysis of the intended cases of buried pipelines and investigation of the efficiency of FRP wraps the path followed for the development of these analysis models needed to be somehow verified. The method to develop mitigated models incorporating FRP

composite wraps was described in detail under Chapter 3. To validate the developed models an approach similar to the one employed for models not including FRP wraps was utilized. The study performed by Mokhtari and Nia (2015) served the basis for this process. In their study Mokhtari and Nia (2015) have adopted a 3D FE model similar to that of Vazouras et al. (2012), assuming the same dimensions and configuration where the FRP wraps were modeled using S4R type shell elements. The study considered four D/t ratios in total: D/t = 57.6, 72, 96 and 144 and assumed a stiff clay soil condition. The FRP type considered within the scope of their study was a CFRP composite with layer thicknesses in the span ranging between 1mm to 13mm. Analysis result depicting the efficiency of the FRP wrap are presented in form of distribution graphs of longitudinal pipeline strains, variation of axial strains along the pipeline and the change in the value of d_{cr} as the CFRP layer thickness increases.

To validate the accuracy of the path followed in the present study the same model was developed using the concepts and approaches assumed in this dissertation. Analysis was performed only for D/t = 144 and 96 and layer thicknesses of t_c equal to 0mm, 1mm and 5mm, the pipe was accepted to be unpressurized. Similar to the reference study, distribution of longitudinal pipeline strains at 1m of fault displacement were derived for the afro-mentioned cases and graphically compared to the ones of the reference study. Figure 4.35 presents the graphical comparison of the longitudinal pipeline strain distribution extracted from both models. A good overall agreement appears to exist between the obtained result, even though values were not exactly the same. In addition, the variation of axial normal strains along the pipeline for D/t = 144 plotted for t_c = 0, 1 and 5mm shown in Figure 4.36 again reveals an acceptable consistency when compared to the results of the reference study.

Existence of an apparent coherence among the compared results was accepted as the source for the validation of the developed numerical models. Further sections present the analysis result for the utilized types and layer thicknesses of FRP composites. Solutions incorporating FRP wraps were performed for all D/t ratios and β values mentioned in sections above, however, for simplicity, only the cases with $\beta = 10°$ have been reported.

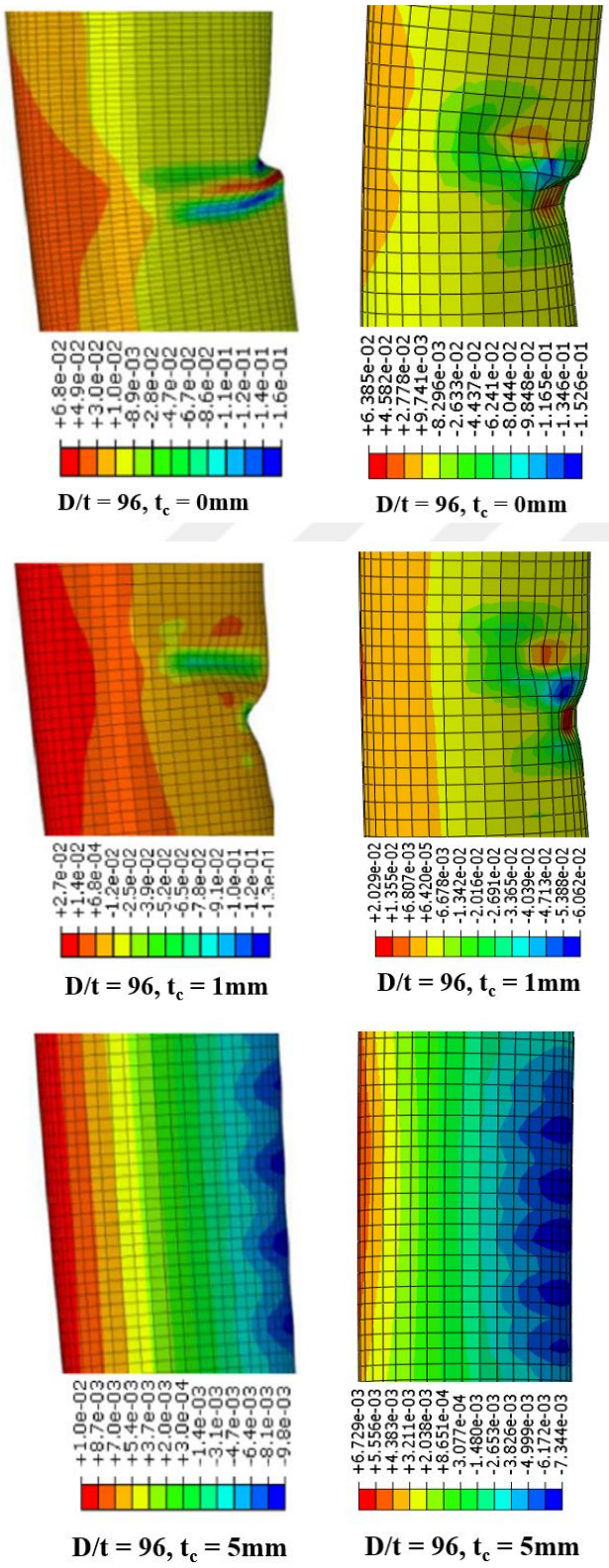

Figure 4.35. Reduction in longitudinal pipeline strains for D/t = 96, left: reference model (Mokhtari and Nia, 2016); right: developed model

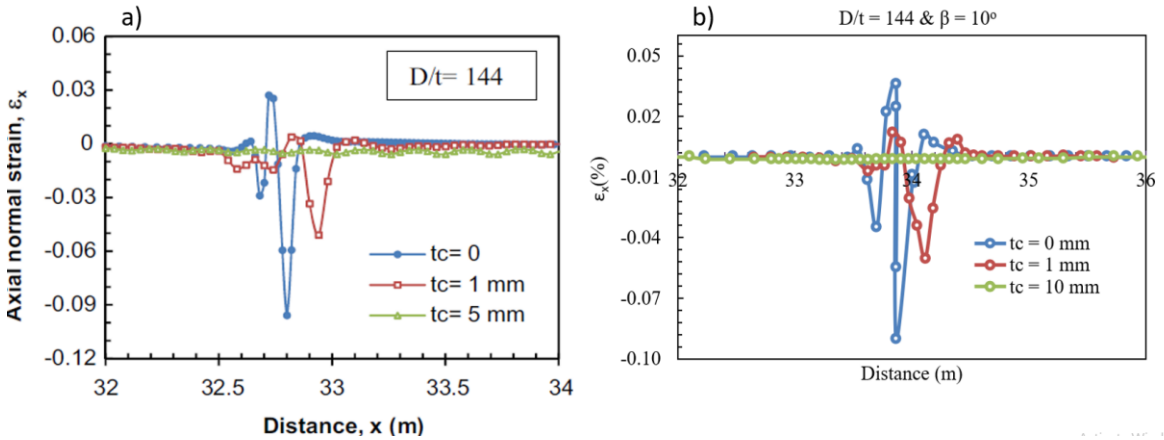

Figure 4.36. Comparison of axial strain result for D/t=144, β = 10°, and d = 1m; a) reference study (Mokhtari and Nia, 2016); b) developed model

4.5.2. Evaluation of the Efficiency of CFRP Wraps

The impact of wrapping the pipe outer surface with CFRP wraps was investigated via reviewing the reduction in longitudinal pipeline strains, reduction in the distribution of axial normal strains along the pipeline, as well as, based on the performance criteria described in Chapter 2. In this aspect the increment in d_{cr} value (i.e., fault displacement value inducing the violation of one these limit states) shift in the mode of failure served the basis for performance evaluation of the applied FRP wraps. As mentioned earlier, the layer thicknesses considered in this study are 1mm, 3mm, 5mm and 10mm. Analysis results were reported only for cases with β = 10°. Figure 4.37a to 4.39e present the reductions achieved for longitudinal pipeline strains for layer thicknesses ranging from 1mm up to 10mm under the applied fault load of 1m and D/t ratios of 144, 96, and 58 respectively. Obtained results indicate that a reduction of as much as 93% is achievable when a CFRP layer of 10mm is used for damage mitigation, a much higher improvement that increasing the wall thickness of the entire pipe from 6.35mm to 15.88m or adjusting the orientation of the buried steel pipe in reference to the fault plane.

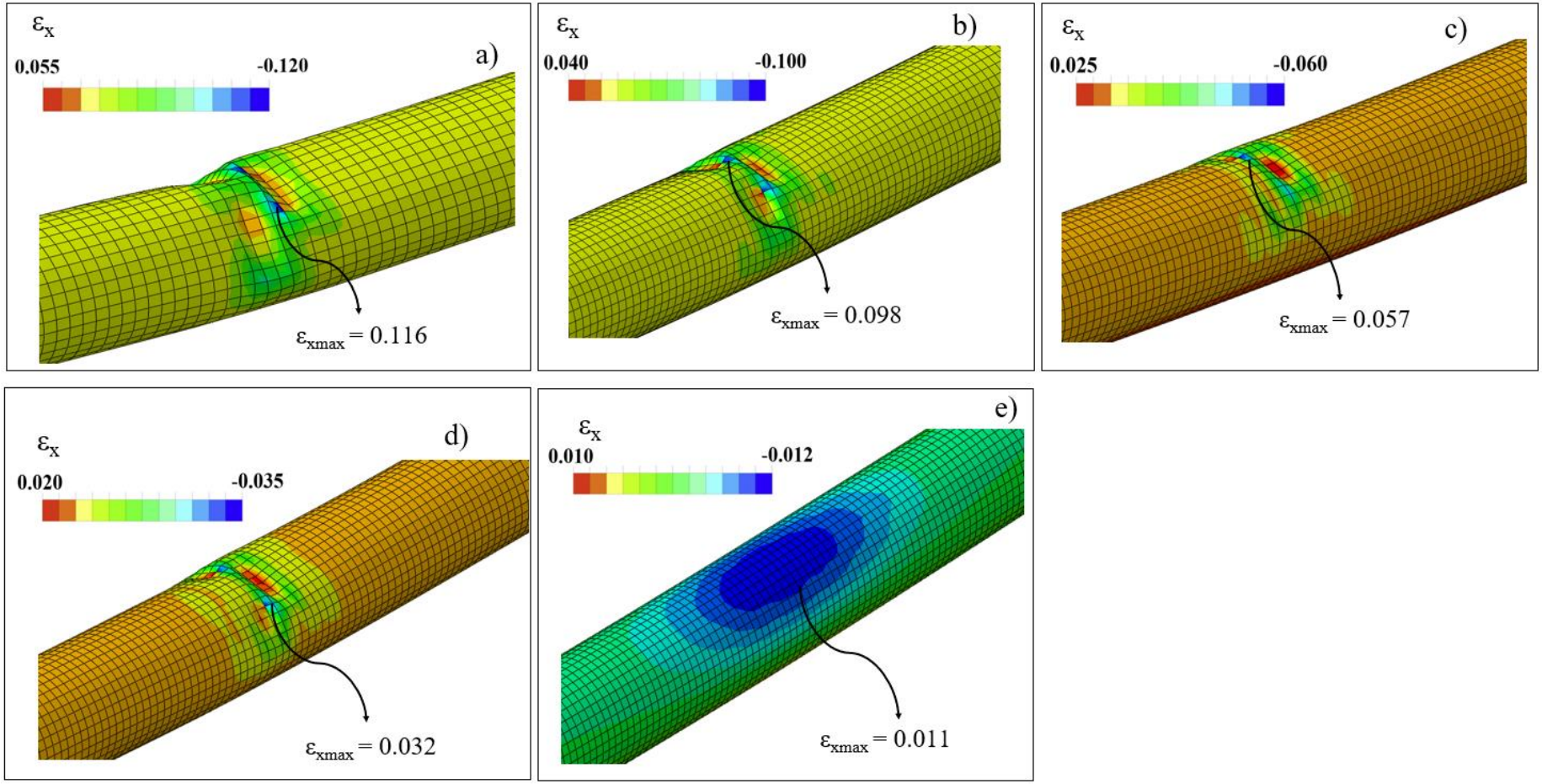

Figure 4.37. Reduction of longitudinal pipeline strains using CFRP wraps of a) t_c = 0mm, b) t_c = 1mm, c) t_c = 3mm, d) t_c = 5mm, and e) t_c = 10mm for D/t = 144, β =10° and d = 1m

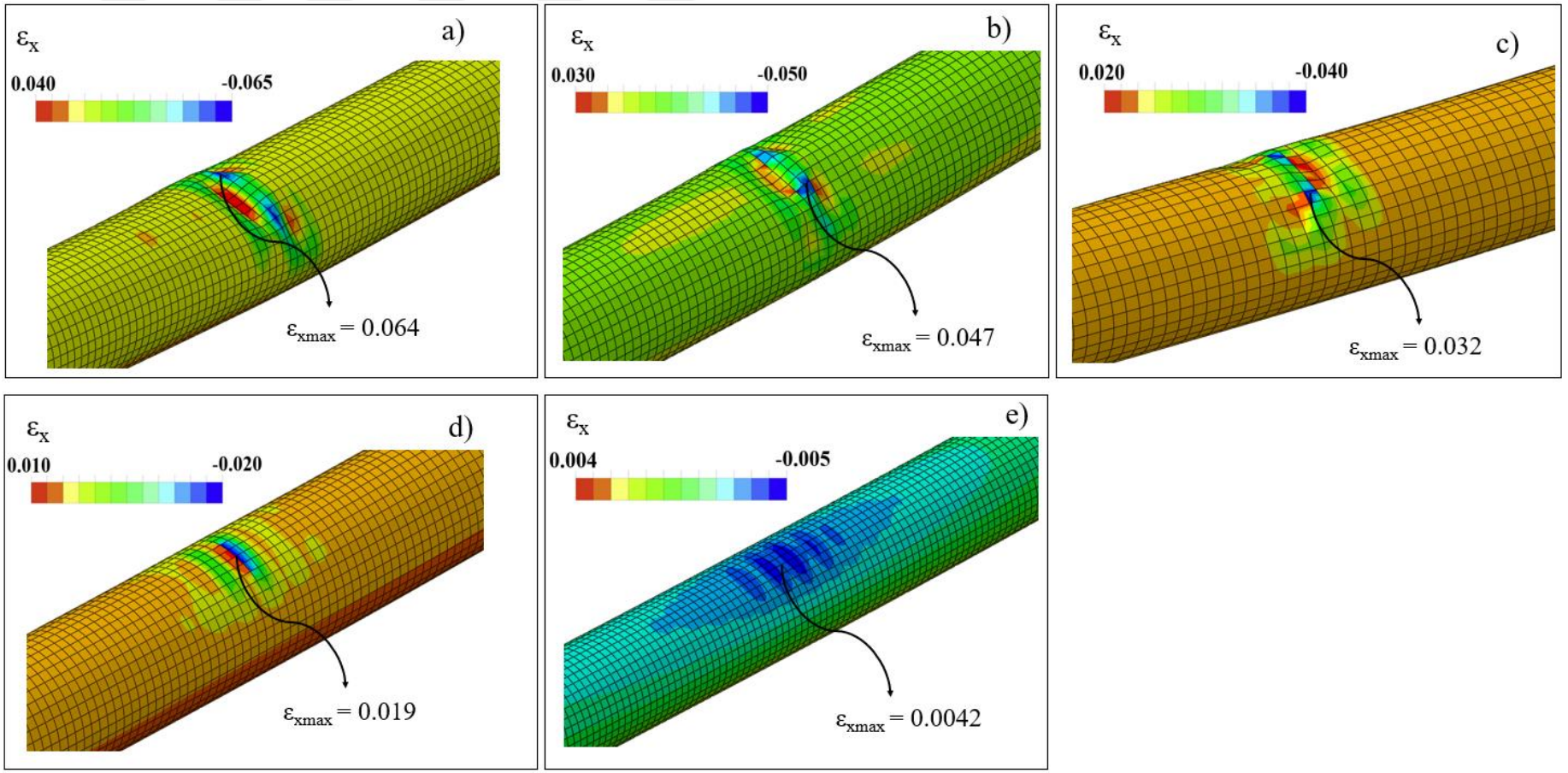

Figure 4.38. Reduction of longitudinal pipeline strains using CFRP wraps of a) t_c = 0mm, b) t_c = 1mm, c) t_c = 3mm, d) t_c = 5mm, and e) t_c = 10mm for D/t = 96, β =10° and d = 1m

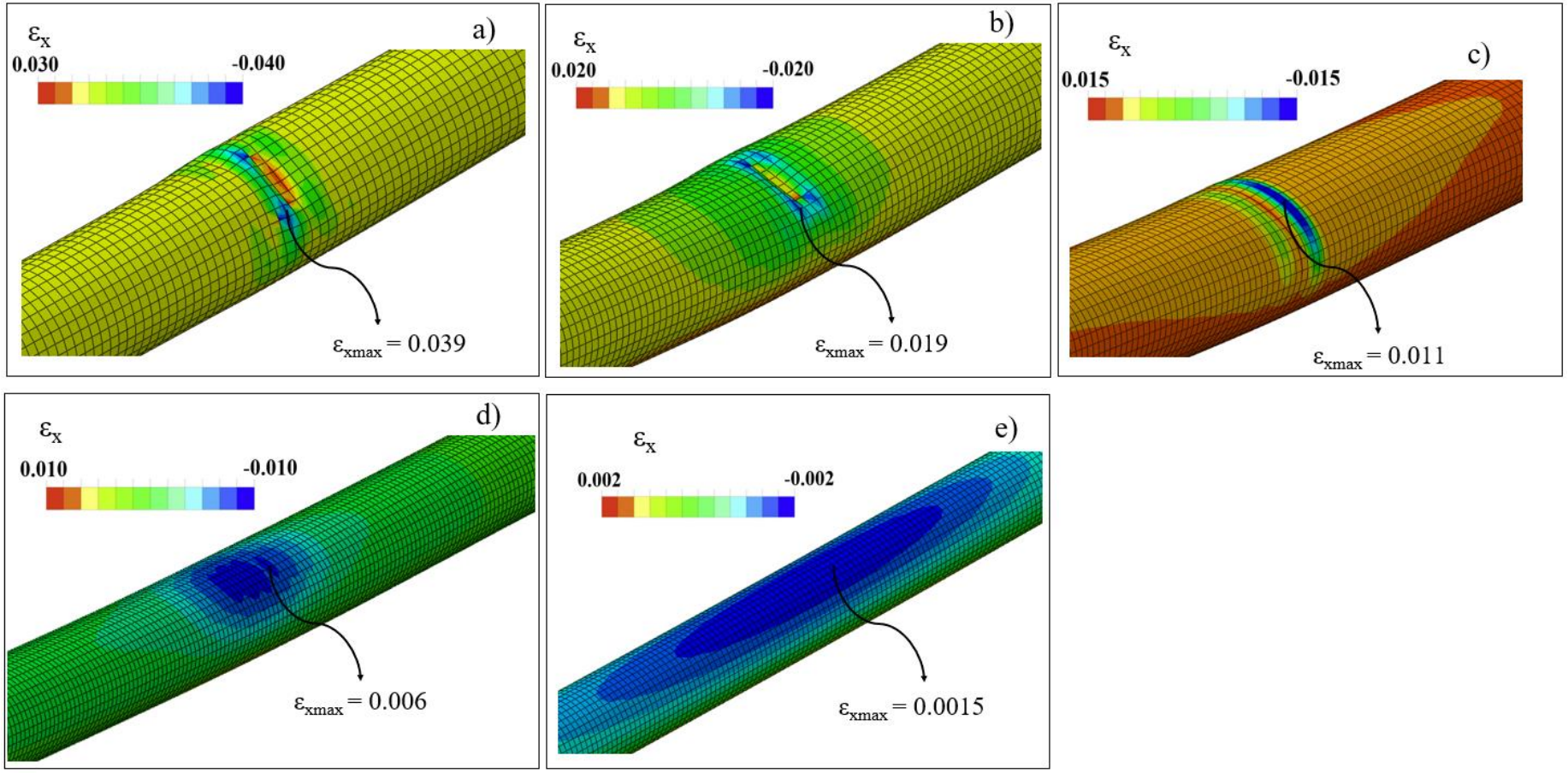

Figure 4.39. Reduction of longitudinal pipeline strains using CFRP wraps of a) t_c = 0mm, b) t_c = 1mm, c) t_c = 3mm, d) t_c = 5mm, and e) t_c = 10mm for D/t = 58, β =10° and d = 1m

In addition to the reduction in the distribution of longitudinal pipeline strains, the mitigation effect of CFRP wraps was also investigated in terms of the reduction of axial normal strains. Result presented in Figure 4.40a to 4.41c reveal that there is a significant reduction in axial strains (up to 82% for t = 10mm) both in tension and compression side of the buckler pipe and that the location of maximum strains shifts as the layer thickness increases. Evaluation of the CFRP wrap thickness in terms of performance criteria is summarized in Table 4.9. While for cases not incorporating FRP wraps the dominant mode of pipeline failure is local buckling as the wrap thickness increases this mode changes to either to maximum tensile strain limit state of 3% (for D/t = 144) or to cross-sectional distortion (for D/t = 96) or CFRP Wrap rupture limit state (for D/t = 58). While investigation made in terms of longitudinal and axial strains did not show any significant effect of D/t ratio on the mitigation offered by CFRP wrap, the data summarized in Table 4.9 underlines and clearly shows that as the D/t gets lower the Wrap rupture limit states becomes the dominant mechanism of failure and eliminates the possibility of the occurrence of other damage modes. In overall, an increment of more than 300% in d_{cr} value is shown to be attainable whenever a CFRP wrap with a layer thickness of 10mm is utilized for damage mitigation.

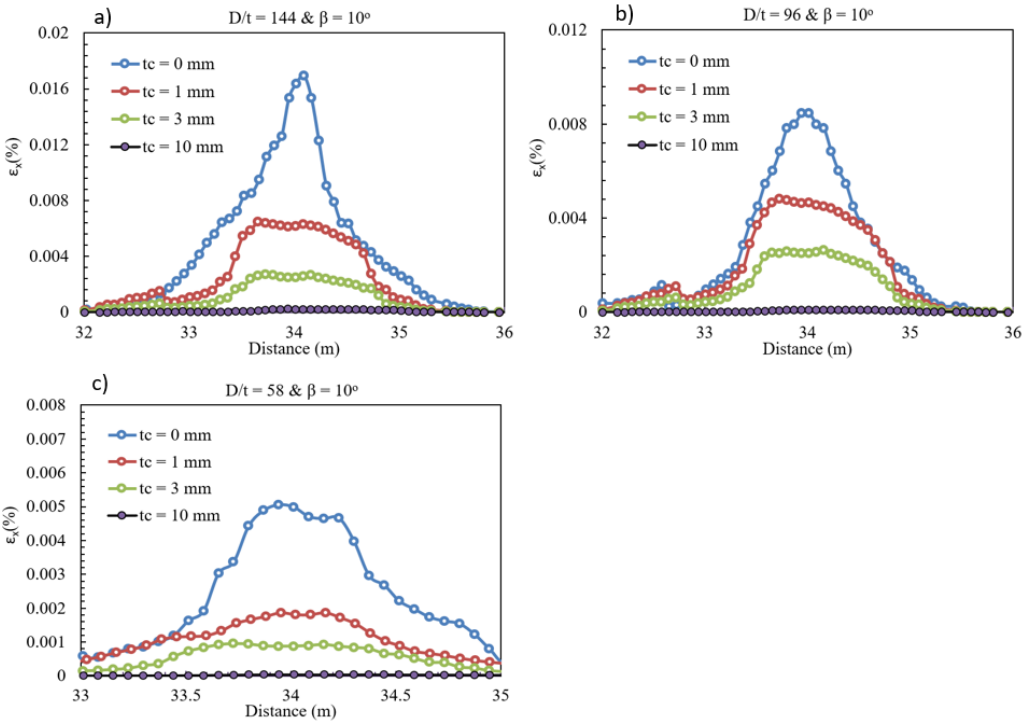

Figure 4.40. Variation of axial strain distribution recorded at the deformed pipe side subjected to tension for, a) D/t =144, b) D/t =96, and c) D/t =58, β = 10°, and t_c varying between 0mm and 10mm

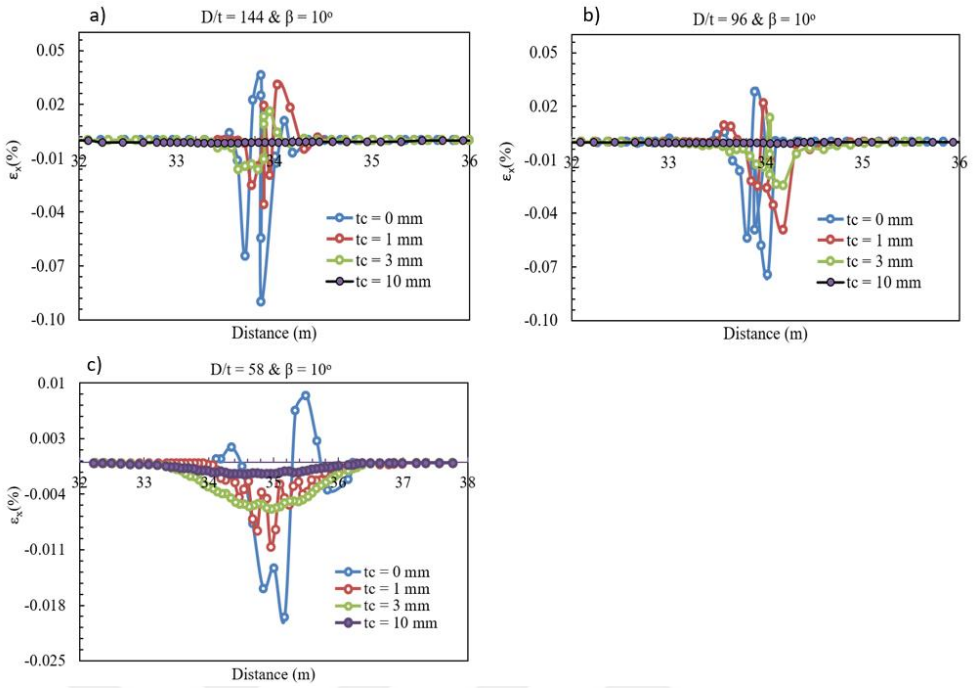

Figure 4.41. Variation of axial strain distribution recorded at the deformed pipe side subjected to compression for, a) D/t =144, b) D/t =96, and c) D/t =58, β = 10°, and t_c varying between 0mm and 10mm

Table 4.9. Variation of the mode of failure and d_{cr} value with respect to CFRP inclusion

D/t	t_c (mm)	d_{cr} (m)	Failure Mode	Limit Value	Increase in d_{cr} (%)
144	0	0.22	Local Buckling	-9.73×10^{3}	0
144	1	0.38	Local Buckling	-9.73×10^{3}	73
144	3	0.54	Ovalization	f = 0.15	145
144	5	0.78	Ovalization	f = 0.15	255
144	10	0.93	Ovalization	f = 0.15	323
96	0	0.31	Local Buckling	-9.73×10^{3}	0
96	1	0.56	3% Tensile Strain	3%	81
96	3	0.74	3% Tensile Strain	3%	187
96	5	0.87	Ovalization	f = 0.15	234
96	10	1.09	Ovalization	f = 0.15	319
58	0	0.59	3% Tensile Strain	3%	0
58	1	0.92	3% Tensile Strain	3%	78
58	3	0.96	CFRP Rupture	0.02182	109
58	5	1.32	CFRP Rupture	0.02182	187
58	10	2.06	CFRP Rupture	0.02182	348

4.5.3. Evaluation of the Efficiency of GFRP Wraps

Similar to the cases incorporating CFRP composites the impact of wrapping the pipe outer surface with GFRP wraps was investigated via reviewing the reduction in longitudinal pipeline strains, reduction in the distribution of axial normal strains accumulated on the buried pipe, as well as, based on the performance criteria described in Chapter 2. In this aspect the increment in d_{cr} value (i.e., fault displacement value inducing the violation of one these limit states) shift in the mode of failure served the basis for performance evaluation of the applied FRP wraps. As mentioned earlier, the layer thicknesses considered for GFRP wraps in this study were 1mm, 3mm, 5mm and 10mm. Analysis results were reported only for cases with $\beta = 10°$. Figure 4.42a to 4.44e present the reductions achieved for longitudinal pipeline strains for layer thicknesses ranging from 1mm up to 10mm under the applied fault load of 1m and D/t ratios of 144, 96, and 58 respectively. Obtained results indicate that a reduction of as much as 76% is achievable when a GFRP layer of 10mm is used for damage mitigation, a much higher improvement that increasing the wall thickness of the entire pipe from 6.35mm to 15.88m or adjusting the buried pipe orientation with regard to the fault plane. In addition to the reduction in the distribution of longitudinal pipeline strains, the mitigation effect of GFRP wraps was also investigated in terms of the reduction of axial normal strains. Result presented in Figure 4.45a to 4.46c reveal that there is a significant reduction in axial strains (up to 64% for t = 10mm) both in tension and compression side of the buckler pipe and that the location of maximum strains shifts as the layer thickness increases. Evaluation of the GFRP wrap thickness in terms of performance criteria is summarized in Table 4.10. While for cases not incorporating FRP wraps the dominant mode of pipeline failure is local buckling as the wrap thickness increases this mode changes to either to maximum tensile strain limit state of 3% (for D/t = 144) or to cross-sectional distortion (for D/t = 96) or CFRP Wrap rupture limit state (for D/t = 58). While investigation made in terms of longitudinal and axial strains did not show any significant effect of D/t ratio on the mitigation offered by GFRP wrap, the data summarized in Table 4.10 underlines and clearly shows that as the D/t gets lower the Wrap rupture limit states becomes the dominant mechanism of deformation and eliminates the possibility of the occurrence of other damage modes. In overall, an increment of more than 300% in d_{cr} value is shown to be attainable whenever a GFRP wrap with a layer thickness of 10mm is utilized for damage mitigation.

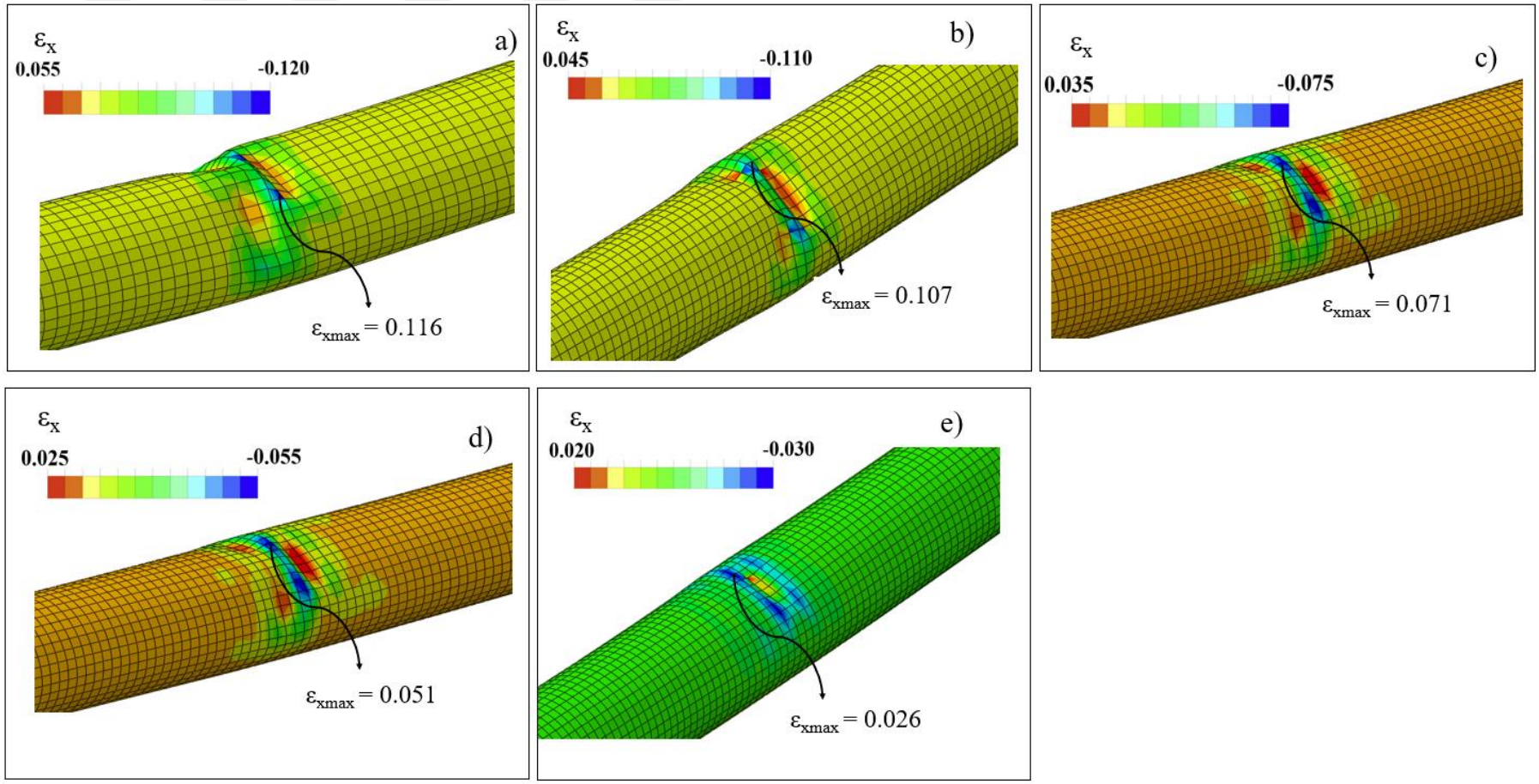

Figure 4.42. Reduction of longitudinal pipeline strains using GFRP wraps of a) t_c = 0mm, b) t_c = 1mm, c) t_c = 3mm, d) t_c = 5mm, and e) t_c = 10mm for D/t = 144, β =10° and d = 1m

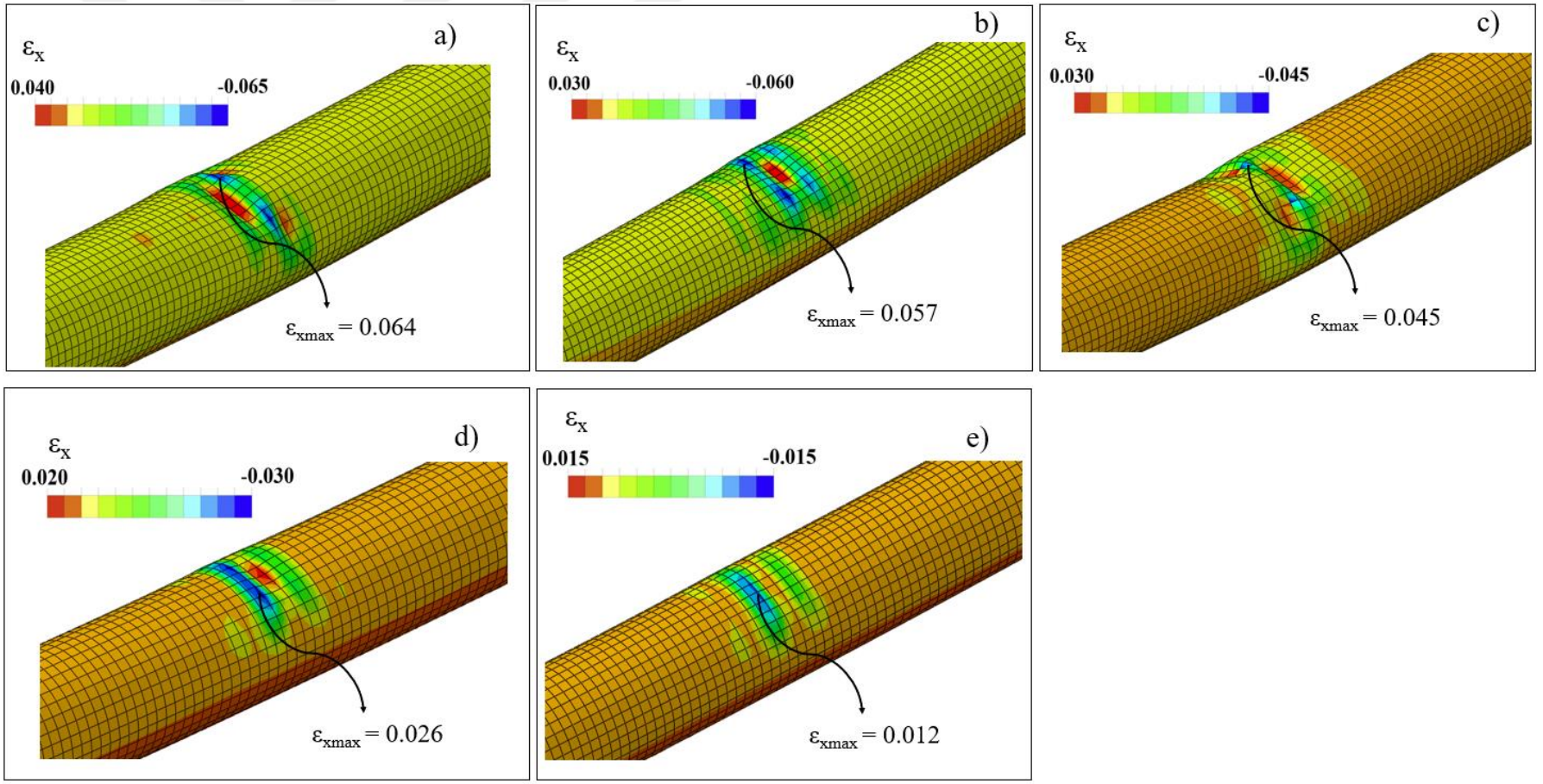

Figure 4.43. Reduction of longitudinal pipeline strains using GFRP wraps of a) t_c = 0mm, b) t_c = 1mm, c) t_c = 3mm, d) t_c = 5mm, and e) t_c = 10mm for D/t = 96, β =10° and d = 1m

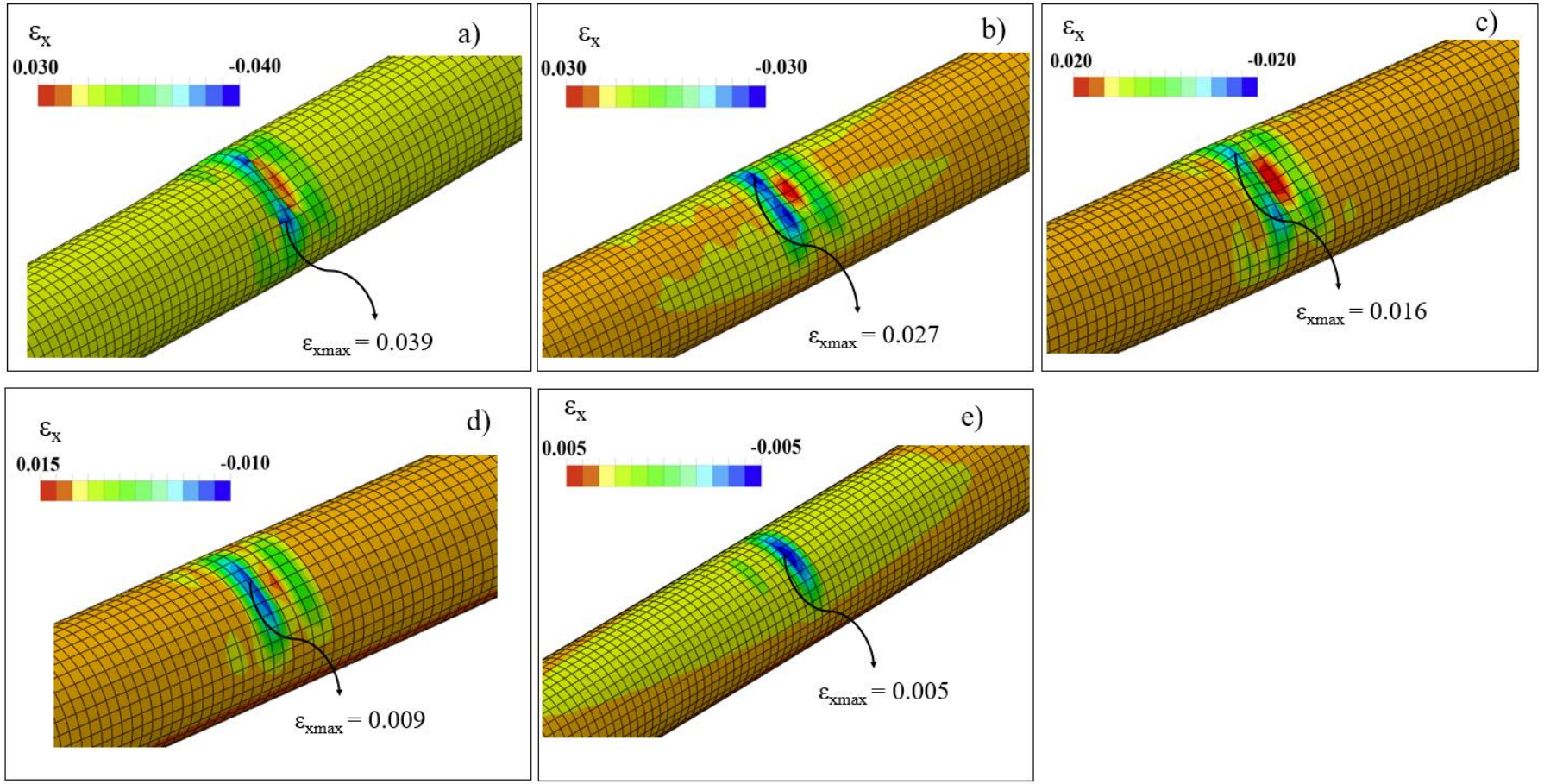

Figure 4.44. Reduction of longitudinal pipeline strains using GFRP wraps of a) t_c = 0mm, b) t_c = 1mm, c) t_c = 3mm, d) t_c = 5mm, and e) t_c = 10mm for D/t = 58, β =10° and d = 1m

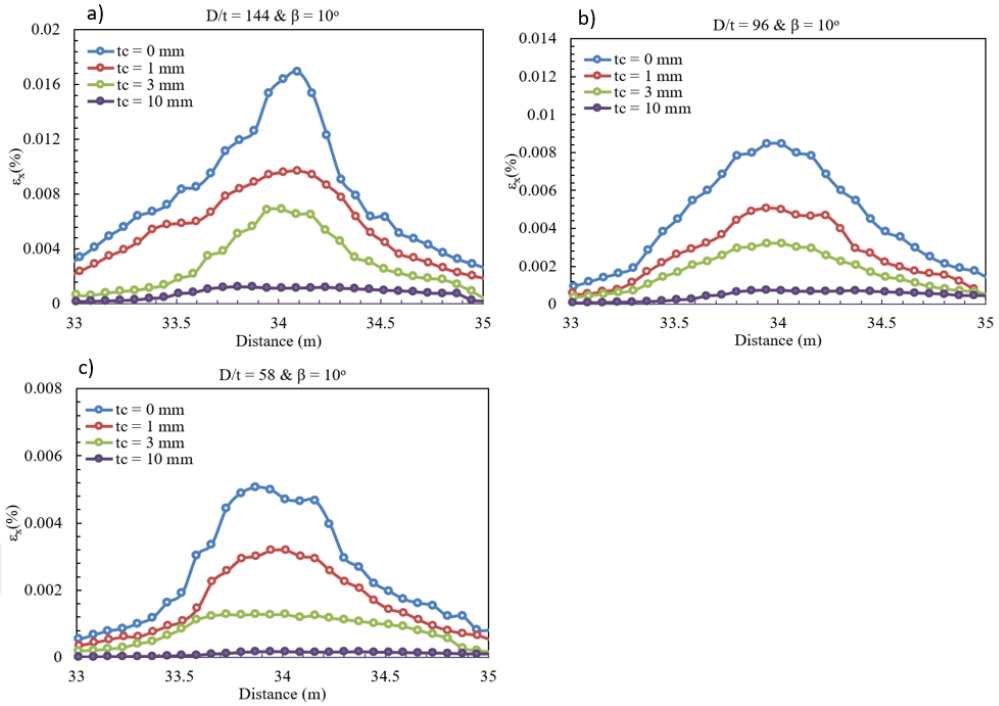

Figure 4.45. Variation of the axial strain distribution recorded at the deformed pipe side subjected to tension for, a) D/t =144, b) D/t =96, and c) D/t =58, β = 10°, and t_c varying between 0mm and 10mm

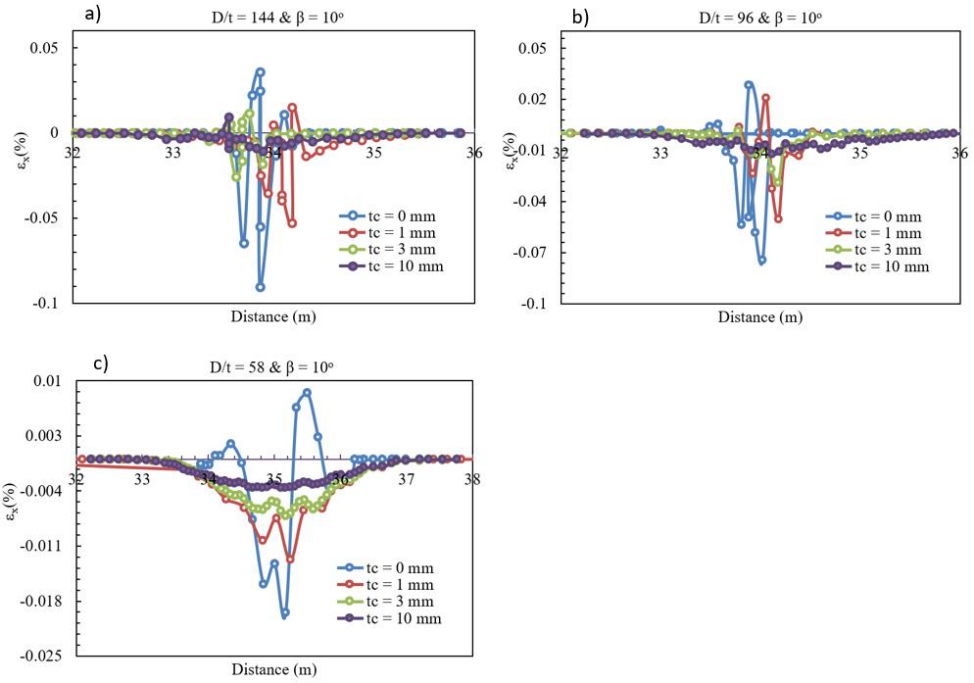

Figure 4.46. Variation of the axial strain distribution recorded at the deformed pipe side subjected to compression for, a) D/t =144, b) D/t =96, and c) D/t =58, β = 10°, and t_c varying between 0mm and 10mm

Table 4.10. Variation of the mode of failure and d_{cr} value with respect to GFRP inclusion

D/t	t_c (mm)	d_{cr} (m)	Failure Mode	Limit Value	Increase in d_{cr} (%)
144	0	0.22	Local Buckling	-9.73×10^3	0
144	1	0.32	Local Buckling	-9.73×10^3	45
144	3	0.46	3% Tensile Strain	3%	109
144	5	0.68	Ovalization	f = 0.15	209
144	10	0.81	Ovalization	f = 0.15	268
96	0	0.31	Local Buckling	-9.73×10^3	0
96	1	0.44	3% Tensile Strain	3%	42
96	3	0.69	3% Tensile Strain	3%	123
96	5	0.81	Ovalization	f = 0.15	161
96	10	1.03	Ovalization	f = 0.15	233
58	0	0.46	Local Buckling	-9.73×10^3	0
58	1	0.73	3% Tensile Strain	3%	59
58	3	0.82	Ovalization	f = 0.15	78
58	5	1.21	GFRP Rupture	0.02182	163
58	10	1.86	GFRP Rupture	0.02182	304

4.5.4. Evaluation of the Efficiency of BFRP Wraps

The impact of wrapping the pipe outer surface with BFRP wraps was investigated via in a manner similar to one utilized for CFRP and GFRP composites. In this aspect the increment in d_{cr} value (i.e., fault displacement value inducing the violation of one these limit states) shift in the mode of failure served the basis for performance evaluation of the applied FRP wraps. As mentioned earlier, the layer thicknesses considered in this study are 1mm, 3mm, 5mm and 10mm. Analysis results were reported only for cases with $\beta = 10°$. Figure 4.47a to 4.49e present the reductions achieved for longitudinal pipeline strains for layer thicknesses ranging from 1mm up to 10mm under the applied fault load of 1m and D/t ratios of 144, 96, and 58 respectively. Obtained results indicate that a reduction of as much as 63% is achievable when a BFRP layer of 10mm is used for damage mitigation, a much higher improvement that increasing the wall thickness of the entire pipe from 6.35mm to 15.88m or adjusting the buried pipe orientation in reference to the fault plane.

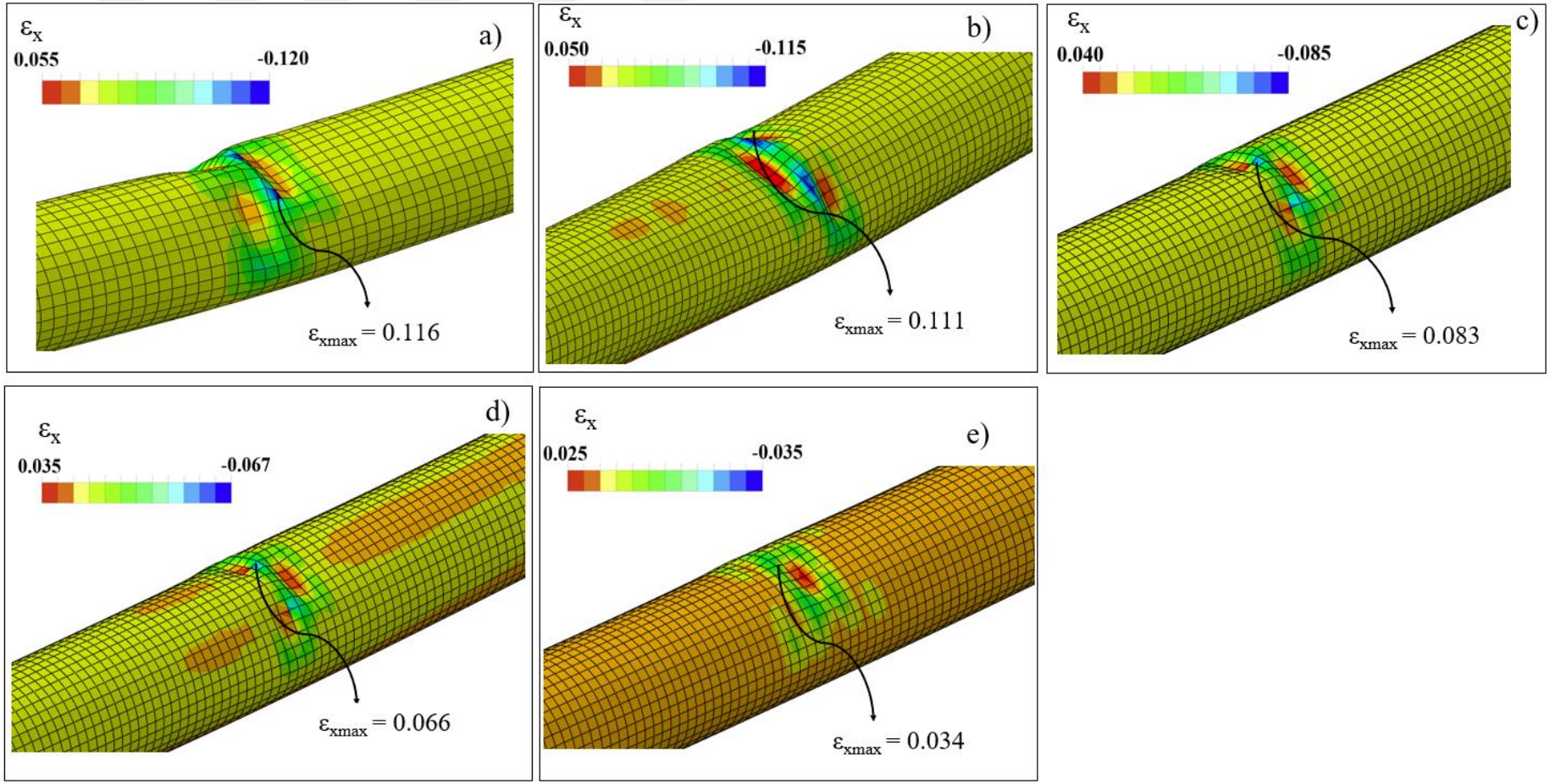

Figure 4.47. Reduction of longitudinal pipeline strains using BFRP wraps of a) t_c = 0mm, b) t_c = 1mm, c) t_c = 3mm, d) t_c = 5mm, and e) t_c = 10mm for D/t = 144, β =10° and d = 1m

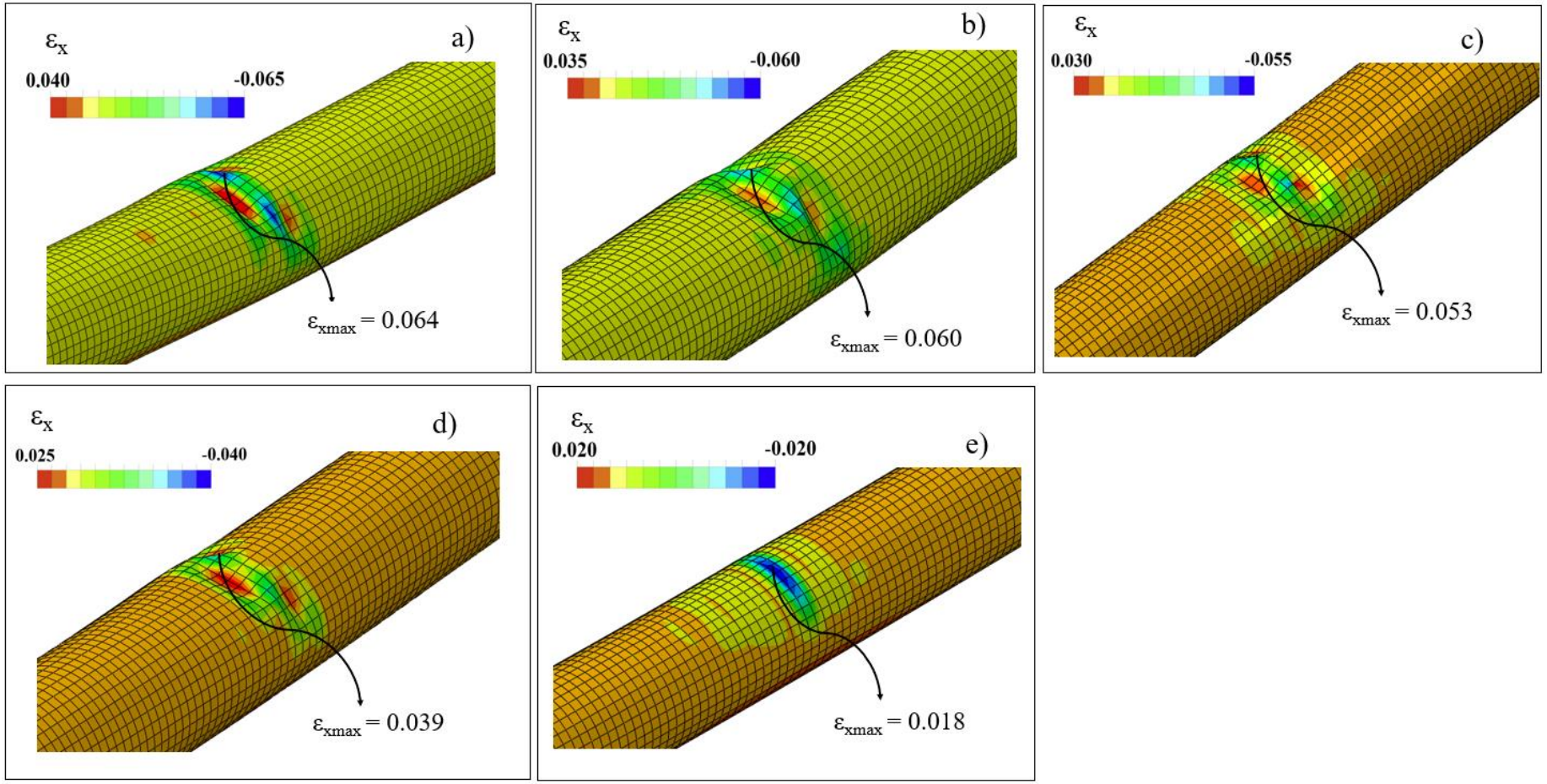

Figure 4.48. Reduction of longitudinal pipeline strains using BFRP wraps of a) t_c = 0mm, b) t_c = 1mm, c) t_c = 3mm, d) t_c = 5mm, and e) t_c = 10mm for D/t = 96, β =10° and d = 1m

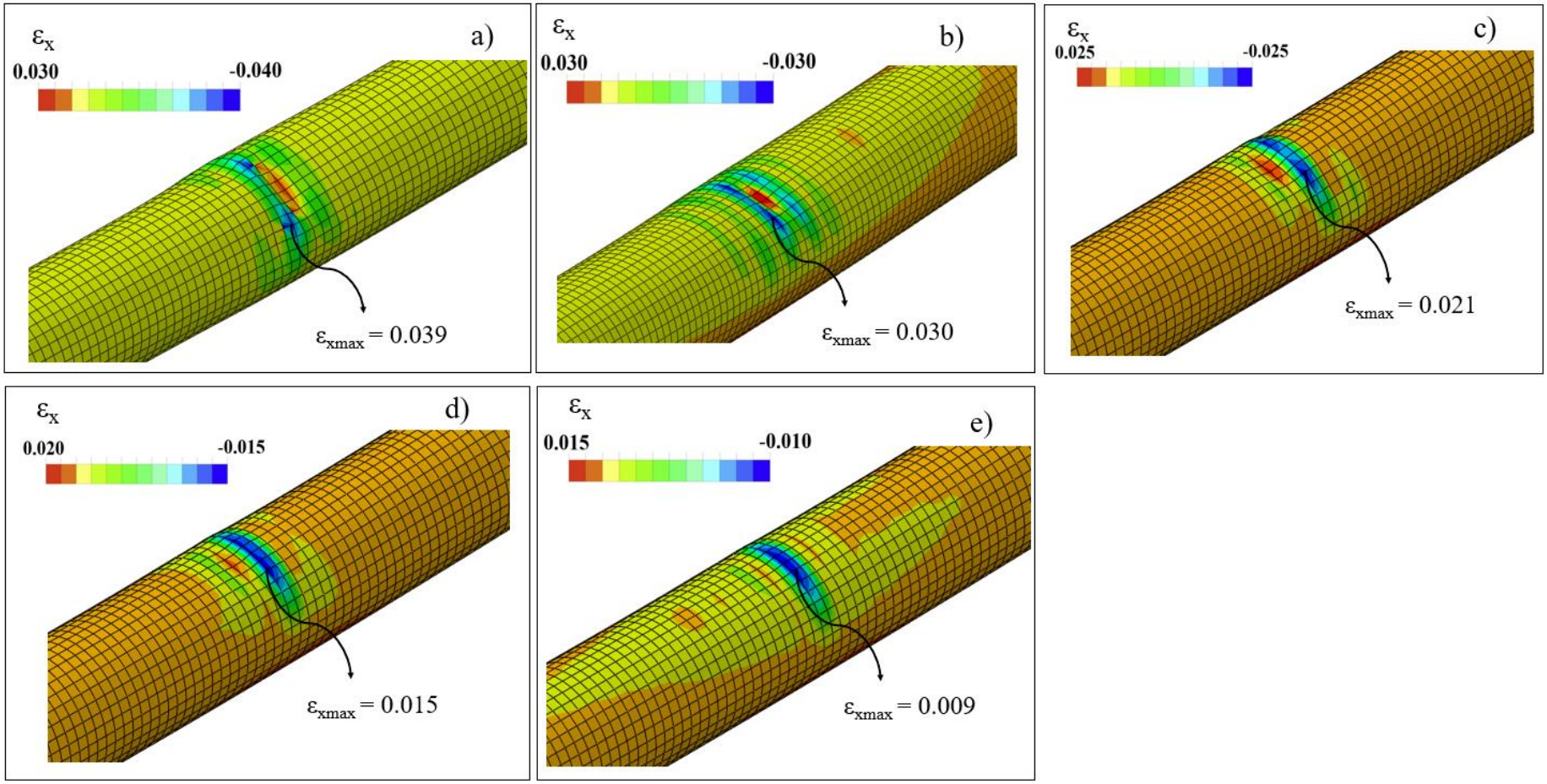

Figure 4.49. Reduction of longitudinal pipeline strains using BFRP wraps of a) t_c = 0mm, b) t_c = 1mm, c) t_c = 3mm, d) t_c = 5mm, and e) t_c = 10mm for D/t = 58, β =10° and d = 1m

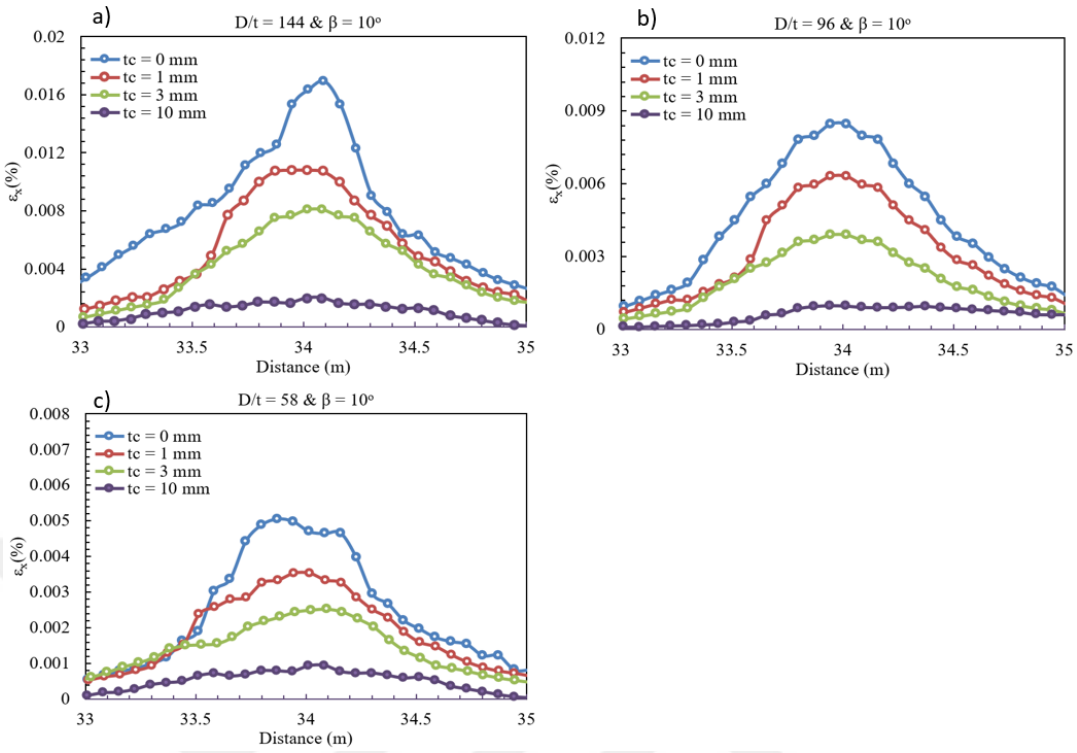

Figure 4.50. Variation of the axial strain distribution recorded at the deformed pipe side subjected to tension, for a) D/t =144, b) D/t =96, and c) D/t =58, β = 10°, and t_c varying between 0mm and 10mm

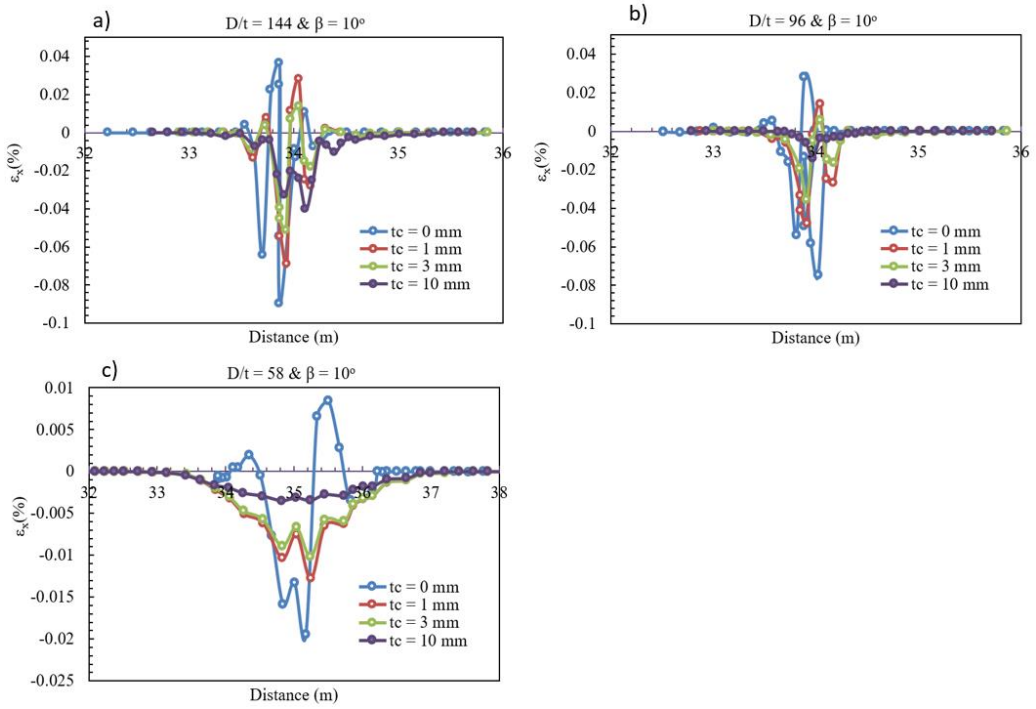

Figure 4.51. Variation of the axial strain distribution recorded at the deformed pipe side subjected to compression for, a) D/t =144, b) D/t =96, and c) D/t =58, β = 10°, and t_c varying between 0mm and 10mm

Evaluation of the BFRP wrap thickness in terms of performance criteria is summarized in Table 4.11. While for cases not incorporating FRP wraps the dominant mode of pipeline failure is local buckling as the wrap thickness increases this mode changes to either to maximum tensile strain limit state of 3% (for D/t = 144) or to cross-sectional distortion (for D/t = 96) or CFRP Wrap rupture limit state (for D/t = 58). While investigation made in terms of longitudinal and axial strains did not show any significant effect of D/t ratio on the mitigation offered by BFRP wrap, the data summarized in Table 4.11 underlines and clearly shows that as the D/t gets lower the Wrap rupture limit states becomes the dominant mechanism of deformation and eliminates the possibility of the occurrence of other damage modes. In overall, an increment of more than 270% in d_{cr} value is shown to be attainable whenever a BFRP wrap with a layer thickness of 10mm is utilized for damage mitigation.

Table 4.11. Variation of the mode of failure and d_{cr} value with respect to BFRP inclusion

D/t	**t_c (mm)**	**d_{cr} (m)**	**Failure Mode**	**Limit Value**	**Increase in d_{cr} (%)**
144	0	0.22	Local Buckling	-9.73×10^3	0
144	1	0.28	Local Buckling	-9.73×10^3	27
144	3	0.37	Local Buckling	-9.73×10^3	68
144	5	0.49	Ovalization	f = 0.15	123
144	10	0.69	Ovalization	f = 0.15	214
96	0	0.31	Local Buckling	-9.73×10^3	0
96	1	0.39	3% Tensile Strain	3%	26
96	3	0.64	3% Tensile Strain	3%	107
96	5	0.66	Ovalization	f = 0.15	154
96	10	0.97	Ovalization	f = 0.15	223
58	0	0.46	Local Buckling	-9.73×10^3	0
58	1	0.64	3% Tensile Strain	3%	39
58	3	0.73	Ovalization	f = 0.15	59
58	5	1.14	Ovalization	0.02182	148
58	10	1.74	BFRP Rupture	0.02182	278

4.5.5. Comparison of the Efficiencies of FRP Composite Wrap Types

The positive influence of wrapping a buried steel pipeline exposed to strike-slip fault motion with a FRP composite wrap was proven separately for each FRP type considered within the scope of this study in the previous sections. This section presents the comparison of the efficiency of FRP types relative to each other. Reviewing the distribution of axial strains and the tension and compression side of the buckled pipe presented in Figures 4.52a to 4.53c for D/t = 96 shows that the use of CFRP wraps has the highest positive impact on the behavior of the same buried pipe configurations exposed to the same loading conditions. Furthermore, graphical comparison of the rate of increment in d_{cr} value presented in Figure 4.54 shows the superiority of CFRP composites for each D/t case considered within the scope of this dissertation. Plot of tensile strain developments under incremental fault displacements ranging from 0m to 0.80m shown in Figure 4.46 indicates that the use of GFRP and BFRP wraps with a layer thickness of 1mm is not sufficient enough to avoid failure due to the exceedance of tensile strain limit of 3%, whereas the use of thicker layers for all FRP composites reduced the resulting strains below the threshold value. Similarly, plots of compressive strains given in Figure 4.55 shows that buckling might be avoided up much increased d_{cr} values through the use of these composites.

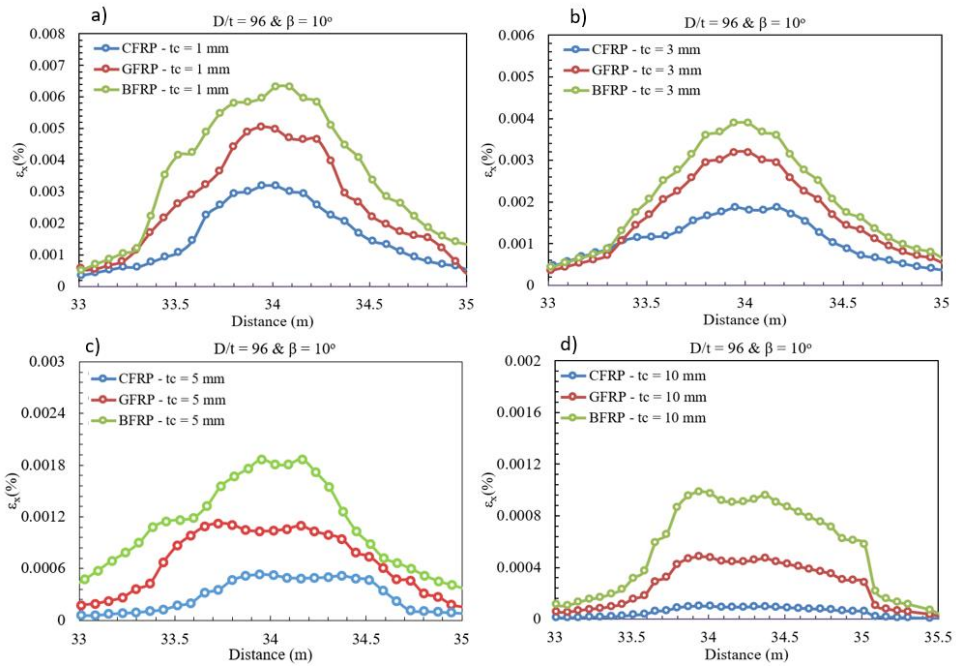

Figure 4.52. Comparison of the efficiency of FRP composite wraps in terms of axial strains at tension side for, a) t_c = 1mm, b) t_c = 3mm, c) t_c = 5mm, and d) t_c = 10mm

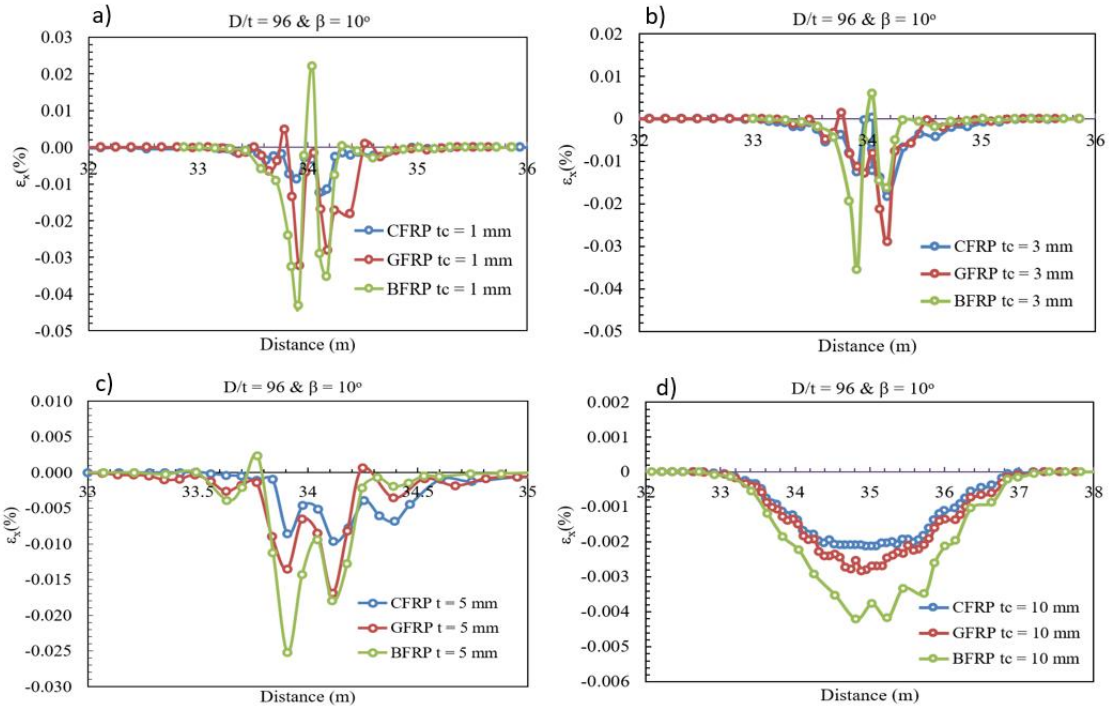

Figure 4.53. Comparison of the efficiency of FRP composite wraps in terms of axial strains at compression side for, a) t_c = 1mm, b) t_c = 3mm, c) t_c = 5mm, and d) t_c = 10mm

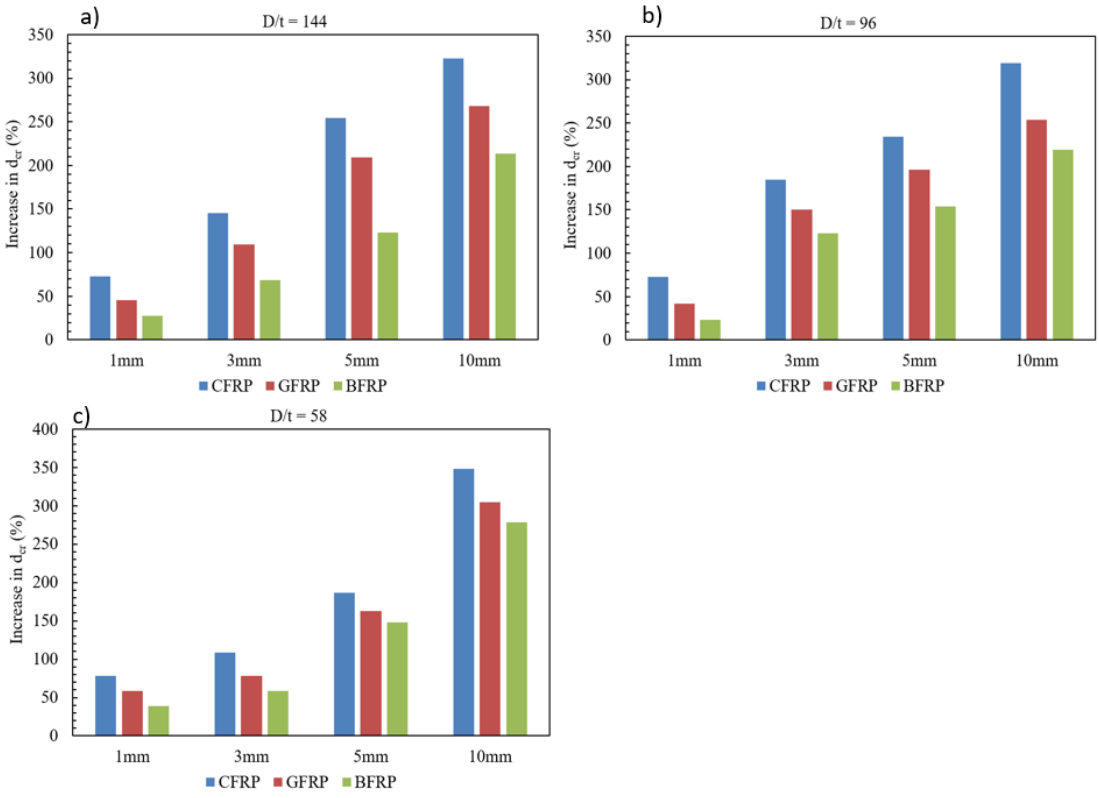

Figure 4.54. Comparison of the efficiency of FRP composite wraps in terms increase in d_{cr} value for, a) D/t = 144, b) D/t = 96, and c) D/t = 58

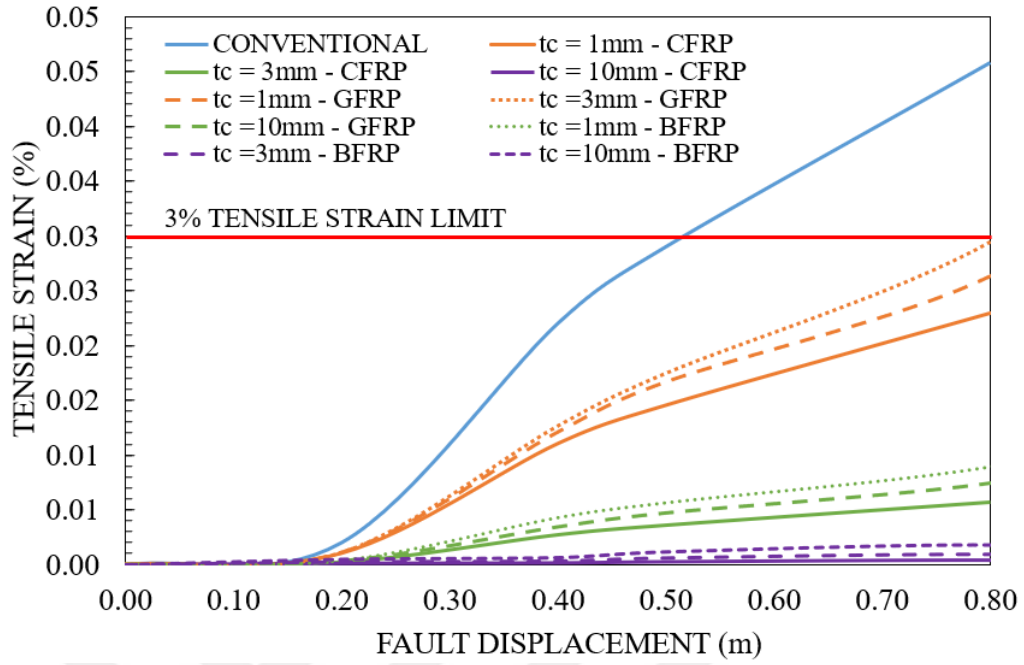

Figure 4.55. Comparison of the variation of pipe axial tensile strains under incremental fault displacements and protected using CFRP, GFRP, and BFRP wraps

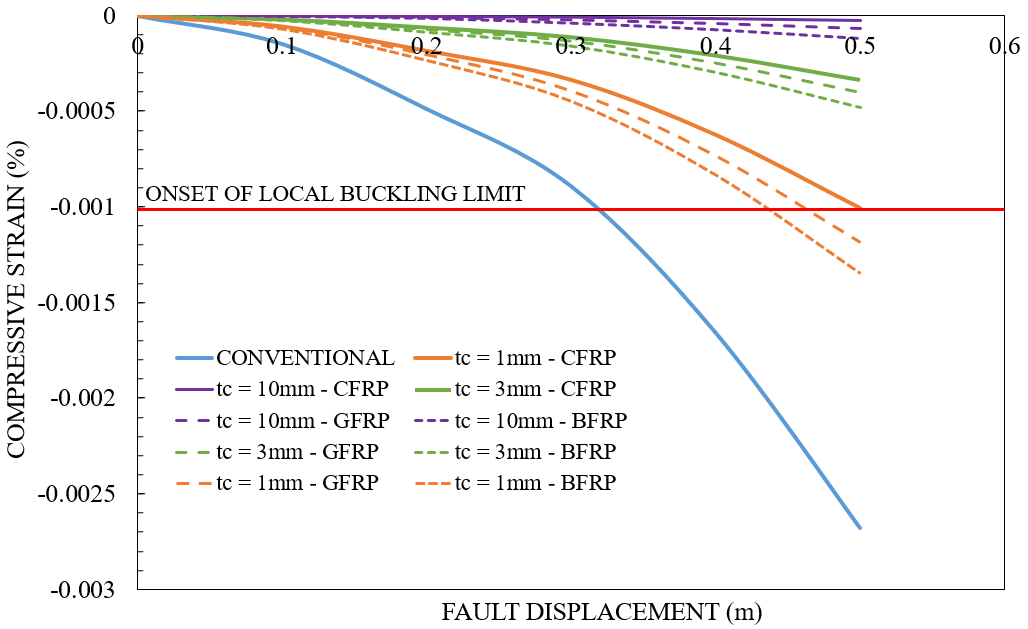

Figure 4.56. Comparison of the variation of pipe axial compression strains under incremental fault displacements and protected using CFRP, GFRP, and BFRP wraps

4.6. Damage Mitigation of Buried Steel Pipes Using EPS Geofoam Blocks

Mitigation of seismic damage and demands on buried steel pipes subjected to strike-slip fault action was also investigated through the use of EPS geofoam blocks with varying strength classes. As a starting point for the evaluation and visualization of the effectiveness of utilizing EPS geofoam blocks for mitigating the seismic deformations originating from the actions of faults (strike-slip in this case) the study compares the results of axial strains at the tension and compression side of the buckled pipe. Figures 4.57a through 4.57d show the obtained axial strain (compression side only) results plotted versus their respective locations (distances) over the buried pipe length accumulated under fault displacement values of 0.50m, 1m, 1.5m and 2m respectively for D/t = 96 and $\beta = 10^{o}$. Comparison of the results indicates a significant reduction in axial strains at all fault displacement values investigated. While as expected the effectiveness of Low Strength EPS geofoam is noted to be less than that of High Strength one, yet the amount of decrements appear to be considerable high. A reduction of as much as 74.8% is observed for HS EPS, whereas the reduction rate for LS EPS was 51.9%. In addition, plots also reveal that the distribution of strains along the length of the pipe changes due to the effect of utilizing EPS geofoam blocks, a more uniform-rather than a concentrated-distribution is clearly observed (Figure 4.58a), for instance an increment from 1.61m to 4.37m is noted under a fault displacement of 0.50m.

Figure 4.49 depicts the change of tensile strains on the buried pipe with respect to applied fault displacement value. Obtained results indicate that the conventional buried pipeline subjected directly to the applied fault displacement exceeds the tensile strain threshold of 3% at exactly 0.46m of fault displacement and undergoes structural failure. However, when protected using EPS geofoam the strains reduce significantly, such that no failure occurs even when the applied fault displacement exceeds 1m incorporating high strength EPS. Comparison in terms of minimum compressive strains along with local buckling limit is shown in Figure 4.59. Plotted for a fault displacement range of 0.1 to 0.50m and for D/t = 96 the results indicate that the conventional buried pipe already undergoes buckling at a considerably low values of fault displacement (31cm), however, when protected using EPS geofoam the response and performance of these buried pipes improves significantly and the fault displacement value leading to buckling increases (from 31cm to 67cm when high strength EPS is used). As shown in Table 4.12 the pipeline modes of failure and the

associated critical fault displacement values leading to it are greatly influenced by the use of EPS geofoam, an increment of as much 130% is determined to be achievable via the use of high strength EPS and a D/t ratio of 58. Moreover, the results indicate that the mode of failure also changes with respect to the use of EPS.

The anticipated benefit of using EPS geofoam protection in distributing the fault rupture induced deformation along a longer length and thus avoiding the accumulation of high level of stresses and strain that would otherwise lead to the failure of the pipe is investigated by obtaining the variation of cross-sectional distortion defined in terms of ovalization factor of f = 0.15 in this study along the pipeline length. Shown in Figures 4.60a through 4.62 is the plot of the variation of this factor along the pipeline length at the vicinity of fault trace at displacement values between 0.20m-0.80m. Results obtained for the conventional case (Figure 4.51) indicate that at d = 0.80m the pipeline has already undergone cross-sectional flattening (exactly at 65cm), however encasing the pipeline within EPS geofoam offsets the d_{cr} value at a value higher than 0.80m (84cm for low strength and 102cm for high strength EPS respectively).

Moreover, the length through which ovalization occurs-distribution of damage-increases from 1.50m for conventional pipe to 3.80m (an increment of more than 150%) for case utilizing high strength EPS. Lastly, Figure 4.63 illustrates the change in pipeline longitudinal strain distributions, while a concentrated stress pattern and localized deformation is observed from the numerical model results corresponding to a fault displacement value of 1m for conventional pipe buried within traditional soil backfill, this changes to a much uniform distribution and no localized damage occurrence when EPS geofoam is utilized.

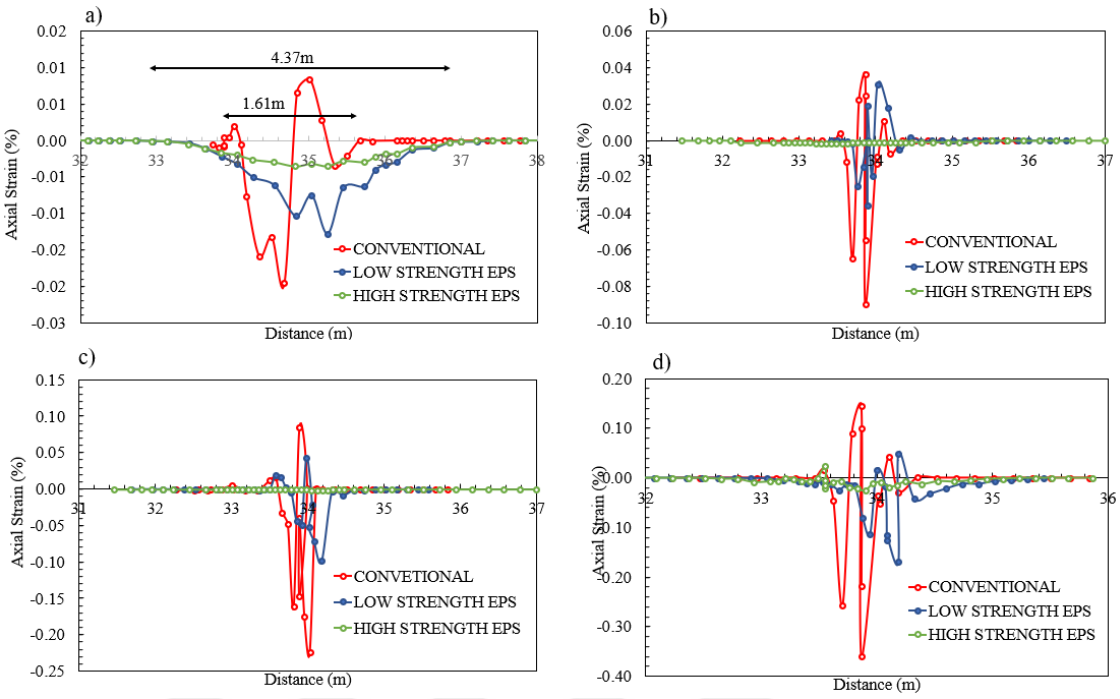

Figure 4.57. Effect of using Low and High Strength EPS geofoam blocks on axial strains recorded at the deformed pipe side subjected to compression for D/t = 96 and β = 10^{o} at fault displacement of a) d = 0.50m, b) d = 1m, c) d = 1.50m and d) d = 2m

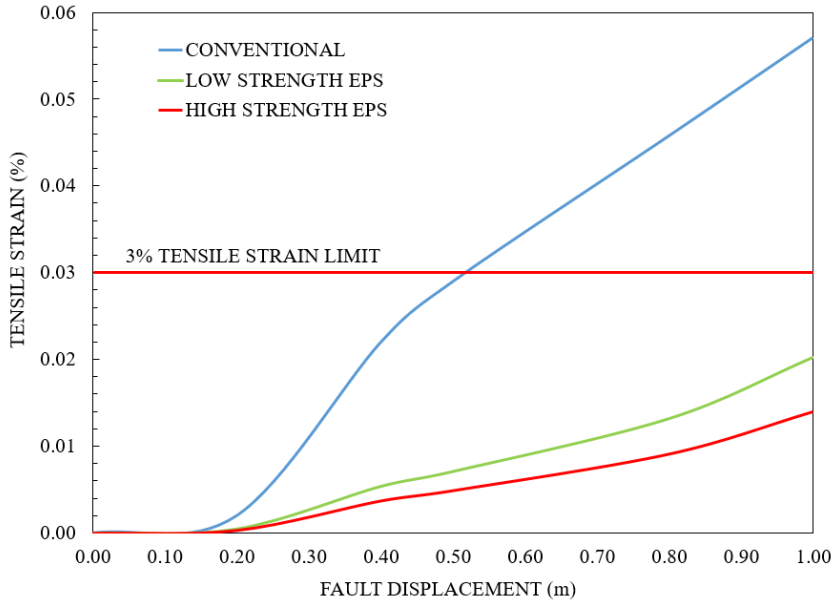

Figure 4.58. Effect of EPS geofoam protection on the evolution of pipeline tensile strains in reference to the fault displacement increment for D/t = 96 and β = 10^{o}

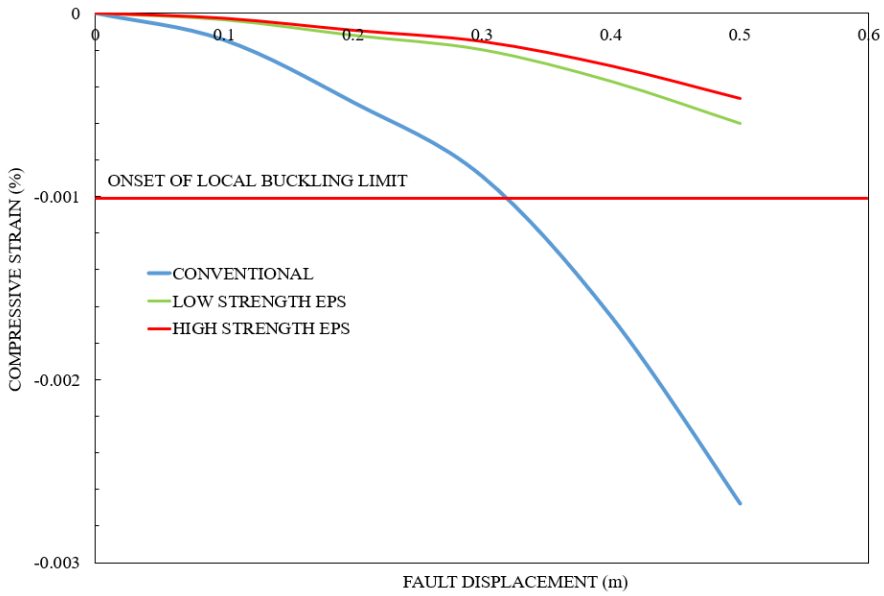

Figure 4.59. Effect of EPS geofoam protection on the evolution of pipeline buckling strains with respect to fault displacement increments up to 0.50m for D/t = 96 and β = 10º

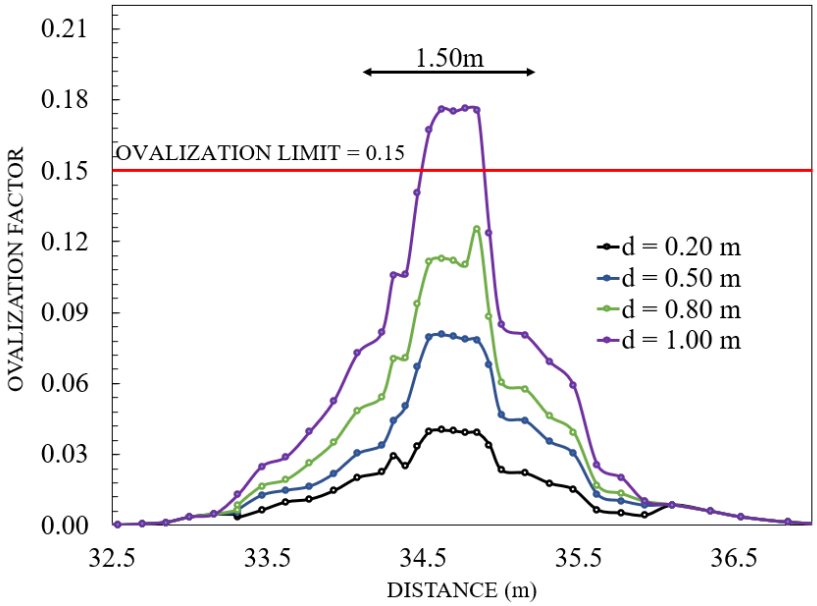

Figure 4.60. Variation of cross-sectional distortion (ovalization factor) along the pipe length for conventional buried pipe for D/t = 96 and β = 10º

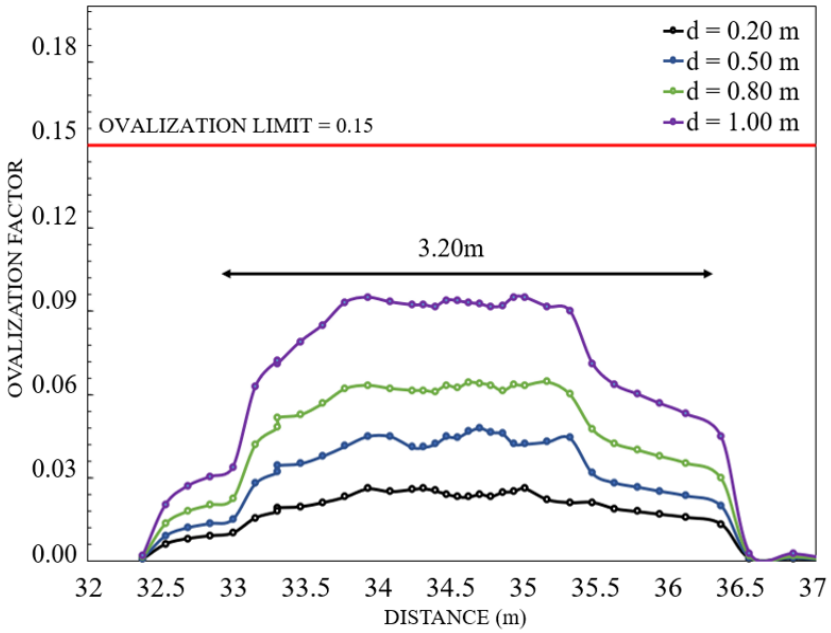

Figure 4.61. Variation of cross-sectional distortion (ovalization factor) along the pipe length for buried pipe protected using Low Strength EPS for D/t = 96 and β = 10º

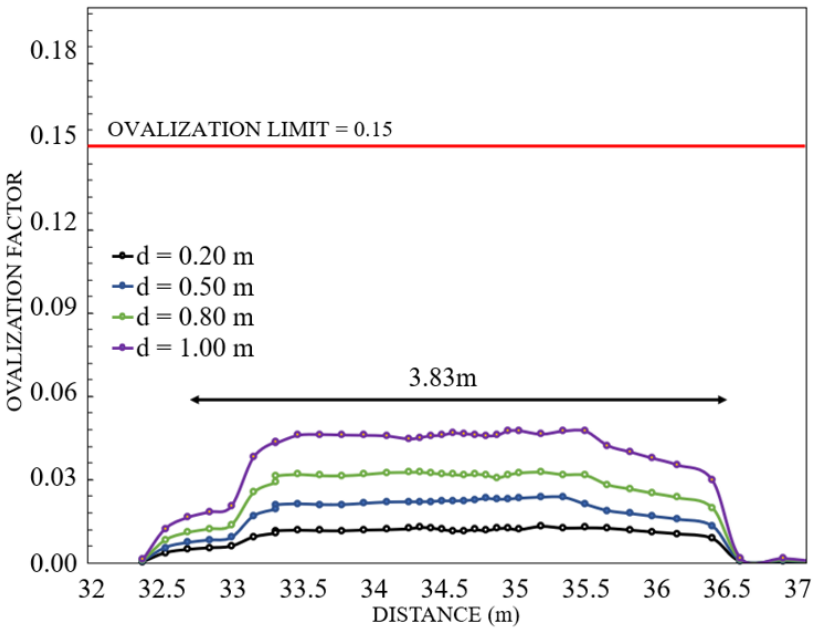

Figure 4.62. Variation of cross-sectional distortion (ovalization factor) along the pipe length for buried pipe protected using High Strength EPS for D/t = 96 and β = 10º

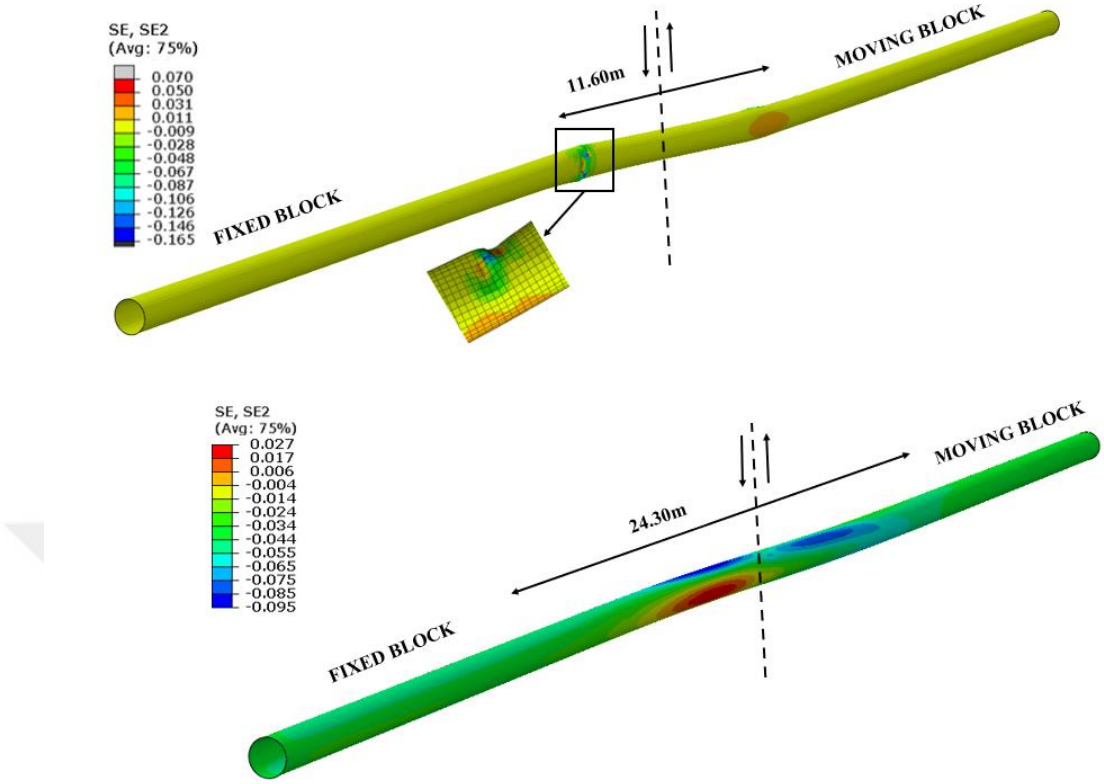

Figure 4.63. Graphical illustration of the variation of longitudinal strains using EPS Geofoam at d = 1.50m and D/t = 96

Table 4.12. Variation of the mode of failure and d_{cr} value with respect to EPS geofoam use

D/t	Condition	d_{cr} (m)	Failure Mode	Limit Value	Increase in d_{cr} (%)
144	Conventional	0.22	Local Buckling	-9.73×10^{3}	0
144	LS EPS	0.41	Local Buckling	-9.73×10^{3}	87
144	HS EPS	0.50	Local Buckling	-9.73×10^{3}	127
96	Conventional	0.46	Local Buckling	-9.73×10^{3}	0
96	LS EPS	0.84	Ovalization	f = 0.15	83
96	HS EPS	1.01	3% Tensile Strain	3%	120
58	Conventional	0.59	3% Tensile Strain	3%	0
58	LS EPS	1.09	Ovalization	f = 0.15	82
58	HS EPS	1.36	3% Tensile Strain	3%	130

4.7. Damage Mitigation of Buried Steel Pipes Using CLSM

Another strategy utilized for seismic damage mitigation of buried steel pipes subjected to faulting actions considered the use of controlled-low strength material (CLSM) encasement. This approach aimed at creating a uniform shield around the pipe that is anticipated to sustain the deformations due to seismic actions and thus reduce their effect on the buried pipe. As described under Chapter 3 within the scope of the study presented in this dissertation a rectangular CLSM box with a width of 2m and height and length equal to that of the analysis model was assumed to exist around the buried. Two strength classes, namely a low and high strength CLSM were considered to evaluate the effect of this parameter. Due to the fact that these materials have properties somewhere between a soil and a cementitious material to evaluate the effect of material modeling approach the study adopted two distinct material models. In particular, each investigated case was run through the use of both Mohr-Coulomb constitutive material model (the same one use for native soil) and concrete damage plasticity model what required the definition of tension and compression behavior.

Figures 4.64a to 4.65c show the variation of longitudinal strain distributions along the buried pipe recorded under fault displacement load of 1m for D/t = 96 and $\beta = 10^{o}$ for cases modeled using both of the above-mentioned material modeling approaches. Investigation of these results reveal that incorporation of CLSM leads to a reduction in the intensity of strains. A reduction of nearly 28% and 35% is noted with the use of low and high strength CLSM respectively, which compared to other mitigation strategies utilized in this dissertation is the lowest value. Comparison of the influence of material modeling approach indicates to a slight difference, where the use of Mohr-Coulomb model led to slightly (around 10%) decreased strains values.

Compared in terms of the effect on the distribution of axial strains at compression side shown in Figure 4.66a to 4.67b for fault displacements of 0.50m, and 1m respectively, results reveal a decrement in axial strains of the pipe using CLSM mixtures. Once again, result indicate that the use of Mohr-Coulomb model instead of concrete damage plasticity approach leads to slightly reduced axial strain values. Hence, it is suggested that the use of CDP model instead of Mohr-Coulomb might be a more accurate approach for this material type.

Investigation of the rate of change in tensile strains under incremental fault displacement shown in Figure 4.68 (only including results obtained using CDP material model) indicates that for this performance criteria avoidance of failure due to the exceedance of the threshold value of 3% is not attainable unlike the use of FRP wraps and EPS geofoam blocks. However, results show that cases incorporating CLSM exceed this threshold at larger fault displacement value. While the steel pipe buried under traditional soil reached the limit value at 46cm, this value was offset to 77cm and 84cm using low and high strength CLSM respectively. Similarly, review of the change in compression strains (see Figure 4.69) show that the conventional buried pipe already undergoes buckling at a considerably low values of fault displacement (31cm), but the use of low and high strength CLSM shifts this displacement value up to 43cm and 56cm respectively. Summarized in Table 4.13, numerical investigation of the rate of change in critical fault displacement value shows that by the use of CLSM mixtures, an increment of as much 51% and 72% is attainable though the use of low and high strength option of this material.

Table 4.13. Variation of the mode of failure and d_{cr} value with respect to CLSM use

D/t	Condition	d_{cr} (m)	Failure Mode	Limit Value	Increase in d_{cr} (%)
144	Conventional	0.22	Local Buckling	-9.73×10^{3}	0
144	LS CLSM - MCHR	0.30	Local Buckling	-9.73×10^{3}	35
144	LS CLSM - CDP	0.34	Local Buckling	-9.73×10^{3}	55
144	HS CLSM - MCHR	0.36	Ovalization	f = 0.15	64
144	HS CLSM - CDP	0.39	Ovalization	f = 0.15	77
96	Conventional	0.31	Local Buckling	-9.73×10^{3}	0
96	LS CLSM - MCHR	0.38	3% Tensile Strain	3%	23
96	LS CLSM - CDP	0.42	3% Tensile Strain	3%	36
96	HS CLSM - MCHR	0.44	Ovalization	f = 0.15	42
96	HS CLSM - CDP	0.47	Ovalization	f = 0.15	52
58	Conventional	0.49	3% Tensile Strain	3%	36
58	LS CLSM - MCHR	0.66	3% Tensile Strain	3%	45
58	LS CLSM - CDP	0.74	3% Tensile Strain	3%	51
58	HS CLSM - MCHR	0.80	Ovalization	f = 0.15	63
58	HS CLSM - CDP	0.84	Ovalization	f = 0.15	72

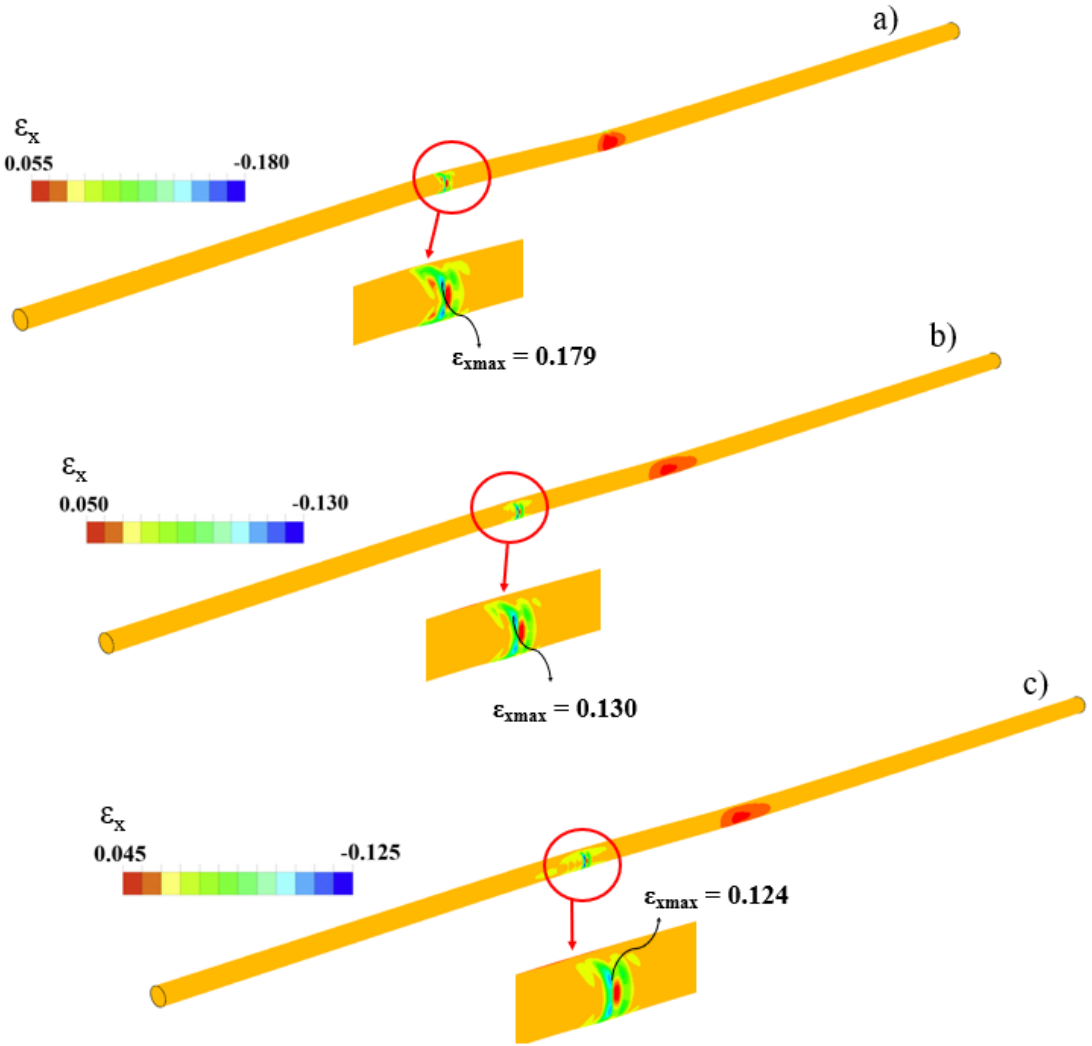

Figure 4.64. Graphical illustration of the variation of longitudinal strains using low strength CLSM assuming, a) No mitigation, b) Mohr-Coulomb model, and c) CDP model recorded at d = 1.00m and D/t = 96

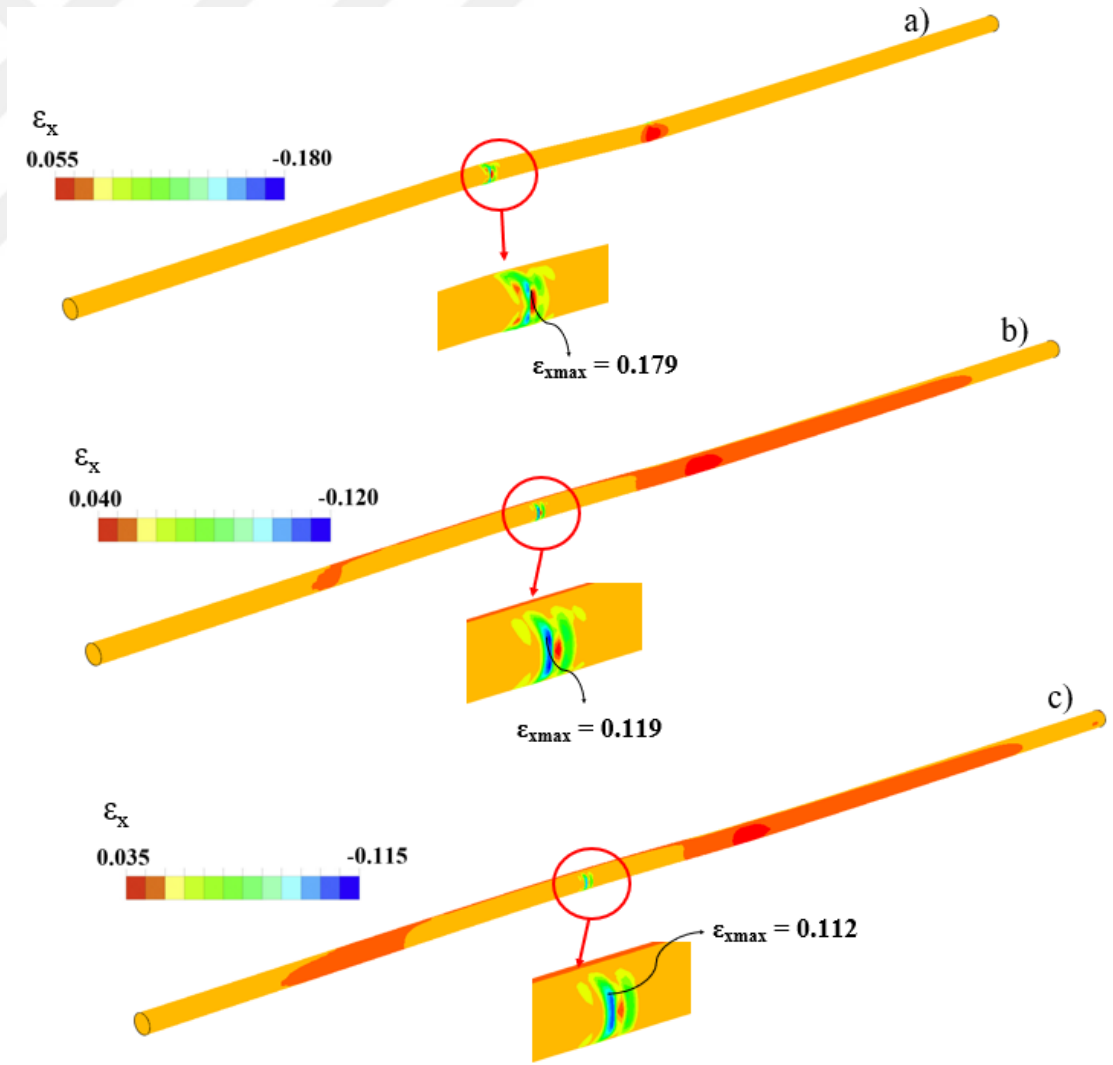

Figure 4.65. Graphical illustration of the variation of longitudinal strains using high strength CLSM assuming, a) No mitigation, b) Mohr-Coulomb model, and c) CDP model recorded at d = 1.00m and D/t = 96

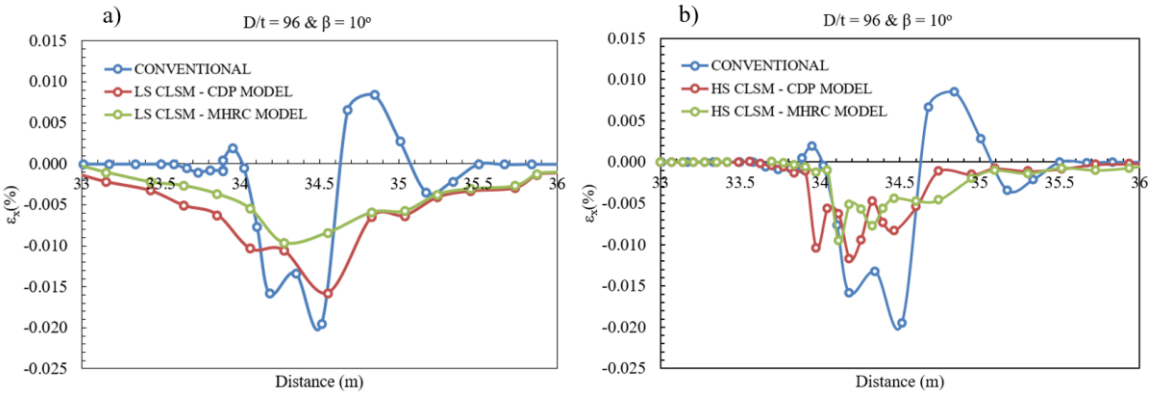

Figure 4.66. Effect of using a) low strength CLSM, and b) high strength CLSM mixture on axial strains recorded at the deformed pipe side subjected to compression for D/t = 96 and β = 10° plotted at d = 0.50m

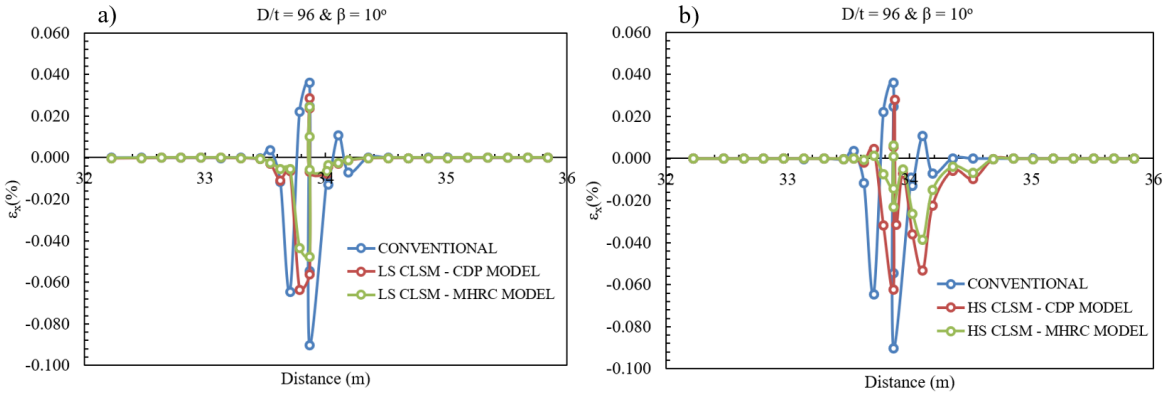

Figure 4.67. Effect of using a) low strength CLSM, and b) high strength CLSM mixture on axial strains recorded at the deformed pipe side subjected to compression for D/t = 96 and β = 10° plotted at d = 1m

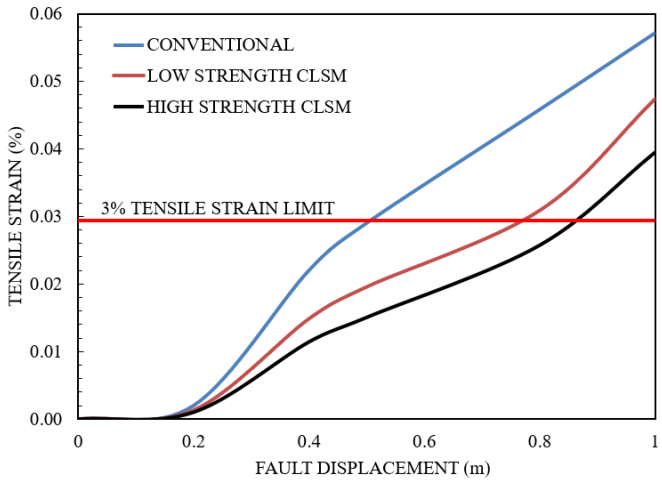

Figure 4.68. Effect of CLSM use on the evolution of pipeline tensile strains in reference to the fault displacement increment for D/t = 96 and β = 10°

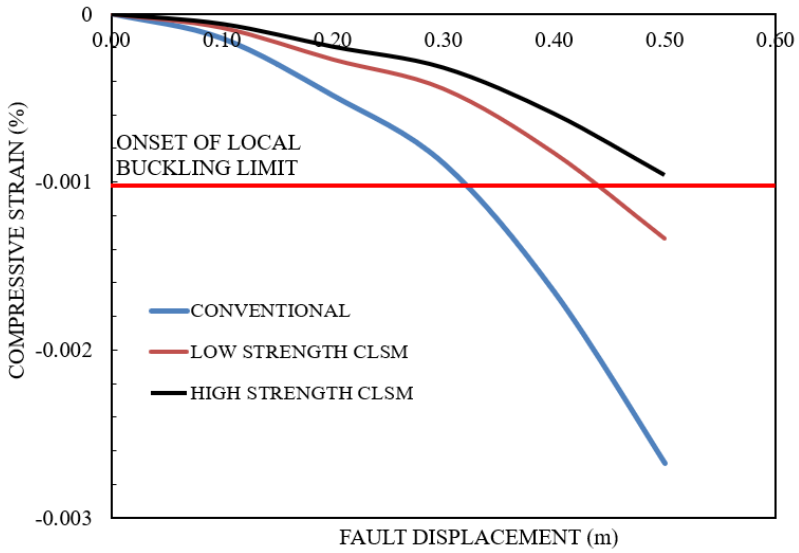

Figure 4.69. Effect of CLSM use on the evolution of pipeline compressive strains in reference to the fault displacement increment for D/t = 96 and β = 10º

4.8. Damage Mitigation of Buried Steel Pipes Using Geogrid Reinforcement

Lastly this thesis investigated the utilization of geogrid reinforcement as a remedy against the detrimental seismic effects induced by the strike-slip fault rupture incidents. Configurations incorporating single and double layers of this material were analyzed developing numerical models where the geometry of the geogrid layers including the apertures have been detailly modeled. As mentioned earlier, studies have shown that the inclusion of geogrid layers within a soil deposit enhances its load bearing properties. Specifically in terms of seismic loads, studies have revealed that geogrid reduces these effects through the widening of the shear zone of the faults trace and thus leading to a reduction. This effects also served the basis for utilization of this material for buries steel pipe cases investigated within the scope of this thesis.

Similar to the cases incorporating FRP composite wraps, EPS geofoam blocks, and CLSM mixtures, a strain-based evaluation approach was utilized also for the evaluation of the performance of buried pipes protected using geogrid. Figures 4.70a through 4.70c show the variation of longitudinal strain distributions along the buried pipe recorded under fault displacement load of 1m for D/t = 96 and β = 10º for cases incorporating single and double layers or geogrid reinforcement. Investigation of these results reveal that the use of this

mitigation strategy leads to a reduction in the magnitude and concentration of strains. A reduction of nearly 53% and 71% is noted with the use single- and double-layer configurations respectively, which comes third following FRP and EPS approaches.

Figures 4.71a and 4.71b show the obtained axial strain (compression side only) results plotted versus their respective locations (distances) along the length of the pipeline accumulated under fault displacement values of 0.50m, and 1m, respectively for D/t = 96 and $\beta = 10^{o}$. Comparison of the results indicates a significant reduction in axial strains at all fault displacement values investigated. While as expected the effectiveness of double layer configuration is noted to be less than that of single layer, yet the amount of decrements appears to be considerable high. A reduction of as much as 64.5% is observed for double layer configuration, whereas the reduction rate for case incorporating single layer was 41.7%.

Investigation of the rate of change in tensile strains under incremental fault displacement shown in Figure 4.72 indicates that for this performance criteria avoidance of failure due to the exceedance of the threshold value of 3% is not attainable unlike the use of FRP wraps and EPS geofoam blocks. However, results show that cases incorporating geogrid exceed this threshold at larger fault displacement value. While the steel pipe buried under traditional soil reached the limit value at 46cm, this value was offset to 92cm and 105cm using single and double layers of geogrid respectively. Similarly, review of the change in compression strains (see Figure 4.73) show that the conventional buried pipe already undergoes buckling at a considerably low values of fault displacement (31cm), but the use of single and double layers of geogrid shifts this displacement value up to 54cm and 63cm respectively. Summarized in Table 4.15, numerical investigation of the rate of change in critical fault displacement value shows that by the use of geogrid, an increment of as much 67% and 96% is attainable though the use of low and high strength option of this material.

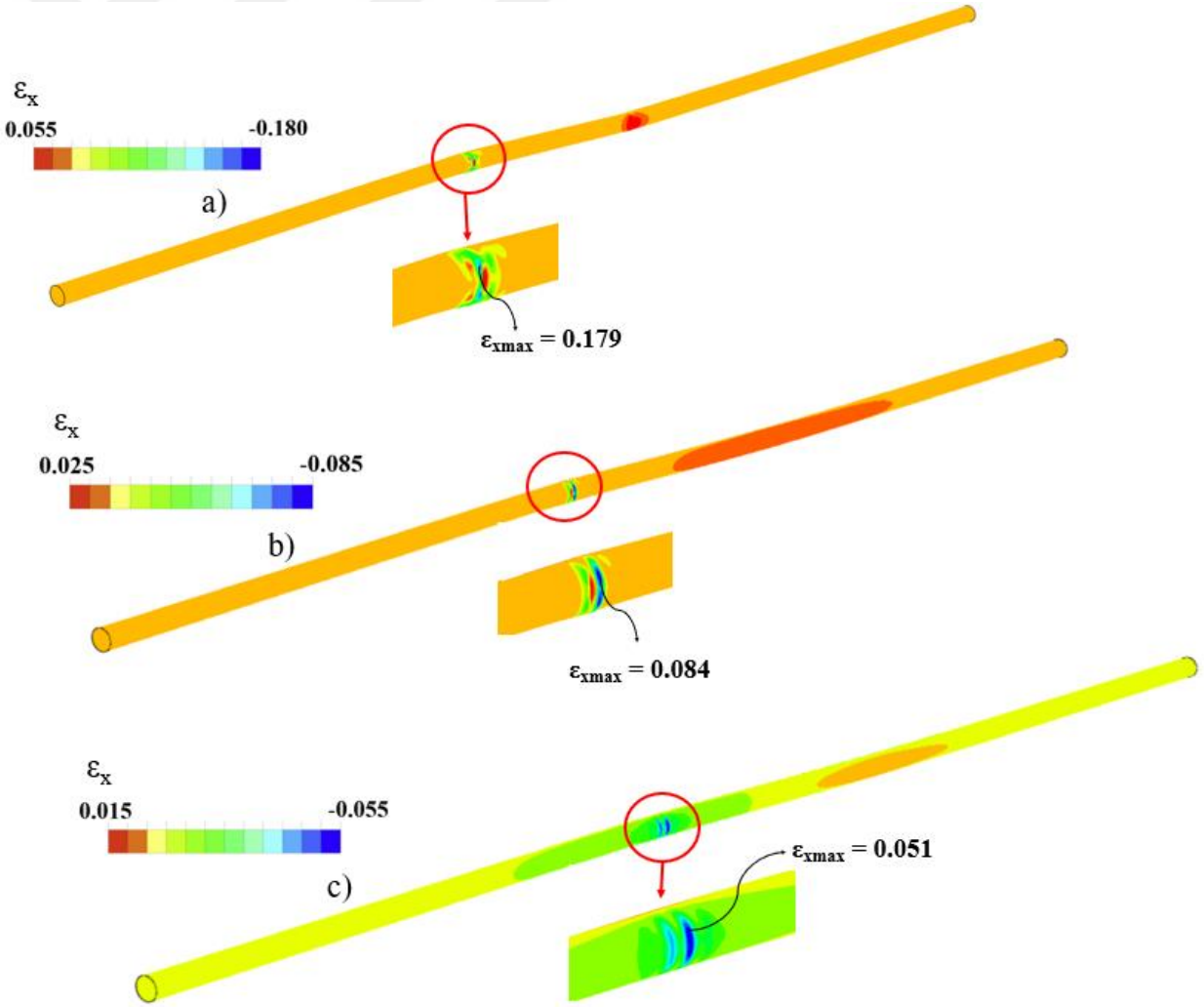

Figure 4.70. Graphical illustration of the variation of longitudinal strains using geogrid reinforcement, a) No mitigation, b) single layer, and c) double layers plotted at d = 1m

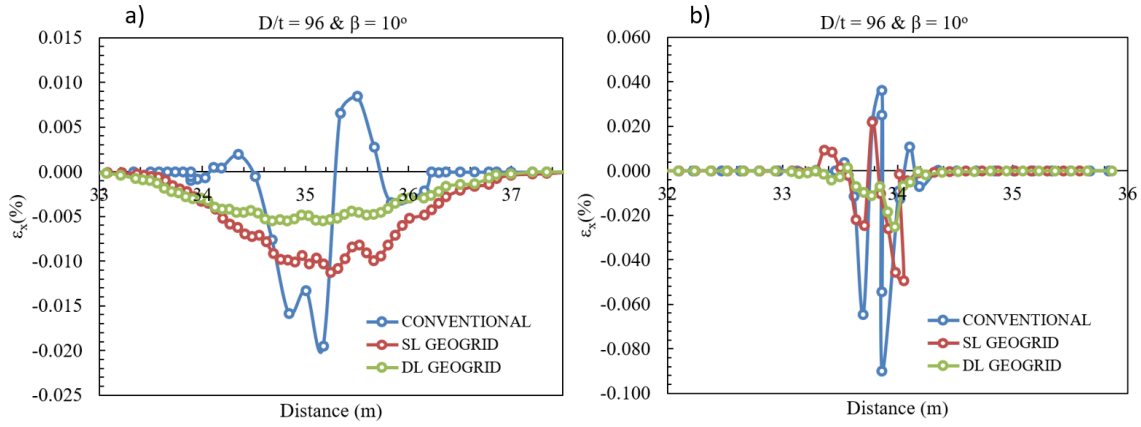

Figure 4.71. Effect of using single and double layers of geogrid reinforcement on axial strains recorded at the deformed pipe side subjected to compression for D/t = 96 and β = 10° plotted at, a) d = 0.50m, and b) d = 1m

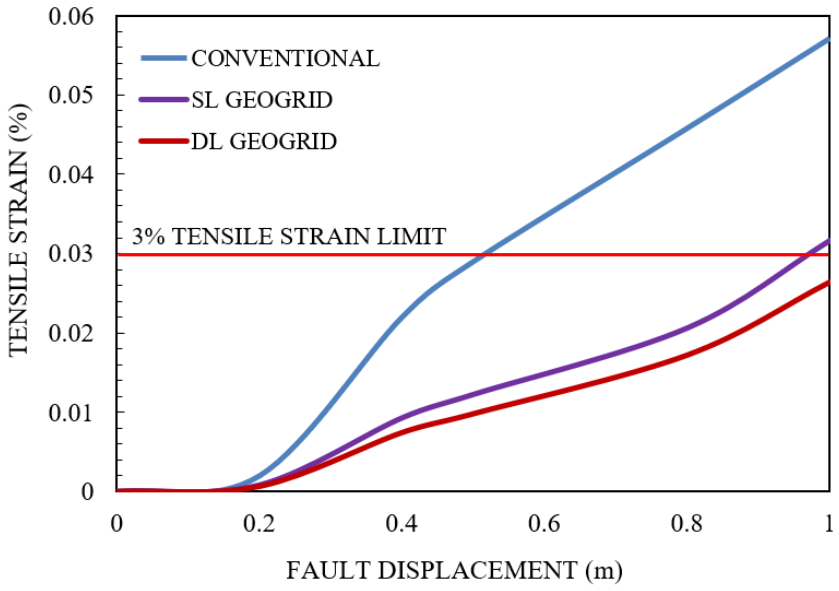

Figure 4.72. Effect of geogrid use on the evolution of pipeline tensile strains in reference to the fault displacement increment for D/t = 96 and β = 10°

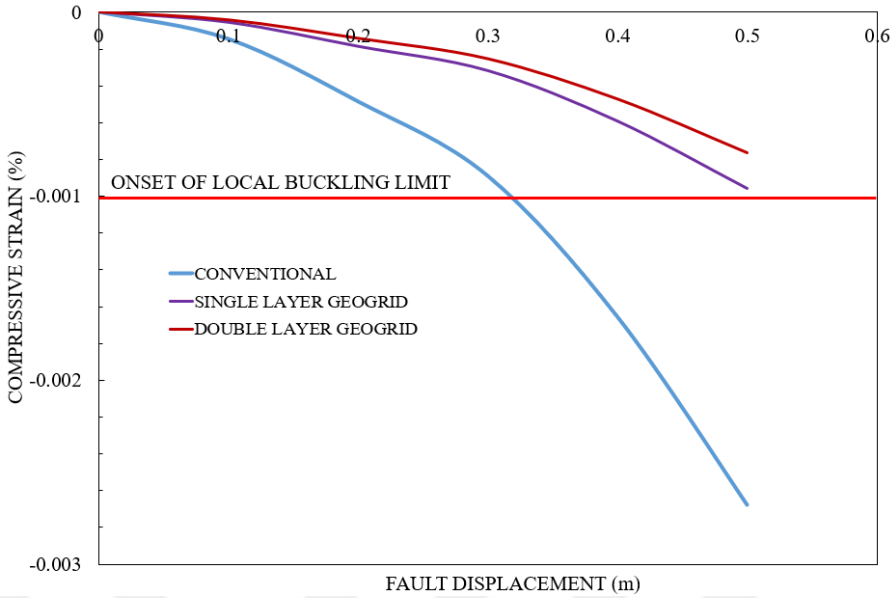

Figure 4.73. Effect of geogrid use on the evolution of pipeline compressive strains in reference to the fault displacement increment for D/t = 96 and β = 10º

Table 4.14. Variation of the mode of failure and d_{cr} value with respect to geogrid use

D/t	Condition	d_{cr} (m)	Failure Mode	Limit Value	Increase in d_{cr} (%)
144	Conventional	0.22	Local Buckling	-9.73×10^{3}	0
144	SL Geogrid	0.36	Local Buckling	-9.73×10^{3}	64
144	DL Geogrid	0.40	Ovalization	f = 0.15	82
96	Conventional	0.46	Local Buckling	-9.73×10^{3}	0
96	SL Geogrid	0.77	Ovalization	f = 0.15	67
96	DL Geogrid	0.85	3% Tensile Strain	3%	85
58	Conventional	0.59	3% Tensile Strain	3%	0
58	SL Geogrid	0.97	Ovalization	f = 0.15	63
58	DL Geogrid	1.16	Ovalization	f = 0.15	96

4.9. Comparison of the Effectiveness of Mitigation Approaches

This dissertation investigated the use of four mitigation approaches involving the utilization of a foreign material and do not include any modifications to the buried pipe itself. Previous sections evaluated the effect of using three types of FRP composite wraps possessing various layer thickness values, effect of shielding the buried pipe from the

surrounding native soil deposit via the use of EPS geofoam blocks, controlled-low strength material encasement, and lastly investigated the performance of buried steel pipes subjected to strike-slip faulting actions protected using Tensar Nr. 3 geogrid meshes. A strain-based evaluation approach comparing the rate of change in parameters such as the distribution of longitudinal and axial strains over the pipe length was utilized to visualize the effectiveness of these mitigation approaches. Moreover, determination and comparison of the critical values of fault displacement load leading to the structural failure of the pipe due to the exceedance of on the performance criteria also enabled to a meaningful and comprehensive comparison for the cases incorporating the use of this materials.

Comparison of the rate of change in d_{cr} values presented in Tables 4.9 through 4.15 and Figure 4.74 reveals that the most effective among the studied approaches is the use of FRP wraps and CFRP ones in particular, where an increment of nearly 350% in d_{cr} value was determined to be possible through the use of 10mm thick CFRP wraps. Results pointed out that the use of geofoam blocks was also effective where an increment of as much as 130% was determined to be possible. Among the studied approaches, placement of the buried pipe within a CLSM box was determined to be least effective approaches with only 75% increment in d_{cr} value.

Figures 4.75 through 4.80 show the comparison of the axial strain distributions along the length of the buried pipe obtained for cases incorporating the use of mitigation techniques studied in detail in previous sections. Recorded under d = 1m and for D/t = 96 plots show figuratively and numerically the effectiveness of the approaches against each other. Plots of the change in tensile and compressive strains obtained for small increments of the fault load given in Figures 4.81 and 4.82 allow a more intuitive look into the effectiveness of each investigated mitigation approach.

Lastly, Tables 4.15 through 4.18 present a cost calculation for each mitigation approach, allowing a simple cost-effectiveness comparison between the methods. Review of computed values show that despite their efficiency FRP wraps result in high additional costs (reaching up to 500,000 USD). Being the least effective method, CLSM has the second highest cost among these mitigation approaches (approaching 100,000 USD).

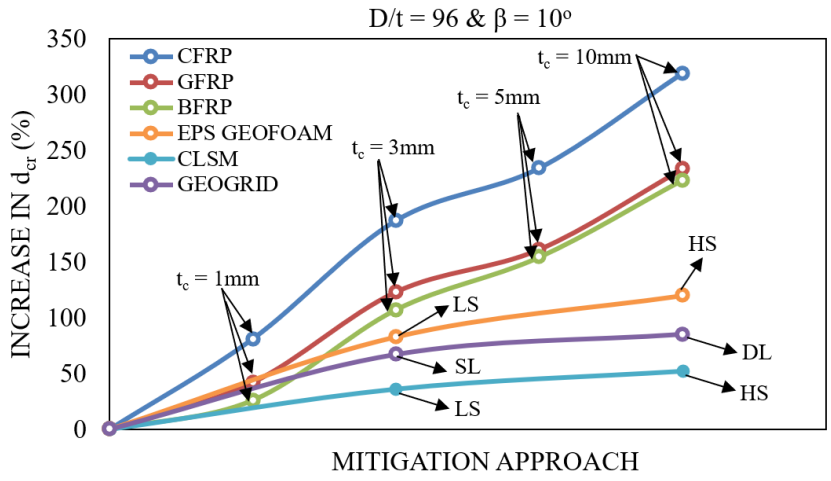

Figure 4.74. Comparison of the effectiveness of mitigation approaches based on the rate of increment in d_{cr} value

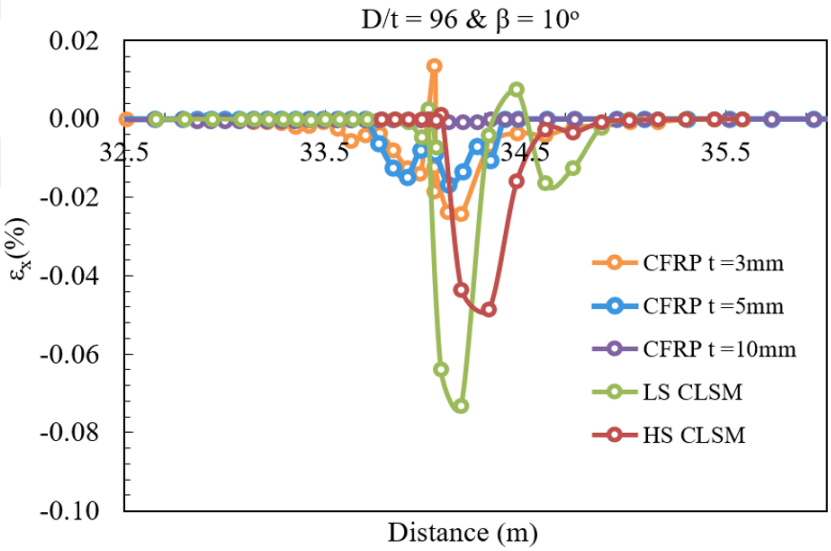

Figure 4.75. Comparison of the effectiveness of CFRP wraps and CLSM mixtures on reducing pipe axial strains at compression side plotted for d = 1m

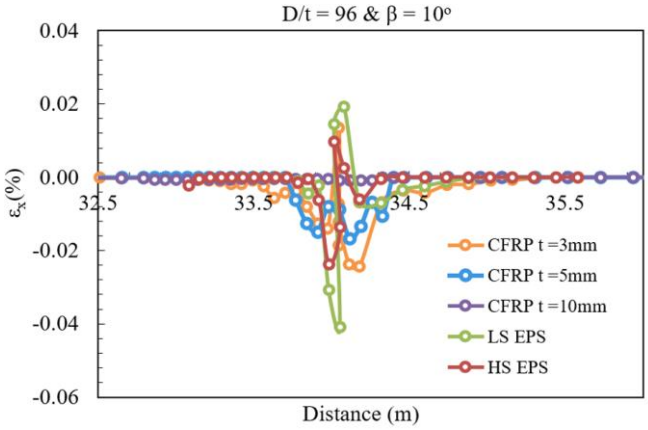

Figure 4.76. Comparison of the effectiveness of CFRP wraps and EPS geofoam blocks on reducing pipe axial strains at compression side plotted for d = 1m

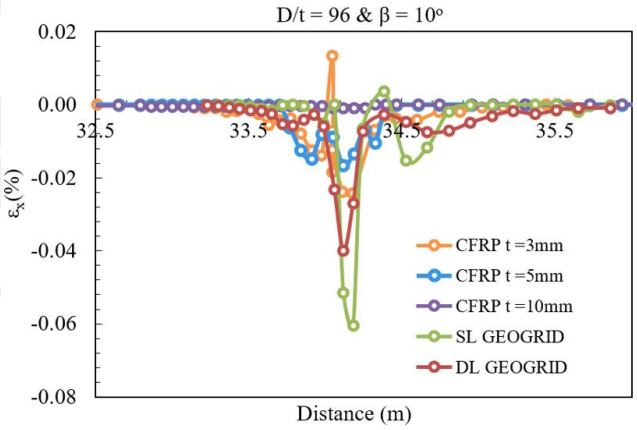

Figure 4.77. Comparison of the effectiveness of CFRP wraps and geogrid layers on reducing pipe axial strains at compression side plotted for d = 1m

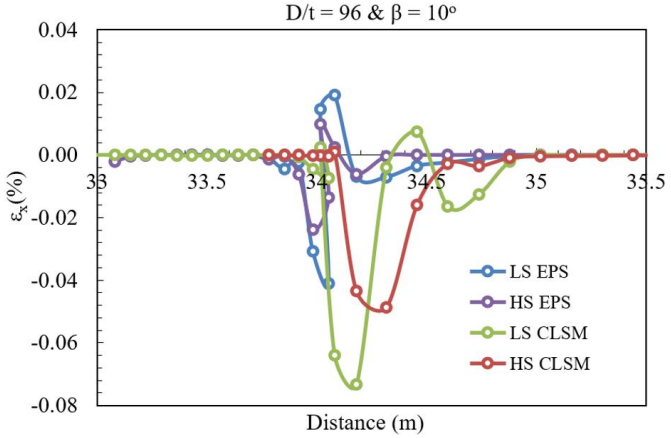

Figure 4.78. Comparison of the effectiveness EPS geofoam and CLSM mixtures on reducing pipe axial strains at compression side plotted for d = 1m

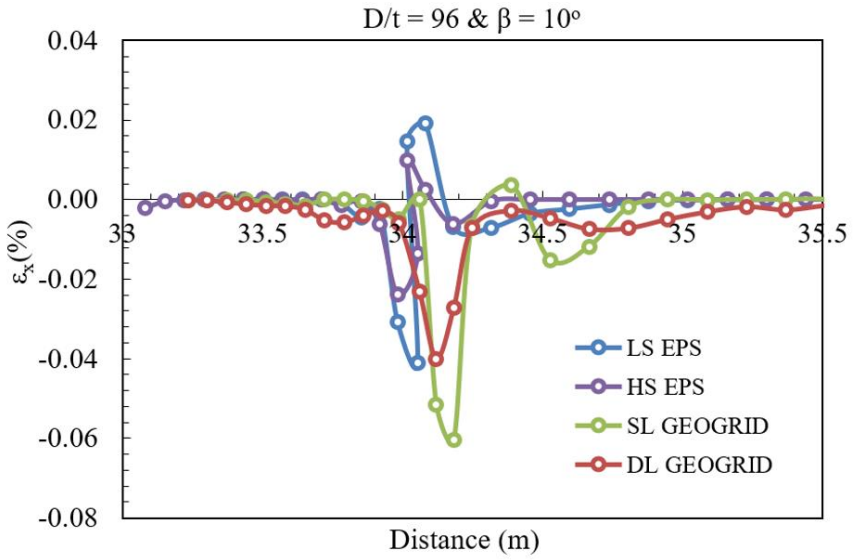

Figure 4.79. Comparison of the effectiveness EPS geofoam and geogrid layers on reducing pipe axial strains at compression side plotted for d = 1m

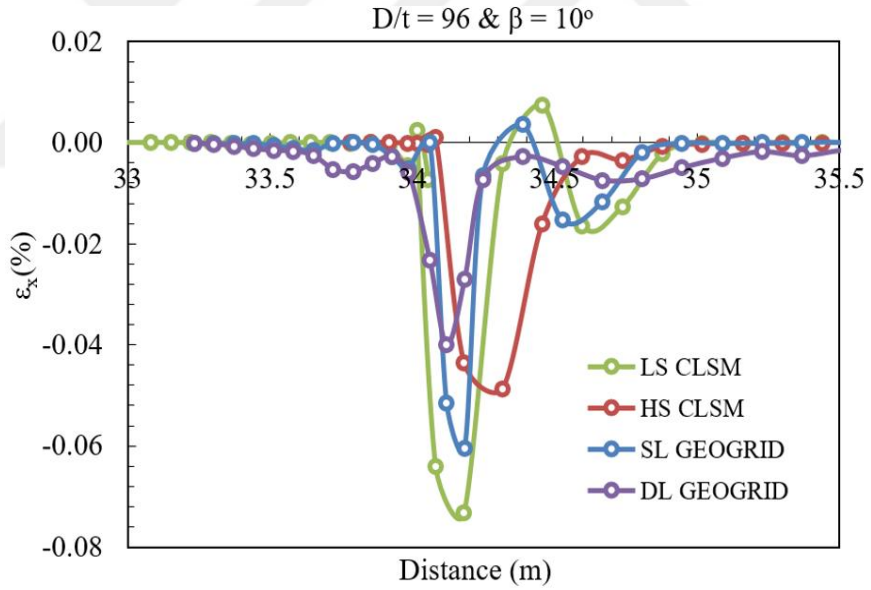

Figure 4.80. Comparison of the effectiveness of geogrid layers and CLSM mixtures on reducing pipe axial strains at compression side plotted for d = 1m

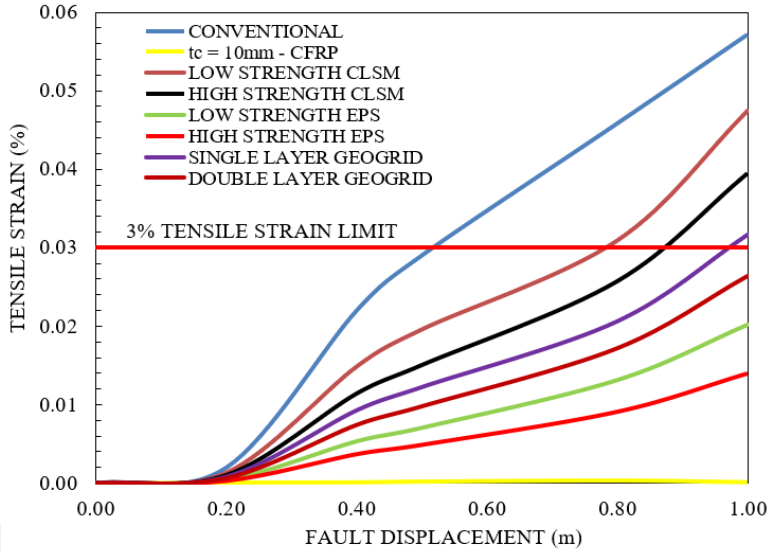

Figure 4.81. Comparison of the effect of investigated mitigation approaches the evolution of pipeline tensile strains in reference to the fault displacement increment for D/t = 96 and β = 10º

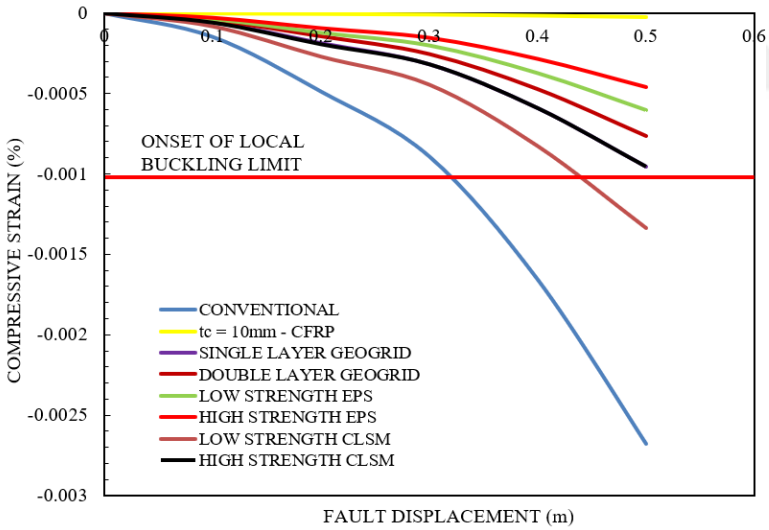

Figure 4.82. Comparison of the effect of investigated mitigation approaches the evolution of pipeline compressive strains in reference to the fault displacement increment for D/t = 96 and β = 10º

Table 4.15. Cost of utilizing CFRP wraps to mitigate buried pipe seismic demands

D/t	t_c (mm)	Increase in d_{cr} (%)	At (m^2)	Cost per m^2 (USD)	Total Cost (USD)
144	1	73	179.20	245.33	43,962.91
144	3	145	179.99	735.98	132,467.69
144	5	255	180.78	1226.65	221,750.60
144	10	323	182.75	2453.30	448,343.40
96	1	81	180.45	245.33	44,270.73
96	3	187	181.24	735.98	133,391.31
96	5	234	182.03	1226.65	223,290.28
96	10	319	184.01	2453.30	451,424.23
58	1	78	182.96	245.33	44,885.68
58	3	109	183.75	735.98	135,236.49
58	5	187	184.54	1226.65	226,366.21
58	10	348	186.52	2453.30	457,579.02

Table 4.16. Cost of utilizing EPS geofoam to mitigate buried pipe seismic demands

D/t	Condition	Increase in d_{cr} (%)	V (m^3)	Cost per m^3 (USD)	Total Cost (USD)
144	LS EPS	87	929.24	75.00	69,692.70
144	HS EPS	127	929.24	91.00	84,560.48
96	LS EPS	83	929.24	75.00	69,692.70
96	HS EPS	120	929.24	91.00	84,560.48
58	LS EPS	82	929.24	75.00	69,692.70
58	HS EPS	130	929.24	91.00	84,560.48

Table 4.17. Cost of utilizing CLSM to mitigate buried pipe seismic demands

D/t	Condition	Increase in d_{cr} (%)	V (m^3)	Cost per m^3 (USD)	Total Cost (USD)
144	LS CLSM	55	560.60	157.70	88,294.50
144	HS CLSM	77	560.60	157.70	91,658.10
96	LS CLSM	36	560.60	157.70	88,294.50
96	HS CLSM	52	560.60	157.70	91,658.10
58	LS CLSM	51	560.60	157.70	88,294.50
58	HS CLSM	72	560.60	157.70	91,658.10

Table 4.18. Cost of utilizing geogrid to mitigate buried pipe seismic demands

D/t	Condition	Increase in d_{cr} (%)	Cost per Unit (USD)	No. of Units	Total Cost (USD)
144	SL Geogrid	64	1,325.00	42	55,650.00
144	DL Geogrid	82	1,560.00	42	65,520.00
96	SL Geogrid	67	1,325.00	42	55,650.00
96	DL Geogrid	85	1,560.00	42	65,520.00
58	SL Geogrid	63	1,325.00	42	55,650.00
58	DL Geogrid	96	1,560.00	42	65,520.00

5. SIMPLIFIED ANALYSIS APPROACH

5.1. Introduction

This chapter presents the details of a simplified method proposed for response analysis of buried continuous steel pipes undergoing deformations due to strike-slip fault actions. The proposed approach aimed at establishing relationships among the bending (deformation) angle (θ) of the pipe, local buckling factor (α) and pipeline tensile strains (ε_T) to finally compute the maximum longitudinal strains on the pipe. An analytical solution scheme based on the well-known requirement of equilibrium between the deformation induced and geometrically required pipeline elongations was employed to compute the bending length of the deformed pipe, which was later used to compute the corresponding bending angle value also dependent on the angle of crossing of the buried pipe in reference to the fault. An iterative solution approach based on the variation of the axial force was used to calculate the required bending length. Computation of tensile strains was performed through the use of a finite element numerical model of the buried pipe. A distributed plasticity model defined through non-linear beam elements was utilized to model the behavior of the buried pipe in order to capture the locations of plastic hinges and large deformations. A bilinear relationship was used to input the isotropic mechanical properties of pipeline steel material. Interaction occurring at the interface of the buried pipe and the native backfill soil was incorporated via the use of equivalent soil springs in corresponding directions. A non-linear static analysis procedure involving the gradual application of fault action as displacement load on half of the pipe section was employed for response analysis. Strain results obtained following the analysis procedure were than used to determine the required relationships through the use of an appropriate a curve fitting technique. The chapter concludes with the comparison of maximum longitudinal pipeline strains obtained using the proposed approach and numerical models described in Chapter 3.

5.2. Outline of the Proposed Simplified Approach

The simplified approach proposed in this dissertation for the computation of maximum longitudinal strains developing on pipes exposed to strike-slip faulting actions consisted of

three phases. The first phase of analysis involved the calculation of bending angle of the pipe determined based on the bending length (L_{cl}) and angle of intersection (β) between the axis of the buried pipe and the fault. Illustrated in Figure 5.1 the bending length corresponds to the length of pipeline section along which bending or deformation occurs. This value was computed for each considered analysis case using the obligation for coherence among the load induced and required (geometrically) pipeline elongations which involved the utilization of an iterative solution approach where the axial force value was calculated and updated until convergence was achieved. The bending or deformation angle values were then calculated using the computed lengths. The details of the adopted calculation procedure are presented in Subsection 5.2.1.

The second phase of the proposed calculation approach involved the use of a finite element model of buried pipe to compute the resulting tensile strains under the applied strike-slip fault load. The developed numerical models aimed at analyzing the response of buried pipes by considering both the geometric and material non-linearities occurring under large deformations due to faulting actions. For this purpose, a non-linear beam element was employed model the buried pipe in order to make use of a distributed plasticity approach enabling the capture of deformation occurring along the length of the pipe. Interaction occurring at the interface of pipe and backfill soil was modeled through equivalent soil spring defined in axial, transverse, vertical upwards, and downwards directions. A static non-linear (pushover) analysis procedure was employed for response analysis, where the strike-slip fault action was defined as a gradually increasing displacement load (from 0m to 4m) defined on the nodes of half of the pipe element. Subsection 5.2.2 describes the details of the developed numerical models.

Following the computation of strains using the developed numerical models, the solution continued with the third phase, where initially plots between the bending angles computed in phase one and strains in phase two along with the consideration of local buckling factor were constructed. These plots were than used to determine relationships between these parameters via the use of the best fitting curve technique. Relationships obtained at the end of this phase were than used to compute maximum longitudinal strains developing on pipe subjected to fault displacements. The flowchart presented in Figure 5.2 summarizes the steps and phases of the proposed simplified approach.

Analysis was carried out considering the same D/t ratios and intersection angle (β) values utilized for numerical models described in Chapter 3 to later allow the comparison of results between the two approaches.

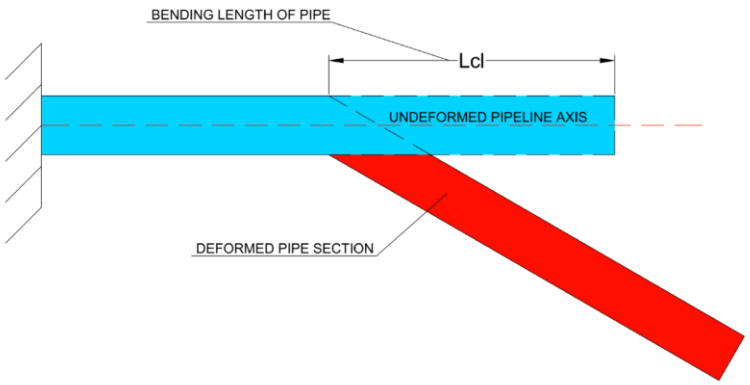

Figure 5.1. Illustration of the bending length of a buried pipe subjected to faulting action

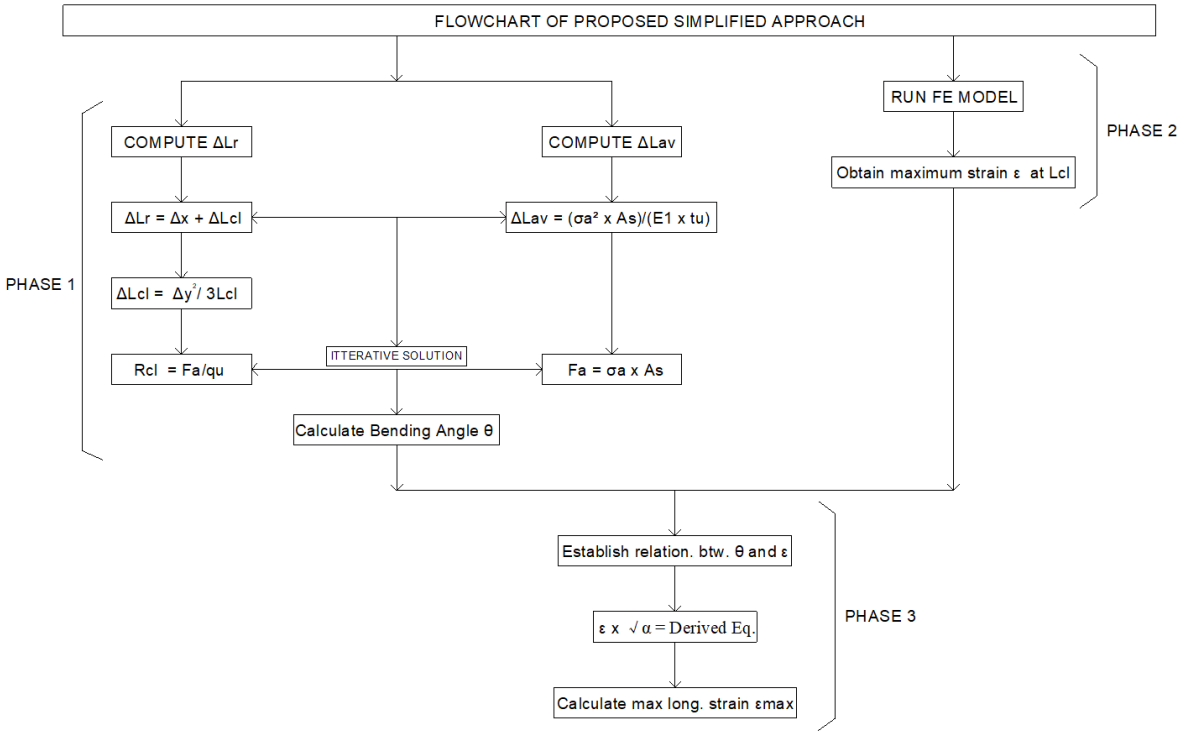

Figure 5.2. Flowchart summarizing the phases of the proposed simplified approach

5.2.1. Details of the Procedure for the Calculation of Bending Angle

The first phase of the proposed methodology dealt with the formulation of a procedure for the calculation of the pipeline bending length (i.e., the length from the fault trace to the pipe where bending occurs). In order to compute this parameter initially the pipeline geometrically required, and stress-induced (available) pipeline elongations were needed to be calculated so as to be able to compute the bending length by using the requirement of compatibility between these two pipeline properties. Obviously, this procedure required the adoption of an iterative solution approach to compute the desired value.

The required pipeline elongation (ΔL_r) was calculated adopting the following steps given in equation 5.1 through 5.6 below:

$$\Delta L_r = \Delta x + \Delta L_{cl} \tag{5.1}$$

where Δx is the buried pipe displacement component in x direction, and ΔL_{cl} is the elongation in the bent part of pipe near the fault in the horizontal plane calculated as:

$$\Delta L_c = \frac{\Delta y^2}{3L_{cl}} \tag{5.2}$$

where Δy is the buried pipe displacement component in y direction, and L_{cl} is the bent length of the pipe in horizontal plane.

$$\Delta x = \delta_h \cos\beta \tag{5.3}$$

$$\Delta y = \delta_h \sin\beta \tag{5.4}$$

Here, δ_h is the applied fault displacement load, and β is the fault angle of intersection.

$$L_{cl} = \left(\frac{R_{cl}}{\Delta y}\right)^{1/2} \tag{5.5}$$

Here, R_{cl} is the radius of curvature in the horizontal plane calculated as follows:

$$R_{cl} = \frac{F_a}{q_u} \tag{5.6}$$

where F_a is the force acting in axial direction of the pipe at its crossing with the fault, and q_u is the limit stress for transverse soil springs, defined per length of the pipe.

The available pipeline elongation ($\Delta L_{avl.}$) defined as the elongation of the pipe emerging from the integration of axial strain over the unsupported length of the pipe (i.e. length of buried pipe where slippage occur between the buried pipe and backfill soil deposit) was calculated adopting the following steps given in equation 5.7 and 5.10 below:

$$\Delta L_{avl.} = 2\int_0^{L_{uanch.}} \varepsilon(L)dL \tag{5.7}$$

$$L_{unanch.} = \frac{F_a}{t_u} = \frac{\sigma_a A_s}{t_u} \tag{5.8}$$

where A_s is the buried pipe cross-sectional area, σ_a is the yield strength of pipe steel, and t_u is the limit soil-pipeline friction force, defined per pipeline length.

When $\Delta L_r = \Delta L_{avl.}$:

$$\Delta L_{avl.} = \frac{{\sigma_a}^2 A_s}{E_1 t_u} \tag{5.9}$$

Irrespective of the magnitude of stresses in axal direction, the resulting force is:

$$F_a = \sigma_a A_s \tag{5.10}$$

As seen from the equations derived above the required bent length value (L_{cl}) is computed via an iterative approach incorporating F_a as the variable of this solution algorithm. Once the bent length values were determined for each case, a finite element model description of which are presented in the following sections was analyzed to find the corresponding maximum pipeline strains developing on these determined bent lengths. After the analysis procedure was completed, the collected data was used to establish a relationship between bending angle and the maximum longitudinal pipeline strain. The general form of these equations are as follows:

$$\theta = \tan^{-1}\left(\frac{\delta \sin\beta}{L_{cl} + \cos\beta}\right) \tag{5.11}$$

where θ is the bending (deformation) angle of the buried pipe.

$$\varepsilon_t\sqrt{\alpha} = Derived\ Equation \tag{5.12}$$

The local buckling factor α is was calculated using the expression given in equation 5.13 below:

$$\alpha = \frac{E_1/\sigma_y}{D/t} \tag{5.13}$$

where E_1 is Young's modulus of pipe steel, D is the external pipeline diameter, and t is the wall thickness of pipe section.

5.2.2. Details of Simplified Numerical Models

The second phase of the proposed simplified approach involved the computation of pipeline strains occurring at the bending length computed using the procedure described in Subsection 5.2.1. For the purpose, a finite element model of the buried steel pipe was constructed using the SAP 2000 V.20 software package. The model used in consists of frame (stick) elements modeled as non-linear elements considering a bilinear stress-strain curve for the steel material assuming the material properties provided under Chapter 3 (Table 3.2) and moment-rotation curves were developed to describe the distributed plasticity behavior expected to occur during the application of fault displacement (see Figure 5.3). In elements defined with distributed plastic behavior, plastic hinges are assumed to occur anywhere along the defined element. To capture the formation of these plastic hinges axial force and bending moment (P-M) hinges (see Figure 5.4) are assigned along the length of the pipe at intervals equal to 2m. Both ends of the pipe were assumed to be restrained using roller supports, in that way the pipe was let free to move along the slip direction of the pipe. The total buried steel pipe length for each analysis case was assumed to be equal to 60m similar to the numerical models developed using ABAQUS CAE software package. Computation of the strains acting on the pipeline for a fault displacement range of 0-4m were conducted separately for three different pipeline cases with varying wall thickness. Similar to models described under Chapter 3 the diameter of the pipeline was kept constant at 0.9144m (36 inch)- which represents one the most common pipeline diameters used to transport oil and natural gas- while the wall thickness attained values of 6.35mm, 9.53mm, and 15.88mm respectively. The backfill soil around the buried pipe was assumed to the same one used in sophisticated numerical models; properties of this soil type are provided in Table 3.1. Once again, to enable the comparison between simplified and rigorous models developed within

the scope of the present study cases with angles of intersection among the buried pipe and fault trace equal to 10º, 15º, and 30º were studied. In addition, cases with angle values of 60º and 80º were also developed to further review the applicability of the proposed approach.

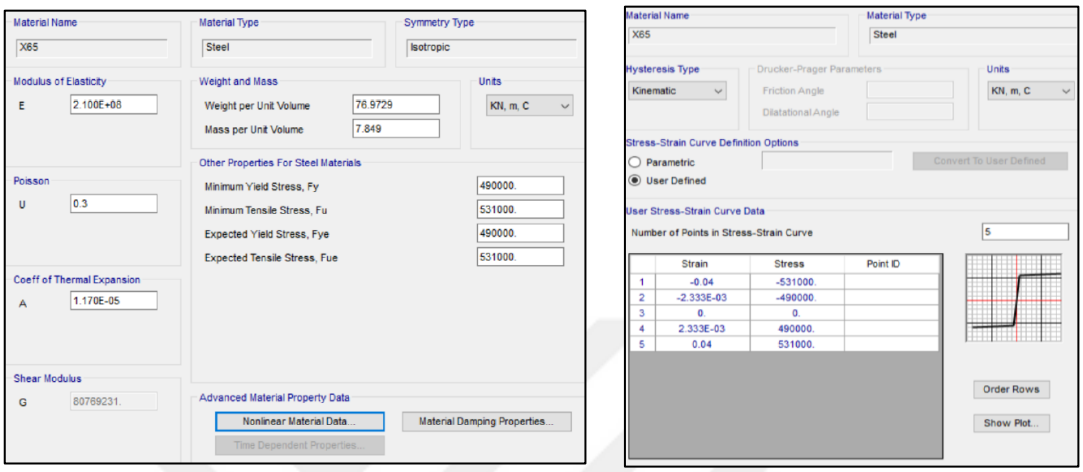

Figure 5.3. Software input for API Grade X65 pipe steel material

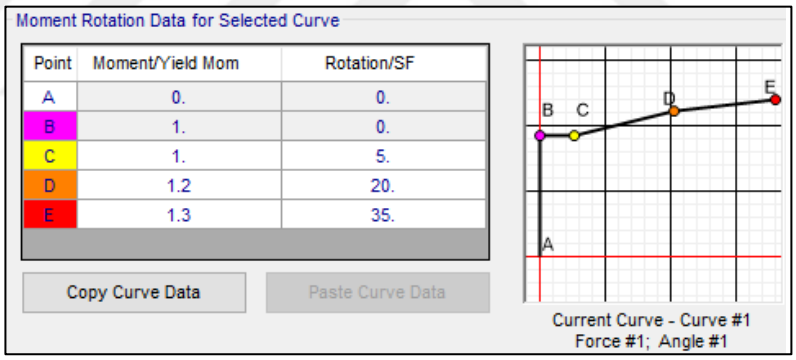

Figure 5.4. Moment-rotation curve and its data utilized for pipeline analysis

The interaction between the buried steel pipe surface and soil deposit around it was represented in these simplified numerical models through the use of equivalent soil spring in axial, transverse, vertical upwards, and downwards directions. As shown in Figures 5.5 an 5.6 in the models these spring (link) elements were defined with the aid of force deformation curves and data obtained using the ALA Guideline (2005) expressions shown in equations 5.14 through 5.17 below. The resulting force and deformation values for each considered direction are summarized in Tables 5.1 through 5.4. Two node link elements with one node attached to the support point and the other one attached to the pipe itself were utilized to define these soils springs.

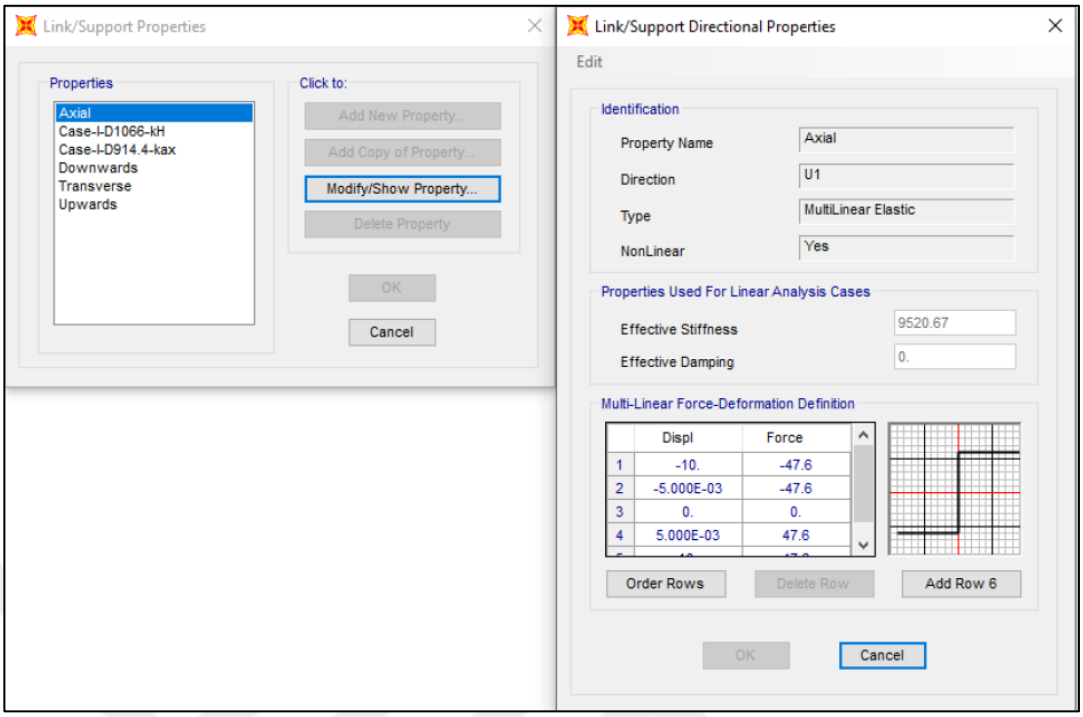

Figure 5.5. Software input for force deformation curves used to define soil springs

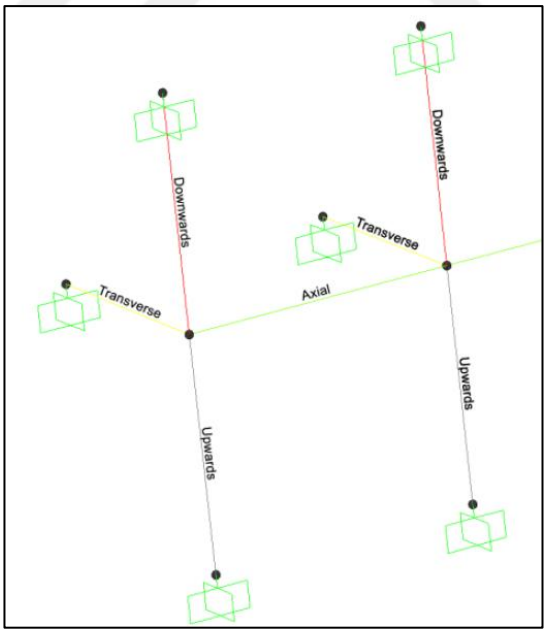

Figure 5.6. Soil springs incorporated into analysis model

Calculation of Soil Spring in Axial Direction:

$$T_u = \pi D \alpha_{adh.} c + \pi D H \gamma_s \frac{1 + K_0}{3} \tan \delta \tag{5.14}$$

where D is the external diameter of buried pipe, c is the soil cohesion value, $\alpha_{adh.}$ is the adhesion factor, H is the burial depth of pipe, K_o is the pressure coefficient at rest condition, γ_s is the unit weight of soil and δ is the friction angle value at interface of soil and pipe.

Table 5.1. Computed properties for axial springs

Property	**D/t = 144**	**D/t = 96**	**D/t = 58**
α (MPa)	1.029	1.029	1.029
δ (°)	35	35	35
c (MPa)	0	0	0
H (m)	1.763	1.766	1.773
D (m)	0.927	0.933	0.946
γ_s (kN/m^3)	18.00	18.00	18.00
T_u (kN/m)	47.60	48.02	48.84
Displ. at T_u (mm)	5.000	5.000	5.000

Calculation of Soil Spring in Transverse (Lateral) Direction:

$$P_u = N_{ch}cD + N_{qh}\gamma_s HD \tag{5.15}$$

where N_{ch} is the horizontal bearing capacity factor for clay soil, N_{qh} is the horizontal bearing capacity factor for sandy soil calculated as per ALA (2005) Appendix A.

Table 5.2. Computed properties for transverse springs

Property	**D/t = 144**	**D/t = 96**	**D/t = 58**
c (MPa)	0	0	0
H (m)	1.763	1.766	1.773
D (m)	0.927	0.933	0.946
γ_s (kN/m^3)	18.00	18.00	18.00
N_{qh}	10.64	10.62	10.58
P_u (kN/m)	293.69	295.81	300.06
Displ. at P_u (mm)	89.060	89.320	89.820

Calculation of Soil Spring in Vertical (Upwards) Direction:

$$Q_u = N_{cv}cD + N_{qv}\gamma_s HD \tag{5.16}$$

where N_{cv} is the vertical bearing capacity factor for clay soil, N_{qv} is the vertical bearing capacity factor for sandy soil calculated as per ALA (2005) Appendix A.

Table 5.3. Computed properties for vertical (upwards) springs

Property	**D/t = 144**	**D/t = 96**	**D/t = 58**
c (MPa)	0	0	0
H (m)	1.763	1.766	1.773
D (m)	0.927	0.933	0.946
γ_s (kN/m^3)	18.00	18.00	18.00
N_{qv}	1.513	1.505	1.491
Q_u (kN/m)	43.66	43.82	44.13
Displ. at Q_u (mm)	17.630	17.660	17.730

Calculation of Soil Spring in Vertical (Downwards) Direction:

$$Q_d = N_c + N_q \gamma_s H D + N_\gamma \gamma_s \frac{D^2}{2} \tag{5.16}$$

where N_c is the vertical downward bearing capacity factor for clay soil, N_q is the load bearing limit of sandy soil in vertical downward direction, and N_γ is vertical downward soil bearing capacity factor calculated as per ALA (2005) Appendix A.

Table 5.4. Computed properties for vertical (downwards) springs

Property	**D/t = 144**	**D/t = 96**	**D/t = 58**
c (MPa)	0	0	0
H (m)	1.763	1.766	1.773
D (m)	0.927	0.933	0.946
γ_s (kN/m^3)	18.00	18.00	18.00
N_q	33.30	33.30	33.30
N_γ	0.0916	0.0916	0.0916
Q_d (kN/m)	961.41	969.75	986.65
Displ. at Q_d (mm)	92.690	93.320	94.590

Simulation of the effect of ground displacement and hence the computation of the developing strains was achieved via performing non-linear static (i.e., pushover) analysis for a fault displacement range of 0.1m-4m with intermediate increments of 100mm. As mentioned earlier, the analysis was repeated for five fault crossing angles (β = 10º, 15º, 30º,60º, 80º) and three different pipeline sections (t = 6.35mm, t = 9.53mm and t = 15.88mm) in order to obtain sufficient data for the derivation of relationships. Displacement values were input into the analysis model as joint displacements in axial and transverse direction (Δx and Δy respectively), Figure 5.7 shows the application of these displacements, it should also be noted that the displacements were applied only to second half of the pipeline while the first half was kept fixed, so as to better simulate the pipeline deformation under fault movements. Figure 5.8 shows the pipeline stresses and deformation along with the fault plane.

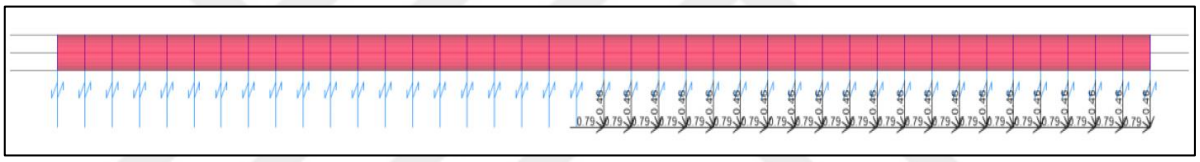

Figure 5.7. Application of fault displacement loads in the analysis models

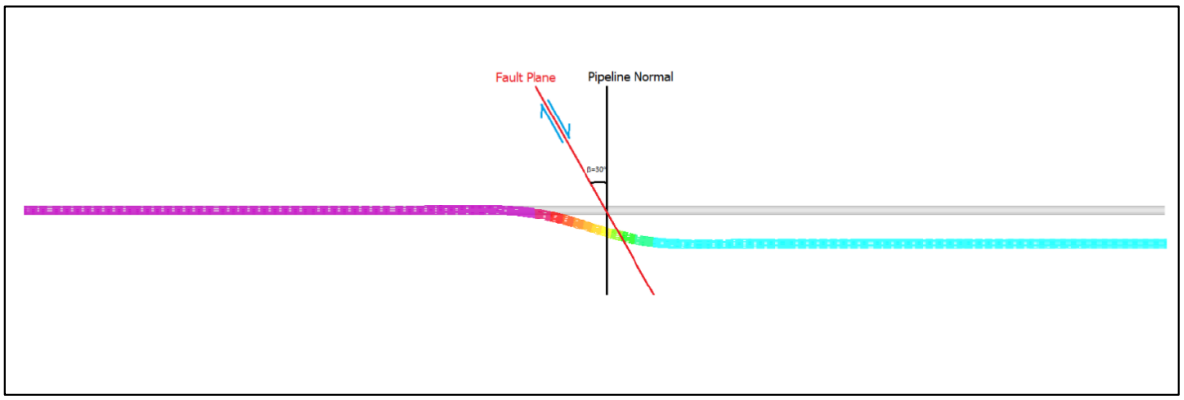

Figure 5.8. Pipeline deformation and accumulated stresses on pipe during the act of fault displacement load (for D/t= 144 and β = 30º)

5.3. Analysis Results

Numerical models described in Subsection 5.2.2 have been analyzed under the applied fault displacement to obtain the maximum pipeline strains occurring at bending lengths

calculated using the algorithm presented under Subsection 5.2.1. Computed bending length values corresponding to the applied fault displacement were also utilized to compute the bending angle (θ) values, where an iterative solution approach based on the need for equilibrium between load induced and geometrically required pipeline elongations was adopted. Strain values obtained at each fault displacement increment along with bending angle values also corresponding to these displacement states were plotted together by also including the local buckling factor (α) to account for non-linear deformations anticipated to occur on the buried pipe during the act of fault load, curve fitting techniques were than employed to determine the type of relationship between these parameters. Following sections of the chapter present the obtained results, initially Subsection 5.3.1 provides a sample calculation for bending angle, whereas Subsections 5.3.2 and 5.3.3 present the derived equations and maximum pipe strains obtained using these expressions respectively. Lastly, in Subsection 5.3.4 a comparison of strains obtained using the simplified approach described in this section and the ones resulting from the advanced models described under Chapter 3 is presented to verify the accuracy of the proposed method.

5.3.1. Sample Calculation of Bending Length L_{cl} and Angle θ

Prior to application of the ground displacements on the developed finite element models to obtain the necessary strain, initially the bending length and bending angle were computed for each case following the procedure given under Subsection 5.2.1. An example calculation for D/t = 144, β = 10^o and δ_h = 0.1m is given below, the remaining values have been calculated similarly, however, due to the large data size have not been numerically presented.

$\Delta x = \delta_h \cos\beta$ = 0.098m — Fault displacement load input in x direction

$\Delta y = \delta_h \sin\beta$ = 0.017m — Fault displacement load input in y direction

Through iteration F_a was found to be equal to:

F_a = 4260kN

A_s = 0.0184m^2

E_1 = 2.1 x 108MPa

$\sigma_a = F_a/A_s$ = 231525.66kN/m2

$\Delta L_{avl.} = \frac{\sigma_a^2 A_s}{E_1 t_u}$ = 0.098m

$R_{cl} = \frac{F_a}{q_u}$ = 97.57m

$L_{cl} = (R_{cl}\Delta y)^{1/2}$ = 1.288m

$\Delta L_{cl} = \frac{\Delta y^2}{3L_{cl}}$ = 0.000075m

$\Delta L_r = \Delta_x + \Delta L_{cl}$ = 0.0981m

$\theta = \tan^{-1}\left(\frac{\delta \sin\beta}{L_{cl}+\delta\cos\beta}\right)$ = 0.0123rad

Through iterative analysis L_{cl} value for this case is determined as 1.288m whereas the bending angle θ is 0.0123rad. Once these values were obtained FE analysis was run to compute the strains at this location.

5.3.2. Derivation of Relationships Between Bending Angle and Computed Strains

Following the calculation of bending angle θ vales corresponding to each pipeline D/t ratio, intersection angle β value and fault displacement δ_h values, strains ε developing at the calculated critical length L_{cl} were obtained through the solution of the numerical models developed for each investigated case. Once results have been obtained plots of strains vs. bending angle were constructed by also including the local buckling factor α to account for non-linear deformation occurring on the pipe at large fault displacements. Through the use of various curve fitting techniques relationships were established among these parameters, to be later used for the computation of strains under the applied fault load. Figures 5.9a through 5.13c show the determined relationships for cases of D/t equal to 144, 96 and 68, and cases of angle β equal to 10^o, 15^o, 30^o, 60^o, and 80^o respectively. Results obtained at the end of calculation procedures revealed that for strike-slip fault cases an exponential relationship exists between the above-mentioned parameters. A R^2 value above 0.9 for each case indicates a good fitting of these curves to the data obtained through analysis.

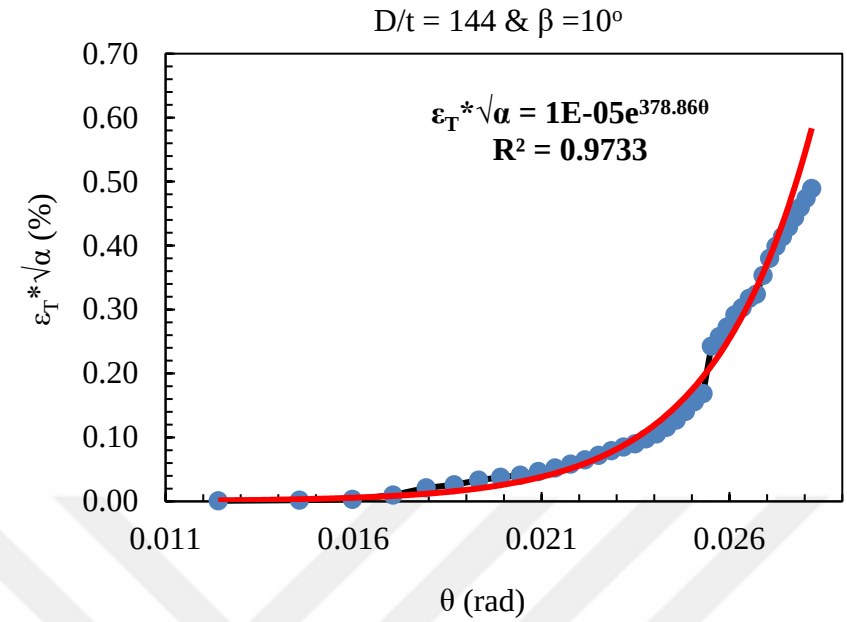

a)

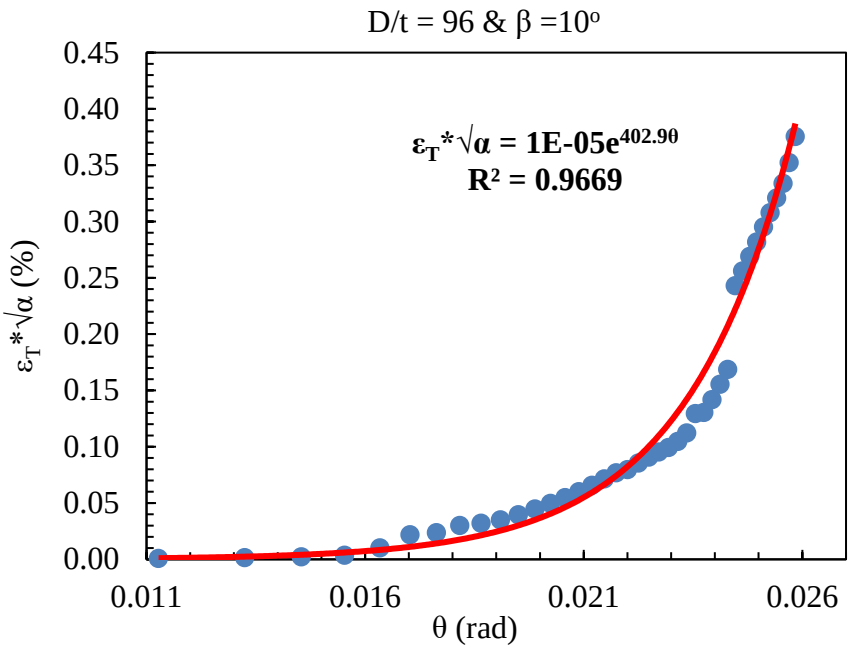

b)

Figure 5.9. Relationships between pipe strains ε, local buckling factor α and bending angle θ derived for β = 10° and, a) D/t = 144, b) D/t = 96, and D/t = 58

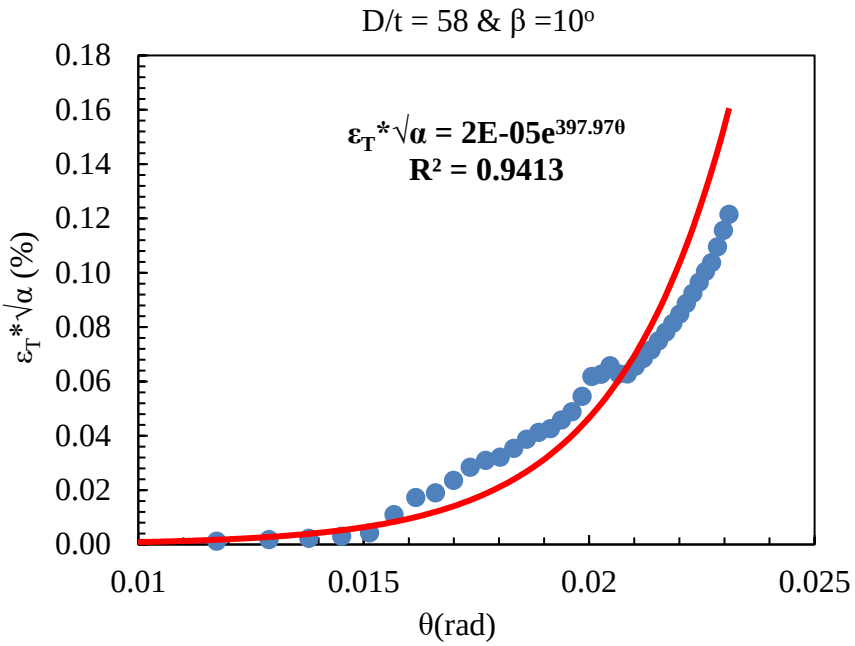

c)

Figure 5.9. Relationships between pipe strains ε, local buckling factor α and bending angle θ derived for β = 10° and, a) D/t = 144, b) D/t = 96, and D/t = 58

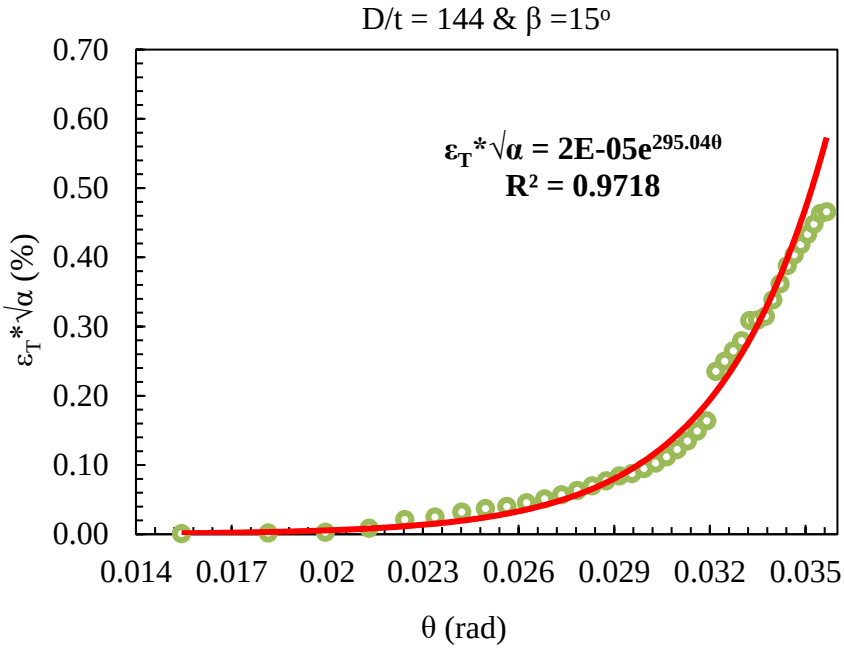

a)

Figure 5.10. Relationships between pipe strains ε, local buckling factor α and bending angle θ derived for β = 15° and, a) D/t = 144, b) D/t = 96, and D/t = 58

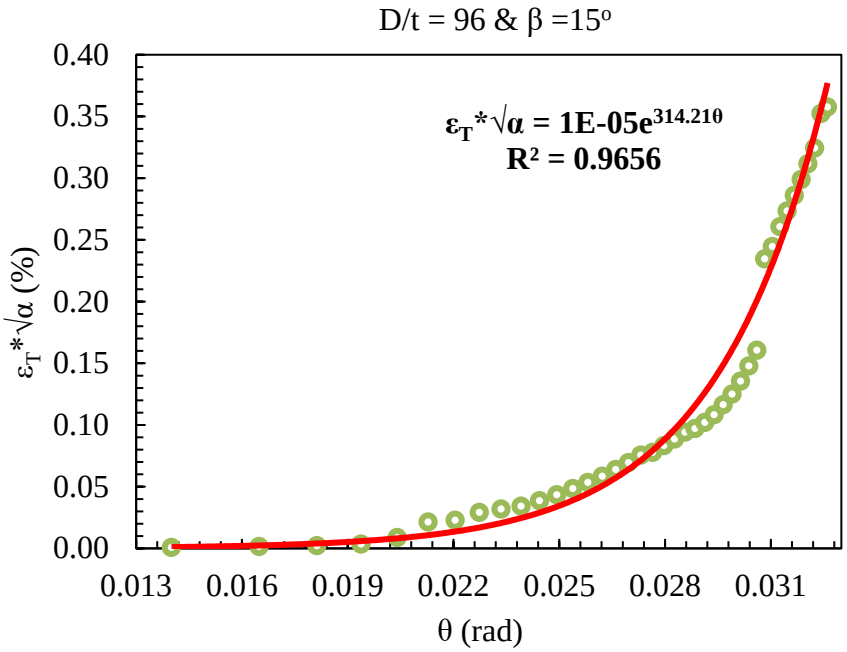

b)

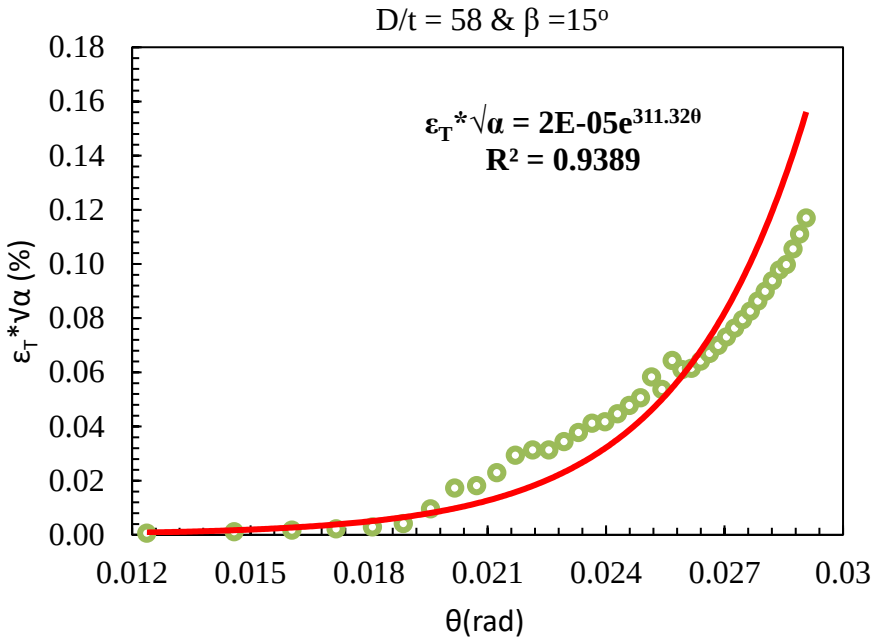

c)

Figure 5.10. Relationships between pipe strains ε, local buckling factor α and bending angle θ derived for β = 15° and, a) D/t = 144, b) D/t = 96, and D/t = 58

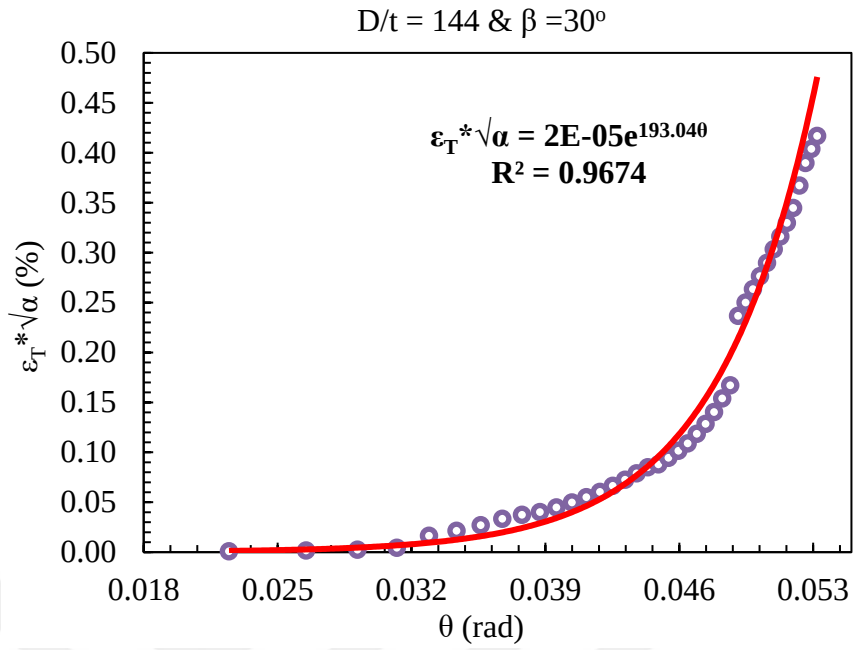

a)

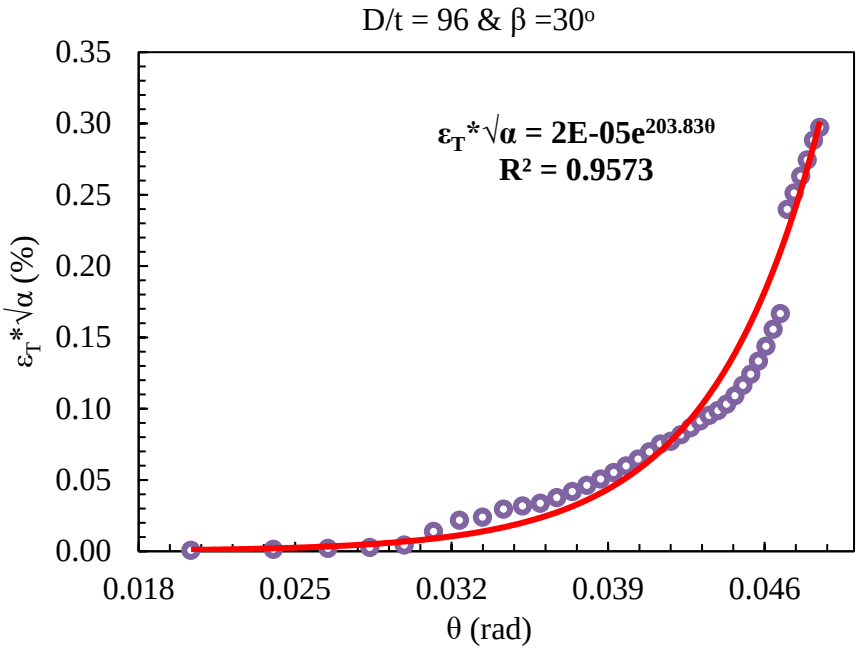

b)

Figure 5.11. Relationships between pipe strains ε, local buckling factor α and bending angle θ derived for β = 30° and, a) D/t = 144, b) D/t = 96, and D/t = 58

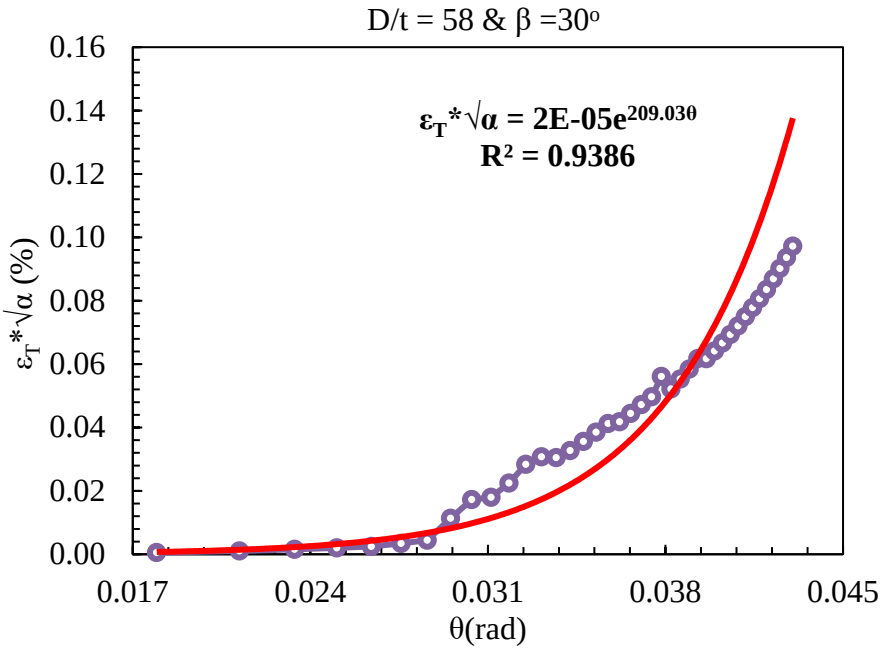

c)

Figure 5.11. Relationships between pipe strains ε, local buckling factor α and bending angle θ derived for β = 30° and, a) D/t = 144, b) D/t = 96, and D/t = 58

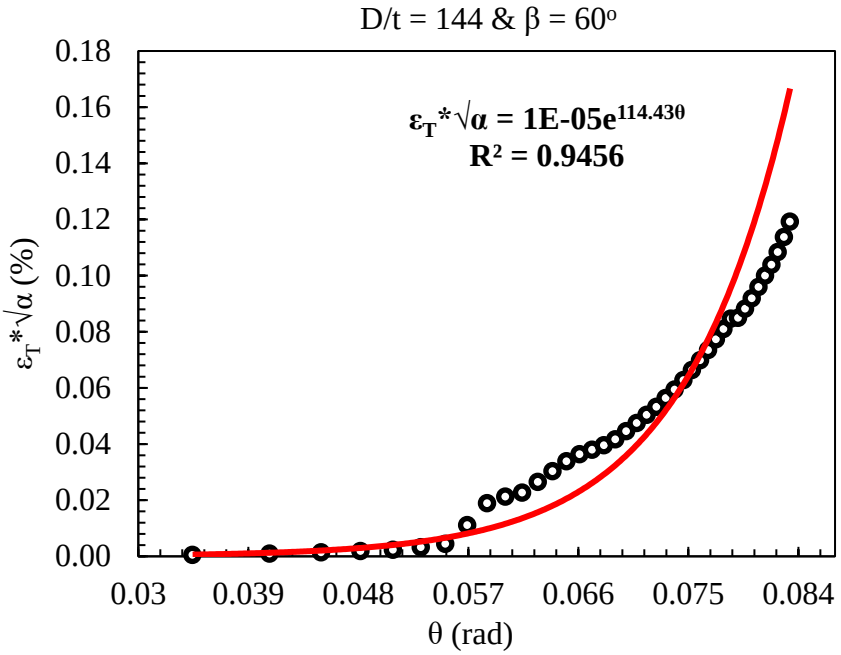

a)

Figure 5.12. Relationships between pipe strains ε, local buckling factor α and bending angle θ derived for β = 60° and, a) D/t = 144, b) D/t = 96, and D/t = 58

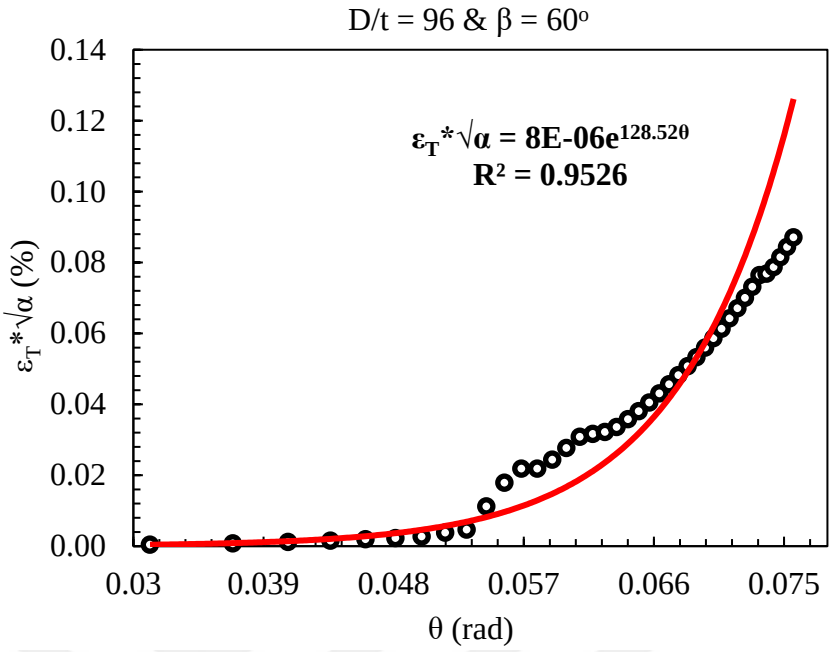

b)

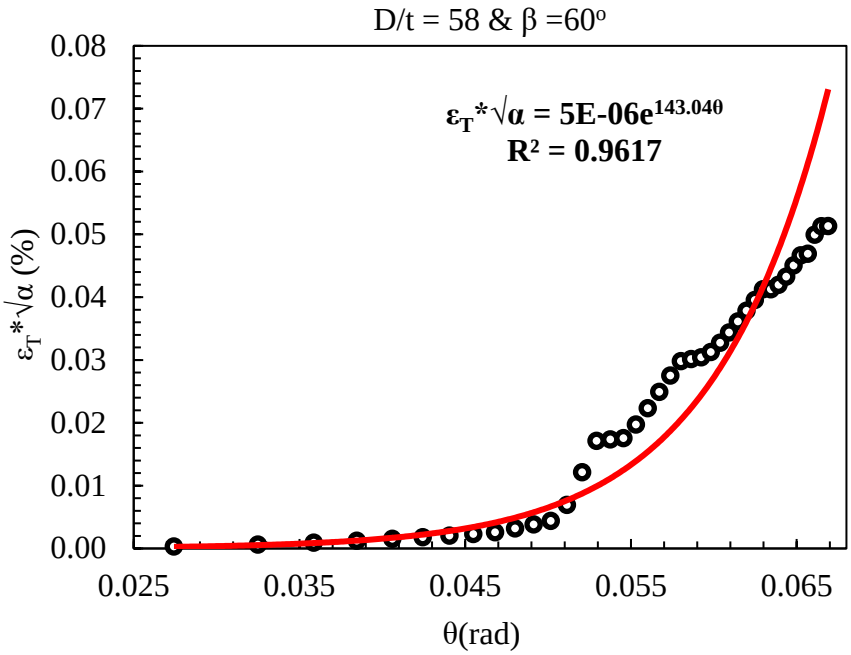

c)

Figure 5.12. Relationships between pipe strains ε, local buckling factor α and bending angle θ derived for β = 60° and, a) D/t = 144, b) D/t = 96, and D/t = 58

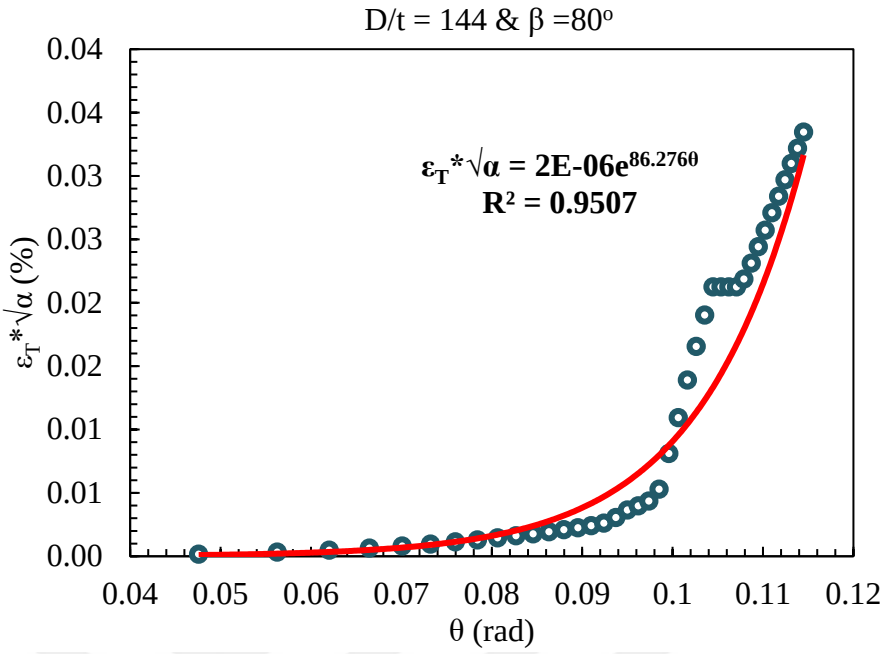

a)

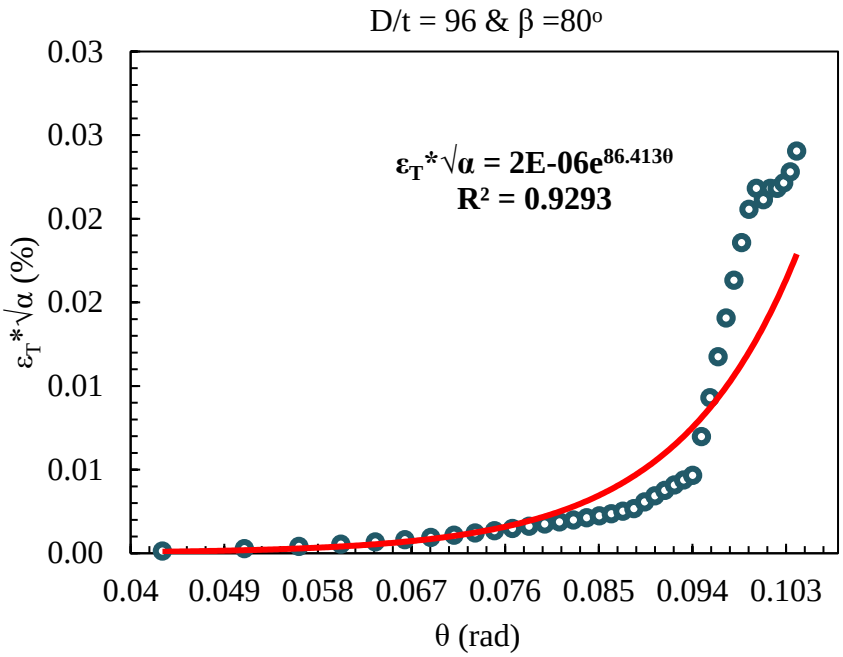

b)

Figure 5.13. Relationships between pipe strains ε, local buckling factor α and bending angle θ derived for β = 80° and, a) D/t = 144, b) D/t = 96, and D/t = 58

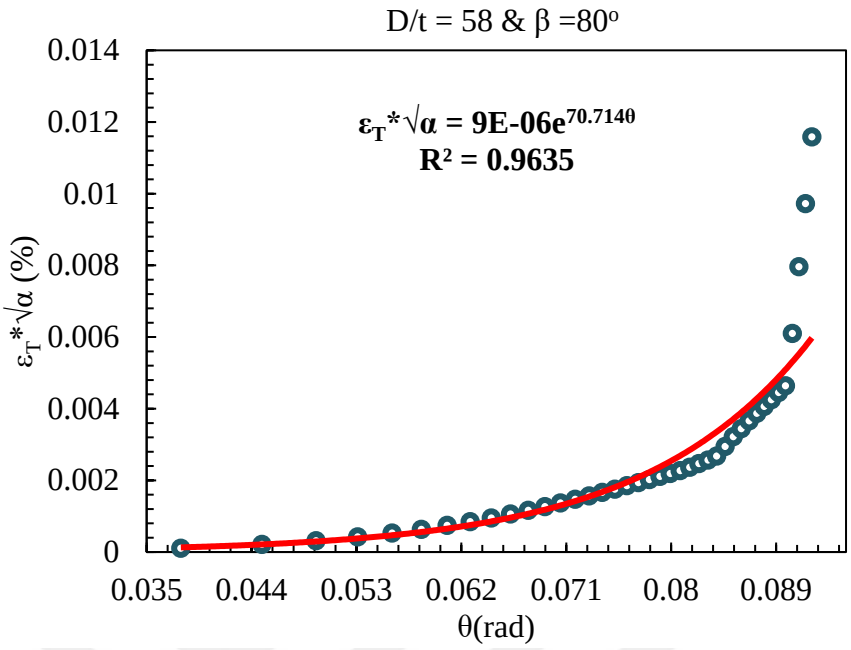

c)

Figure 5.13. Relationships between pipe strains ε, local buckling factor α and bending angle θ derived for β = 80° and, a) D/t = 144, b) D/t = 96, and D/t = 58

5.3.3. Calculation of Longitudinal Pipe Strains Using the Derived Equations

The expressions derived above in Subsection 5.3.2 indicate that the maximum pipeline strains might be computed by incorporating the sectional deformation using an exponential equation that in essence relates the local buckling factor α and the bending angle θ. Strains computed using these expressions for each analysis case are plotted against fault displacement normalized in reference to the pipe diameter D and are presented in Figures 5.14 through 5.16 for D/t ratios equal to 144, 96, and 58 respectively. Review of the resulting strain values showed that tensile strains of a buried pipe subjected to faulting actions reduce as the fault crossing angle increases, which is an expected phenomena due to the fact that as the crossing angle increases and approaches 90° compression becomes the dominant mode of deformation for the pipeline, an observation similar to that of emerging from sophisticated numerical models. Moreover, results indicate that as expected the performance of the buried pipe improves with the increment of pipe wall thickness, again an observation that agrees with that of rigorous models incorporating explicit modeling of soil-pipe interaction.

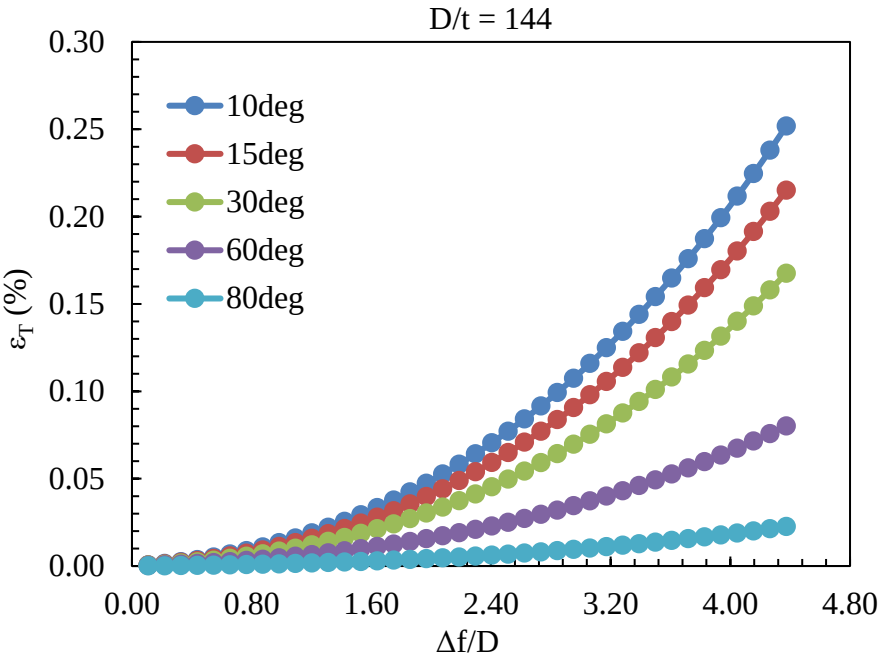

Figure 5.14. Maximum pipeline strains computed using the derived equations for D/t = 144 and β values varying between 10º and 80º

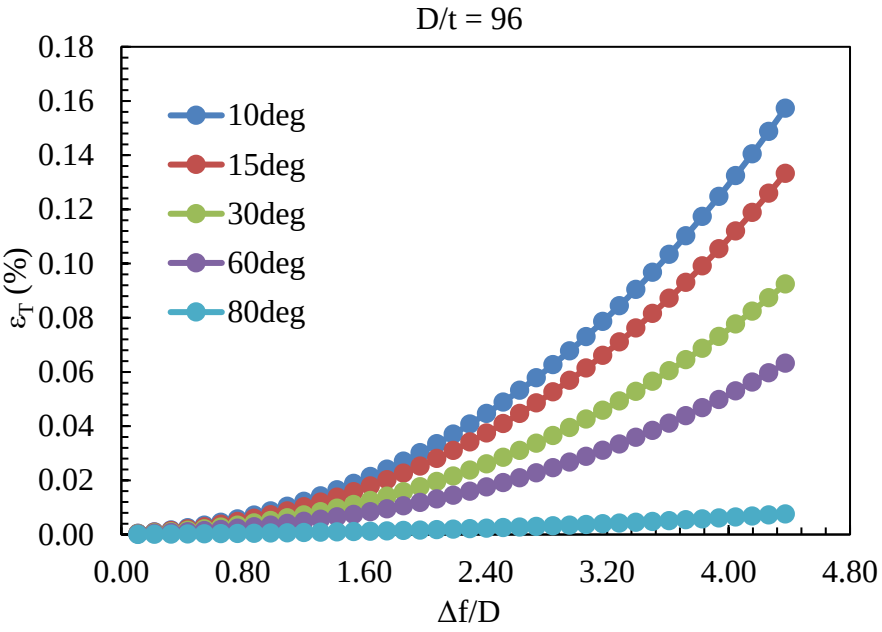

Figure 5.15. Maximum pipeline strains computed using the derived equations for D/t = 96 and β values varying between 10º and 80º

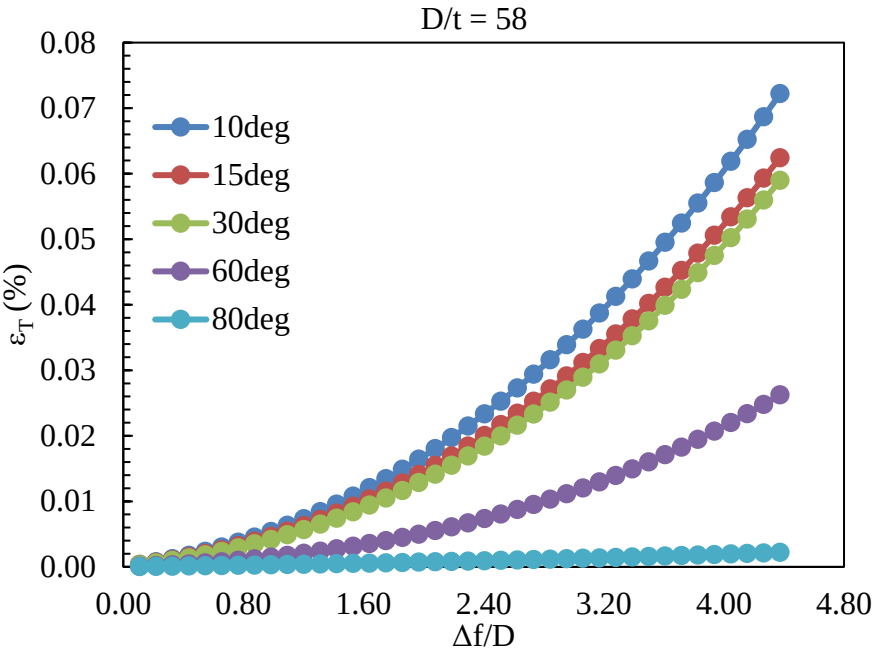

Figure 5.16. Maximum pipeline strains computed using the derived equations for D/t = 58 and β values varying between 10º and 80º

5.3.4. Comparison With Rigorous Numerical Models

The method proposed in this chapter aimed at calculating the maximum longitudinal strains on buried pipes subjected to strike-slip actions using a three-phase analytical and numerical calculation algorithm. Plots given under Subsection 5.3.3 presented the strains on the pipe calculated adopting this method. Numerical models of the buried pipe involving the detailed modeling of the problem including the precise simulation of the interaction occurring at the interfaces of soil and buried pipe and accurate definition of the mechanical behavior of these material under the applied fault displacement load have been described detailly under Chapter 3. Result obtained using these models are presented under Chapter 4. The longitudinal strains corresponding to fault displacement values also utilized for the simplified models have obtained using these models as well. Comparison of the results of these two approaches are presented in Figures 5.17a through 5.19c for D/t equal to 144, 96, and 58 and β equal to 10º, 15º, and 30º. Review of results indicate that the computed strain values are in good overall agreement with each other and have an acceptable margin of difference, results show that strain values computed using the simplified approach are always smaller than those obtained from sophisticated numerical models.

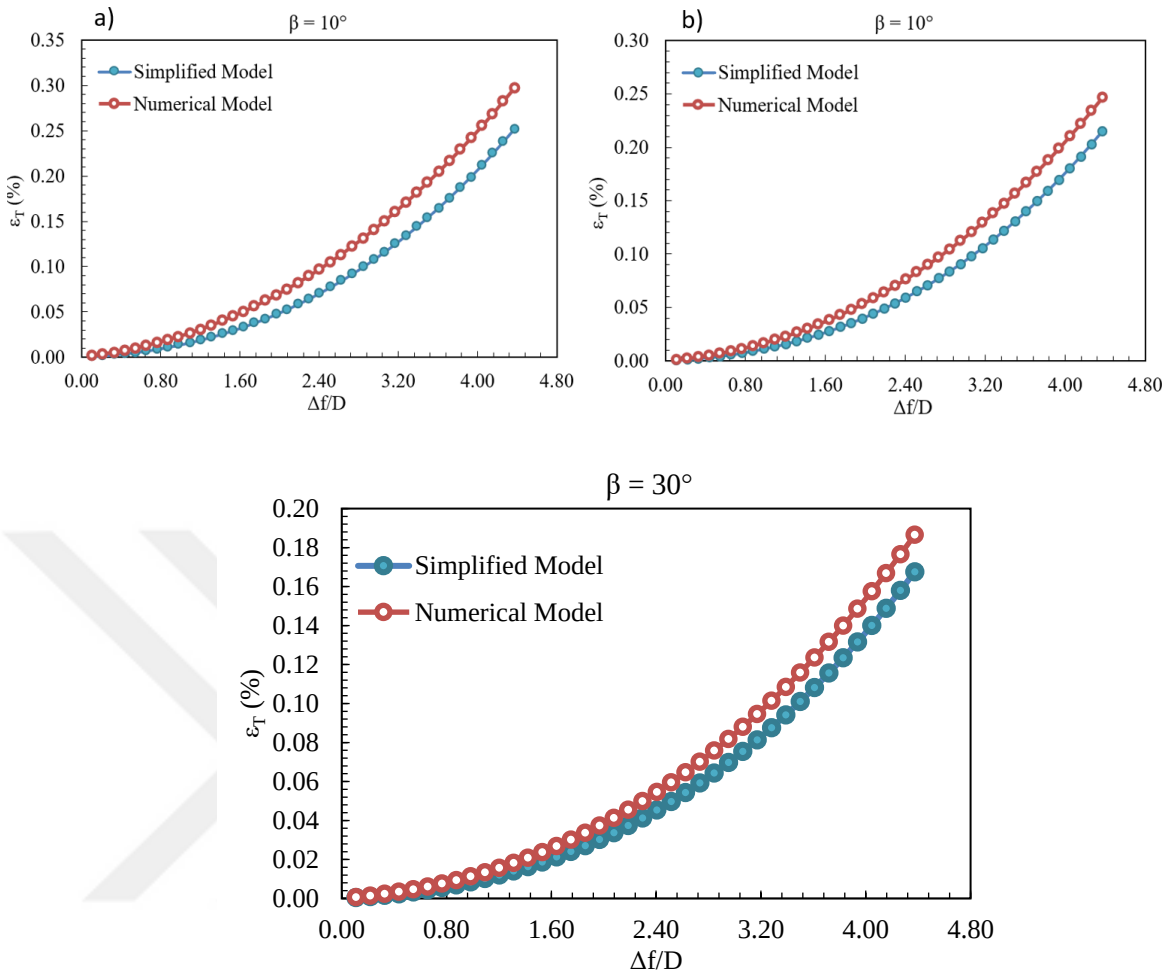

c)

Figure 5.17. Comparison of strain results obtained using the simplified models (blue) and numerical models (red) for, a) D/t = 144 and β = 10º, b) D/t = 144 and β = 15º, and c) D/t = 144 and β = 30º

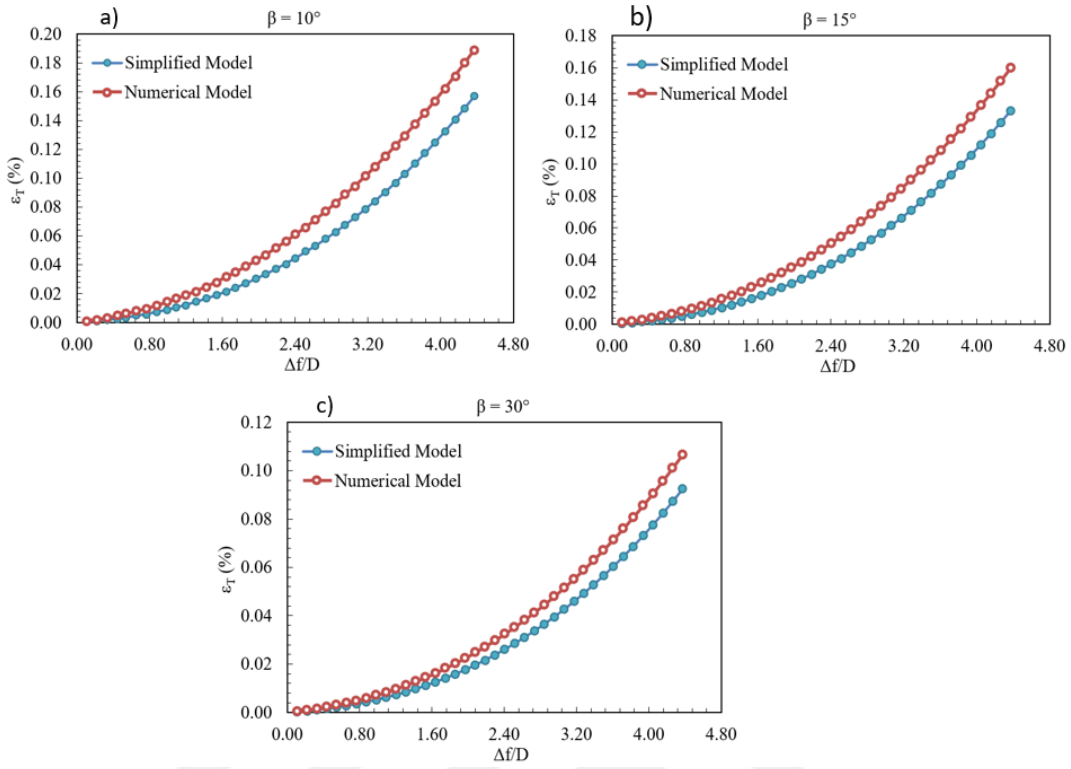

Figure 5.18. Comparison of strain results obtained using the simplified models (blue) and numerical models (red) for, a) D/t = 96 and β = 10º, b) D/t = 96 and β = 15º, and c) D/t = 96 and β = 30º

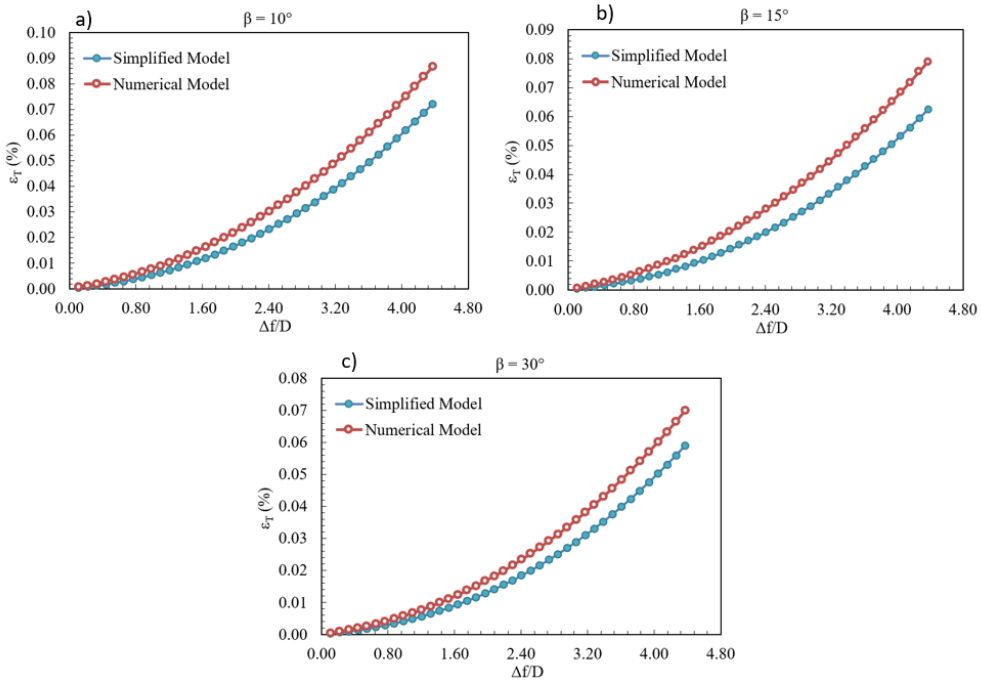

Figure 5.19. Comparison of strain results obtained using the simplified models (blue) and numerical models (red) for, a) D/t = 58 and β = 10º, b) D/t = 58 and β = 15º, and c) D/t = 58 and β = 30º

6. CASE STUDY: THAMES WATER PIPE

Known as Thames water pipe, a welded steel pipe with a diameter of 2.2m running along the city of Izmit in Turkey and used to transport water over a large area suffered irreparable damage during the earthquake that hit the city in 1999, the severity of damage deemed the pipe to be eventually shut down causing significant socio-economic consequences. This chapter presents a case study involving the numerical modelling of this pipe and evaluation of its response under a strike-slip fault displacement load used to simulate the effects of this earthquake event. Initial sections of the chapter cover background information regarding this conduit and the damage sustained by it during the 1999 Izmit earthquake. The chapter proceeds with a brief review of existing literature on this topic, going through the developed numerical models, performed field measurements and evaluations. Later sections of the chapter describe the details of the advanced model proposed in this thesis to evaluate the response of this pipe. Results obtained using this model is compared to the results of existing studies to ensure their validity. Lastly, the possibility of reducing the induced seismic damages is investigated through the use of CFRP composites. Numerical models incorporating these wraps were developed following the concept described in Chapter 3. Results obtained in terms of strains, stresses and rotational demands were then used to assess the magnitude of improvement offered by this mitigation approach.

6.1. Background Information

Being a devastating major event the 1999 Izmit earthquake occurring due the rupture of the North Anatolian fault took o heavy toll on the general population spread along a large area claiming thousands of lives and causing detrimental material losses. With a moment magnitude of 7.6 this devastating event ruined large significant portions of numerous mid-sized towns and cities leading to irreparable damages on many residential and public structures as well as heavily damaging many infrastructure lines of critical importance (Şahin and Tari, 2000; Erdik, 2001). As an industrial city with then a population of approximately 500.000 the city of Izmit was the place which took the heaviest hit by this major earthquake suffering loss of both life and property damage (Marza, 2004).

As a major industrial zone, the city was the crossing zone of many large scale buried steel pipelines which naturally sustained damage during this catastrophic damage. Among this pipeline, the one crossing the cities of Kullar and Izmit and named as Thames pipeline suffered great damage during the earthquake and was forced to shut down a few days following the event. Thames pipe was a welded steel pipe with an out-to-out diameter of 2.2m and wall thickness of 18mm, with its primary function being to deliver water from the Yuvacik Dam to many urban areas in the vicinity (Tang, 2000). As shown in Figure 6.1 the pipe crosses the North Anatolian fault at the exact location of latitude and longitude values of N40° 43.174' and E29° 58.098' respectively. Excluding a short duration of suspension required for field investigations and interventions, the pipe remained functional for almost the next eight months following this devastating incident. The pipeline begin service about a year before the event happened. The pipe was used to deliver water to the city of Izmit from a dam located in Yuvacik where along its path it passed through a facility used for water treatment purposed located near the city of Kullar, where the fault with the same name crossed through. The welded steel pipe at this location crossed the fault at an intersection angle of 55º, and damage occurred on the pipe due to rupture (right lateral direction) of the strike-slip fault at that zone that caused a total fault displacement of 3m. The components of fault rupture (offsets) at lateral and axial directions were 2.32 to 2.49m and 1.71m, respectively (Eidinger, 2001).

Within a few days following the earthquake, the buried steel pipe was excavated and exposed so as to gather more complete information and enable a better comprehension of the magnitude and features of the deformations sustained by this particular pipe. The soil deposit covering the buried steel pipe was excavated, exposing the better part of the buried pipeline for exploration and field measurements. After draining the content of the line, a cut allowing entrance to the inside of the pipe was made, field observations and measurement revealed the existence of three major damages located at stations 1+320, 1+337 and 1+349 (See Figure 6.2). The buried pipe suffered damage in form of local buckling, sustaining major wrinkling at these stations. The wrinkles observed at stations 1+337 and 1+320 (see Figures 6.3 and 6.4) resulted in a folding with a depth of approximately 200mm or more. These deformations resulted in a reduced cross-sectional area which in turn lead to a reduced flow capacity (Eidinger et al., 2002). Observations revealed that leakage of pipe content occurred at a single area where a crack in the steel had appeared (area of major wrinkle).

Field measurements determined that the pipe was losing around 1% of its water flow at this location, however, this was not considered to be a major failure in terms of safety.

The fact that the Thames Water Pipeline sustained damage during this earthquake that took place along the North Anatolian tectonic plate is not much of surprise considering to features of the fault slip and the pipe design aspects. This pipe intersected the fault at an angle of 50° to 55.5°±, which put it under compression effects due to the fault movement in right lateral direction (Eidinger et al., 2002).

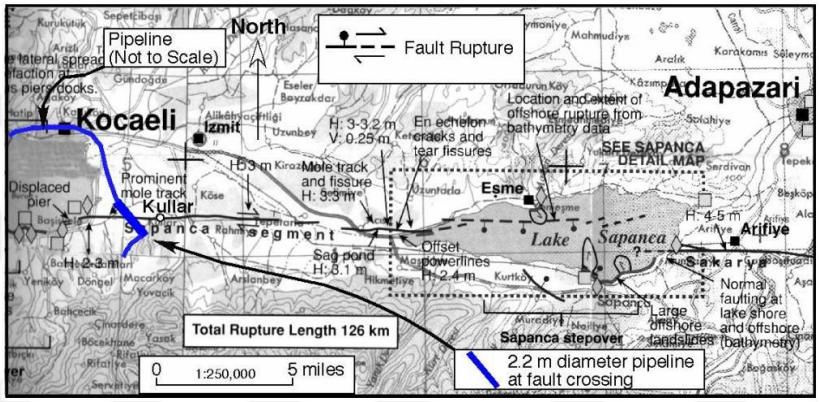

Figure 6.1. Location of the Thames Pipe at the vicinity of Kullar fault (Tang, 2000)

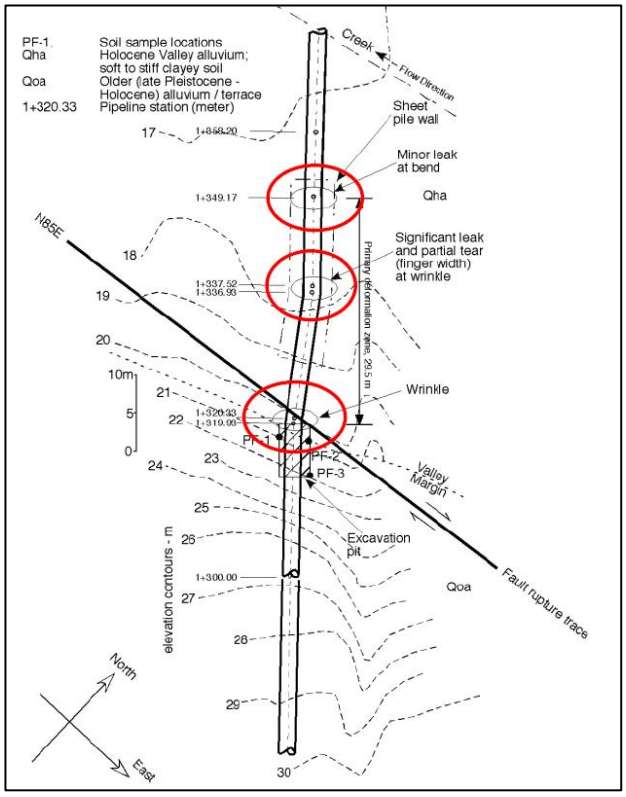

Figure 6.2. Damage locations along Thames Pipe (Eidinger et al., 2002)

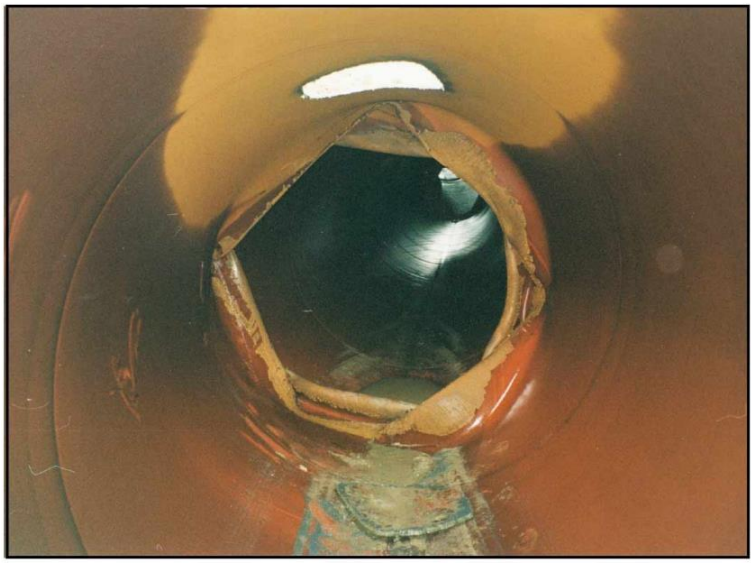

Figure 6.3. Major wrinkle occurred at station 1+337 (Eidinger et al., 2002)

Figure 6.4. Major wrinkle occurred at station 1+320 (Eidinger et al., 2002)

6.2. Review of Previous Studies

There exists a considerable number of research in literature dealing with the performance evaluation of Thames water pipe during the 1999 Izmit, Kocaeli earthquake. Some of the studies involve field evaluations mainly by means of in-situ observations and measurements performed using a variety of tools, while other studies made use of the observed data to construct numerical analysis models adopting a variety of approaches ranging from simple approaches to rigorous FE models to better understand and simulate the behavior of this pipe.

In their study Liu et al., (2014) have proposed a finite element model consisting of shell elements to analyze the response of Thames pipe. Due to the fact that during its service the pipe was operating with 10MPa of internal pressure the wall thickness was increased from 18mm to 28mm on purpose to account for this condition. The developed FE shell model was subjected to incremental lateral displacement reaching up to 3m. Obtained results indicate a good overall agreement with field observations. Two points of major wrinkling and one point of minor wrinkling is observed on the developed model due to induced compression strains. As expected, due to the difference in soil properties at the right- and left-hand side of the pipe, the largest wrinkling occurred at the point located on the soft soil side, it was also concluded that despite the considerably low amount of compression strains yet due to the difference in soil properties a third minor wrinkle also occurred on the pipe.

Takada et al. (2001) have performed a similar study which involved the development of a shell finite element model of the pipe having equivalent boundary conditions. The study proposes a new simplified model which primarily aims at lowering the required computational time caused by the extremely long pipeline portion affected during the earthquake (approximately 200m) needed to be modeled using shell elements, which typically requires lengthy hours of computational effort. To reduce this length, a model was constructed where only the pipeline portions close to the fault are modeled via shell elements and assuming fixed boundary conditions at ends of the pipe. Whereas, for pipeline segments located away from the fault plane, pipeline material was assumed to have an elastic perfectly plastic behavior modeled via the computation and use of non-linear soil springs. Results obtained using this method appear to be in good overall agreement with field observations, where similar to other studies and observations two major and one minor wrinkle area are found to occur along the pipeline under the applied compression strains.

A series of detailed field surveys and subsequent development of numerical model of analysis was performed by Edinger and O'Rourke (2001, 2002). The ANSR-III analysis software was adopted for numerical modeling of the response of Thames pipe in these studies. The most vital features and properties of the model were as follows: The length of the buried was modeled to be 1400 feet long. Segments of the pipe were represented via 3D ANSR type 6 elements featuring distributed plasticity. Truss elements (type 1 nonlinear elements) were utilized to model the behavior of soil in the corresponding (axial and

transverse) directions. Bilinear stress strain curves were assumed for material behavior representation. 3D gap elements with single degree of freedom were used to model soil in vertical upwards and downwards directions. Two reflect the change in soil pattern two different vertical elements were utilized. The obtained results presented in terms of peak pipeline strains and moments on pipeline indicate the presence of three distinct point where the strain and bending moments attain large values, an observation that is in agreement with field observations noting two major and one minor point of wrinkling.

Among the latest attempts to establish a more sophisticated FE model of analysis for the Thames pipe is the study published by Kaya et al. (2017). In this research a 3D non-linear continuum model of the pipe-soil system was developed using ABAQUS CAE software. In this context as shown in Figure 6.5 a 3D model of 100m length 20m width and 5m depth was constructed to simulate the response of the pipe. The fault trace was modelled as a discontinuity plane crossing the pipe with an intersection angle of 55^{o}, and thus dividing the soil into two blocks of equal length (50m of length on both sides). The fault load caused by the right lateral movement of the Kullar fault was imposed onto the model as incremental nodal displacement up to the magnitude of 3m. In addition to the evaluation of the response for free end boundary conditions models involving the evaluation of the effect of different end boundary conditions was also investigated. In particular, the fixed end and equivalent spring conditions were investigated within the scope of the presented work. The studied boundary conditions are illustrated in Figure 6.6. The findings of the study indicate that the analysis model is able of capturing the behavior of the pipe under the applied fault load with low margins of deviance. As expected, due to the difference in soil conditions on both sides of the pipe the wrinkle locations were not symmetric and were closer to the site with stiff soil conditions. Changing the support (boundary) conditions restricting the movement of the pipe at the ends was determined to play a significant role on the overall response of the pipe. Compared to fixed end case the strains obtained at free end solutions increased considerably. This study also served as the basis for the development of the analysis model presented in this dissertation and was utilized for model validation purposes and shown in later sections of this chapter.

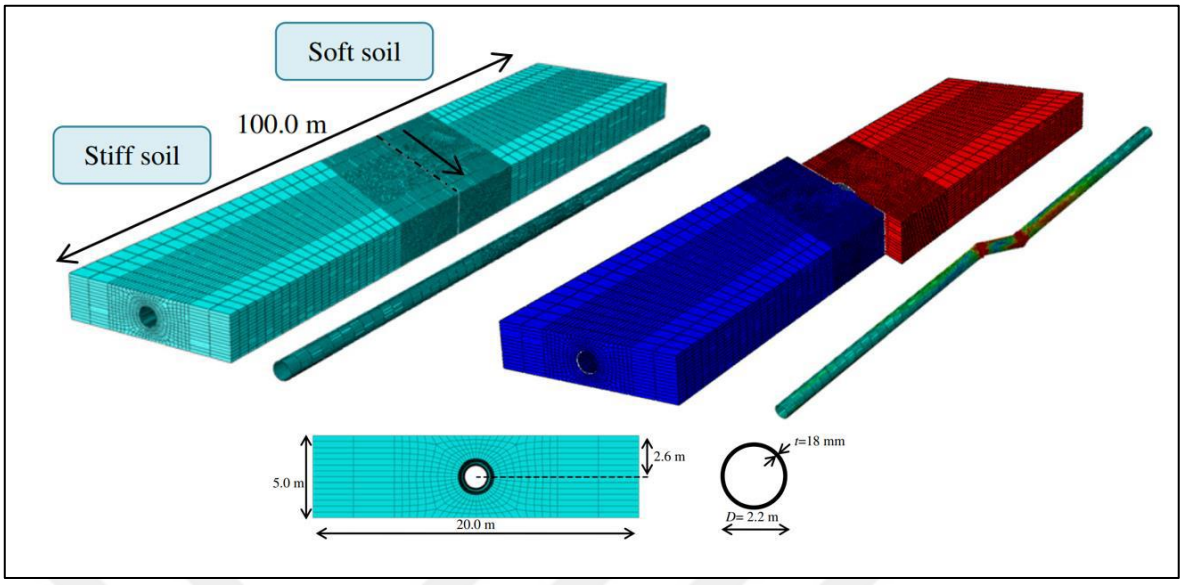

Figure 6.5. Numerical FE model of Thames pipe proposed by Kaya et al. (2017)

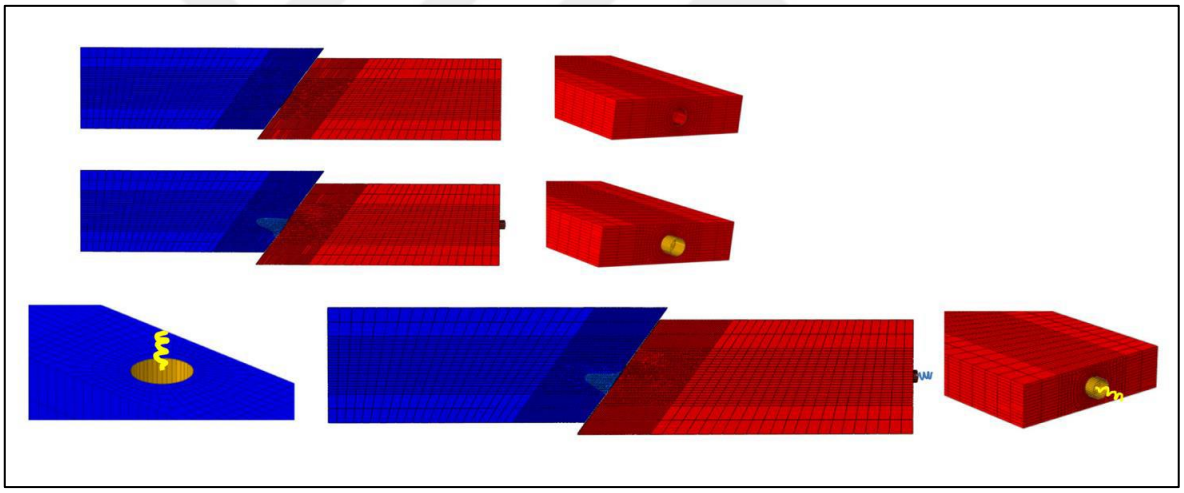

Figure 6.6. Pipe end conditions investigated in Kaya et al. (2017) study, top left: free end, top right: fixed end, and bottom: equivalent spring model

6.3. Description of the Developed Numerical Model

The FE model developed to study the behavior of Thames welded steel pipe in essence follows the steps utilized in the models developed throughout the course of this dissertation. Similar to other models, the developed model consists of three parts in total, two soil blocks divided at equal length by the fault plane modeled as a plane of discontinuity which, soil blocks were modeled using solid continuum elements with hourglass control, while the buried steel pipe was modeled using shell elements capable of capturing the non-linear

response of it. Different from the cases studied within the scope of this dissertation, in order to realistically capture the full response and behavior of the buried steel pipe the length of the developed model was assumed to be equal to 100m in total and the width and depth were 20m and 5m respectively (similar to dimension of the model developed by Kaya et al. (2017)). Figure 6.7 shows the dimension and meshing pattern of the developed model. The fault was modeled to cross the pipeline at an intersection angle of 55^{o}, causing compression strains, where an incremental fault displacement reaching up to value of 3m was imposed onto the external nodes of the moving soil block as depicted in Figure 6.8. Similar to the model developed by Kaya et al. (2017) fixed end conditions were assumed for the pipe so as to obtain more realistic solutions. Field observation performed by Edinger et al. (2002) indicate the presence of two different soil conditions along the length of the pipeline, to simulate this condition, blocks at the opposite sides of the fault plane were assumed to possess the characteristic of a stiff and soft clay soil respectively. The steel material used for the buried pipe was API Grade B steel. The Mohr Coulomb material model was assumed for the native soil whereas the Von Misses approach was utilized for the pipe steel material.

The diameter of the pipe in the model was equal to 2200mm with a wall thickness of 18mm, the burial depth was equal to 2.6m as per field observation data. An internal pressure value of 10MPa was assumed during the analysis, which added one extra step to the solution algorithm. The surface-to-surface contact algorithm assuming full contact among the surfaces of buried pipe and the backfill soil with an initial penalty friction value of 0.30 was assumed to exist between the two.

A quasi-static full Newtonian solution approach was adopted as the solution technique. The analysis encompassed three stages in total, initially the stresses developing due to the dead load of soil were analyzed in the geostatic loading case solved using the general static method, in step number two a 11MPa load was imposed as pressure on internal walls of the buried steel pipe, lastly, in step 3 the incremental fault load is applied on the moving soil block while the other is kept fixed. The sectional view of system subjected to fault load and the accumulation of Von Misses stresses and deformations is illustrated in Figure 6.9. The results obtained through the analysis of the developed model are validated through comparison with data obtained from field observation and numerical models developed by

researchers. As discussed in later sections results obtained from the developed method and in good agreement with the data of other studies.

Lastly this chapter also includes the investigation of the possibility of damage mitigation for the Thames pipe using the most efficient technique determined based on result and comparisons presented in Chapter 4. In particular, models of the Thames water pipe incorporating the use of CFRP wraps of 3mm and 10mm thickness were developed to evaluate the effectiveness of this techniques. The model configurations and paths followed to construct these models were essentially the same with the ones used for other models studied in this dissertation. Figure 6.10 shows the configuration for models incorporating CFRP wraps.

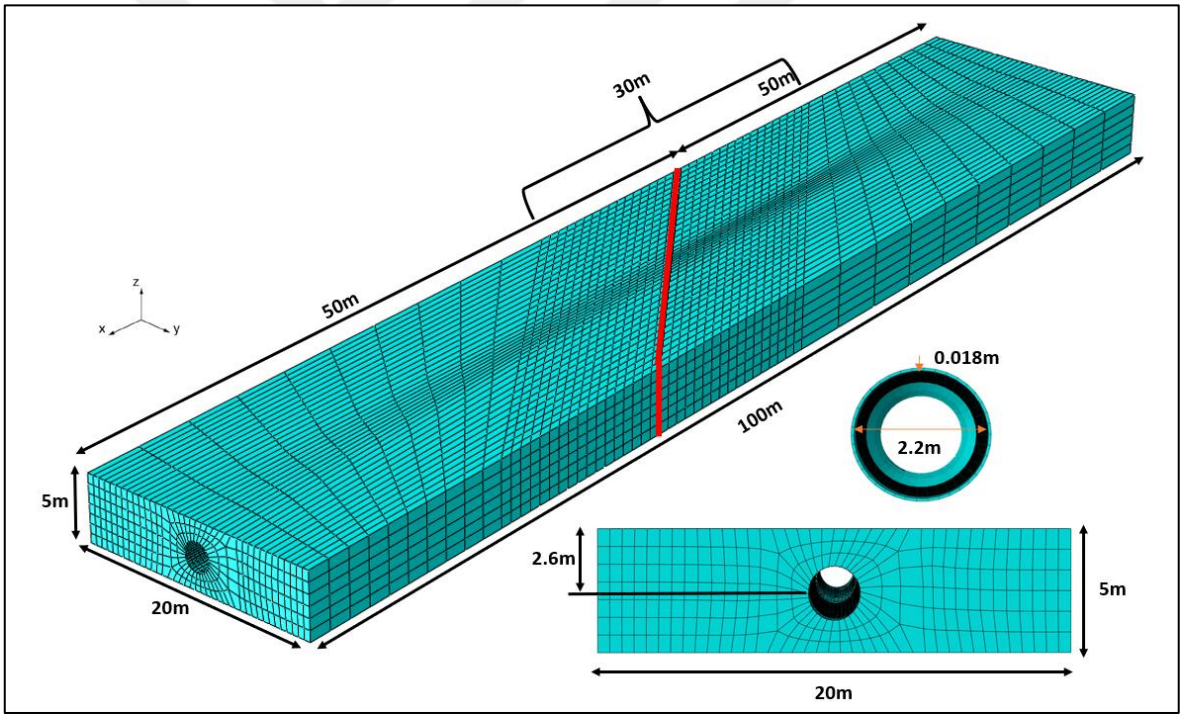

Figure 6.7. Model configuration and mesh pattern utilized for Thames pipe

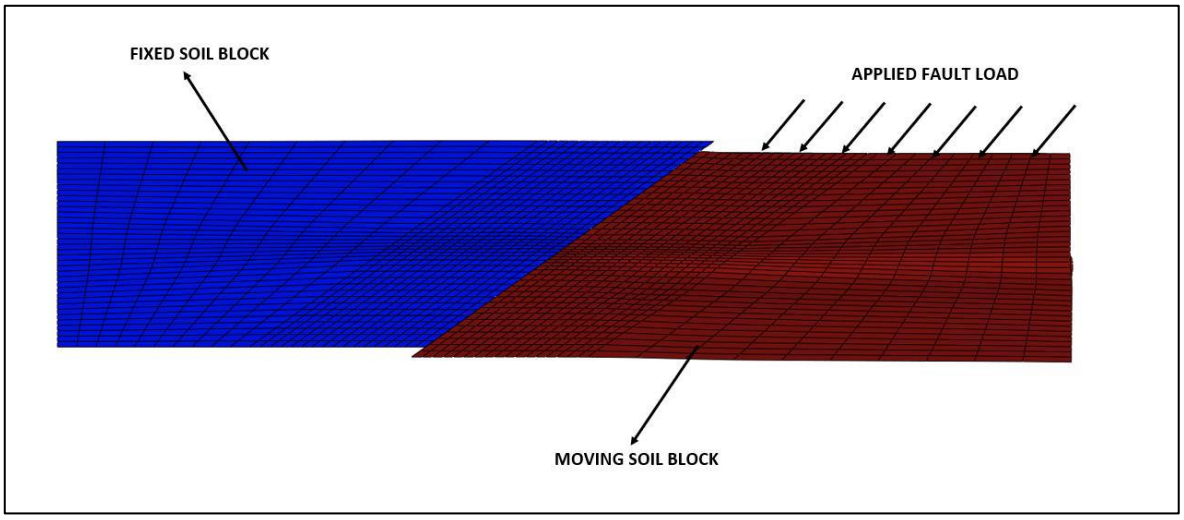

Figure 6.8. Illustration of the applied fault load and response of the pipe-soil system

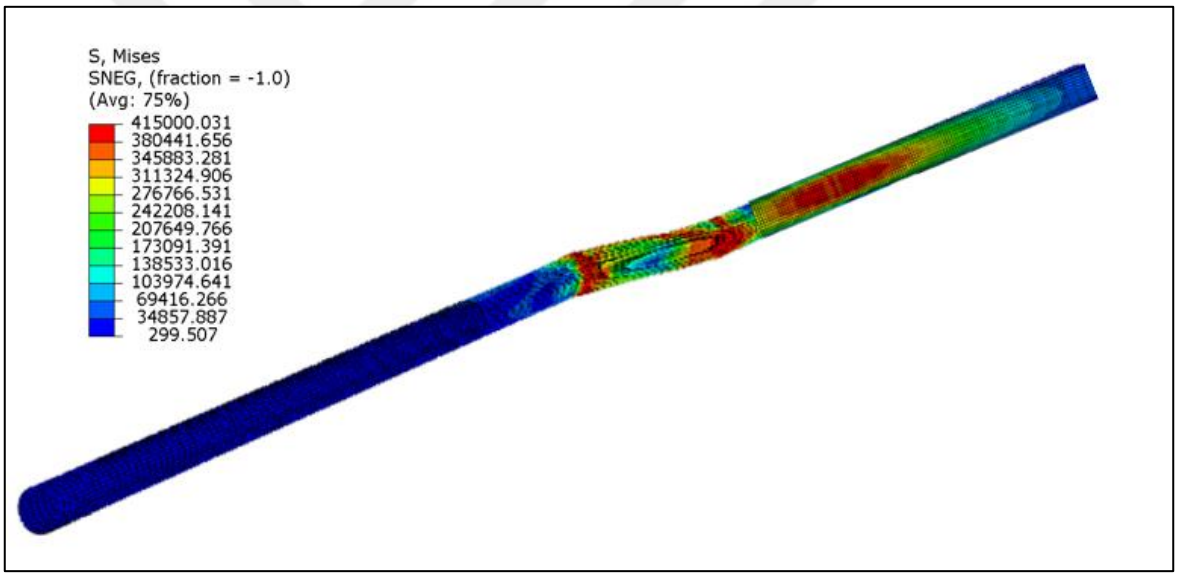

Figure 6.9. Onset of Von Misses Stresses due to the applied fault load

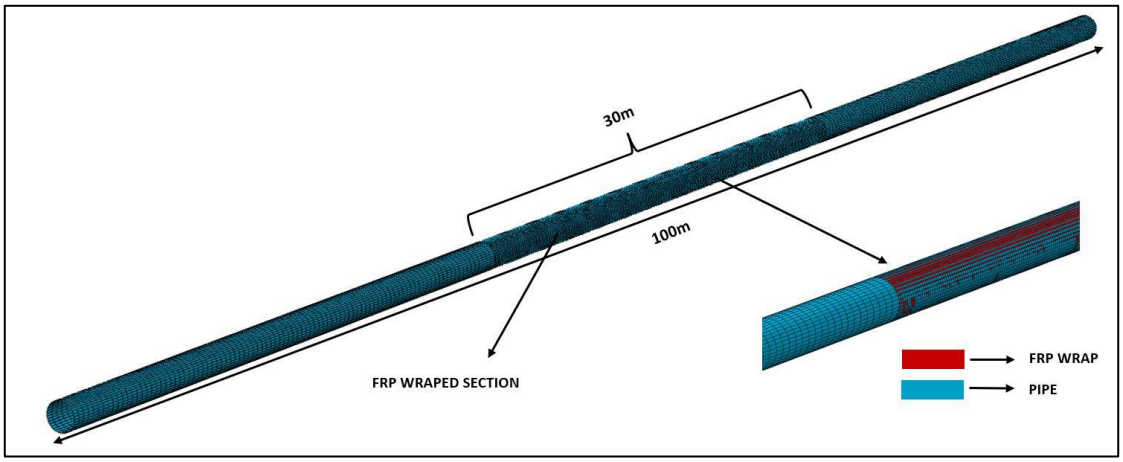

Figure 6.10. Model configuration used for CFRP wrapping of Thames pipe

6.4. Model Validation

The accuracy of the developed FE model for the Thames water pipe was verified through comparison with data reported by field surveys, data yielded from published numerical models explicitly developed to simulate the behavior of this pipe (such as the model of Kaya et al. (2017) and outcomes of other simplified theoretical approaches. Existing data contain information regarding the location of the major and minor wrinkles developed during the act of the seismic load imposed by the 3m offset of the strike-slip fault of Kullar, maximum attained axial strains on the pipeline, rotation demands imposed onto the pipeline, buckling strain and wavelength.

The data mentioned above was also derived from the developed ABAQUS model and summarized for comparison with other models. In this context, Table 6.1 summarizes the data for the location of axial strains, average axial strain demands, rotation demands, buckling strains and their location along the length of the pipe. Obtained results indicate that the outcomes of the proposed model are in close vicinity into the ones obtained by field surveys as well as other numerical models. In addition, Figures 6.11 and 6.12 illustrate the distribution of plastic strains along the pipeline obtained by the numerical model developed by Kaya et al. (2017) as well as the model presented in the study herein, for fault displacements of 0.5m and 3m respectively. As it can clearly be observed from the Figures the data obtained from the models are in very good agreement. Moreover, Figure 6.13 shows the developed Von Misses stresses at 3m of fault displacement obtained using the proposed

methods. Again, a good overall agreement seems to exists among the two. Lastly, to prove the exactness of the proposed method the deformed shape of the buried pipe obtained at the end of the analysis was compared to pictures taken during field surveys. As shown in Figures 6.14 and 6.15 a good agreement exists between the actual and the simulated response of the pipe.

Table 6.1. Comparison of data obtained using the proposed model and other researches

	Separation Dist. Btw. Wrinkles (m)	**Avr. Axial Strains at Wrinkles 1&2 (%)**	**Rotational Demands at Wrinkles 1&2 (deg.)**	**Location of the 3rd Minor Wrinkle (m)**	**Local Buckling Wavelength (m)**	**Local Buckling Strain (%)**
Field Data	17.10-17.60	15-50	7.50-8.50	13.00	50-60	-
Kaya et al. (2017)	16.50	15-20	7.50-8.00	13.10	50-55	0.210
Theoretical (1986)	-	-	-	-	48	0.190
Developed Model in This Study	16.10	13-17.90	6.90-7.85	13.50	48-52	0.205

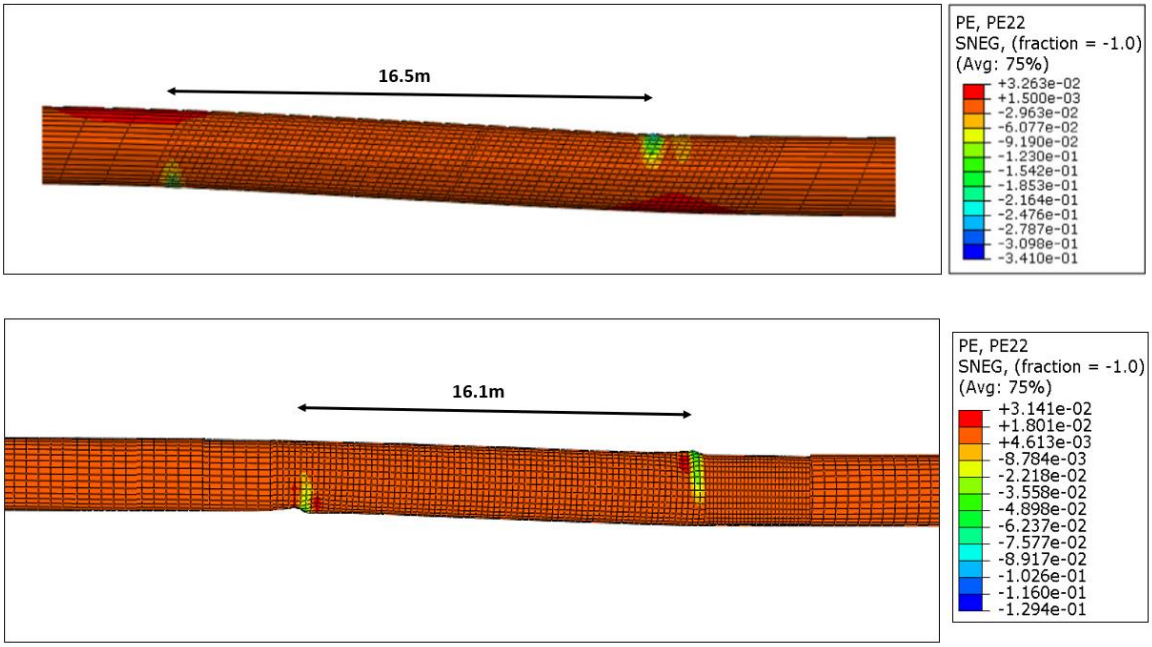

Figure 6.11. Model distribution of plastic strains at d = 0.50m and the corresponding wrinkle separation distances obtained through the model of Kaya et al. (2017) (top) and the developed model (bottom)

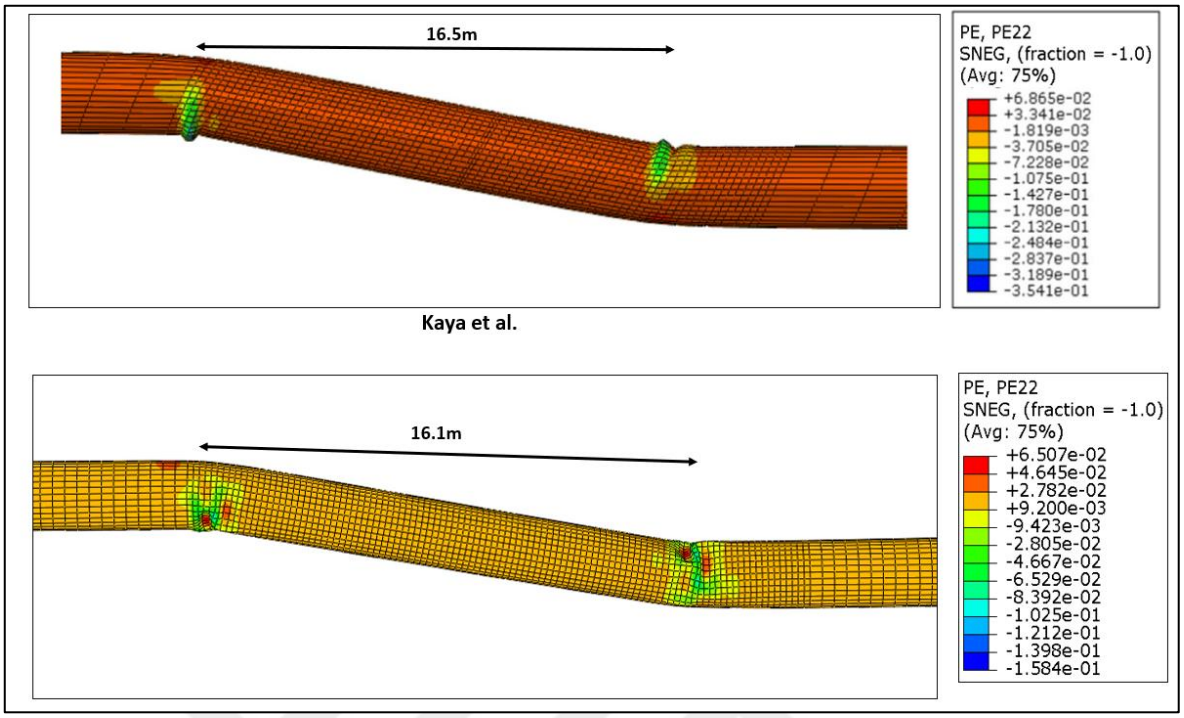

Figure 6.12. Model distribution of plastic strains at d = 3m and the corresponding wrinkle separation distances obtained through the model of Kaya et al. (2017) (top) and the developed model (bottom)

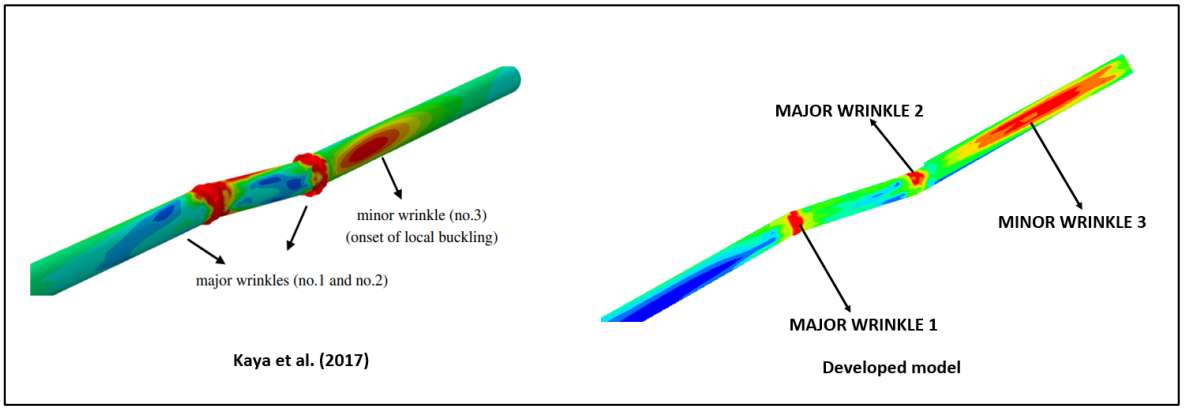

Figure 6.13. Illustration of the distribution of wrinkles along the pipeline obtained using Kaya et al. (2017) model (left) and the model developed in this study (right)

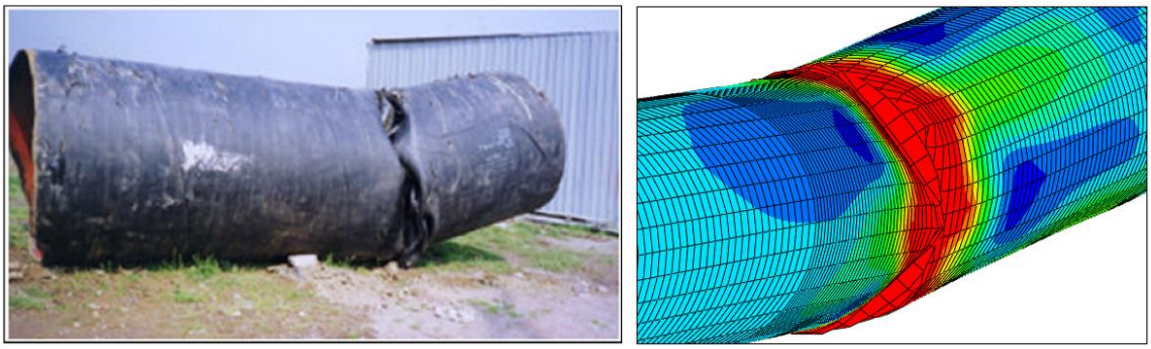

Figure 6.14. Comparison of wrinkle formation using field data (left) and the developed model (right)

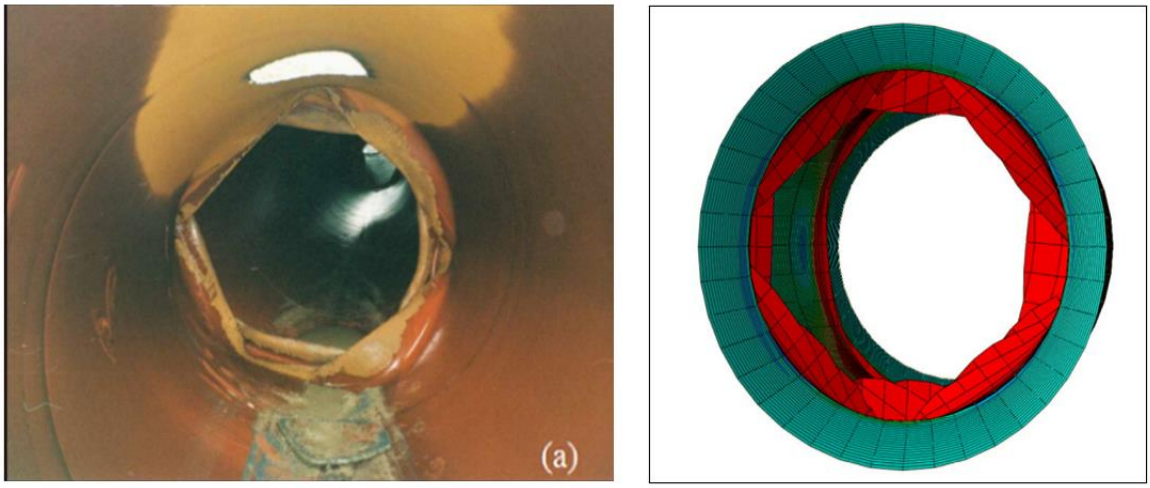

Figure 6.15. Sustained pipeline damage: field survey data (left) simulated data (right)

6.5. Damage Mitigation Using CFRP Composites

Possibility of the mitigation of seismic demands exerted on the Thames water pipe by the strike-slip fault action was investigated via incorporating FRP composite wraps within the analysis models described above. In particular, the impact of utilizing Carbon Fiber (CFRP) wraps with a 3mm and 10mm of layer thickness was investigated within the scope of this study. As shown in Figure 6.10 the CFRP wrap was modeled using the same element type (S4R shell element) used for pipeline modelling. Again, contact algorithm incorporating the definition of slave and master surfaces was utilized to simulate the interaction between the pipe and the CFRP composite wrap. Details of the properties of these interaction

algorithms are discussed under Chapter 3. A performance criterion (limit state) is defined to account for the rupture of the FRP wrap, owing to the fact that a hard contact with no possibility of slippage among the pipe and FRP was enforced into the analysis model once the rupture will take place on the FRP the same amount of tensile strains will also be sustained by the pipeline. Hence, as described detailly in previous chapters a tensile strain capacity calculated using elastic material properties of the CFRP (due to fact that the behavior of CFRP is almost linear up to the point of rupture) was utilized as the limit state for CFRP wrap rupture.

The efficiency of utilizing CFRP as means of damage mitigation for the Thames pipe was evaluated via initially comparing the formation of wrinkles. Figure 6.16 illustrates the distribution of damage along the pipeline at the fault displacement value of 3m. As seen from the figure, the minor wrinkles developing at the far end of the pipe disappeared when a CFRP wrap of 3mm thickness is used for damage mitigation, in addition the amount of plastic strains developing at wrinkle 1&2 locations appear to have been reduced by as much as 47% as the pipe is wrapped with CFRP composites, a truly desirable achievement which could have possibly eliminated the need to cease the function of the pipe immediately following the earthquake. Moreover, the use of a 10mm thick CFRP layer was determined to eliminate the occurrence of major wrinkling at location 2, with only a minor amount wrinkling appearing at location 1, results indicate a reduction of 87.3% in plastic strains as well.

In addition, graphical comparison of axial strains given in Figures 6.17 through 6.19 illustrates the variation of strains for the wrapped and non-mitigated cases at fault displacement values of 1, 2 and 3m respectively. Comparison of the results indicates a clear reduction in the resulting plastic strains, however, wrapping the pipeline with CFRP does not seem to affect the length at which the major wrinkles occur. As per the stresses developed at fault displacement value of 3m as shown in Figures 6.20 again a significant reduction is seen to have been obtained using CFRP composite wraps. Lastly, comparison of results between mitigated and non-mitigated cases in terms of rotation demands is shown in Figure 6.21 to 6.23 where once again a considerable reduction can be noticed for CFRP wrapped cases. Despite the remedy offered through the use of this mitigation strategy, yet the results

indicate that complete elimination of seismic demands is not achievable for this case study, revealing the level of severity of this earthquake and importance of soil properties.

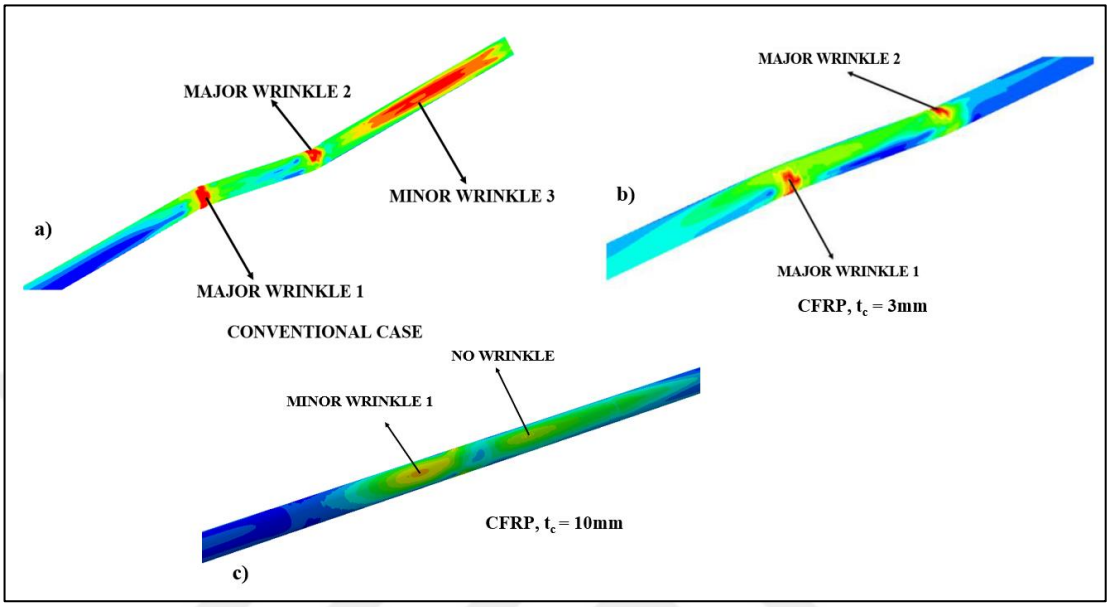

Figure 6.16. Damage locations on buried pipe for a) conventional case, b) case with 3mm thick CFRP, and c) case with 10mm thick CFRP layer recorded at d = 3m

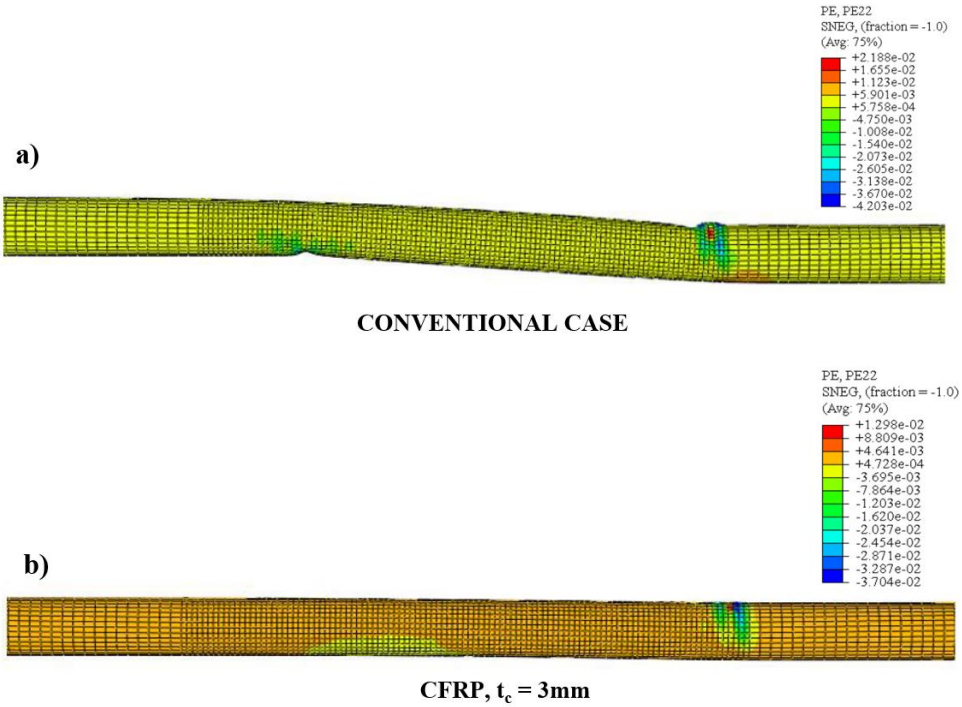

Figure 6.17. Plastic strains developed on the pipe for a) conventional case, b) case with 3mm CFRP wrap, and c) case with 10mm CFRP wrap recorded at d = 1m

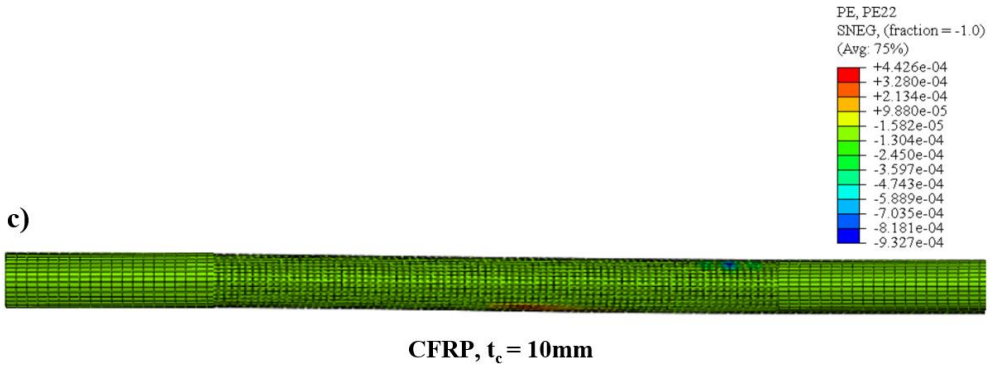

Figure 6.17. Plastic strains developed on the pipe for a) conventional case, b) case with 3mm CFRP wrap, and c) case with 10mm CFRP wrap recorded at d = 1m

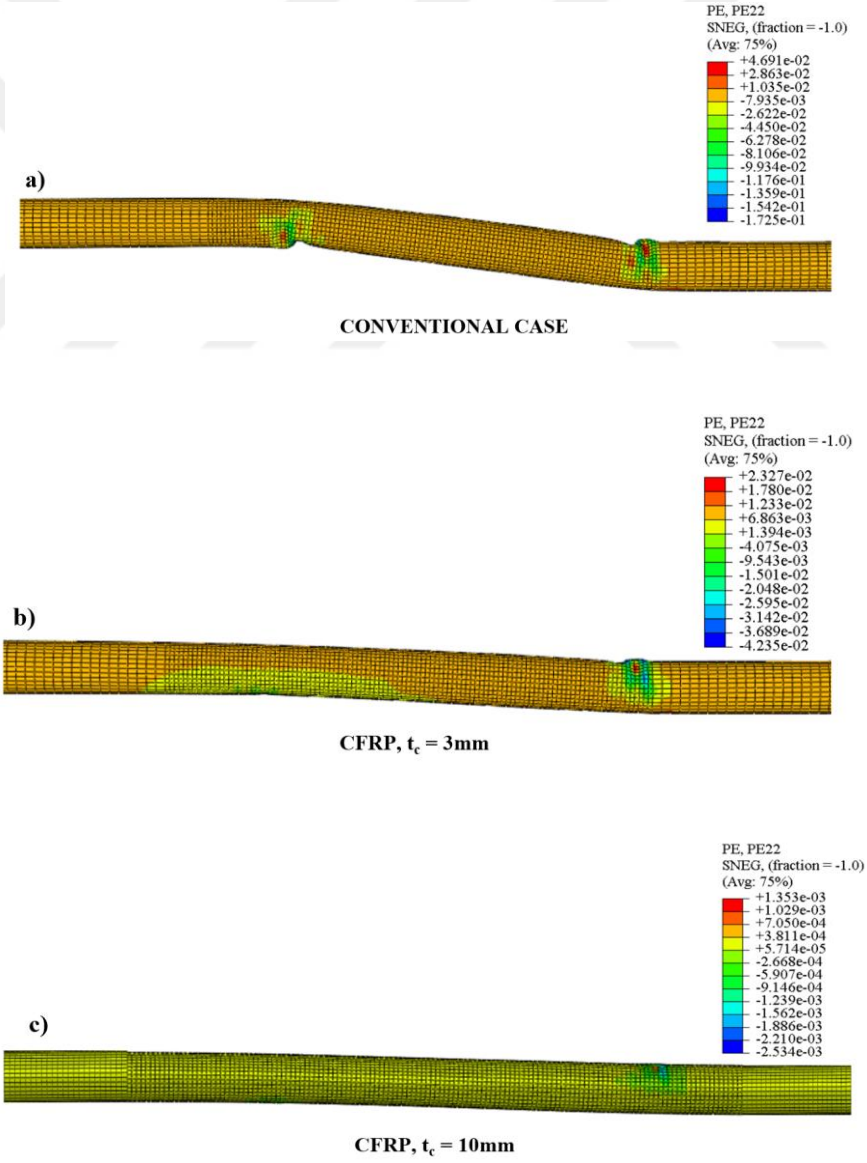

Figure 6.18. Plastic strains developed on the pipe for a) conventional case, b) case with 3mm CFRP wrap, and c) case with 10mm CFRP wrap recorded at d = 2m

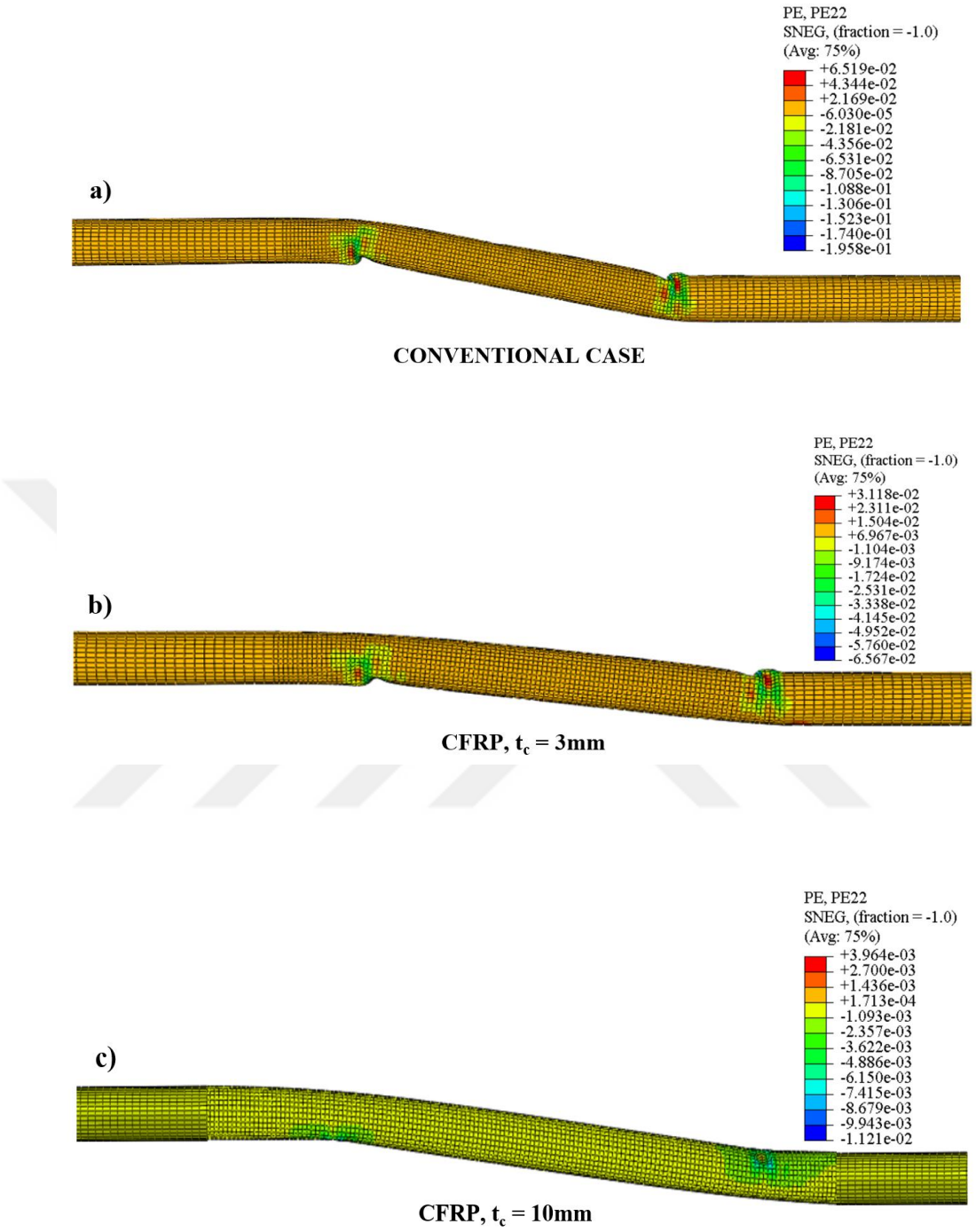

Figure 6.19. Plastic strains developed on the pipe for a) conventional case, b) case with 3mm CFRP wrap, and c) case with 10mm CFRP wrap recorded at d = 3m

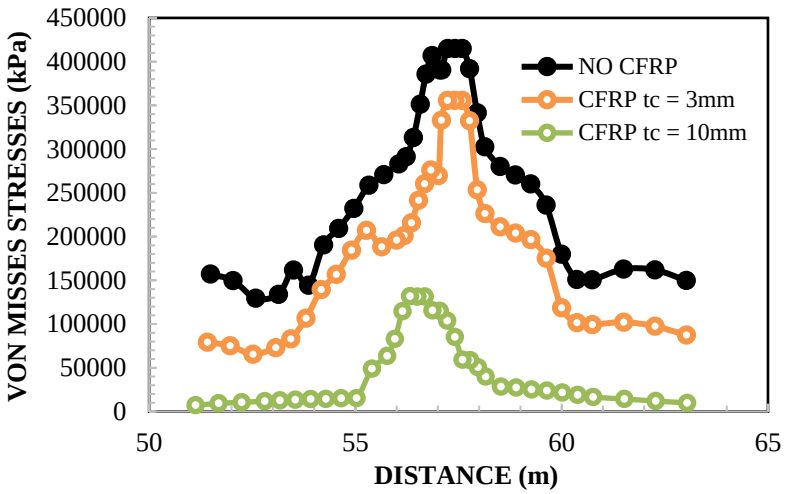

Figure 6.20. Plot of Von Misses Stresses along the pipeline length for non-mitigated (black) and CFRP mitigated (orange and green) cases at d = 3m

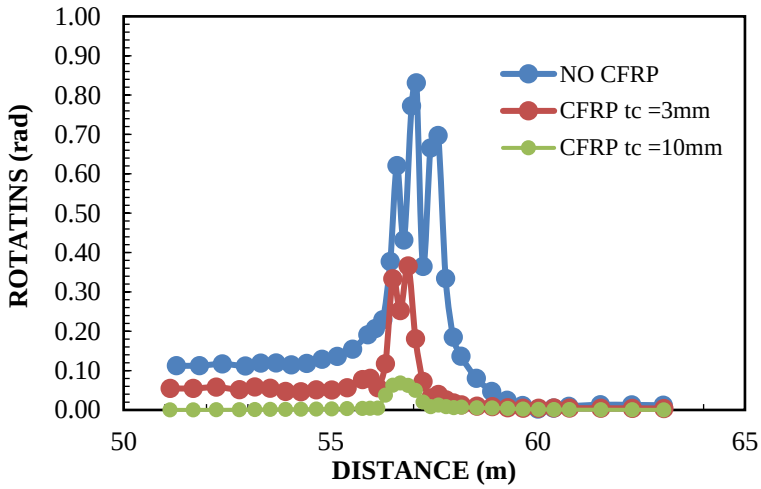

Figure 6.21. Plot of rotation demands along the pipeline length for non-mitigated (blue) and CFRP mitigated (red and green) cases at d = 1m

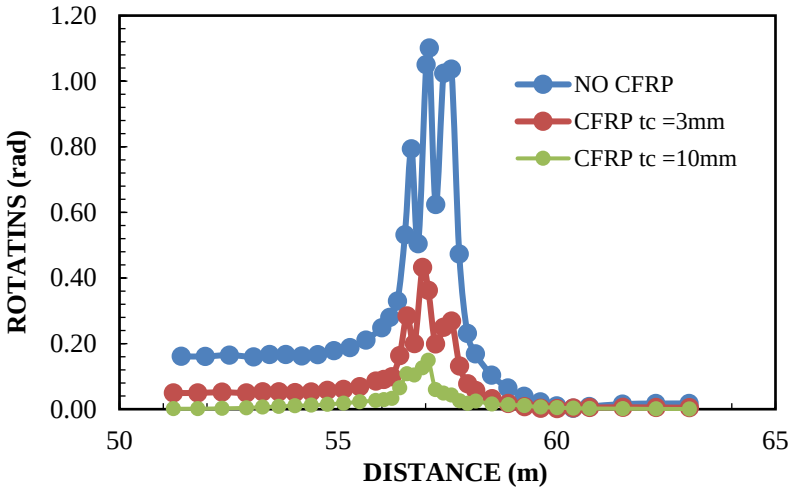

Figure 6.22. Plot of rotation demands along the pipeline length for non-mitigated (blue) and CFRP mitigated (red and green) cases at d = 2m

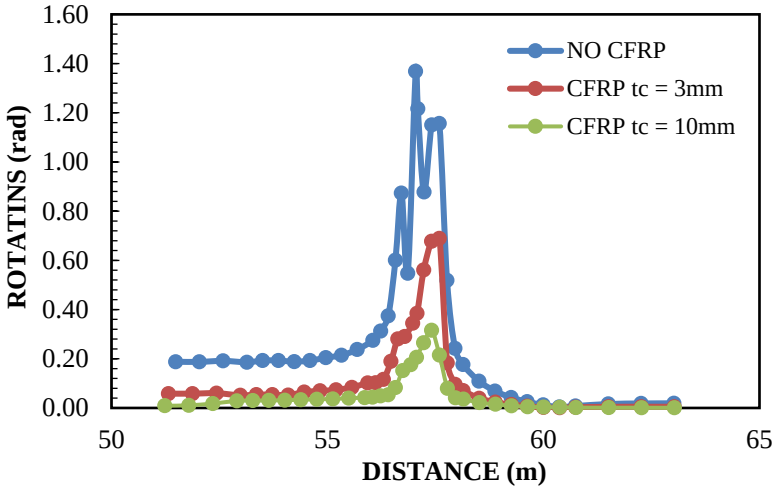

Figure 6.23. Plot of rotation demands along the pipeline length for non-mitigated (blue) and CFRP mitigated (red and green) cases at d = 3m

7. CONCLUSIONS AND DISCUSSION

This dissertation concerned itself with the assessment of the performance and behavior of steel buried continuous (welded) pipes subjected to fault actions resulting from the rupture of a strike-slip fault. Advanced three-dimensional finite element numerical models of the problem incorporating the modelling of material and geometric non-linearities as well as explicit simulation of the interaction and contact among the surfaces of the buried pipe and the backfill soil deposit have been developed and utilized to estimate the pipe response subjected to effects emerging from the rupture of faults applied in the developed models as a quasi-static displacement load. Influence of design parameters such as fault crossing angle and pipe D/t ratio on the performance of the buried pipe have been investigated within the scope of this thesis. A strain-based approach was utilized for performance evaluation purpose where strain limits defining the failure of the pipe due to the occurrence of phenomena such as local buckling, exceedance of tensile strains and cross-sectional distortion have been calculated for each investigated case. Apart from developing numerical models to simulate the buried pipe behavior under fault movement, this thesis also investigated the effect of four mitigation techniques to improve the buried pipe performance exposed to severe seismic actions. In particular, utilization of FRP composite wraps (three types, CFRP, GFRP and BFRP with layer thicknesses varying from 1mm to 10mm), EPS geofoam blocks (low and high strength), controlled-low strength material (low and high strength) and Tensar Nr. 3 geogrid meshes (single and double mesh configurations) has been investigated to assess the level of improvement that might offered following the same strain-based evaluation scheme. In addition to the developed complex numerical models this thesis also aimed at proposing a simplified-easier to construct and use-numerical model to accurately predict the peak longitudinal pipe strains and to be adopted for preliminary design and evaluation purposes. A case study involving the investigation of the efficacy of utilizing CFRP wraps for seismic damage mitigation was conducted within the scope of this thesis where the Thames Water Pipe which suffered severe damage during the notorious 1999 Izmit earthquake and was shut down as a consequence of this event was modeled and evaluated.

damage during the earthquake that hit the city in 1999, the severity of damage deemed the pipe to be eventually shut down causing significant. The followings are the main concluding remarks emerged from this dissertation:

- Advanced numerical finite element models of the buried pipe-soil model considering the explicit modeling of the complex interaction occurring at the interface of buried pipe and backfill soil were utilized to evaluate the impact of the angle of crossing β between the pipe and the fault trace. Compared in terms of longitudinal strain distributions along the length of the buried pipe recorded at various fault displacements results indicate that increasing the angle value from 10^o to 30^o improves its performance. Strain (axial direction) distributions at tension and compression sides of the deformed pipe further underline this positive influence. Effect of the pipe placement or orientation in reference to the fault plane was also investigated in terms of rate of change in critical fault displacement value, results indicate an increment of at least 25% in d_{cr} value for each strain limit for β value equal to 30^o.

- Evaluation of the impact of increasing the wall thickness of the pipe or reducing the D/t ratio showed that as expected better seismic performance is attainable through the use of thicker pipes. Graphical and numerical investigation of the change in longitudinal strain distribution revealed to an improved performance where the strains reduced by 66%, a more pronounced improvement than that of caused by the increment of angle β. Axial strains at compression and tension sides also were determined to reduce significantly with the increment of pipe wall thickness. Utilized as a useful parameter for performance assessment, critical fault displacement values corresponding to limits states of tensile strains of 3% and 5%, onset of local buckling, and cross-sectional distortion expressed in terms of ovalization, were determined to increase manifold with the increment of thickness from 6.35mm to 15.88mm, with the highest increment noted to be around 90%.

- Possibility of the mitigation of seismic demands imposed on buried pipes by strike-slip fault rupture actions was studied through the use of three types of fiber reinforced

polymers. Namely, the effect of carbon fiber (CFRP), glass fiber (GFRP), and basalt fiber (BFRP) polymers with layer thicknesses of 1mm, 3mm, 5mm, and 10mm were investigated through the development of numerical models incorporating these polymers as wraps around the buried pipe. In overall, Analysis results obtained from mitigated models revealed that the use of FRP wraps lead to significant reduction in strains as well the critical fault displacement value (d_{cr}) that leads to permanent pipeline deformation under one of the limit states considered in this study. Numerical results indicate that a reduction of as much as 96% in pipeline longitudinal strains and 348 % in d_{cr} is possible with the use of FRP wraps with a layer thickness of 10mm. Results also indicate that among the studied FRP types CFRP (carbon fiber) results in the highest reduction and hence performance improvement when compared to other two types. Use of GFRP and BFRP wraps instead of CFRP leads to a reduction of 50-65% and 35-40% respectively in overall Wrap efficiency for the same wrap thickness. As expected, increasing the thickness of FRP Wrap leads to a significant variation in terms of efficiency for all FRP types considered. Plot of tensile strain developments under incremental fault displacements ranging from 0m to 0.80m indicates that the use of GFRP and BFRP wraps with a layer thickness of 1mm is not sufficient enough to avoid failure due to the exceedance of tensile strain limit of 3%, whereas the use of thicker layers for all FRP composites reduced the resulting strains below the threshold value. Similarly, plots of compressive strains given shows that buckling might be avoided up much increased d_{cr} values through the use of these composites.

- Performance of buried pipes against fault rupture induced actions was also evaluated for configurations incorporating EPS geofoam blocks replacing a certain portion of native soil around the buried pipe. Obtained results indicate that the pipeline buried conventionally within backfill soil without EPS geofoam protection could not escape failure occurring either due to exceeding the axial tensile strain limit of 3%, or due to onset of local buckling. A fault displacement value of 46cm and 31cm was determined to be enough to cause failure due to over accumulation of tensile strains and buckling of the pipeline wall respectively. Results also indicate that the pipeline would undergo excessive cross-sectional distortion at a relatively early stage of fault rupture incident with ovalization factor exceeding the limit of 0.15 at 65cm of fault

displacement. Using EPS geofoam blocks to safeguard the buried pipe against fault rupture induced damages proves to be a beneficial approach. Evaluated in terms of axial strains at the compression side of the buckled pipe section shows that a strain reduction of as much as 61.9% and 84.8% is attainable through the use of Low and High Strength EPS geofoam blocks respectively. In addition, utilizing EPS geofoam increases the length of distribution of deformations along the pipeline, hence, avoiding the localized concentration of stresses and strains that would lead to the failure of pipe. A reduction of as much as 171% is noted under the fault displacement of 0.50m when using high strength EPS. Moreover, an increment of as much as 130% in dcr value was achievable through the use of high strength EPS, in which way the pipeline failure under strike-slip fault rupture is offset to much larger displacement values. Distribution of ovalization factor along the length of the pipeline increases by as much as 150% with the use of geofoam, leading to the mitigation of severe deformations and avoiding the flattening of the pipe cross-section.

- Use of controlled-low strength material mixtures as encasement for buried pipes so as to shield them from the detrimental effects of fault actions was also investigated through the development of numerical models. Results indicate that this methodology is the least effective one compared to other studied mitigation approaches leading to only a mere 35% reduction in longitudinal and axial strains. Furthermore, the increase in dcr value was determined to around 70%. Two distinct material modeling approaches have been utilized to assess their impact on theobtained results. Results were obtained for cases solved using the Mohr-Coulomb and concrete damaged plasticity approaches owing to the fact that CLSM has properties between a soil and low strength concrete. Comparison of the results showed that cases modeled using the Mohr-Coulomb approach had the tendency of being higher that those resulting from cases modeled using CDP approach.

- Lastly, the improvement of seismic performance of buried pipes was evaluated for cases incorporating the reinforcement of native soil using geogrid layers. Obtained analysis results reveal that the use of this material considerably improves the performance of buried steel pipelines exposed to actions induced by fault movements. The performance of the pipe under tension was determined to improve

significantly with the use of geogrid, where the critical fault displacement value causing failure due to the exceedance of the threshold value of 3% increased from 46cm for conventional case to 72cm and 96cm for cases incorporating single and double layers of geogrid. The conventional buried pipe already undergoes buckling at a considerably low values of fault displacement (31cm), however, when protected using single and double layers of geogrid the performance of the pipeline improves significantly and the fault displacement value leading to buckling increases from 31cm to 56cm when double layer geogrid configuration is used. The use of double layers of geogrid was also determined to cause a maximum increment of 96% in critical fault displacement value.

- Comparison of the effectiveness of the utilized mitigation approaches revealed that the most effective approach is the use of FRP composite wraps, which led to highest reduction in strains and increase in d_{cr} value. Use of EPS geofoam blocks appears to be second most effective remedy for the improvement of seismic performance of buried pipes. CLSM mixtures have been determined to possess the lowest beneficial effect among the considered approaches. In addition, cost comparison of the approaches showed that despite the high benefits of using FRP wraps, these tend to have the highest cost of use. The use EPS geofoam seemed to be the optimum choice for damage mitigation considering its cost-effectiveness.

- A simplified semi analytical-numerical approach for the calculation of maximum pipeline strains was developed within the scope of this dissertation to provide a simplified tool for preliminary evaluation purposes. Relationships between pipe bending length calculated based on the need of equilibrium among the available and geometrically required pipeline elongations and the tensile strains obtained using a numerical model of buried pipe were determined. Developed simplified numerical models made use of distributed plasticity model approach to simulate the anticipated buried pipe response, while the interaction between the pipe and soil was represented via the use of equivalent soil springs. Use of curve fitting techniques reveled the existence of exponential relationships between the tensile strains, local buckling factor, and the bending angle. Expressions obtained for investigated buried pipe cases were then utilized to compute the maximum longitudinal pipeline strains. Obtained

strains were lastly compared to those emerging from rigorous numerical models, comparison of results reveled a good overall agreement between the strains obtained using both of these approaches, with a low margin of difference.

- Lastly, a case study involving the numerical modeling of Thames Water pipe, a lifeline damaged during the 1999 Izmit earthquake and consequently shut down was investigated within the scope of this dissertation. Existing numerical, and analytical results, as well as field measurements were utilized to validate the developed numerical models, where a good agreement between the results was determined. Mitigation of seismic damage for this buried pipe was investigated through the use of CFRP wraps with a layer thickness of 3mm and 10mm. Results showed that the minor wrinkles developing at the far end of the pipe disappeared when a CFRP wrap of 3mm thickness is used, while the use of 10mm thick layer caused the second wrinkle to also disappear, while the first wrinkle still remained but was significantly mitigated. In addition, the amount of axial strains developing at wrinkle 1&2 locations appear to have been reduced by as much as 47% as the pipe is wrapped with 3mm CFRP composites, whereas a reduction of 87.3% was noted for the case incorporating 10mm thick CFRP layer, truly desirable achievement which could have possibly eliminated the need to cease the function of the pipe immediately following the earthquake. The results indicate a clear reduction in the resulting axial strains, as well however, wrapping the pipeline with CFRP does not seem to affect the length at which the major wrinkles occur. As per the stresses developed at various fault displacement values again a significant reduction is seen to have been obtained using CFRP composite wraps. Lastly, comparison of results between mitigated and non-mitigated cases in terms of rotation demands showed once again a considerable reduction for CFRP wrapped cases. Despite the remedy offered through the use of this mitigation strategy, yet the results indicate that complete elimination of seismic demands is not achievable for this case study, revealing the level of severity of this earthquake and importance of soil properties.

Future Work:

- Effectiveness of the utilized mitigation approaches might be studied for different soil conditions.

- Parametric studies regarding the change of the length of FRP wraps might be performed.
- Effect of the variation of EPS geofoam block thicknesses might be studied through parametric studies.
- Effect of the variation of geogrid layer depths might be studied to better understand the remedy offered using this mitigation strategy.

8. REFERENCES

ABAQUS CAE User's Manual, Dassault System, US, 2020.

Abdel-Rahman, K., T. Gerlach, and M. Achmus, 2020, "Numerical Investigation on Rigid and Flexible Pipelines Embedded in Granular and Self-Compacting Materials.", *Innovative Infrastructure Solutions,* Vol. 5, pp. 1-10.

AbdelSelam, S.S., R.A. Jama, and M.A. Salah, 2019, "EPS Inclusion to Reduce Vertical Stresses on Shallow Tunnels.", *Geosynthetics International,* Vol. 26, pp. 121-135.

Adams, C.A., E. Apraku, and R. Opoku-Boahen, 2015, "Effect of Triaxial Geogrid Reinforcement on CBR Strength of Natural Gravel Soil for Road Pavements.", *Journal of Civil Engineering Research,* Vol. 5, pp. 45-51.

Ahmed, M.R., V.D.H Tran, and M.A. Meguid, 2015, "On the Role of Geogrid Reinforcement in Reducing Earth Pressure on Buried Pipes: Experimental and Numerical Investigations.", *Soils and Foundations,* Vol. 55, pp. 588-599.

Al-Barqawi, M., R. Aqel, M. Wayne, H. Titi, and R. Elhajjar, 2021, "Polymer Geogrids: A Review of Material, Design and Structure Relationships.", *Materials,* Vol. 14, p. 4745

Alexander, C., and O.O. Ochoa, 2013, "Extending Onshore Pipeline Repair to Offshore Steel Risers with Carbon–Fiber Reinforced Composites.", *Composite Structures,* Vol. 92, pp. 499-507.

American Lifeline Alliance - ALA, 2005, "Guidelines for the Design of Buried Steel Pipe."

American Society of Civil Engineers, 2009, "Buried Flexible Steel Pipe; Design and Structural Analysis."

Anastasopoulos, I., A. Callerio, M.F. Bransby, M.C. Davies, A. Nahas, E. Faccioli, G. Gazetas, A. Masella, R. Paolucci, A. Pecker, and E. Rossigniol, 2008, "Numerical Analyses of Fault Foundation Iinteraction.", *Bulletin of Earthquake Engineering,* Vol. 6, pp. 645-675.

Anastasopoulos, I., G. Gazetas, M.F. Bransby, M.C. Davies, A. Nahas, 2007, "Fault Rupture Propagation through Sand: Finite Element Analysis and Validation Through Centrifuge

Experiments.", *Journal of Geotechnical and Geoenvironmental Engineering,* Vol. 133, pp. 943-958.

Aksoy, H.S., G.O.R Mesut, and I.N.A.L Esen, 2017, "Determination of Friction Angles Between Soil and Steel-FRP Piles.", *Turkish Journal of Science and Technology,* Vol. 13, pp. 19-23.

Ballard, J.C, and R. Jewell, 2013, "Observations of Pipe-Soil Response From in-situ Measurements.", *Offshore Technology Conference*.

Bartlett, S.F., B.N. Lingwall, and J. Vaslestad, 2015, "Methods of Protecting Buried Pipelines and Culverts in Transportation Infrastructure Using EPS Geofoam.", *Geotextiles and Geomembranes,* Vol. 43(5), pp. 450-461.

Bartlett, S.F., E.C. Lawton, A.C. Trandafir, and B.N. Lingwall, 2011, "Applications of EPS Geofoam in Design and Construction of Rarthquake Resilient Infrastructure.", *EPS 2011 Conference.*

Bartolini, L., B. Roberto, and L. Vitali, 2013, "Strain Based Design Crossing of Local Features in Arctic Environment.", *Proceedings of the 32nd International Conference on Ocean, Offshore and Arctic Engineering.*

Bathurts, R.J., and F.M. Ezzein, 2017, "Insights into Geogrid–Soil Interaction Using a Transparent Granular Soil.", *Géotechnique Letters,* Vol. 7, pp. 179-183.

Brinch-Hansen, J., 1961, "The Ultimate Resistance of Rigid Piles Against Transversal Forces.", *Geoteknisk Instit., Bull.*

Canadian Standard Association, 2007, "Oil and Gas Pipeline Systems."

Canadian Foundation Engineering Manual, Canadian Geotechnical Society, Richmond, BC, 2006.

Carol, I., E. Rizzi, and K. William, 2001, "On the Formulation of Anisotropic Elastic Degradation. I. Theory Based on a Pseudo-Logarithmic Damage Tensor Rate.", *International Journal of Solids and Structures,* Vol. 38, pp. 491-518.

Cheung, T., D.C. Jansen, and J.L. Hanson, 2008, "Engineering Controlled Low Strength Materials Using Scrap Tire Rubber.", *Geotechnical Special Publication.*

Choo, Y.W., T.H. Abdoun, M.J. O'Rourke, and D. Ha, 2007, "Remediation for Buried Pipeline Systems Under Permanent Ground Deformation.", *Soil Dynamics and Earthquake Engineering,* Vol. 27, pp. 1043-1055.

Comite Europeen de Normalisation, 2006, "Eurocode 8, Part 4: Silos, Tanks and Pipelines."

Crapps, J.M, X. Yue, R.A. Berlin, H.A. Suarez, P.A. Pribytkov, B.A. Vyvial, and J.S. Proegler, 2018, "Strain-Based Pipeline Repair via Type B Sleeve.", *International Journal of Offshore and Polar Engineering,* Vol. 28(03), pp. 280-286.

Dama, E., S.A. Karamanos, and A.M. Gresnigt, 2007, "Failure of Locally Buckled Pipelines.", *Journal of Pressure Vessel Technology,* Vol. 129, pp. 272-279.

Das, S., J.J.R. Cheng, D.W. Murray and N. Nazemi, 2008, "Effect of Monotonic and Cyclic Bending Deformations on NPS12 Wrinkled Steel Pipeline.", *Journal of Structural Engineering,* Vol. 134, pp. 1810-1817.

Dash, S.R., and S.K. Jain, 2007, "IITK-GSDMA Guidelines for Seismic Design of Buried Pipelines."

Desmond, T.P., M.S. Power, C.L. Taylor, and R.W. Lau, 1995, "Behavior of Large-Diameter Pipelines at Fault Crossings.", *ASCE, TCLEE.,* Vol. 6, pp. 296-303.

Demirci, H.E., M. Karaman, and S. Bhattacharya, 2021, "Behaviour of Buried Continuous Pipelines Crossing Strike-Slip Faults: Experimental and Numerical Study.", *Journal of Natural Gas Science and Engineering.,* Vol. 92, p. 103980.

Dezfooli, M.S., A. Abolmaali, Y. Park, and M. Razavi, and F. Ballever, 2015, "Staged Construction Modeling of Steel Pipes Buried In Controlled Low-Strength Material Using 3D Nonlinear Finite-Element Analysis.", *International Journal of Geomechanics,* Vol. 15, pp. 4-14.

Do, T.M., and Y.S. Kim, 2016, "Engineering Properties of Controlled Low Strength Material (CLSM) Incorporating Red Mud.", *International Journal of Geo-Engineering,* Vol. 7, pp. 1-17.

Eidinger, J., 2001, "Performance of Thames Water 2.2 Meter Diameter Pipeline at North Anatolian Fault Crossing.", *G&E Engineering Systems Inc. Report,* No. 48.01.

Eidinger, J., M. O'Rourke, and J. Bachhuber, 2002, "Performance of Pipelines at Fault Crossings.", *Proceedings of the 7th US National Conference of Earthquake Engineering*, No. pp. 21-25.

El Naggar, H., A. Turan, and A. Valsangkar, 2015, "Earth Pressure Reduction System Using Geogrid-Reinforced Platform Bridging for Buried Utilities.", *Journal of Geotechnical and Geoenvironmental Engineering*, Vol. 141, p. 04015024.

Elshesheny, A., M. Mohamed, and T. Sheehan, 2019, "Performance of Buried Rigid Pipes Under the Application of Incrementally Increasing Cyclic Loading.", *Soil Dynamics and Earthquake Engineering*, Vol. 125, p. 105729.

Ferellec, J.F., and G.R. McDowell, 2012, "Modelling of Ballast–Geogrid Interaction Using the Discrete-Element Method.", *Geosynthetics International*, Vol. 19, pp. 470-479.

Fredj, A., and A. Dinovitzer, 2012, "Simulation of the Response of Buried Pipelines to Slope Movement Using 3D Continuum Modeling.", *Proceedings of the 9th International Pipeline Conference.*

Gantes, C., and G. Bouckovalas, 2013, "Seismic Verification of the High Pressure Natural Gas Pipeline Komotini–Alexandroupoulis–Kipi in Areas of Active Fault Crossings.", *Structural Engineering International,* , Vol. 23(2), pp. 204-208.

Gantes, C.J., and V.E. Melissianos, 2016, "Evaluation of Seismic Protection Methods for Buried Fuel Pipelines Subjected to Fault Rupture.", *Frontiers in Built Environment,* Vol. 2, p. 34.

Gazetas, G., I. Anastasopoulos, and M. Apostolou, 2007, "Shallow and Deep Foundation Under Fault Rapture or Strong Seismic Shaking.", *Earthquake Geotechnical Engineering*, pp. 185-215.

Gresnigt, A., 1986, "Plastic Design of Buried Steel Pipelines in Settlement Areas.", *Heron (Delft),* Vol. 31, pp. 1-113.

Günaslan, S.A., A. Karaşin, and M.E. Öncü, 2014, "Properties of FRP Materials for Strengthening.", *International Journal of Innovative Science, Engineering & Technology,* Vol. 1, pp. 656-660.

Ha, D., T.H. Abdoun, M.J. O'Rourke, M.D. Symans, T.D. O'Rourke, M.C. Palmer, and H.E. Stewart, 2008, "Centrifuge Modelling of Earthquake Effects on Buried High-Density Polyethylene (HDPE) Pipelines Crossing Fault Zones.", *ASCE Journal of Geotechnical and Geoenvironmental Engineering,* Vol. 134, pp. 1501-1515.

Ha, D., T.H. Abdoun, M.J. O'Rourke, M.D. Symans, T.D. O'Rourke, M.C. Palmer, and H.E. Stewart, 2008, "Buried High-Density Polyethylene Pipelines Subjected to Normal and Strike-Slip Faulting-A Centrifuge Investigation.", *Canadian Geotechnical Journal,* Vol. 45, pp. 1733-1742.

Hafezolghorani, M., F. Hajezi, R. Vaghei, M.S.B. Jafaar, and K. Karimzade, 2017, "Simplified Damage Plasticity Model for Concrete.", *CICTP 2012: Structural Engineering International,* Vol. 27, pp. 68-78.

Hashin, Z., 1980, "Failure Criteria for Unidirectional Fiber Composites.", *Journal of Applied Mechanics,* Vol. 47, pp. 329-334.

Hashin, Z., and A. Rotem, 1973, "A Fatigue Failure Criterion for Fiber Reinforced Materials.", *Journal of composite materials,* Vol. 7, pp. 448-464.

Holloway, L.C., 2010, "A Review of the Present and Future Utilization of FRP Composites in the Civil Infrastructure with Reference to Their Important In-Service Properties", *Construction and Building Materials,* Vol. 24, pp. 2419-2445.

Humphreys, M., 2003, "The Use of Polymer Composites in Construction.", *Proceedings of the CIB 2003 Int'l conference on Smart and Sustainable Built Environment,* pp. 1-9.

Hussein, M.G., and M.A. Meguid, 2016, "A Three-Dimensional Finite Element Approach for Modeling Biaxial Geogrid with Application to Geogrid-Reinforced Soils.", *Geotextiles and Geomembranes,* Vol. 44, pp. 295-307.

Jayasuriy, S., B. Chegeni, and S. Das, 2020, "Use of BFRP Wrap for Rehabilitation of Pipeline in Bending with Various Corrosion Depths.", *Journal of Pipeline Systems Engineering and Practice,* Vol. 11, pp. 38-48.

Jung, J.K., T.D. O'Rourke, and N.A. Olson, 2013, "Lateral Soil-Pipe Interaction in Dry and Partially Saturated Sand.", *Journal of Geotechnical and Geoenvironmental Engineering,* Vol. 139, pp. 2028-2036.

Karamitros, D.K., G.D. Bouckovalas, and G.P. Kouretzis, 2007, “Stress Analysis of Buried Steel Pipelines at Strike-Slip Fault Crossings.”, *Soil Dynamics and Earthquake Engineering*, Vol. 27(3), pp. 200-2011.

Karimian, H., D. Wijewickreme, and D. Honegger, 2009, “Response of Buried Pipelines Subjected to Relative Axial Soil Movement.”, *Canadian Geotechnical Journal*, Vol. 46(7), pp. 735-752.

Kaya, E.S., E. Uckan, M.J. O’Rourke, S.A. Karamanos, B. Akbas, F. Cakir, and Y. Cheng, 2017, “Failure Analysis of a Welded Steel Pipe at Kullar Fault Crossing.”, *Engineering Failure Analysis*, Vol. 71, pp. 43-62.

Kennedy, R.P., and R.H. Kincaid, 1983, “Fault Crossing Design for Buried Gas Oil Pipelines.”, *ASME, PVP Conference*, Vol. 77, pp. 1-9.

Kennedy, R.P., R.A. Williamson, and A.M. Chow, 1977, “Fault Movement Effects on Buried Oil Pipeline.”, *Transportation Engineering Journal of ASCE*, Vol. 103(5), pp. 617-633.

Kibey, S., X. Wang, K. Minaar, M.L. Macia, D.P. Fairchild, W.C. Kan, S.J. Ford, and B. Newbury, 2010, “Tensile Strain Capacity Equations for Strain-Based Design of Welded Pipelines.”, *International Pipeline Conference*, Vol. 44236, pp. 355-363.

Labuz, J.F., and A. Zang, 2012, “Mohr–Coulomb Failure Criterion.”, *Rock mechanics and rock engineering*, Vol. 45, pp. 975-979.

Larsson, S., R. Malm, B. Charbit, and A. Ansell, 2012, “Finite Element Modelling of Laterally Loaded Lime–Cement Columns Using a Damage Plasticity Model.”, *Computers and Geotechnics*, Vol. 44, pp. 48-57.

Ling, T.C, S.K. Kaliyavaradhan, and C.S. Poon, 2018, “Global Perspective on Application of Controlled Low-Strength Material (CLSM) for Trench Backfilling–An Overview.”, *Construction and Building Materials*, Vol. 158, pp. 535-548.

Lingwall, B., and S. Bartlett, 2014, “Full-Scale Testing of an EPS Geofoam Cover System To Protect Pipelines at Locations of Lateral Soil Displacement.”, *Pipelines 2014: From Underground to the Forefront of Innovation and Sustainability*, pp. 606-615.

Liu, A., S. Takada, and Q. He, 2014, "The Failure Performance of Thames Water Pipeline at Fault Crossing in Kocaeli Earthquake.", *Second European Conference on Earthquake, Engineering and Seismology.*

Liu, M., H. Zhang, M. Li, M. Xia, W. Zheng, K. Wu, and Y. Han, 2016, "Effects of Steel Properties on the Local Buckling Response of High Strength Pipelines Subjected to Reverse Faulting.", *Journal of Natural Gas Science and Engineering,* Vol. 33, pp. 378-387.

Liu, X., S. Takada, and Q. He, 2014, "The Failure Performance of Thames Water Pipeline at Fault Crossing in Kocaeli Earthquake.", *Second European Conference on Earthquake, Engineering and Seismology.*

LS-DYNA, 2007, "Keywords User's Manual.", *Livermore Software and Technology Corporation.*

MaCaffrey, M.A., 1983, "Buried Pipeline Response to Reverse Faulting During the 1971 San Fernando Earthquake.", *ASME, PVP.,* Vol. 77, pp. 151-159.

Marto, A., M. Oghabi, and A. Eisazadeh, 2013, "The Effect of Geogrid Reinforcement on Bearing Capacity Properties of Soil Under Static Load; A Review.", *Electronic Journal of Geotechnical Engineering,* Vol. 18, pp. 1881-1896.

Marza, V. I., 2004, "On the Death Toll of the 1999 Izmit (Turkey) Major Earthquake.", *ESC General Assembly Papers, European Seismological Commission, Potsdam.*

Masada, T., and S.M. Sargand, 2002, "Measured Structural Performance of HDPE Pipe Installed In CLSM-CDF.", *Pipelines 2002: Beneath Our Feet: Challenges and Solutions,* pp. 1-12.

Meguid, M.A., and M.O.G. Hussein, 2017, "A Numerical Procedure for The Assessment of Contact Pressures on Buried Structures Overlain by EPS Geofoam Inclusion.", *International Journal of Geosynthetics and Ground Engineering,* Vol. 3, pp. 1-14.

Meguid, M.A., M.G. Hussein, M.R. Ahmed, Z. Omeman, and J. Whalen, 2017, "Investigation of Soil-Geosynthetic-Structure Interaction Associated with Induced Trench Installation.", *Geotextiles and Geomembranes,* Vol. 45, pp. 320-330.

Mehjardi, G.D., and S. Tafreshi, 2008, "Buried Pipes Analysis in Reinforced Sand Under Repeated Loading.", *Proceedings of the Second BGA International Conference on Foundations, ICOF2008.*

Melissianos, V.E., G.P. Korakitis, C.J. Gantes, and G.D. Bouckovalas, 2016, "Numerical Evaluation of The Effectiveness of Flexible Joints in Buried Pipelines Subjected to Strike-Slip Fault Rupture.", *Soil Dynamics and Earthquake Engineering,* Vol. 39, pp. 395-410.

Mokhtari, M., and A.A. Nia, 2015, "The Influence of Using CFRP Wraps on Performance of Buried Steel Pipelines Under Permanent Ground Deformations.", *Soil Dynamics and Earthquake Engineering,* Vol. 73, pp. 29-41.

Nederlands Normalisatie-Instituut, 2006, "Requirements for Pipeline Systems, NEN 3650, Part-1: General, and Part-2: Steel Pipelines."

Newmark, N.M., and W.J. Hall, 1975, "Pipeline Design to Resist Large Fault Displacement.", *Proceedings of US National Conference on Earthquake Engineering,* Vol. 1975, pp. 416-425.

O'Rourke, M.J., and X. Liu, 2012, "Seismic Design of Buried and Offshore Pipelines", *MCEER Monograph MCEER-12-MN04,* p. 380.

O'Rourke, T.D., H.E. Stewart, M.C. Palmer, T.K. Bond, J.M. Jezerski, M.J. O'Rourke, M.D. Symans, T. Abdoun, and D. Ha, 2009, "Evaluation of Ground Rupture Effects on Critical Lifelines.", *NSF Program Solicitation 03-589.*

O'Rourke, T.D., M.D Grigoriu, and M.M. Khater, 2012, "A State of The Art Review: Seismic Response of Buried Pipelines", *Decade of Progress in Pressure Vessel Technology, (C. Sundararajan, Editor), ASME.*

Odina, L., and R. Tan, 2009, "Seismic Fault Displacement of Buried Pipelines Using Continuum Finite Element Methods.", *Proceedings of the ASME 2009 28th International Conference on Ocean, Offshore and Arctic Engineering.*

Odina, L., and R.J. Conder, 2010, "Significance of Lüder's Plateau on Pipeline Fault Crossing Assessment.", *Proceedings of the ASME 2010 29th International Conference on Ocean, Offshore and Arctic Engineering.*

Oskouei, A.V., A. Tamjidi, and P. Pourshabani, 2019, "Effects of Burial Depth in the Behavior of Buried Steel Pipelines Subjected to Strike-Slip Fault.", *Soil Dynamics and Earthquake Engineering,* Vol. 123, pp. 252-264.

Panico, M, M.L. Macia, D.P. Fairchild, and W. Cheng, 2017, "A Case Study of Design and Integrity Management Framework for Strain-Based Pipelines.", *The 27th International Ocean and Polar Engineering Conference.*

Perkins, S.W., and M.Q. Edens, 2003, "Finite Element Modeling of a Geosynthetic Pullout Test.", *Geotechnical & Geological Engineering,* Vol. 21, pp. 357-375.

Pinho-Lopes, M., A.M. Paula, and M.D.L. Lopes, 2015, "Pullout Response of Geogrids After Installation.", *Geosynthetics International,* Vol. 22, pp. 339-354.

PLE4Win, 2003, "Short Introduction to Ple4, A Pipeline Stress, Strain and Stability Analysis Computer Program.", *Expert Design Systems.*

Puppala, A.J., A. Banarjee, and S.S. Congress, 2020, "Geosynthetics in Geo-Infrastructure Applications.", *Geotechnique,* Vol. 11, pp. 339-353.

Potyondy, J.G., 1961, "Skin Friction Between Various Soils and Construction Materials.", *Durability of Composite Systems,* pp. 289-312.

Rasouli, H., and B. Fatahi, 2020, "Geofoam Blocks to Protect Buried Pipelines Subjected to Strike-Slip Fault Rupture.", *Geotextiles and Geomembranes,* Vol. 48, pp. 257-274.

Saadeldin, R., Y. Hu, and A. Henni, 2015, "Numerical Analysis of Buried Pipes Under Field Geo-Environmental Conditions", *International Journal of Geo-Engineering,* Vol. 6(1), pp. 1-22.

Sahin, M., and E. Tari, 2000, "The August 17 Kocaeli and The November 12 Duzce Earthquakes in Turkey.", *Earth, Planets and Space,* Vol. 52, pp. 753-757.

Sarvanis, G.C., S.A. Karamanos, P. Vazouras, E. Mecozzi, A. Lucci, and P. Dakoulas, 2018, "Permanent Earthquake-Induced Actions in Buried Pipelines: Numerical Modeling and Experimental Verification.", *Earthquake Engineering & Structural Dynamics,* Vol. 47, pp. 966-987.

Scarpelli, G., S. Sakellariadi, and G. Furlani, 2003, "Strain Based Design Crossing of Local Features in Arctic Environment.", *Proceedings of the 32nd International Conference on Ocean, Offshore and Arctic Engineering.*

Seed, R.B., K.O. Cetin, R.E. Moss, A.M. Kammerer, J. Wu, J.M. Pestana, M.F. Riemer, R.B. Sancio, J.D. Bray, R.E. Kayen, and A. Faris, 2003, "Recent Advances in Soil Liquefaction

Engineering: A Unified and Consistent Framework.", *Proceedings of the 26th Annual ASCE Los Angeles Geotechnical Spring Seminar*.

Shang, K., Q. Guo, Z. He, and Y. Ye, 2012, "A Study of the Torsional Behavior of Reinforced Concrete Trough Girder Based on ABAQUS.", *CICTP 2012: Multimodal Transportation Systems—Convenient, Safe, Cost-Effective, Efficient,* Vol. 10, pp. 3029-3035.

Shewbridge, S.E., and N. Sitar, 1996, "Formation of Shear Zones in Reinforced Sand.", *Journal of Geotechnical Engineering,* Vol. 122, pp. 873-885.

Shitamoto, H., M. Hamada, S. Okaguchi, N. Takahashi, I. Takeuchi, and S. Fujita, 2010, "Evaluation of Compressive Strain Limit of X80 SAW Pipes for Resistance to Ground Movement.", *Proceedings of the Twentieth International Offshore and Polar Engineering Conference.*

Shouman, A., and F. Taheri, 2011, "Compressive Strain Limits of Composite Repaired Pipelines Under Combined Loading States.", *Composite Structures,* Vol. 93, pp. 1538-1548.

Shuwang, Y., F. Shouzhong, and B. Barr, 1998, "Finite-Element Modelling of Soil-Geogrid Interaction Dealing with the Pullout Behaviour of Geogrids.", *Acta Mechanica Sinica,* Vol. 14, pp. 371-382.

Somboonyanon, P., and C. Halmen, 2021, "Seismic Behavior of Steel Pipeline Embedded in Controlled Low-Strength Material Subject to Reverse Slip Fault.", *Journal of Pipeline Systems Engineering and Practice,* Vol. 12, pp. 25-41.

Somboonyanon, P., and C. Halmen, 2021, "Seismic Behavior of Steel Pipeline Embedded in Controlled Low-Strength Material Subject to Reverse Slip Fault.", *Journal of Pipeline Systems Engineering and Practice,* Vol. 12, pp. 21-25.

Sugimoto, M., and A.M.N Alagiyawanna, 2003, "Pullout Behavior of Geogrid by Test and Numerical Analysis.", *Journal of Geotechnical and Geoenvironmental Engineering,* Vol. 129, pp. 361-371.

Taechakumthorn, C., and R. Rowe, 2013, "Reinforced Embankments on Soft Deposits: Behavior, Analysis and Design.", *Geotechnical Engineering,* Vol. 44, pp. 69-76.

Tafreshi, S.M., N.J. Durabi, and A.R. Dawson, 2020, “Combining EPS Geofoam with Geocell to Reduce Buried Pipe Loads and Trench Surface Rutting.”, *Geotextiles and Geomembranes,* Vol. 48, pp. 400-418.

Takada, S., N. Hassani, and K. Fukuda, 2001, “A New Proposal for Simplified Design of Buried Steel Pipes Crossing Active Faults.”, *Earthquake Engineering & Structural Dynamics,* Vol. 30, pp. 1243-1257.

Talebi, F., and J. Kiyono, 2021, “Comparison of 3D Solid and Beam–Spring FE Modeling Approaches in the Evaluation of Buried Pipeline Behavior at a Strike-Slip Fault Crossing.”, *Energies,* Vol. 14, pp. 4539.

Tang, A. K., 2000, “Izmit (Kocaeli), Turkey, Earthquake of August 17, 1999 Including Duzce Earthquake of November 12, 1999: Lifeline Performance.”, *ASCE Publications,* Vol. 17.

Tsubakihara, Y., H. Kishida, and T. Nishiyama, 1993, “Friction Between Cohesive Soils and Steel.”, *Soils and Foundations,* Vol. 33, pp. 145-156s.

Tran, V.D.H., M.A. Meguid, and L.E. Chouinard, 2015, “Three-Dimensional Analysis of Geogrid-Reinforced Soil Using a Finite-Discrete Element Framework.”, *International Journal of Geomechanics,* Vol. 15, p. 04014066.

Trautmann, C.H., 1983, “Behavior of Pipe in Dry Sand Under Lateral and Uplift Loading.”, *Cornell University.*

Turner, J., 2004, *Lateral Force–Displacement Behavior of Pipes in Partially Saturated Sand*, M.S. Thesis, Cornell University.

Vazouras, P., P. Dakoulas, and S.A. Karamanos, 2015, “Pipe–Soil Interaction and Pipeline Performance Under Strike-Slip Fault Movements”, *Soil Dynamics and Earthquake Engineering,* Vol. 72, pp. 48-65.

Vazouras, P., S.A Karamanos, and P. Dakoulas, 2010, “Finite Element Analysis of Buried Steel Pipelines Under Strike-Slip Fault Displacements”, *Soil Dynamics and Earthquake Engineering,* Vol. 30(11), pp. 1361-1376.

Wang, L.L., and L.J. Wang, 1995, “Parametric Study of Buried Pipelines Due to Large Fault Movements.”, *ASCE, TCLEE.,* Vol. 6, pp. 152-159.

Wang, L.R.L., and Y.H. Yeh, 1985, "A Refined Seismic Analysis and Design of Buried Pipeline for Fault Movement.", *Earthquake Engineering & Structural Dynamics,* Vol. 13(1), pp. 75-96.

Wang, X, S. Kibey, H. Tang, W. Cheng, K. Minnaar, M. Macia, W.C. Kan, S.J. Ford, and B. Newbury, 2010, "Strain-Based Design-Advances in Prediction Methods of Tensile Strain Capacity.", *The 20th International Offshore and Polar Engineering Conference.*

Xu, C., C. Liang, and P. Shen, 2019, "Experimental and Theoretical Studies on the Ultimate Bearing Capacity of Geogrid-Reinforced Sand.", *Geotextiles and Geomembranes,* Vol. 47, pp. 417-428.

Yogarajah, I., and K.C. Yeo, 1994, "Finite Element Modelling of Pull-Out Tests with Load and Strain Measurements.", *Geotextiles and Geomembranes,* Vol. 13, pp. 43-54.

Yoshizaki, K., and T. Sakanoue, 2003, "Experimental Study on Soil-Pipeline Interaction Using EPS Backfill.", *New Pipeline Technologies, Security, and Safety*, pp. 1126-1136.

Yoshizaki, K., T.D. O'Rourke, T. Bond, J. Mason, and M. Hamada, 2001, "Large Scale Experiments of Permanent Ground Deformation Effects on Steel Pipelines.", *Available from MCEER. Buffalo. edu/publications/resaccom/01-sp01/rpa_pdfs/03orourke_tkyogas. pdf [accessed 14 October 2022].*

Yimsiri, S., K. Soga, K. Yoshizaki, G.R. Dasari, and T.D. O'Rourke, 2004, "Lateral and Upward Soil-Pipeline Interactions in Sand for Deep Embedment Conditions.", *Journal of Geotechnical and Geoenvironmental Engineering,* Vol. 130, pp. 830-842.

Yu, T., J. Teng, Y. Wong, and S. Dong, 2010, "Finite Element Modeling of Confined Concrete-II: Plastic-Damage Model.", *Engineering Structures,* Vol. 32, pp. 680-691.

Zaman, A., S.A. Gutub, and M.A. Wafa, 2013, "A Review on FRP Composites Applications and Durability Concerns in the Construction Sector.", *Journal of Reinforced Plastics and Composites,* Vol. 32, pp. 1966-1988.

Zhan, C., and B. Rajani, 1997, "Load Transfer Analyses of Buried Pipe in Different Backfills.", *Journal of Transportation Engineering,* Vol. 123, pp. 447-453.

Zhou, J., J.F. Chen, J.F. Xue, and J.Q. Wang, 2012, “Micro-Mechanism of the Interaction Between Sand and Geogrid Transverse Ribs.”, *Geosynthetics International,* Vol. 19, pp. 426-437.